Faculty of Aerospace Engineering

Dynamic Stall Modeling for the Cessna Citation II

Joost van Ingen

25 October 2017

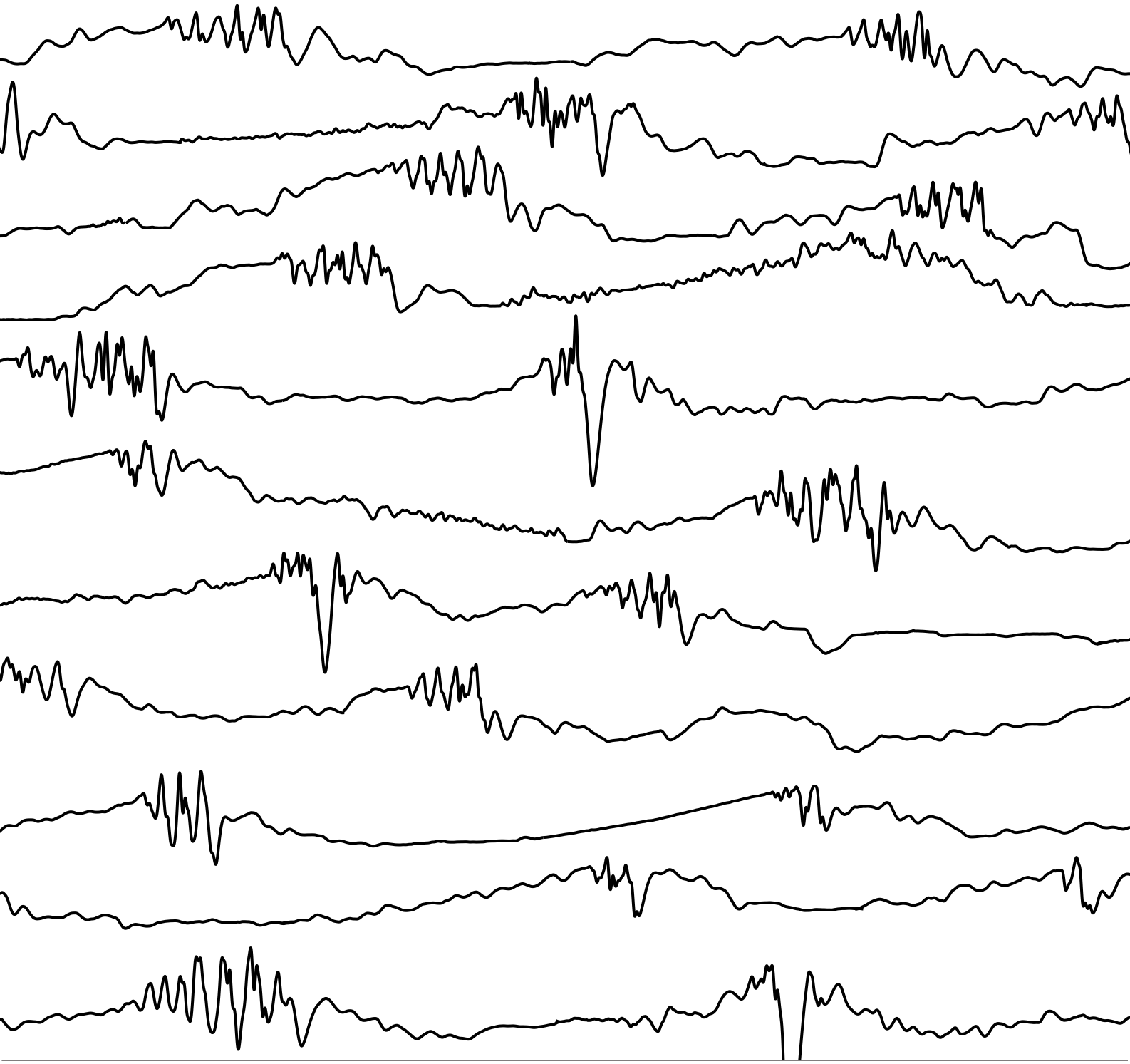

TU Delft Delft University of Technology

Challenge the future

Dynamic Stall Modeling for the Cessna Citation II

MSc Thesis

by

J.B. van Ingen

to obtain the degree of Master of Science at Delft University of Technology,
to be defended publicly on Wednesday 25 October 2017 at 14:00.

Student number:	4049705	
Project duration:	22 August 2016 – 25 October 2017	
Assessment committee:	Prof. dr. ir. M. Mulder	TU Delft, AE, Control & Simulation
	Dr. ir. D.M. Pool	TU Delft, AE, Control & Simulation
	Dr. ir. C.C. de Visser	TU Delft, AE, Control & Simulation
	Dr. ir. M.M. van Paassen	TU Delft, AE, Control & Simulation
	Dr. ir. S.J. Hulshoff	TU Delft, AE, Aerodynamics
	Dr. ir. S.K. Advani	IDT & ICATEE

TU Delft

Preface

Before you lies the final piece of work I will produce during my time as a student in Delft. It is the product of more than twelve months of efforts, which, according to true TU Delft tradition, is longer than initially planned. Along the way, the process has surely been very difficult at times, but overall, I look back and am quite proud of the end result. As you will be able to read, this thesis is part of a longer program that is to eventually result in proven and effective simulator training programs that teach pilots to recognize, prevent, and recover from dangerous stalled flight conditions. It is my hope that a step in that direction has been made, no matter how small that step might be.

Back in the summer of 2016, when I was looking for a thesis project, I was immediately excited by the possibility of working on stall modeling of a real aircraft. It appeared to have everything I was looking for: a challenging system identification problem, the fact that I would not have to sit in a simulator control room for weeks on end, a relevant application to industry, and also the opportunity of doing actual flight tests! However, these flight tests also introduced a large amount of uncertainty into the feasibility and planning this project, which made me doubt whether I should commit to this subject.

However, in the end, my enthusiasm and optimism won; in August 2016, I officially started my thesis. As with all students, the first months were spent with reading up on literature and trying to wrap my head around the suddenly enormously-appearing task that stood before me. Then, already in November 2016, it turned out that my initial doubts were unfounded. A full day of flight tests took place during probably the most beautiful day of weather of that year's Fall. The fact that I could work with real flight data has been both a privilege and a challenge. During these months I have become so familiar with the view of the plots, that I decided to use them to decorate the cover page of this report, so that others might see them too as I did. Moreover, I feel that they have been used to build a high-quality model, but I will leave the final judgement of that to the examination committee.

I would like to use this section to thank all the people that have helped me during this project. First of all a big thanks to Daan and Coen, my daily supervisors, for all the feedback, encouragement, and support. Our meetings were really enjoyable, and provided me with (sometimes much needed) positive reinforcement to push on. Next, Max, thanks for your feedback on those important decision moments, and for finding the time in your busy schedule to read and comment on my paper. René, thank you for your comments on my paper, and for updating DUECA to support the latest changes to Matlab. Olaf, thank you for all your assistance (and patience) in getting the stall model running in SIMONA. Hans and Xander, Citation pilots, for your help in designing the flight tests, and for managing all that paperwork (and the bureaucrats of the NLR). Aircraft technicians, Ferdinand and Menno, thanks for preparing and planning the aircraft, and for guiding a student who has very little experience with real-world aircraft operations. Sunjoo, for supporting the research project, your industry insights, your enthusiasm, and for agreeing to be part of the examination committee. Steven Hulshoff, for also taking place in the examination committee as external member. And finally, a big shout-out to all the boys and girls of room NB2.44 and SIM0.08. Thanks for all the coffee breaks, lunches, Friday drinks, bad jokes, time-outs for really bad jokes, and being a place where all the daily struggles and frustrations could be discussed. Without you, it would have been no fun at all!

This preface is already turning out much longer than I thought, much like this whole report itself. A short note on how it is structured: it consists of four parts. First comes the research paper I have written, which is intended to summarize my research in a scientific way. Next is the prelminary thesis report, which covers roughly the first half of the thesis project. After that, there are two parts containing appendices, which present additional findings, details, and conclusions that did not make it to the final paper.

Contents

List of Figures vii

List of Tables viii

Nomenclature ix

I Scientific Paper 1

II Preliminary Thesis Report 33

1 Introduction 34

2 Background & Literature Review 37
2.1 Aerodynamic Stall Definition . . . 37
2.2 New FAA Regulations Regarding Stall Modeling in FSTDs . . . 38
2.3 ICATEE List of Effects of Aerodynamic Stall . . . 39
2.4 A Literature Survey of Stall Modeling Research . . . 40
2.4.1 Early Efforts . . . 41
2.4.2 Kirchoff's Theory of Flow Separation . . . 42
2.4.3 Other Extensions to Aerodynamic Model Equations . . . 43
2.4.4 Application of Fighter Methods to Civil Aircraft . . . 44
2.4.5 Founding of ICATEE . . . 45
2.4.6 Bihrle Applied Research . . . 45
2.4.7 Recent Developments . . . 46
2.5 Chapter Summary . . . 46

3 Flight Test Experiments 48
3.1 Test Aircraft and FTIS . . . 48
3.2 Flight Test Design . . . 49
3.2.1 Objectives For Flight Tests . . . 49
3.2.2 Maneuver Descriptions . . . 50
3.3 Notes on the Flight Tests . . . 50

4 Flight Path Reconstruction 51
4.1 Unscented Kalman Filter . . . 51
4.1.1 UKF Implementation . . . 51
4.1.2 UKF Parameters . . . 53
4.2 Navigation Equation . . . 53
4.2.1 Position, Velocity, Attitude . . . 53
4.2.2 Wind, IMU Sensor Biases . . . 54
4.2.3 Air Data Boom Vane Parameters . . . 54
4.2.4 Full Navigation Equation. . . . 55
4.3 Observation Equation. . . . 55
4.3.1 Position Measurements . . . 55
4.3.2 Attitude Measurements . . . 56
4.3.3 Air Data Measurements . . . 56
4.3.4 Full Observation Equation . . . 56
4.4 Observability and Final System . . . 57
4.4.1 Local Observability Analysis . . . 57
4.4.2 State Covergence On a Real Data Set . . . 57
4.4.3 Final System . . . 58
4.5 Example of UKF Performance on Data . . . 60

5 Stall Model Structure **66**
5.1 Conventional Aerodynamic Model Equations . . . 66
5.2 Extensions to the Conventional Aerodynamic Model Equations . . . 68
5.2.1 Terms Based on Kirchoff's Theory of Flow Separation . . . 68
5.2.2 Higher Order Polynomial Terms . . . 70
5.2.3 Univariate Splines of State Variables . . . 71
5.2.4 Other Model Extensions . . . 71
5.3 Buffet Model . . . 71
5.4 Merging the Stall Model with the Regular Aerodynamic Model . . . 72
5.5 Chapter Conclusion . . . 72

6 Parameter Estimation **73**
6.1 Evaluating Model Fit Quality . . . 73
6.1.1 Mean Squared Error . . . 73
6.1.2 Variance Accounted For . . . 73
6.1.3 Regularization . . . 73
6.1.4 Parameter Correlations . . . 74
6.1.5 Cramèr-Rao Lower Bounds . . . 74
6.2 Nonlinear Parameter Estimation . . . 75
6.2.1 Nonlinear Optimization in MATLAB . . . 75
6.2.2 Parameter Sensitivity of the Solution of an ODE . . . 76
6.3 Linear Parameter Estimation . . . 76
6.4 Chapter Conclusion . . . 77

7 Preliminary Results **78**
7.1 Model Identification Approach . . . 78
7.1.1 Selected Model Structure . . . 78
7.1.2 Cost Function & Solver Algorithm . . . 79
7.2 Estimated Parameter Values . . . 79
7.2.1 As Function of Flight Condition . . . 79
7.2.2 Parameter Correlations . . . 84
7.3 Time-History Comparisons . . . 85
7.3.1 Training Data Example . . . 85
7.3.2 Validation Data Example . . . 85
7.4 Sensitivity Analysis . . . 88

8 Conclusion & Outlook **90**
8.1 Conclusion . . . 90
8.2 Outlook For Remainder of the Thesis . . . 91

Bibliography **93**

III Appendices to Preliminary Thesis Report **97**

A AHRS Data Corrections **98**
A.1 Specific Force to Acceleration . . . 98
A.2 AHRS Output to Specific Force . . . 98
A.3 Complete Correction Method . . . 100

B Usability of Old Flight Data **101**
B.1 Analysis Method . . . 101
B.2 Results . . . 101
B.3 Discussion . . . 102

C Vibrations in the Air Data Boom **109**
C.1 Power Spectral Density Estimate of Vibrations . . . 109
C.2 Filtering the Vibrations . . . 110

D Example Flight Test Card **111**

IV Appendices to Final Report **115**

E Time History Plots of All Flight Data Sets **116**

F Analysis of Flight Test Maneuver Effectiveness **123**
F.1 Methodology & Results 123
F.2 Conclusions. 123

G SIMONA Implementation of Model **128**
G.1 Current State of SIMONA Implementation 128
G.2 Recommended Next Steps 128

H List of Recommendations for Future Research **130**

List of Figures

1.1 The structure of the proposed thesis research methodology . . . 35

2.1 Progression of trailing edge flow separation . . . 37
2.2 Statistics of civil aviation fatalities by category, 2006-2015 . . . 38
2.3 Example of nonlinear control and stability derivatives of an F-15 during stall . . . 41
2.4 Illustration of internal variable X . . . 42
2.5 Non-pysical model behavior . . . 43
2.6 Mechanization of aircraft angular rate vector . . . 44

3.1 A picture of the PH-LAB laboratory aircraft of DUT and NLR, note that the air data boom is not installed in this picture . . . 48
3.2 Schematic views of the PH-LAB . . . 49

4.1 Negative correlation between $C_{\alpha_{\text{up}}}$ and C_{α_0} . . . 58
4.2 UKF state convergence (1/2) . . . 59
4.3 UKF state convergence (2/2) . . . 59
4.4 UKF reconstructed states (1/2) . . . 61
4.5 UKF reconstructed states (2/2) . . . 62
4.6 UKF reconstructed measurements . . . 63
4.7 UKF reconstructed input signals . . . 64
4.8 UKF measurement innovations . . . 65

5.1 Illustration of internal variable X . . . 68
5.2 Effect of varying τ_1 . . . 69
5.3 Effect of varying τ_2 . . . 69
5.4 Effect of varying a_1 . . . 69
5.5 Effect of varying α^* . . . 70

7.1 Scatter of X-parameters . . . 80
7.2 Scatter of C_L-parameters . . . 81
7.3 Scatter of C_D-parameters . . . 81
7.4 Scatter of C_Y-parameters . . . 82
7.5 Scatter of C_l-parameters . . . 82
7.6 Scatter of C_m-parameters . . . 83
7.7 Scatter of C_n-parameters . . . 83
7.8 Time history of training data fit . . . 86
7.9 Time history of validation data fit . . . 87
7.10 Sensitivity analysis of X and C_L-parameters . . . 88

A.1 Raw AHRS output visualization . . . 99
A.2 Corrected AHRS output visualization . . . 100

B.1 Detailed plots of α, β, for a longitudinal stall . . . 102
B.2 Reconstructed measurement signals, for a longitudinal stall . . . 103
B.3 Reconstructed state (1/2), for a longitudinal stall . . . 104
B.4 Reconstructed state (2/2), for a longitudinal stall . . . 105
B.5 Reconstructed input signal, for a longitudinal stall . . . 106
B.6 Detailed plots of α, β, for a partially lateral stall . . . 107
B.7 Reconstructed state (1/2), for a partially lateral stall . . . 107

C.1 PSD of raw and filtered boom signals . . . 109
C.2 Time history of raw and filtered boom signals . . . 110

E.1 Time history plots of training sets 1, 2, and 3. . . . 116
E.2 Time history plots of training sets 4, 6, and 8. . . . 117
E.3 Time history plots of training sets 9, 10, and 11. . . . 117
E.4 Time history plots of training sets 13, 14, and 15. . . . 118
E.5 Time history plots of training sets 17, 18, and 19. . . . 118
E.6 Time history plots of training sets 20, 21, and 24. . . . 119
E.7 Time history plots of training sets 26, 27, and 28. . . . 119
E.8 Time history plots of training sets 29, 30, and 31. . . . 120
E.9 Time history plots of training sets 32, 33, and 34. . . . 120
E.10 Time history plots of validation sets 5, 7, and 12. . . . 121
E.11 Time history plots of validation sets 16, 22, and 23. . . . 121
E.12 Time history plots of validation sets 22, and 23, which are repeated from previous figure and 25. 122

F.1 Flight test maneuver analysis plots for the X-parameters. . . . 124
F.2 Flight test maneuver analysis plots for the C_L-parameters. . . . 125
F.3 Flight test maneuver analysis plots for the C_D-parameters. . . . 125
F.4 Flight test maneuver analysis plots for the C_Y-parameters. . . . 126
F.5 Flight test maneuver analysis plots for the C_l-parameters. . . . 126
F.6 Flight test maneuver analysis plots for the C_m-parameters. . . . 127
F.7 Flight test maneuver analysis plots for the C_n-parameters. . . . 127

G.1 Overview of the complete Citation II aircraft model as implemented in Simulink . . . 129
G.2 Aerodynamic stall model part of the Simulink model. . . . 129

List of Tables

3.1 Mass and geometry properties of the Cessna Citation II . . . 48
3.2 FTIS signals that are measured in-flight . . . 50
3.3 Air data boom dimensions w.r.t. datum line . . . 50

4.1 UKF parameters used for the FPR in this thesis. . . . 53
4.2 The range from which the random states were sampled for the local observability analysis. . . . 57

7.1 Parameter bounds used in preliminary results . . . 79
7.2 Largest absolute parameter correlation values (repeated from Table 7.3) . . . 84
7.3 Parameter correlations from preliminary results . . . 89

A.1 AHRS output, specific force, acceleration symbol notation definitions . . . 98

E.1 List of all gathered data sets, showing whether they were a wings-level or accelerated stall, and wheter they were used as training (T) or validation (V) data. . . . 116

F.1 List of the properties and metrics that were used in the analysis if flight test maneuver effectiveness. . . . 124

Nomenclature

List of Roman Symbols

Symbol	Description	Unit
a_1	Shape parameter of flow separation point X	-
A	Specific force output signal of AHRS (includes a correction on z_b-axis)	ms^{-2}
b	Wing span	m
C	Force or moment coefficient (see subscripts)	-
$\bar{c}$	Mean aerodynamic chord	m
g_0	Standard gravitational acceleration (9.0865)	ms^{-2}
h	Altitude	m
I	Rotational moment of inertia	kgm^2
J	Cost function value	-
K	UKF Kalman gain	-
M	Mach number	-
m	Mass	kg
p	Roll rate	$rads^{-1}$
P	UKF state auto-covariance matrix	-
q	Pitch rate	$rads^{-1}$
Q	UKF process noise matrix	-
r	Yaw rate	$rads^{-1}$
R	UKF measurement noise matrix	-
S	Wing surface area	m^2
S	Periodogram, power spectrum estimate	-
t	Time	s
u	Wind velocity in x_b	ms^{-1}
$\mathbf{u}$	UKF input vector	-
v	Wind velocity in y_b	ms^{-1}
$\mathbf{v}$	UKF process noise variables vector	-
V_{TAS}	True airspeed	ms^{-1}
W	UKF weights or wind velocity	- or ms^{-1}
w	Wind velocity in z_b or random variable	ms^{-1} or -
$\mathbf{w}$	UKF measurement noise variables vector	-
X	Normalized flow separation point position	-
x	x-position in current axis system	m
$\mathbf{x}$	UKF state vector	-
y	y-position in current axis system	m
$\mathbf{y}$	UKF measurement vector	-
z	z-position in current axis system	m

List of Greek Symbols

Symbol	Description	Unit
α	angle of attack	rad
α^*	Angle of attack for which $X = 0.5$	rad
α_{crit}	critical angle of attack	rad
β	Angle of sideslip	rad
$\delta_a, \delta_e, \delta_r$	Aileron, elevator, and rudder deflections	rad
λ	Bias term	-
ϕ	Aircraft roll angle	rad
θ	Aircraft pitch angle	rad
ψ	Aircraft yaw angle	rad
τ	Time constant	s
τ_1	Lag time constant of flow separation point X	s
τ_2	Hysteresis time constant of flow separation point X	s
$\mathcal{X}$	UKF set of sigma points	-
$\mathcal{Y}$	UKF transformed set of sigma points	-
ω	Aircraft rotation vector or frequency	rads^{-1} or Hz

List of Subscripts

Subscript	Meaning
0	Static term
b	Body reference frame
D	Drag force
E	Earth-fixed reference frame
k	Time sample
L	Lift force
l	Roll moment
L, R	Left and right
m	Pitch moment
N	Normal force
n	Yaw moment
osc	Oscillatory
si	Sidewash
ss	Steady-state
T	Tangential force
up	Upwash
v	Air data boom vane
xx, yy, zz, xz	Aircraft body planes
Y	Lateral force

List of Superscripts

Superscript	Meaning
$\cdot$	Time derivative
$\hat{}$	Estimate
$\tilde{}$	Dimensionless variant of variable
a	Augmented state with process and measurement noise variables
$\top$	Matrix transpose

List of Abbreviations

Abbreviation	Meaning
AHRS	Attitude and heading reference system
AvSP	Aviation safety programme
BAR	Bihrle applied research
CAST	Commercial aviation safety team
CFD	Computational fluid dynamics
CFIT	Controlled flight into terrain
CRLB	Cramèr-Rao lower bound
DADC	Digital air data computer
DASMAT	Delft University aircraft simulation model and analysis tool
DUT	Delft University of Technology
EU	European Union
FAA	Federal Aviation Administration
FL	Flight level
FSTD	Flight simulation training device
FTIS	Flight test information system
GPS	Global positioning system
ICATEE	International Committee for Aviation Training in Extended Envelopes
JAR	Joint aviation requirements
LOC-I	Loss off control in-flight
MLE	Maximum likelihood estimate
MSE	Mean squared error
NASA	National Aeronautics and Space Administration
NLR	Netherlands Aerospace Laboratory
ODE	Ordinary differential equation
QTG	Qualification test guide
RE	Runway excursion
SRS	SIMONA research simulor
SUPRA	Simulation of upset recovery in aviation
UKF	Unscented Kalman filter
US	United States
VAF	Variance accounted for

I

Scientific Paper

Stall Model Identification of a Cessna Citation II from Flight Test Data Using Orthogonal Model Structure Selection

Joost van Ingen*

Delft University of Technology, Delft, 2629HS, the Netherlands

From 2019 onwards, airline pilots will be required to follow stall training in simulators. A major open research question is which level of model fidelity is required for effective training. As part of an effort to answer this question, a stall model of a Cessna Citation II aircraft is developed from specifically-gathered flight test data. The model is based on Kirchoff's theory of flow separation. During identification, the nonlinear and linear parameters of the model are estimated in separate steps. This distinction enables the application of a semi-objective model structure selection method using multivariate orthogonal functions. It is shown that stall-related effects should be included in the model equations for lift, drag, and pitch moment. The model parameters are accurately estimated, and model output is validated around a flight condition of 5,500 m altitude. The developed methodology is concluded to be well-suited for stall model identification of small business jets.

Nomenclature

Roman

A	Matrix of regression variables
A_*	Specific force in $*$-direction [m/s^2]
$\mathbf{a}$	Regression variable vector
a_1	X-parameter for shape [-]
b	Aircraft span [m]
C_*	Force/moment coefficient [-]
$\bar{c}$	Average chord length [m]
I_*	Angular moment of inertia around $*$-axis [kgm^2]
J	Cost function value
M	Mach number [-]
m	Mass [kg]
N	Amount of time samples
n	Amount of terms in a model structure
p	Roll rate [rad/s]
q	Pitch rate [rad/s]
R^2	Coefficient of determination
r	Yaw rate [rad/s]
S	Wing surface area [m^2]
$\mathbf{p}$	Orthogonalized regression variable vector
U	Theil statistic

Greek

α	Angle of attack [rad]
α_*	X-parameter for scheduling [rad]
β	Angle of sideslip [rad]
$\gamma_{k,j}$	Gram-Schmidt scaling parameter
ϵ	Vector of remnant
δ_a	Aileron deflection [rad]
δ_e	Elevator deflection [rad]
δ_r	Rudder deflection [rad]
θ	Pitch angle [rad] *or* parameter vector
$\hat{\theta}$	Optimal estimate of parameter vector
ρ	Correlation
σ	Standard deviation
τ_1	X-parameter for time delay [s]
τ_2	X-parameter for hysteresis [s]
ϕ	Roll angle [rad] *or* orthogonal parameter vector
$\hat{\phi}$	Optimal estimate of orthogonal parameter vector
ψ	Heading angle [rad]

*MSc student, supervised by: dr. ir. D.M. Pool, dr. ir. C.C. de Visser, dr. ir. M.M. van Paassen, and prof. dr. ir. M. Mulder; all from the Faculty of Aerospace Engineering, Control and Simulation Division. Email: joostingen@gmail.com

Roman (continued)

V_{TAS}	True airspeed [m/s]
x	Regression variables
x_E, y_E, z_E	Cartesian position in F_E [m]
$\dot{x}_E, \dot{y}_E, \dot{z}_E$	Velocity components in F_E [m/s]
X	Flow separation point variable [-]
$\mathbf{y}$	Measurement vector
$\hat{\mathbf{y}}$	Model output vector

Subscripts

D	Drag
L	Lift
l	Roll moment
m	Pitch moment
n	Yaw moment
T	Thrust force
Y	Lateral force

I. Introduction

Loss of control in-flight currently is the largest category of fatal civil and general aviation accidents,[1] and aerodynamic stall is an important contributor.[2] Better training of pilots in recognizing, preventing, and recovering of stalls is seen as an important step for increasing safety.[3] From March 2019 onwards, such training will become mandatory for all airline pilots.[4] Due to cost and safety considerations, this stall training will take place in simulators. As a result, there is an increased demand for stall models of civil aviation aircraft.

Currently, aerodynamic stall models are difficult to obtain. Stalls are characterized as highly nonlinear, unsteady, configuration-dependent, and fundamentally unpredictable.[5] Current stall modeling methods generally fall in either of two categories. The first category is based on modeling methods that were originally developed for fighter jets. Starting in the 1980s, these were also applied to civil aviation aircraft. NASA[6,7] and the EU[8,9] both have had dedicated research programs based around this "fighter" method. This method relies on extensive wind tunnel testing, is complex and expensive to implement, but can be used for modeling even extreme maneuvers such as spins. The second category is based on Kirchoff's theory of flow separation.[10] It involves modeling of an internal flow separation point variable X, which in turn affects lift and possibly other forces or moments. The potential range of application of "Kirchoff's method" is smaller – spins cannot be modeled – but it is simpler to implement. Research has shown that the flow separation point parameters can be identified from flight test data.[11,12,13] Both these approaches have resulted in stall models of varying fidelity. Recently, novel modeling methods have appeared, such as those based on CFD[14] or representative methods based on aircraft geometry and/or configuration.[15,16] Regardless of modeling method, a major unanswered question is what level of fidelity is actually required for effective pilot stall training. A pilot-in-the-loop evaluation of several stall models of varying fidelity found no differences in subjective ratings from a group of experienced pilots.[17] The Faculty of Aerospace Engineering at the TU Delft is uniquely positioned to contribute to this question; it has access to both a research simulator, as well as a test aircraft.

However, a full model of the stall dynamics of this test aircraft – a Cessna Citation II – does not exist yet. Previous research[18] has resulted in a partial stall model based on Kirchoff's method, which includes only longitudinal dynamics. Because flight data of only quasi-static stall maneuvers were available, it was shown to be difficult to identify dynamic stall effects. Moreover, a thorough substantiation of which terms to include in the model remained to be done, specifically considering control surface degradation, which was not yet included in the model.

Therefore, the existing Citation II stall model has been extended. Dedicated flight tests are done to gather data that contains sufficient dynamic excitation as well as control surface perturbations during stall maneuvers. An air data boom is installed that measures side slip angle, enabling the identification of lateral model terms. System identification is aided by objective model structure selection using multivariate orthogonal functions modeling. Finally, the nonlinear parameter estimation problem is approached efficiently, by optimizing the flow separation point parameters separately from the rest of the model.

The structure of this paper is as follows. Section II describes the flight test vehicle and the maneuvers that were flown to gather the data. Section III presents the stall modeling methodology. The parameter estimation and model structure selection techniques that were used are discussed separately. Results are presented in Section IV. Section V follows with a discussion of the work, and Section VI presents the conclusions.

II. Flight Test Data

A. Flight Test Vehicle

Flight tests were performed in a Cessna Citation II (callsign PH-LAB). This aircraft is jointly owned by the Faculty of Aerospace Engineering of Delft University of Technology, and the Netherlands Aerospace Center (NLR). The aircraft is equipped with an advanced flight test instrumentation system (FTIS), which connects and logs data from installed sensors. Schematic views of the aircraft can be found in Figure 1. Tables 1 and 2 describe general mass and geometric properties, and list the flight test equipment relevant to this research. Critical to this research is the air data boom, which is mounted on the nose of the aircraft, and is illustrated on the left-hand side of Figure 1. The boom enables accurate measurements of the angle of attack and angle of sideslip.[19]

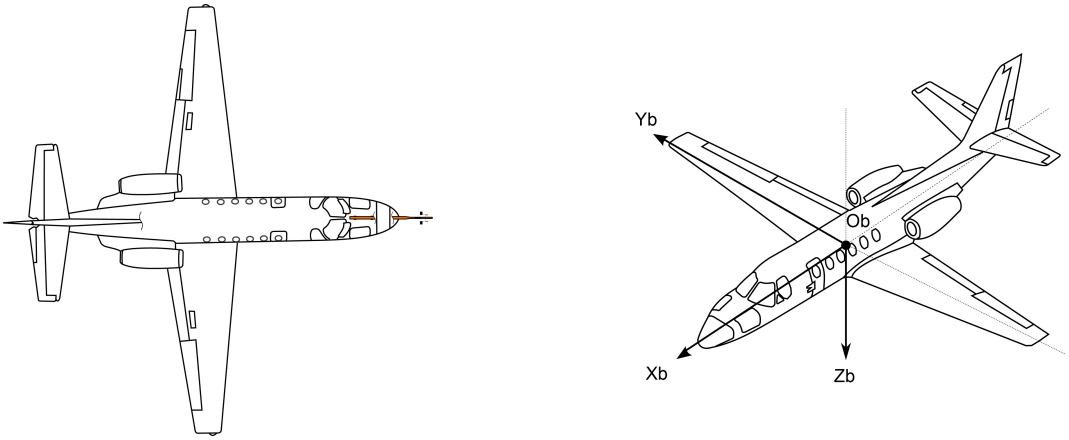

Figure 1. Schematic views of the PH-LAB, including the body-fixed reference frame axes definition. The left schematic also illustrates the installed air data boom.

Table 1. PH-LAB dry mass & dimensions.

Dimensions	
b	15.9 m
$\bar{c}$	2.09 m
S	30.0 m^2
Mass and inertia	
m	4,157 kg
I_{xx}	12,392 kgm^2
I_{yy}	31,501 kgm^2
I_{zz}	41,908 kgm^2
I_{xz}	2,252.2 kgm^2

Table 2. List of flight test equipment installed in the Cessna Citation II aircraft PH-LAB, including the variables they measure, which are relevant to this research.

Name	**Explanation**	**Measures**	**Variables**	**Units**
GPS	Global positioning system	Position in F_E	x_E, y_E, z_E	m
		Velocity in F_E	$\dot{x}_E, \dot{y}_E, \dot{z}_E$	m/s
DADC	Digital airdata computer	Total airspeed	V_{TAS}	m/s
AHRS	Attitude & heading reference system	Aircraft attitude	ϕ, θ, ψ	rad
		Body rotation rates	p, q, r	rad/s
		Body specific forces	A_x, A_y, A_z	m/s^2
Synchro	Angle measurements	Contr. surf. defl.	$\delta_a, \delta_e, \delta_r$	rad
Boom	Air data boom	Air incidence ang.	α, β	rad

B. Flight Test Maneuvers

Two flights were conducted in order to gather the stall data required for this research. Special maneuvers were flown for the specific goal of stall model identification. In total, 34 stall maneuvers were recorded, all in clean configuration (i.e., no flaps, and gear retracted). Each stall maneuver was trimmed to include stall entry, stall itself, as well as recovery phases.

Figure 2 visualizes several key characteristics of the data sets. Figure 2a shows that the majority of data sets were gathered around 5,500 m flight altitude. As a result, this is the only condition for which the model output could be validated. Figure 2b shows that angles of attack up to 22 degrees were achieved, where the Citation would stall around 12 degrees. Figure 3 shows the gathered flight data in a V-n diagram.

Two types of stall were flown: **wings-level symmetric** and **accelerated** stalls. This distinction was made in an attempt to distinguish $\dot{\alpha}$-related effects from q-related ones. The difference between these maneuver types can seen in the ϕ-plot in Figure 2c. The former was entered by achieving trimmed, level flight, and then reducing airspeed by 1 kts/s by closing the throttle. During the stall, effort was put into keeping the wings-level condition with aileron inputs. The accelerated stall entry was similar, but started from a coordinated turn of either about 30 or 45 degrees bank (approximately 1.1 or 1.3 g). In the stall, the pilots aimed to keep the same bank angle and turn rate. Maneuvers 1-15, 33, and 34 are wings-level, the rest are accelerated stalls. All accelerated stalls were right-hand turns, except maneuver 29, which was a left-hand turn.

A piloting technique was developed in collaboration with the test pilots, based on one described by Morelli.[20] The main principle is that pilot inputs are composed of two components: one part to keep the aircraft at or close to the desired flight condition, and a second component with (semi-)random disturbances to excite the aircraft. Figures 2d, e, and f visualize the use of control surfaces during each maneuver. In Figure 2f it can be seen that large rudder inputs were only applied during maneuvers 3-6 and 27-34. This is because rudder inputs were only applied as "disturbance". The response of the aircraft to rudder excitations during stall was unknown, which is why rudder deflections were carefully increased during the experiments. The end result is that not all data sets contain sufficient rudder excitations for identifying a yaw moment model. The aileron and elevator were used during all maneuvers.

For the conditions that were tested, the aircraft's stall behavior was quite benign and showed a strong self-recovering tendency. Active pilot elevator inputs were required to direct the Citation II back into a stalled condition after the aircraft would recover itself. As a result, some of the stall maneuvers are actually a sequence of short stalls. Examples of this can be seen later on in this thesis, for instance in Figure 27.

C. Data Pre-Processing

Before the model identification, two data pre-processing steps were taken. First, all recorded signals were filtered using a zero-phase low-pass filter using MATLAB's `filtfilt` function. A Butterworth filter of order 4 was used. There were two main disturbance sources: vibrations due to the stall buffet, and amplified noise in signals that are obtained through numerical differentiation (e.g., $\dot{p}$, or $\dot{\alpha}$). The buffet vibrations are vital to a realistic stall model implementation in a simulator, but these are modeled by a separate buffet model,[18] and are not in the scope of this research. The cut-off frequencies for the filtered signals are listed in Table 3. An example of filtering can be seen in Figures 4 and 5, where part of a time history and a power spectral density estimate are shown both before and after low-pass filtering.

After applying the low-pass filter, the second pre-processing step was to apply an optimal state reconstruction using an Unscented Kalman Filter (UKF). This filter was developed and shown to be effective in previous research,[18] and was adjusted to use the α and β signals from the air data boom.

Table 3. Cut-off frequencies used for low-pass filtering measured signals.

Signal(s)	f_c [Hz]
α, β	4.0
$\dot{\alpha}$, $\dot{\beta}$	4.0
δ_a, δ_e, δ_r	4.0
A_x, A_y, A_z	1.5
p, q, r	1.5
$\dot{p}$, $\dot{q}$, $\dot{r}$	4.0

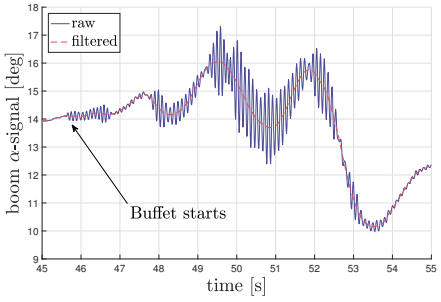

Figure 4. Detail of boom α-signal time history showing oscillatory vibrations due to buffet.

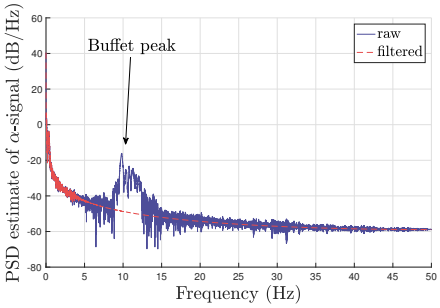

Figure 5. Power spectral density estimate of α-signal before and after low-pass filtering.

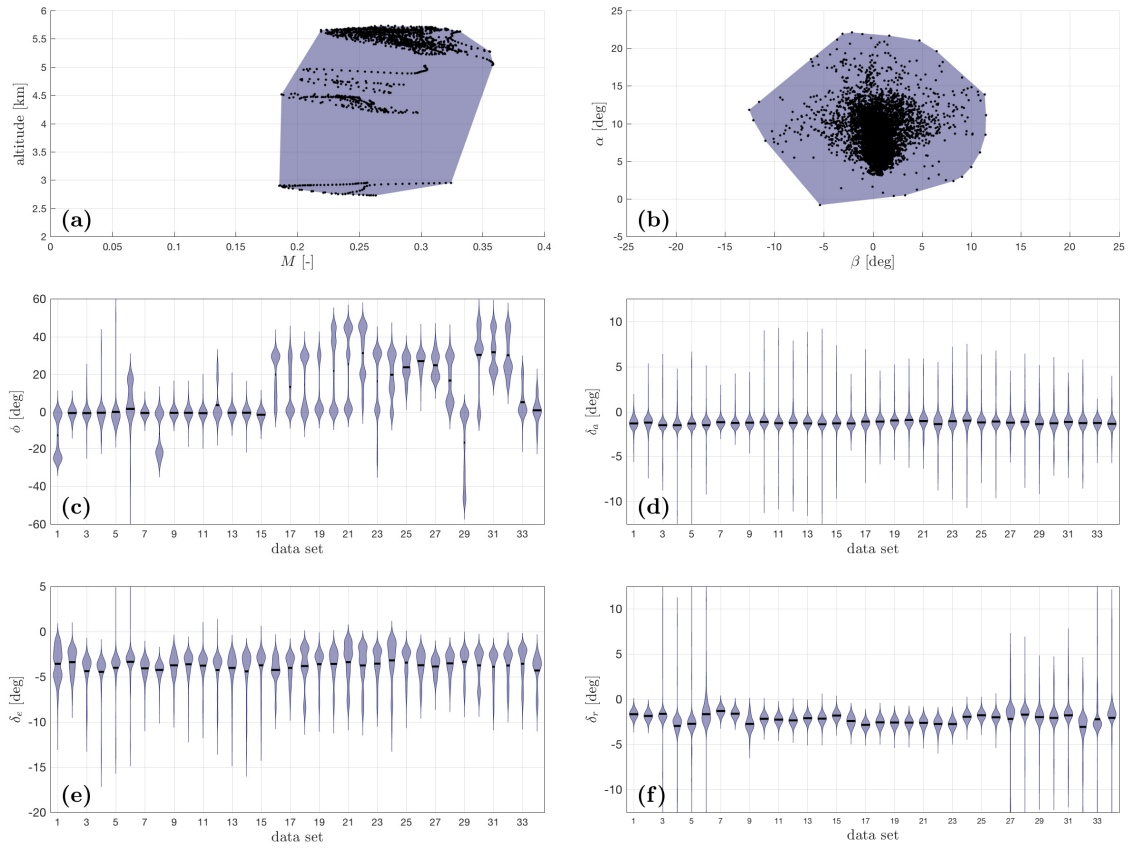

Figure 2. Visualization of several properties of the gathered flight test data. Plots a and b show the Mach-altitude and α-β envelope, respectively. Plots c-f are violin plots, which show approximations of the distribution of the bank angle and control inputs. Black marks are means. The difference between longitudinal and lateral maneuvers can clearly be seen, as well as the fact that the rudder was used very little in maneuvers 7-26.

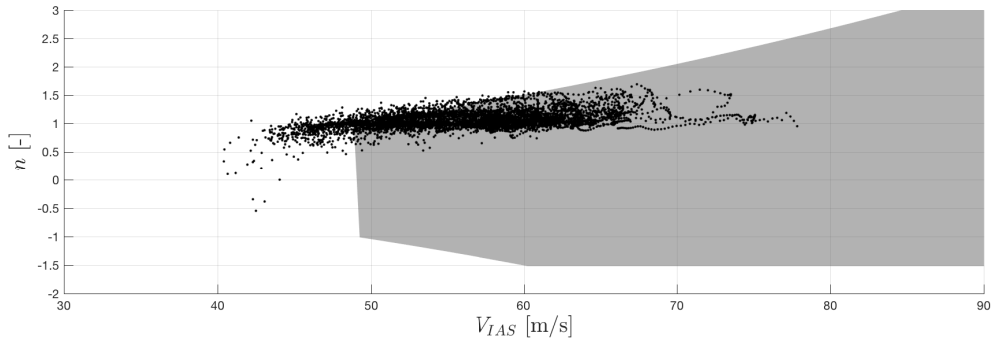

Figure 3. Decimated view of all the time samples in the flight data sets on the maneuvering load factor limit diagram of the Cessna Citation 550 II, defined for a take-off weight of 11,500 lbs. All airspeeds were converted to indicated airspeeds. The grey plot area marks the flight envelope where normal flight maneuvers are possible. It can clearly be seen that part of the recorded flight data fall to the left of this area, which corresponds to stalled flight.

III. Methodology

The stall model consists of six separate models; one for each of the force (C_L, C_D, C_Y) and moment (C_l, C_m, C_n) coefficients. The methodology that was followed for the identification of these models is explained in this section. First, the general modeling principle is explained, which is based on Kirchoff's theory of flow separation. After that, a general overview of the system identification process is given. Finally, the methods used for model structure selection and parameter estimation, which form the core of the novel approach in this research, are presented separately.

A. Kirchoff's Theory of Flow Separation

In the early 1990s, a relatively simple model structure was published that is able to explain the nonlinear, dynamic, and time-dependent phenomena caused by aerodynamic stall.[10] Previous research has shown the validity of this modeling approach for several different aircraft.[12,13] This model is based on the assumption that the effect of stall on airfoil lift can be described by Kirchoffs theory of flow separation, which states that the relation between airfoil lift and the flow separation point X, which represents the fraction of the chord length affected by flow separation, can be modeled by:

$$C_L = C_{L_\alpha} \left(\frac{1 + \sqrt{X}}{2} \right)^2 \alpha \, . \tag{1}$$

The variable X represents the distance along the wing chord where the flow separates, and ranges from 1 (flow is fully attached) to 0 (flow is fully separated). It was shown that the dynamics of X can be adequately modeled by a first-order ordinary differential equation (ODE):

$$\tau_1 \frac{\mathrm{d}X}{\mathrm{d}t} + X = \frac{1}{2} \left(1 - \tanh \left[a_1 \left(\alpha - \tau_2 \dot{\alpha} - \alpha^* \right) \right] \right) \, . \tag{2}$$

Only four parameters are needed for this ODE, and each represents a physical effect of the stall. τ_1 sets the time delay in the dynamics of X, which is caused by inertia in the flow; it takes time before the air flow has reacted to sudden changes in α. τ_2 encodes hysteresis effects on X. The static mapping between X and α is parametrized by a_1, which is a shape parameter that determines the "abruptness" of the stall, and by α^*, which schedules the angle of attack at which the stall occurs. These four parameters will from here on be referred to as X-parameters. Visualizations of the effect of varying these parameters on C_L and X can be found in previous research.[18]

Because of Equation 2, solving for the model parameters is a nonlinear optimization problem, which makes it sensitive to intial conditions, and computationally more demanding to solve. Another challenge is that a direct measurement of X is not available. The solution is to estimate the parameters via another measurement that *is* available, and which is influenced by X. The most obvious candidate for this is C_L, which is directly affected by X as described in Equation 1. A special system identification methodology, detailed in the next section, was used to deal with these challenges.

B. System Identification Methodology

A key idea in this research is to split the parameter estimation problem into two parts. First, the X-parameters are estimated using nonlinear methods. After that, they are assumed fixed and X can be calculated for all data sets. This is followed by model structure selection, and finally the estimation of the remaining parameters using conventional linear methods. These three steps are visualized in Figure 6.

The most important advantage is that X can be regarded as a regressor during model structure selection. This enables quick iterations between selecting a model structure, estimating its parameters, and evaluating the result of any changes. Due to the iterative and interactive nature of a system identification task, this is seen as a highly desirable advantage. Moreover, if this distinction was not made, the semi-objective model structure selection method would have not been possible.

The X-parameters are identified using the measured C_L, as this relation is best documented in literature. An initial assumption on the model structure of C_L needs to be made. The implicit assumption is made that the dependence of the X-parameters on the model structure is mild. When, during the later model structure selection step, a different

model for C_L is found, the X-parameters will be re-estimated, and this process is repeated until it has converged. The next sections describe the steps in Figure 6 in detail.

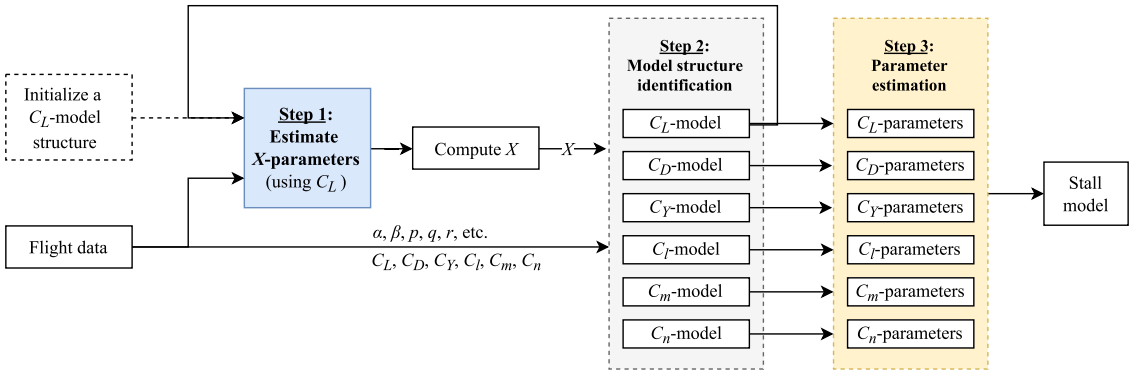

Figure 6. Block diagram of the steps and flow in the system identification approach.

C. Parameter Estimation

As shown in Figure 6, parameter estimation is split into two parts. The linear parameter estimation in step 3 is done using the familiar ordinary least-squares methods, whilst the nonlinear estimation of step 1 is done using a gradient-based solver built into Matlab.

1. Linear Parameter Estimation

Once the model structures of the force and moment coefficient equations are set, the parameter estimation problem is straightforward. For this research, it was chosen to use the model structures in polynomial form, i.e.,

$$\hat{\mathbf{y}} = \theta_1 \mathbf{a}_1 + \theta_2 \mathbf{a}_2 + \ldots + \theta_n \mathbf{a}_n \ , \tag{3}$$

where $\hat{\mathbf{y}}$ is the model output vector, $\mathbf{a}_i$ are the regression variable vectors, and θ_i are parameters. Note that $\mathbf{a}_i$ is allowed to contain non-linear polynomial terms, such as α^2. Equation 3 can be written in matrix notation as:

$$\hat{\mathbf{y}} = A\theta, \quad \text{where} \quad A = [\mathbf{a}_1 \ \mathbf{a}_2 \ \ldots \ \mathbf{a}_n] \, , \quad \text{and } \theta = [\theta_1 \ \theta_2 \ \ldots \ \theta_n]^\intercal \, . \tag{4}$$

To minimize the error between measurement and model output $\epsilon = \mathbf{y} - \hat{\mathbf{y}}$, ordinary least squares (OLS) is used. This leads to the well-known closed-form solution for the parameter estimate $\hat{\theta}$:

$$\hat{\theta} = (A^\intercal A)^{-1} A^\intercal \mathbf{y}. \tag{5}$$

This procedure is the same for all aerodynamic model equations.

2. Nonlinear X-Parameter Estimation

A second parameter estimation method was used for estimating the X-parameters. An optimization problem was created with the goal of minimizing the mean squared error between the measured lift coefficient C_L, and the model output $\hat{C}_L(\theta, x)$. Both are defined as $N \times 1$ vectors, and x indicates the flight data.

$$\hat{\theta} = \arg\min_{\theta} J(\theta, x) \quad \text{with} \quad J(\theta, x) = \tfrac{1}{N} \left(C_L - \hat{C}_L(\theta, x) \right)^\intercal \left(C_L - \hat{C}_L(\theta, x) \right) \ . \tag{6}$$

This method requires a choice for the model structure of $\hat{C}_L$. During the **initial step only** of the system identification procedure, the following model was used:

$$\hat{C}_L(\theta, x) = C_{L_0} + C_{L_\alpha} \left(\frac{1+\sqrt{X}}{2} \right)^2 \alpha + C_{L_q} \frac{q\bar{c}}{V} \,, \tag{7}$$

with X as in Equation 2. Upper and lower bounds were set on all parameters as constraints. The initial conditions were randomly and uniformly sampled from the parameter space constrained by these boundaries. The active set algorithm, as available from Matlab's `fmincon` function was used to solve for the X-parameters. Multiple runs were done on each data set. Since the cost function surface tended to be flat near the solution, the best few percent of runs were averaged to obtain a point estimate for each data set. This final step reduced the variance of the results. To deal with the numerical difficulties of the parameter sensitivity of the solution of an ODE,[21] at each iteration, the gradient of the cost function with respect to the parameters was explicitly computed using the method described in Appendix A.

For the initial step, which used the model structure as shown in Equation 7, the upper and lower bounds are presented in Appendix B. For the final optimization results, the boundaries are presented in Table 4.

Regarding the choice for the initial model structure: the only hard requirement is that some dependency on X is included, otherwise estimating the X-parameters is impossible. The Kirchoff term found in literature was selected, as its effectiveness has been shown before. The q-term was added because it is commonly found in models for lift. On subsequent iterations, the model structure that followed from the model structure selection step was used instead, so the initial model structure of $\hat{C}_L$ was not seen as critical.

D. Model Structure Selection Method

Before estimating the model parameters, a model structure needs to be selected. In other words, this means identifying which regressors are required for capturing the dynamics in the measured data. Note that it is during this step in the system identification process that choices are made *if* e.g., changes in control surface effectiveness or dynamic effects need to be included, and if so, *how* this is done.

A good model structure must be effective at explaining the patterns in the data, and be parsimonious. The model structure has a large influence on the trade-off between bias (model cannot represent data) and variance (model does not generalize well to previously unseen data).[22] In general, evaluating the usefulness of separate model terms is hard, since these influence each other i.e., adding an extra term to some model structure is very likely to change the estimated parameter values of the other terms. Further complexities are caused by the fact that the flight data will inevitably contain errors, have interdependencies/correlations, and is limited in quantity.

An multivariate orthogonal function modeling algorithm was developed as a tool to deal with these challenges. Its block diagram is presented in Figure 7, and will be explained in the next sections. Section D-3 will explain the way it is used and how its results were interpreted.

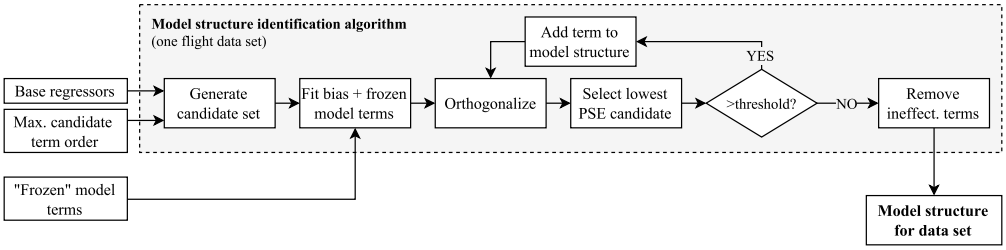

Figure 7. Block diagram visualization of the multivariate orthogonal function modeling algorithm used for model structure selection. During step 2 in Figure 6, this algorithm is run for each model (C_L, C_D, ...) for each training data set.

1. *Multivariate Orthogonal Function Modeling Algorithm*

An algorithm for creating and selecting model terms that lead to a good model was developed based on the multivariate orthogonal function (MOF) modeling method described by Morelli.[20] To avoid correlations of model terms,

all candidate model terms are orthogonalized. The most important consequence of this is that it becomes possible to compute the effect of adding terms independently of each other. This makes it an objective and (semi-)automated procedure for model structure selection.

The algorithm's basic principle is that it iteratively "builds up" model structures from scratch, using a pool of orthogonalized candidate regressor terms. This iterates until a cost function is minimized, which penalizes both any errors between model output and the dependent variable, as well as model complexity. In the following, orthogonalized regression variables will be denoted by $\mathbf{p}_i$ to distinguish them from the regular regression variables $\mathbf{a}_i$. The algorithm starts by generating a set of candidate model terms, based on a set of base regressors and a maximum term order. This will be discussed in the next section. After that, the first step is to include a bias term:

$$\mathbf{a}_1 = \mathbf{p}_1 = \mathbf{1} \,. \tag{8}$$

Then at each iteration, a Gram-Schmidt orthogonalization procedure is used for making all remaining candidate model terms orthogonal to the terms that are already in the selection.

$$\mathbf{p}_j = \mathbf{a}_j - \sum_{k=1}^{j-1} \gamma_{k,j} \mathbf{p}_k \,, \quad j = 2, 3, \ldots, n \,, \qquad \text{where:} \qquad \gamma_{k,j} = \frac{\mathbf{p}_k^\intercal \mathbf{a}_j}{\mathbf{p}_k^\intercal \mathbf{p}_k} \,. \tag{9}$$

Note that the orthogonal regressors are linear combinations of the original regressors. Once orthogonalized, all candidates are evaluated based on the effect that they would have on the predicted square error (PSE). This cost metric consists of two parts: a fit error (equal to the mean squared error), and a penalty term for complexity:

$$\text{PSE} = \frac{(\mathbf{y} - \hat{\mathbf{y}})^\intercal (\mathbf{y} - \hat{\mathbf{y}})}{N} + \sigma_y^2 \frac{n}{N} \,. \tag{10}$$

N is the number of data points, n is the number of terms currently used in the model, and σ_y^2 is the variance of the modeled signal $\mathbf{y}$ (e.g., C_m, C_Y, etc.), which is used as a scaling term. Because of the orthogonality, the change in PSE which would result from adding candidate j can be computed independently for each candidate as:

$$\Delta\text{PSE}_j = -\frac{\left(\mathbf{p}_j^\intercal \mathbf{y}\right)^2}{\mathbf{p}_j^\intercal \mathbf{p}_j} + \sigma_y^2 \frac{1}{N} \,. \tag{11}$$

The candidate leading to the greatest reduction in cost is selected and added to the model. After that, the procedure is repeated: all candidates are again made orthogonal to the selected terms, the best one is selected, etc. This goes until $\Delta\text{PSE}_j \geq 0$ for all j, which means that the added penalty of increasing the model complexity is no longer be offset by the decrease in mean square error.

At this point, a matrix $P = [\mathbf{p}_1 \, \mathbf{p}_2 \, \ldots \, \mathbf{p}_n]$ has been constructed, which can be used to find the vector of maximum-likelihood parameters $\hat{\phi}$ connected to the orthogonalized regressors. For this, the OLS procedure that was explained can be used in exactly the same way. The result $\hat{\mathbf{y}} = P\hat{\phi}$ can then be transformed back to the "normal" non-orthogonalized regressors and associated parameters $\hat{\mathbf{y}} = A\hat{\theta}$. When the $\gamma_{j,k}$ are collected in a matrix:

$$\Gamma = \begin{bmatrix} 1 & \gamma_{1,2} & \gamma_{1,3} & \cdots & \gamma_{1,n} \\ 0 & 1 & \gamma_{2,3} & \cdots & \gamma_{2,n} \\ 0 & 0 & 1 & \cdots & \gamma_{3,n} \\ \vdots & \vdots & \vdots & \ddots & \vdots \\ 0 & 0 & 0 & \cdots & 1 \end{bmatrix} , \tag{12}$$

then $A = P\Gamma$, and thus the optimal parameter vector $\hat{\phi}$ can easily be transformed back to the original regressor definition by applying the following substitution:

$$\hat{\mathbf{y}} = P\hat{\phi} = PI\hat{\phi} = P(\Gamma\Gamma^{-1})\hat{\phi} = A\Gamma^{-1}\hat{\phi} \,, \quad \text{hence:} \quad \hat{\theta} = \Gamma^{-1}\hat{\phi} \,. \tag{13}$$

Once A and $\hat{\theta}$ are obtained, the algorithm checks all the terms that have been selected for their contribution to the final model output. It does so by computing the root mean square RMS $= \frac{1}{N}\sqrt{\hat{\mathbf{y}}^\intercal\hat{\mathbf{y}}}$ of the model output $\hat{\mathbf{y}}$, and comparing that with the RMS of the model output that would occur if that term would be simply ignored, without making any other changes to the parameters or regressors. If the change in RMS is lower than a threshold, for which 0.5% was used, the term would be regarded as ineffective and removed.

The output of the MOF modeling algorithm is a selection of regressor terms A for the specific flight data set that was used as input. As a final step, the results of all data sets need to be generalized. This is done based on a simple count of how many times each model term appears in the output for each flight data set. If a term is selected in 50% of data sets or more, it generally is concluded to be useful, and included in the general model structure. This threshold was used since it was found to work well in the identification of the regular flight envelope model of the Citation II.[23] However, the results were always interpreted alongside other analyses such as the effect on MSE, consistency in the estimate of the associated parameter, or correlations between estimated parameters.

2. Candidate Model Terms

The described algorithm iteratively searches within a set of candidate terms for the best contribution to a model. Any decision that influences the terms that are included in this set will have a strong influence on the final results. If the pool does not contain any useful terms, the quality of the model will never be good. Or, if many similar terms are included, it will be impossible to choose between them since the results will be inconsistent across data sets. This section explains how the candidate model terms are generated, and explains several design choices that were made.

The most straightforward approach for creating candidates is to simply use the common regressors such as α, δ_e, or p. In this research, the thrust force coefficient C_T and Mach number M were also included. Appendix C explains why including C_T is important in the current application. This approach is extended by also including X and several mathematical transformations of X as regressors. These will play a crucial role in including the effects of aerodynamic stall on the aircraft dynamics. Again, note that this is only possible because the parameter estimation problem is split into two separate parts, which enables the assumption that the X-parameters can be considered constants during model structure selection. The following terms were used as "base regressors":

$$\begin{gathered}\mathbf{1},\ \alpha,\ \dot{\alpha},\ \beta,\ \dot{\beta},\ p,\ q,\ r,\ \delta_a,\ \delta_e,\ \delta_r,\ C_T,\ M,\\ X,\ (1-X),\ \left(\tfrac{1+\sqrt{X}}{2}\right)^2,\ \max(0.5, X)\ .\end{gathered}$$

These are named "base regressors" since they form the basis for the automatic generation of any potential higher-order candidate regressors. A routine was implemented that **automatically generates** from these **all unique product-wise combinations** up to and including **a user-defined maximum order** n.

Four base regressors that contain X were included, and it is important to consider why these were selected. In this, it is relevant to re-state that for attached flow $X = 1$, and for fully separated flow $X = 0$. The regressor X itself can be used for explaining an effect that reduces or disappears during stall. $(1 - X)$ does the opposite, it only takes effect during flow separation. The third term is part of the term appearing in Kirchoff's classical theory of flow separation, which would be created by taking the product of this term with α. Finally, the term $\max(0.5, X)$ was used to take into account some effects that change during stall, but do not completely disappear for fully separated flow.

Obviously, many more potential base regressors are possible. However, it was found that it is important to avoid similar candidate regressors i.e., those that have strong correlations with each other. If two regressors are correlated, they explain the same patterns in the data. The result of this is that it is not clear which regressor to select, which makes the results ambiguous. For example, consider a feature that is present in 90% of the data. Then, say there are three regressors that are equally suitable for explaining this feature. Each will then, on average, be selected on 30% of the data sets, which is below the 50% threshold. When viewing these results, the user should recognize that these terms are the same, or the result would not be noticed.

In practice it was found that by setting the maximum model order higher than $n = 2$, the results became much less useful because this led to correlated terms being included in the candidate pool. Next to that, the amount of terms increases very quickly for increasing model order, which complicates the interpretation of the results by a user. As a result, the algorithm was used in quite a specific way, which will be explained in the next section.

3. *Practical Use of Algorithm*

Ideally, the model structure selection algorithm converges to the same model structure for all data sets. It was found that this was not the case. When setting the maximum order of candidate terms higher than two, models full of higher-order model terms were the result. This conflicted with the goal of selecting a parsimonious model structure.

The suspected reason for why this occurs is that the flight data contains nonlinear effects that cannot easily be modeled, as well as significant random disturbances. While simpler regressor terms might be able to explain general trends just fine, it is likely that there exists a higher-order term that does the job better on that specific data set alone. The disturbances differ for each data set. Hence if the described algorithm is given the choice, it will select different higher-order terms for each data set. This makes it hard to identify model terms that generalize well across data sets.

The solution that was implemented was to change the way in which the algorithm was used. This is visualized in Figure 8. The algorithm is run for both $n = 1$ and $n = 2$ separately. The results are then interpreted manually to make conclusions about useful model terms. In most cases, useful new model terms are only found for $n = 1$, but there are two exceptions (C_L and C_m) that will be discussed in the results. The usefulness of terms is judged by the effect on the total model fit quality (MSE and R^2) on the validation data sets.

Any useful terms that are found are "frozen" into the model structure such that they will always be included during future iterations. Iterations are run until no more new good model terms are found. In all cases, only 1 or 2 iterations were needed. The resulting model structure is passed on to the parameter estimation step of the system identification process.

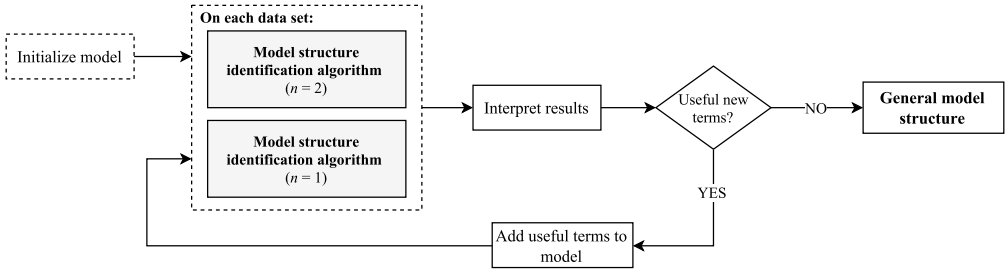

Figure 8. Flow chart of the practical way that the model structure selection algorithm was used. Usefulness of model terms is judged by the effect on MSE and R^2 on the validation data sets.

IV. Results

To identify the aerodynamic model though the proposed methodology, 34 flight data sets were available. It was chosen to split this data into 27 training and 7 validation sets (roughly a 80-20 split). Sets 5, 7, 12, 16, 22, 23, and 25 were used for validation. The split was made randomly, but a check was done that both training and validation sets contained wings-level as well as accelerated stalls. First, the final model structure that was obtained from the model structure selection method described in previous section will be presented. Next, the results of the nonlinear X-parameter optimization are presented. Third, the parameter estimates for the aerodynamic model equations are shown. The final subsection gives the results of model validation, which showcases the current quality of the stall model.

A. Stall Model Structure

The final stall model structure, which resulted from multiple iterations of the process described in Figure 6 is given in Equation 14. The model for each of the aerodynamic model equations will be discussed separately.

$$
\begin{aligned}
\hat{C}_L &= C_{L_0} + C_{L_\alpha}\left(\tfrac{1+\sqrt{X}}{2}\right)^2 \alpha + C_{L_{\alpha^2}}(\alpha - 6^\circ)_+^2 \\
\hat{C}_D &= C_{D_0} + C_{D_\alpha}\alpha + C_{D_{\delta_e}}\delta_e + C_{D_X}(1-X) + C_{D_{C_T}}C_T \\
\hat{C}_Y &= C_{Y_0} + C_{Y_\beta}\beta + C_{Y_p}\tfrac{pb}{2V} + C_{Y_r}\tfrac{rb}{2V} + C_{Y_{\delta_a}}\delta_a \\
\hat{C}_l &= C_{l_0} + C_{l_\beta}\beta + C_{l_p}\tfrac{pb}{2V} + C_{l_r}\tfrac{rb}{2V} + C_{l_{\delta_a}}\delta_a \\
\hat{C}_m &= C_{m_0} + C_{m_\alpha}\alpha + C_{m_{X\delta_e}}\max(\tfrac{1}{2}, X)\delta_e + C_{m_{C_T}}C_T \\
\hat{C}_n &= C_{n_0} + C_{n_\beta}\beta + C_{n_r}\tfrac{rb}{2V} + C_{n_{\delta_r}}\delta_r
\end{aligned}
\tag{14}
$$

1. C_L-model

The obtained C_L-model contains the classical Kirchoff term, and a spline term using the angle of attack squared, $(\alpha - 6^\circ)_+^2$, which will be discussed later. The model structure selection algorithm was run as explained in Figure 8. The results of the first iteration are shown in Figure 9a. The grey bar for the bias term indicates that it was frozen into the model; it was not left up to the algorithm itself to select it. Three terms were found to be useful (i.e., occuring in more than 50% of dat sets): α, $((1+\sqrt{X})/2)^2$, and the combination of the two, the Kirchoff term: $((1+\sqrt{X})/2)^2\alpha$. It was decided to include the latter, since it resulted in the largest improvement in model validation fit quality.

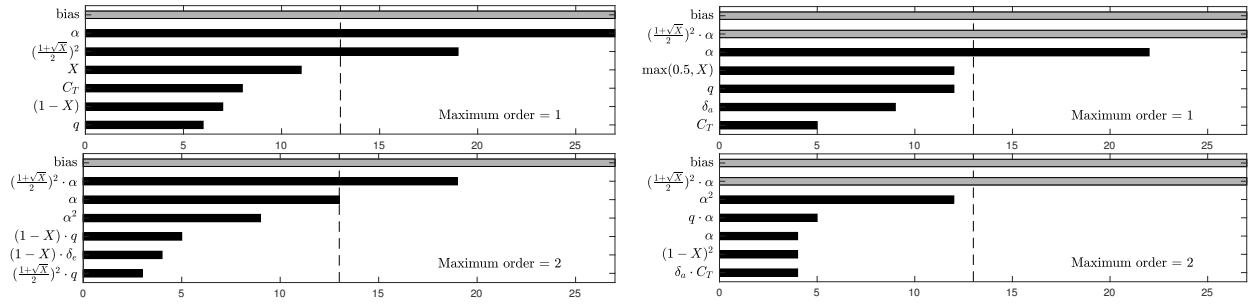

(a) First iteration **(b) Second iteration**

Figure 9. Results of model structure selection algorithm for C_L displaying the count of how many times a model structure is selected. Dashed bar marks 50% of training data sets. Grey bars indicate that a term was forced to the model structure manually.

Next, the algorithm was re-run with the Kirchoff term frozen in the model structure. The results of this second iteration are in Figure 9b, and they indicate that another dependency on the angle of attack is a potentially good term: either as α or α^2. This was surprising, as initially it was expected that all dependency on the angle of attack would be modeled by the Kirchoff term. However, after experimenting with several variations of α-related terms, the term $(\alpha - 6^\circ)_+^2$ was added to the model. This notation indicates a univariate spline in α with zero-order continuity:

$$
(\alpha - 6^\circ)_+^2 = \begin{cases} (\alpha - 6^\circ)^2 & \text{when} \quad \alpha \geq 6^\circ \\ 0 & \text{when} \quad \alpha < 6^\circ \end{cases} . \tag{15}
$$

In understanding why this extra term is useful to have in addition to the Kirchoff term, consider what happens when the aircraft enters a deep stall. Kirchoff's theory of flow separation predicts the lift due to α will decrease by a factor of 0.25 when X goes to zero. However, this reduction is too strong for our data, the measured reduction in lift is less. Discrepancies such as these make sense: Kirchoff's theory was derived for airfoils, whereas the flight data is

of a full aircraft in three-dimensional flow. The term $(\alpha - 6°)_+^2$ contributes a positive effect to the aircraft lift at high angles of attack, even when X goes to zero. It thus mitigates part of the lift reduction due to stall. The beneficial effect on the C_L-model is visualized in Figure 10, where during the deepest part of the stall ($t = 40$-50 s), the spline corrects part of the lift reduction modeled by the Kirchoff term.

Although the difference in model validation fit was modest (difference is <1% on MSE), it was decided to use the spline term instead of simply α^2. There were two reasons for this. First, the spline term's effects are limited to higher angles of attack ($\alpha > 6°$) which reduces the correlation with the Kirchoff term. This led to lower variance in the parameter estimates. Secondly, if α^2 was used, this term would contribute positive lift for negative angle of attack, which can occur during a stall recovery maneuver, which is clearly unphysical. The spline term prevents this. The threshold of 6° resulted in the best fit, and was found using trial and error.

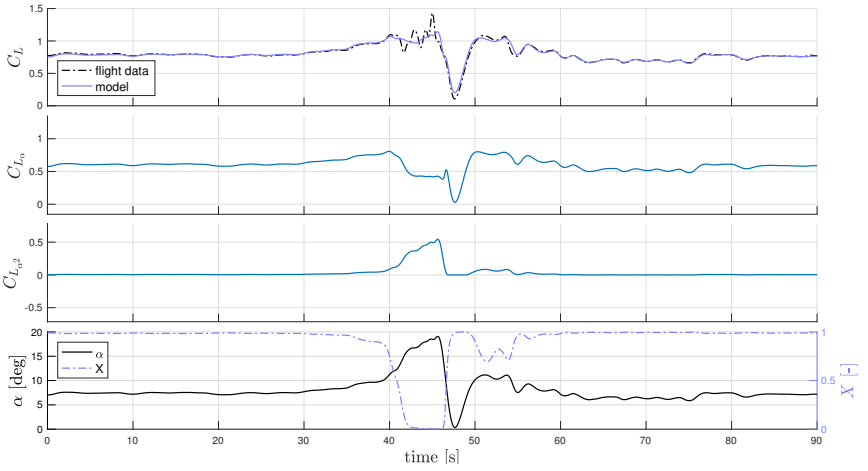

Figure 10. Contributions of individual C_L-model terms for data set 5 (validation).

During a third iteration, no new model terms were found. The way the model structure selection algorithm was used for C_L is a good illustration of both its strengths and limitations. It provided no clear-cut answer, but its results were insightful to guide further analysis.

2. *C_D-model*

For the drag coefficient model structure selection process, Figure 11a shows the results of the first iteration. Many contributing model terms were identified, including C_T. The appearance of the thrust coefficient term has to do with suspected errors in the engine model. This is discussed in Appendix C in detail. The useful second-order terms in the first iteration all contained C_T. No clear underlying physical phenomenon was found for this. Also, further analysis showed that these terms generalized badly across data sets, so they were not selected.

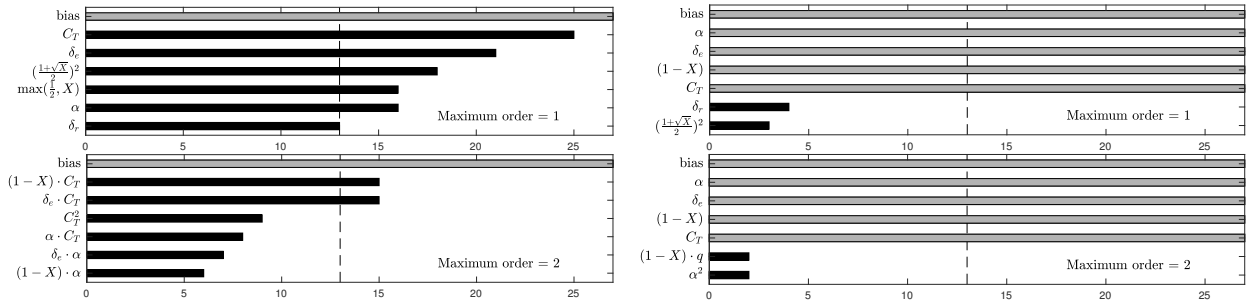

(a) First iteration

(b) Second iteration

Figure 11. Results of model structure selection algorithm for C_D displaying the count of how many times a model structure is selected. Dashed bar marks 50% of training data sets. Grey bars indicate that a term was forced to the model structure manually.

During the first iteration, multiple X-related terms were found. It was decided that including $(1 - X)$ was most desirable, for two reasons. First, the difference in model quality between the X-terms was very small. This is interesting to note, and is indicative of the difficulties in selecting the best model terms. Secondly, the effect of $(1 - X)$ is constrained to just the stalled flight conditions, which means that the effect on the other model terms (especially the bias term) is limited as much as possible. To conclude, after the first iteration C_T, δ_e, α, and $(1 - X)$ were added.

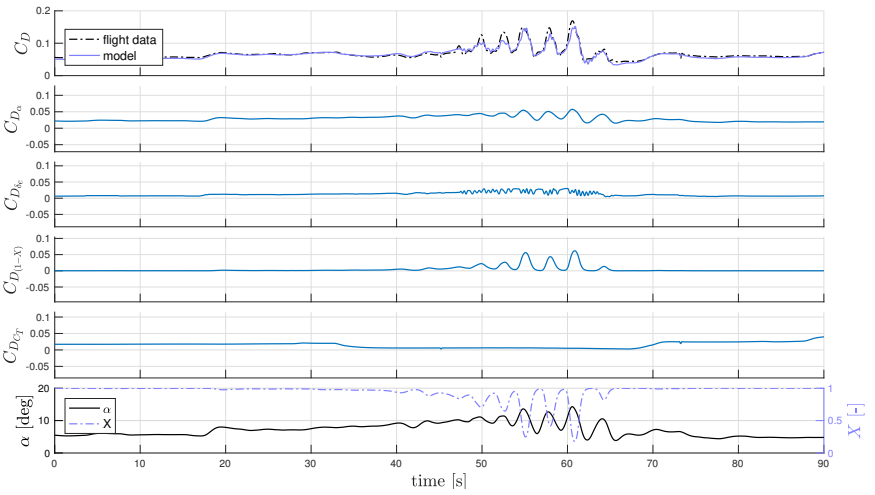

Figure 12. Contributions of individual C_D-model terms for data set 23 (validation).

Figure 11b shows the results of the second iteration. The part of C_D not modeled by the selected terms does not correlate clearly to any remaining candidate. This can be interpreted either as that the current model structure captures all relevant dynamics, or as that the candidate set is missing suitable candidates. Either way, no new terms were added to the model.

Figure 12 shows the contributions of the individual terms in the model for C_D. It is seen that the largest influences are produced by the angle of attack and by flow separation point X. Also the effect of including C_T is clear, none of the other terms can explain the sudden rise in drag that occurs after the stalled flight. Finally, the elevator term is used to explain high-frequency fluctuations in drag, which are also seen in the measured C_D data.

3. C_Y-model

The obtained stall model structure for the lateral force contains no stall-related terms. The data does not suggest that special additions to the conventional aerodynamic modeling terms are necessary. Furthermore, only first-order terms are included in the model, as no support for more complex terms is found in the results of the model structure selection algorithm. β, p, r, and δ_a were included after the first model iteration. In the second iteration δ_r was also identified as a potentially good contribution, but further analysis showed a small negative effect on the validation fit quality. Plots of individual model contributions are presented in Appendix D.

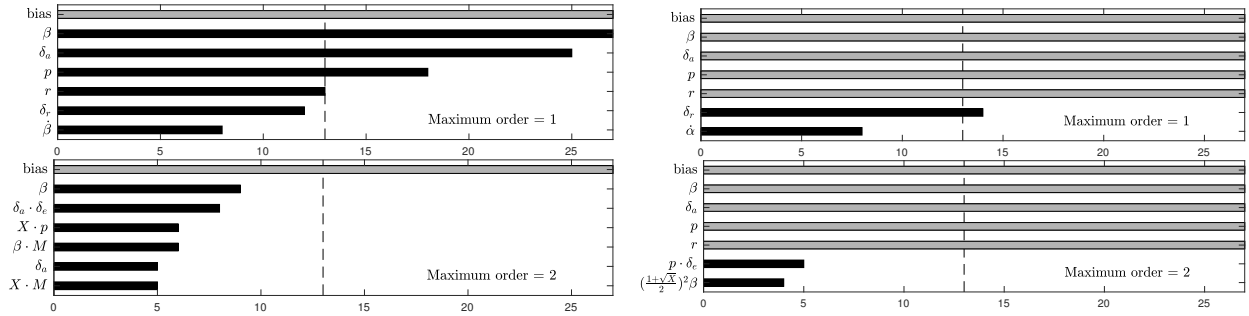

(a) First iteration

(b) Second iteration

Figure 13. Results of model structure selection algorithm for C_Y displaying the count of how many times a model structure is selected. Dashed bar marks 50% of training data sets. Grey bars indicate that a term was forced to the model structure manually.

4. C_l-model

Figure 14 shows the results of the model structure selection algorithm for the roll moment coefficient. As for the lateral force, only first-order terms were found to be useful. Interesting to see is that both $\dot{\beta}$ and r are found to be good options, of which only the latter is selected since it led to a (slightly) lower MSE. On the second iteration, the angle of attack and elevator also received good scores. Since there is little physical justification for including these terms in the roll moment model, and because they did not increase the fit of the model on validation data, they were not added.

No stall-related terms were selected; the data does not suggest that being in a stall results in changes to the roll dynamics. This only partially agrees with experience from the flight tests. One the one hand, it was commented by the test pilots that roll control was not noticeably affected during stall. This suggests that changes to aileron effectiveness are not needed in the model. On the other hand, during some maneuvers the stall resulted in significant roll-off motions, and these are currently not included in the model. Plots of individual model contributions are presented in Appendix D.

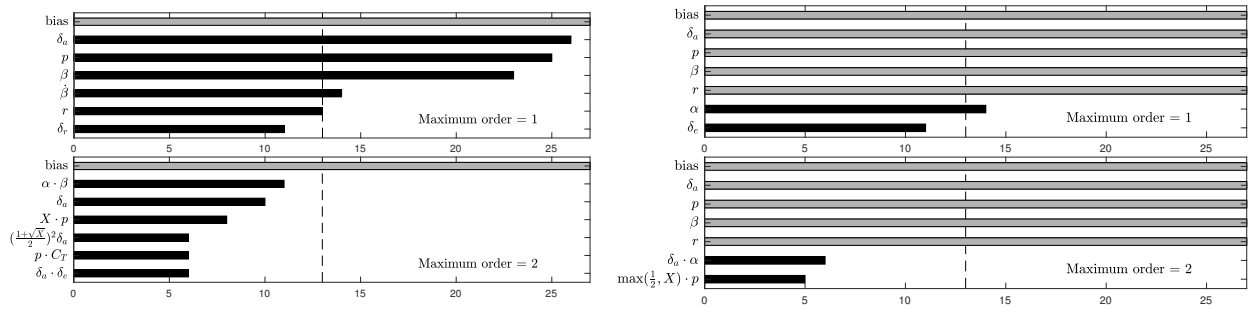

(a) First iteration

(b) Second iteration

Figure 14. Results of model structure selection algorithm for C_l displaying the count of how many times a model structure is selected. Dashed bar marks 50% of training data sets. Grey bars indicate that a term was forced to the model structure manually.

5. C_m-model

The obtained model for the pitch moment includes the flow separation point variable in the form $\max(\frac{1}{2}, X) \cdot \delta_e$. From Figure 16a, it can be seen that this second-order term is selected in the majority of data sets, indicating a strong match with flight data. This model structure reduces the elevator effectiveness by up to half its original value during stall. Physically, this makes sense. In the stall, the horizontal tail can be in the wake of the main wing, reducing its effectiveness. This also agrees with comments from the test pilots, who stated that in stall, pitch controllability was reduced but still clearly present.

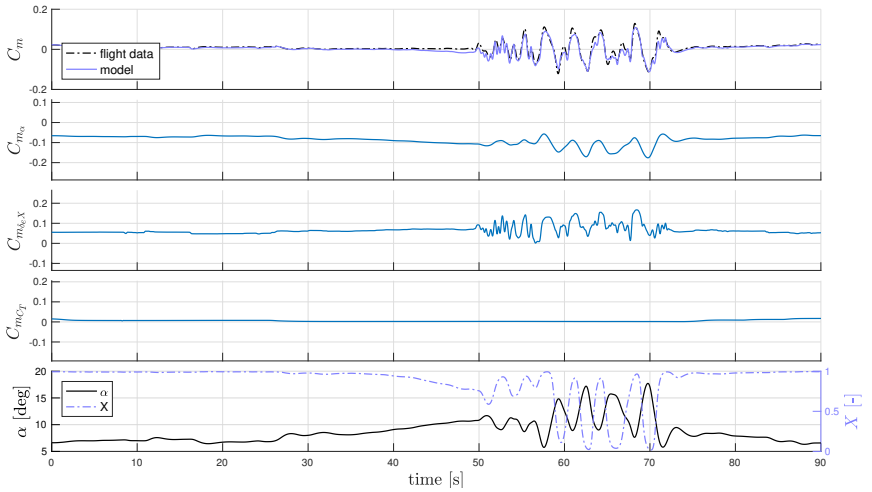

Figure 15. Contributions of individual C_m-model terms for data set 12 (validation).

Next to the modified control term, terms depending on α and C_T are selected. Due to the vertical offset of the engines, the thrust setting influences the pitch moment. The contributions of the individual model terms are visualized in Figure 15. During the stall onset (40-50 s), a (small) negative bias occurs. This is seen in more data sets. One possible reason for this is that the modeled change in control effectiveness is inaccurate during stall onset, which is possible since $\max(\frac{1}{2}, X)$ is a crude mapping. Another possible reason is that an important effect is not included in the model. However, no solutions to this issue were found.

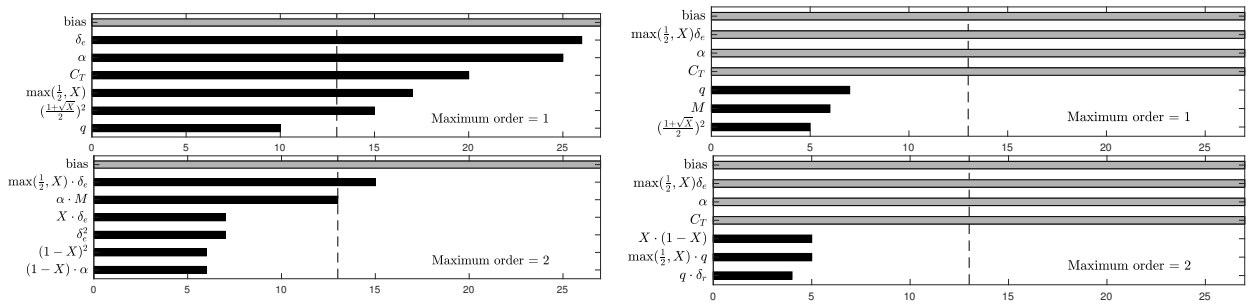

(a) First iteration **(b) Second iteration**

Figure 16. Results of model structure selection algorithm for C_m displaying the count of how many times a model structure is selected. Dashed bar marks 50% of training data sets. Grey bars indicate that a term was forced to the model structure manually.

6. C_n-model

For training the yaw moment model, only 11 out of the 27 training sets could be used. As shown in Figure 2, elevator and ailerons were used in all stall maneuvers to keep the aircraft at desired pitch and bank angles, but rudder inputs were only applied as deliberate disturbance inputs, and only for some of the data sets. It was found that without the rudder disturbances, C_n identification results were not reliable.

Using only the 11 data sets that were suitable, the same model structure selection procedure was applied. After the first iteration, β and δ_r were added, as is shown in Figure 17a. The second iteration of the algorithm did not select any new model terms. Based on engineering insight, the effect of adding r as a term was also tested. Although it was not picked by the model structure selection algorithm, it did lead to a small improvement in model quality. Plots of individual model contributions are presented in Appendix D.

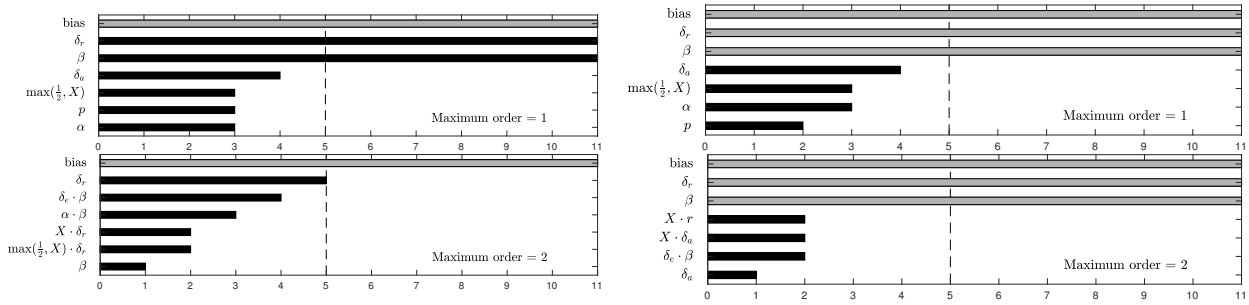

(a) First iteration **(b) Second iteration**

Figure 17. Results of model structure selection algorithm for C_n displaying the count of how many times a model structure is selected. Dashed bar marks 50% of training data sets. Grey bars indicate that a term was forced to the model structure manually.

B. X-parameter Estimates

As shown in Figure 7, the estimation of X-parameters was done iteratively. After the C_L model structure had converged to the form in Equation 14, one final optimization was done. The results of this optimization are presented in this section. Table 4 lists the numerical results and the outcomes of several statistical tests. Figure 19 is a matrix plot of the parameter estimates, which visualizes the distributions and correlations of the estimates. In each figure, the diagonal plots are histograms that visualize an approximation of the parameter distributions. The off-diagonals are scatter plots of each of the parameter combinations. If correlations are present, the data points will form a clear diagonal. The red star marks the median value, and the values of the correlations are shown (ρ).

Table 4. Results of estimating the X-parameters and several statistical tests. For the KS-test a significance of $\alpha = 0.1$ was used. $h = N$ means that the distribution can be assumed to be approxmately normal, $h = \times$ when that this is not possible. The t-test and signed rank test were run with $\alpha = 0.01$ and a Bonferroni correction (here $n = 4$). For these, $h = *$ if the null hypothesis is rejected, and the parameter value is expected to differ from zero.

Parameter		Results				KS-test		t-test		Signed rank	
Name	Unit	$\hat{\theta}$	θ_{lb}	θ_{ub}	$\sigma(\hat{\theta})$	p	h	p	h	p	h
τ_1	[s]	**0.2547**	0.001	0.80	0.1565	0.147	N	0.000	*	0.000	*
τ_2	[s]	**0.0176**	0.000	0.50	0.0819	0.020	$\times$	0.002	*	0.000	*
a_1	[-]	**27.6711**	15.000	40.00	6.7177	0.781	N	0.000	*	0.000	*
α^*	[rad]	**0.2084**	0.100	0.35	0.0202	0.594	N	0.000	*	0.000	*

On each of the 27 training data sets, the optimization was run 300 times from random initial conditions. These initial conditions were uniformly sampled from the parameter space defined by the upper an lower parameter boundaries (θ_{ub} and θ_{lb}), see Table 4. On each data set, the results of the 300 runs were ordered by the MSE of the model output. It was found that the cost function surface was relatively flat near the optimal solution. Therefore, to reduce the variance of the parameter estimates, it was decided to take the average of all runs that reached an MSE within 2% of the best run as the point estimate for that data set. After that, the median over all data sets was taken to obtain the final parameter estimates $\hat{\theta}$.

Three statistical tests were performed. The Kolmogorov-Smirnov (KS) test was used to determine whether it is reasonable to assume that the distribution of the estimates is approximately normal. Next, both parametric (t-test) and non-parametric (Wilcoxon's signed-rank) one-sample tests were done to check with what degree of certainty it can be stated that the *real* parameter value is different from zero, given the data available. The one-sample tests use a Bonferroni correction on their significance level to determine the result h.

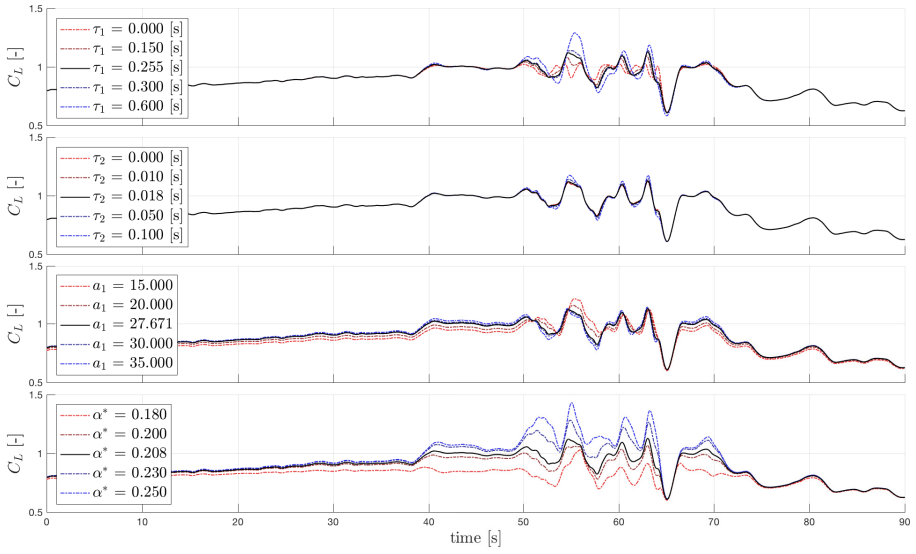

Figure 18. Visualization of the sensitivity of the model output to the X-parameters. Whereas the static parameters influence almost the entire time-history, the dynamic parameters only affect the part where the aircraft actually stalls. Data set 3 (training) is shown.

The outcome of the statistical tests shows that only the distribution of τ_2 cannot be considered normal, which agrees with observing the histograms in Figure 19. The

skewed distribution is likely to be caused by the lower bound of the parameter: the parameters are clustered around $\tau_2 = 0$. It was decided to keep the lower bound in place because negative values of τ_1 and τ_2 are unphysical. Furthermore, all four X-parameters were found to be significantly different from zero. This was found surprising, considering the low value of τ_2. Also this result is likely to have been influenced by the lower parameter bound on τ_2. If negative values of τ_2 had been allowed, its distribution is expected to be spread around the zero value, which would have reduced the significance of the results of the one-sample tests.

In general, the static parameters (a_1 and α^*) were easier to estimate than the dynamic parameters (τ_1 and τ_2). Two main reasons were found for this. First, the cost function surface tended to become rough for large values of τ_1 and τ_2, as is shown in Figure 20. Since a gradient-based optimization algorithm was used, this reduced its effectiveness. This problem was mostly solved by setting θ_{ub} small enough for τ_1 and τ_2. A second reason is that the sensitivity of the model output to changes in a_1 or α^* is greater than the sensitivity to changes in τ_1 or τ_2, as is visualized in Figure 18. Whereas the static parameters influence the output during almost all times of the maneuver, the dynamic parameters only influence C_L during the stall itself.

Finally, the estimated X-parameters were compared to those found in literature. Table 5 contains the results from several other studies. The dynamic parameters were made dimensionless for better comparison. Compared to the other aircraft types, a_1 and α^* are similar. However, τ_1 is about a factor 2 lower, and τ_2 is about a factor 5 lower compared to the values found for other aircraft. These differences could be caused by the choice of model structure, parameter estimation, or simply because of differences in the physical flow phenomena around the aircraft. The final column contains the results of previous research on the same aircraft.[18] This previous research used only data on quasi-static stall maneuvers; data with very little dynamic excitation. Furthermore, a very different approach to estimating τ_1 and τ_2 was used, namely through the stall buffet vibrations. Since in the current research a *direct* estimation of these parameters is used, instead of via the buffet, it is concluded that the newly obtained X-parameter values are more accurate. The static parameters are equivalent between the two Citation II stall models.

Table 5. Comparison of estimated X-parameter values to literature, where for the Cessna Citation II: $\bar{c}$ = 2.06 m, and $V_{\text{stall}} \approx$ 75 m/s (approximate average from flight test data).

Parameter	Unit	Citation II	VFW-614[11]	C-160[11]	AT-26[24]	Citation II[18]
$\tau_1 \frac{V}{\bar{c}}$	[-]	9.27	15.6	14.5	-	22.44
$\tau_2 \frac{V}{\bar{c}}$	[-]	0.64	4.45	3.46	-	13.18
a_1	[-]	27.67	15.00	25.70	25.00	25.87
α^*	[rad]	0.21	0.34	0.36	0.25	0.25

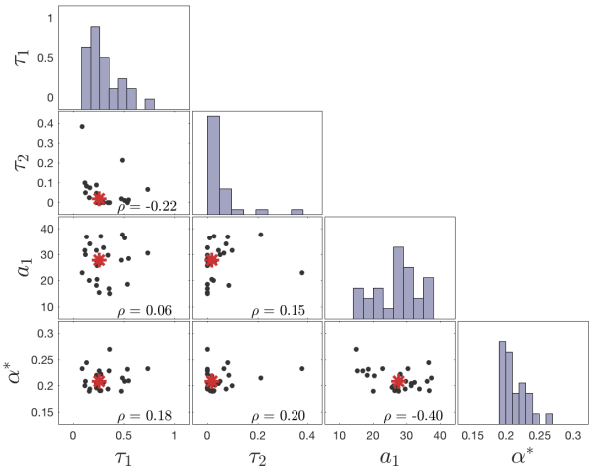

Figure 19. Matrix plot of the estimated X-parameters

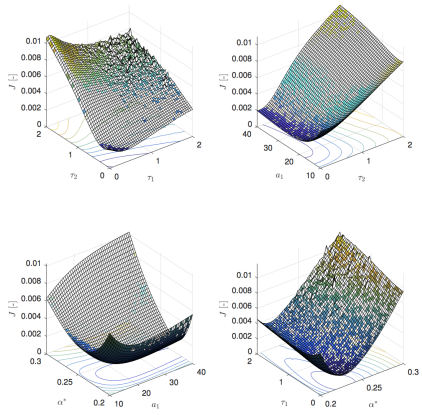

Figure 20. Example of the cost function surface for the optimization of X-parameters. Note the roughness of the cost function surface for values of τ_1 and τ_2 larger than 1 s.

C. Aerodynamic Model Parameter Estimates

The results of the parameter estimation for the aerodynamic model equations can be found in Table 6. This table shows the estimated aerodynamic coefficient values, the standard deviations of the estimates over the data sets, and the outcomes of the same statistical tests as for the X-parameters. Matrix plots of the parameter estimates are shown in Figure 21.

All parameters in Table 6 can be assumed to come from a normal distribution, except for $C_{m_{\delta_e X}}$. This agrees with the histograms for this parameter, found in Figure 21e. Furthermore, the one-sample statistical tests indicate that all model parameters are statistically different from zero, except for C_{D_0}. Because this is a bias parameter, it was still kept in the model. The fact that the drag bias is estimated to be small is surprising. It is hypothesized that this can be explained by the inclusion of $C_{D_{C_T}}$ into the model. Because the thrust is constant for the most part of the maneuvers, this term already accounts for a large part of the bias effect. This is problematic for the current model for C_D, but is expected to be solved once an updated engine model will become available.

Table 6. Parameters estimation results and statistical tests. For the KS-test a significance of $\alpha = 0.1$ was used. $h = N$ means that the distribution can be assumed to be approxmately normal, $h = \times$ when that this is not possible. The t-test and signed rank test were run with $\alpha = 0.01$ and a Bonferroni correction. For these tests, $h = *$ if the null hypothesis is rejected, and the parameter value is expected to differ from zero, $h = \circ$ otherwise.

Parameter		Results		KS-test		t-test		Signed rank	
Name	Unit	$\hat{\theta}$	$\sigma(\hat{\theta})$	p	h	p	h	p	h
C_{L_0}	[-]	**0.1758**	0.0423	0.9135	N	0.0000	*	0.0000	*
C_{L_α}	[-]	**4.6605**	0.3965	0.9399	N	0.0000	*	0.0000	*
$C_{L_{\alpha^2}}$	[-]	**10.7753**	3.8895	0.7665	N	0.0000	*	0.0000	*
C_{D_0}	[-]	**0.0046**	0.0223	0.2648	N	0.2801	○	0.0837	○
C_{D_α}	[-]	**0.2372**	0.1443	0.5802	N	0.0000	*	0.0000	*
$C_{D_{\delta_e}}$	[-]	**-0.1857**	0.0781	0.4845	N	0.0000	*	0.0000	*
$C_{D_{(1-X)}}$	[-]	**0.0732**	0.0317	0.1101	N	0.0000	*	0.0000	*
$C_{D_{C_T}}$	[-]	**0.3788**	0.0852	0.2042	N	0.0000	*	0.0000	*
C_{Y_0}	[-]	**0.0032**	0.0035	0.8693	N	0.0000	*	0.0003	*
C_{Y_β}	[-]	**-0.5222**	0.0682	0.9894	N	0.0000	*	0.0000	*
C_{Y_p}	[-]	**-0.5000**	0.2244	0.9694	N	0.0000	*	0.0000	*
C_{Y_r}	[-]	**0.8971**	0.4794	0.8368	N	0.0000	*	0.0000	*
$C_{Y_{\delta_a}}$	[-]	**-0.2932**	0.0685	0.8481	N	0.0000	*	0.0000	*
C_{l_0}	[-]	**-0.0017**	0.0001	0.8529	N	0.0000	*	0.0000	*
C_{l_β}	[-]	**-0.0454**	0.0167	0.9067	N	0.0000	*	0.0000	*
C_{l_p}	[-]	**-0.1340**	0.0620	0.7478	N	0.0000	*	0.0000	*
C_{l_r}	[-]	**0.1412**	0.1287	0.5916	N	0.0000	*	0.0000	*
$C_{l_{\delta_a}}$	[-]	**-0.0853**	0.0248	0.6586	N	0.0000	*	0.0000	*
C_{m_0}	[-]	**0.0183**	0.0138	0.9811	N	0.0000	*	0.0000	*
C_{m_α}	[-]	**-0.5683**	0.1329	0.8496	N	0.0000	*	0.0000	*
$C_{m_{\delta_e X}}$	[-]	**-1.0230**	0.1542	0.0736	×	0.0000	*	0.0000	*
$C_{m_{C_T}}$	[-]	**0.1443**	0.0498	0.8103	N	0.0000	*	0.0000	*
C_{n_0}	[-]	**0.0013**	0.0000	0.3076	N	0.0000	*	0.0010	*
C_{n_β}	[-]	**0.0804**	0.0093	0.5920	N	0.0000	*	0.0010	*
C_{n_r}	[-]	**-0.0496**	0.0308	0.9029	N	0.0000	*	0.0010	*
$C_{n_{\delta_r}}$	[-]	**0.0492**	0.0040	0.9162	N	0.0000	*	0.0010	*

In the lift, drag, and moment coefficient models, the bias and α parameters show clear correlations. Especially for the drag coefficient model, this can be regarded as a problem affecting the accuracy of the estimate (see Fig 21b, $\rho = -0.95$). These correlations are likely to be caused by the fact that the angle of attack is approximately constant for the largest part of the maneuvers. Hence, it is not easy to distinguish between α-related effects, and bias. Removing either of these parameters in these models lead to a strong increase in modeling error, so no action was taken.

D. Model Validation

Of the 34 recorded flight data sets, 7 were kept aside for model validation (80-20 split). Table 7 compares the MSE and coefficient of determination (R^2) for both the training and validation data. Time histories comparing model output to measured data are presented for three selected validation data sets in Figure 24. It was chosen to show the best, worst, and an average quality fit, measured by average normalized MSE over all coefficients.

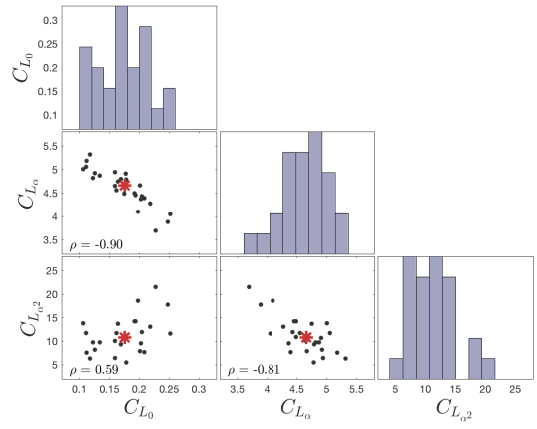

(a) C_L **parameter estimates**

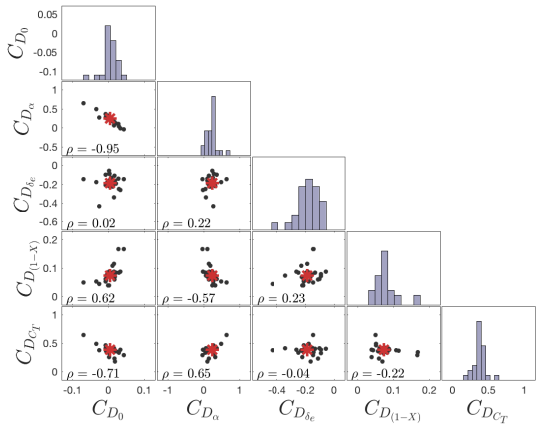

(b) C_D **parameter estimates**

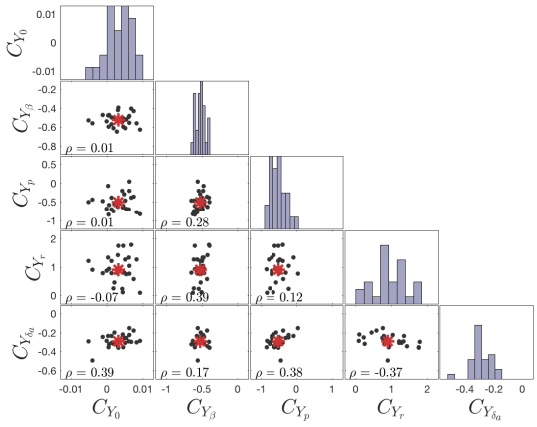

(c) C_Y **parameter estimates**

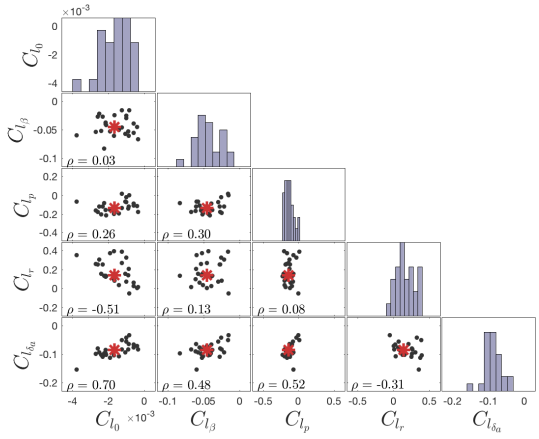

(d) C_l **parameter estimates**

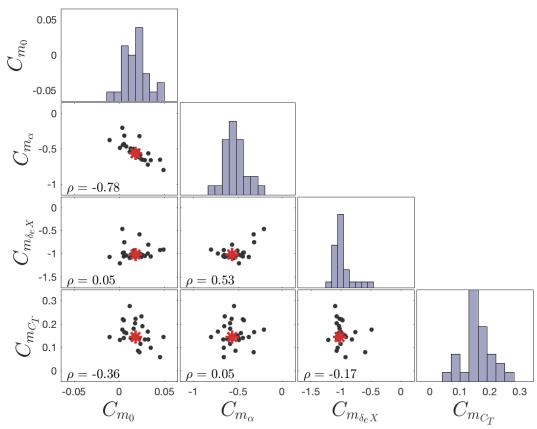

(e) C_m **parameter estimates**

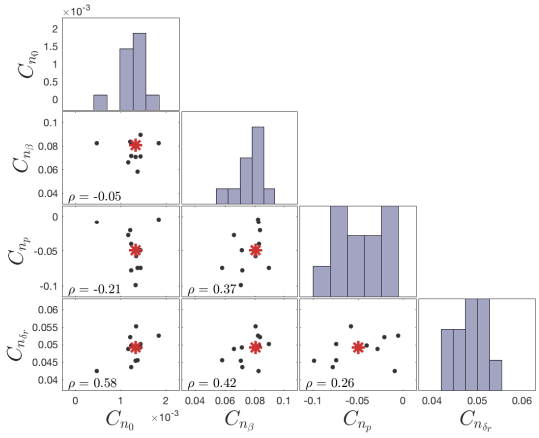

(f) C_n **parameter estimates**

Figure 21. Matrix plots of the parameters estimates. The diagonal plots are histograms that visualize an approximation of the parameter distributions. The off-diagonals are scatter plots of each of the parameter combinations. The red star marks the median value, and the values of the correlations are shown (ρ)

As Table 7 shows, the model quality is approximately the same on training and validation sets, indicating that the model is neither under- nor overfitting. In some cases, the validation fit is even slightly better. This is caused by the random allocation of flight data maneuvers; some of them led to much lower errors. Because there are only 7 validations set, the average over them is influenced more significantly by the random allocation than for the training data. It can be seen that for some sets, the worst R^2 scores are even negative. This holds often the asymmetric models (lateral force, roll, yaw), which on average also show a lower quality fit than for the longitudinal model equations (lift, drag, pitch). In part, this can be explained by the definition of R^2:

$$R^2 = 1 - \frac{\sum(\mathbf{y} - \hat{\mathbf{y}})^2}{\sum(\mathbf{y} - \mu_y)^2} \,. \tag{16}$$

In the extreme case that the measurement is (nearly) a constant, i.e., $\mathbf{y} \approx \mu_y$, then the denominator is (close to) zero. The more a time history is like a constant, the more any present errors will lead to a reduction in R^2, which is the case for the asymmetric models, as can be seen in Figure 24.

Table 7. Properties of the estimated parameters of the aerodynamic model equations. MSE and R^2 are averages over the sets.

	Training data (27 sets)				**Validation data** (7 sets)			
Coefficient	MSE	R^2	min(R^2)	max(R^2)	MSE	R^2	min(R^2)	max(R^2)
C_L	1.65×10^{-3}	0.92	0.71	0.98	1.45×10^{-3}	0.91	0.77	0.96
C_D	1.01×10^{-4}	0.74	-1.47	0.97	6.72×10^{-5}	0.89	0.84	0.94
C_Y	4.68×10^{-5}	0.66	-0.67	0.91	4.55×10^{-5}	0.57	0.29	0.82
C_l	2.40×10^{-6}	0.54	-0.60	0.85	1.97×10^{-6}	0.47	0.08	0.92
C_m	9.93×10^{-5}	0.68	-0.39	0.92	9.87×10^{-5}	0.73	0.26	0.92
C_n	8.21×10^{-7}	0.49	-0.66	0.96	8.66×10^{-7}	0.12	-0.43	0.80

To gain more insight into the types of errors that occur in the model output, use is made of Theil statistics.[25] Theil's U-coefficient is a normalized metric for model quality, and ranges from 1 (worst case) to 0 (perfect fit). The error U can further divided into a bias error U_{bias}, a variance error U_{var}, and a covariance error U_{cov}. These can be calculated as:

$$U = \frac{\sqrt{\frac{1}{N}\sum(\mathbf{y} - \hat{\mathbf{y}})^2}}{\sqrt{\frac{1}{N}\sum \mathbf{y}^2} + \sqrt{\frac{1}{N}\sum(\hat{\mathbf{y}})^2}} \,, \tag{17}$$

$$U_{\text{bias}} = \frac{(\bar{\mathbf{y}} - \hat{\bar{\mathbf{y}}})^2}{\frac{1}{N}\sum(\mathbf{y} - \bar{\mathbf{y}})^2} \,, \tag{18}$$

$$U_{\text{var}} = \frac{(\sigma_y - \sigma_{\hat{y}})^2}{\frac{1}{N}\sum(\mathbf{y} - \bar{\mathbf{y}})^2} \,, \tag{19}$$

$$U_{\text{cov}} = \frac{2(1 - \rho_{y\hat{y}})\sigma_y \sigma_{\hat{y}}}{\frac{1}{N}\sum(\mathbf{y} - \bar{\mathbf{y}})^2} \,. \tag{20}$$

Here, σ and ρ indicate the standard deviation and the cross-correlation, respectively. Bias, variance, and covariance errors always add up to one due to their definition, so they can be used to divide U into fractions. U_{var} relates to scaling errors, while U_{cov} is caused by any errors that are uncorrelated to the signals. These statistics were computed for all the validation data sets, and the result is shown in Figure 22. Within each coefficient group, the order of data sets is the same. They are ordered by average, normalized U over the six coefficients.

This figure confirms the previous observation that the longitudinal models have a higher quality fit. Furthermore, what can be seen is that generally speaking, the same trend can be seen for all coefficients; there is a relation between the fit quality for all models. In other words, some data sets (e.g., set 7) have a high error for all aerodynamic force coefficients, some have low error.

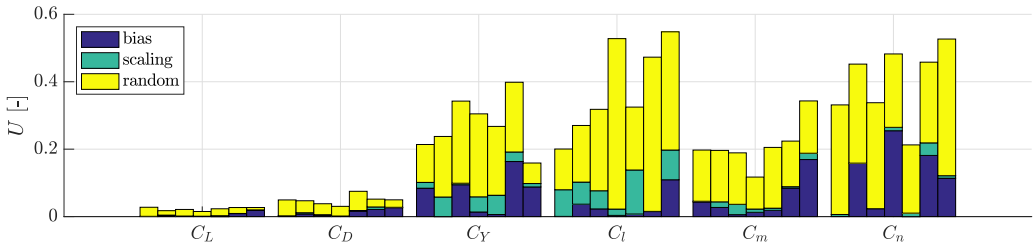

Figure 22. Theil statistics of the 7 validation sets, grouped by coefficient model. Lower means better fit. Groups are sorted by average U-score over all coefficients, normalized by average score over that coefficient (from left to right: 12, 23, 25, 16, 5, 22, 7).

Furthermore, it can be seen that the largest part of the error can be attributed to U_{cov}. This indicates that generally, the model parameters have been properly estimated. However, some maneuvers show that large parts of the error are caused by bias. The contribution of scaling errors to the total model error is small.

Figure 24 shows time-history plots of three selected validation sets, one with the lowest error, one with an average error, and the set with the largest error. Overall, the model output shows good agreement with the flight data, also during the stall. There are some stall-related effects that are not reflected by the model, for instance in the C_L and C_D time histories of the "average" plot in Figure 24. However, the model re-aligns with data once the aircraft recovers from the stall. An attempt was made to explain (part of) these features by considering X on left and right wings separately, as some authors in literature have proposed,[12] but this did not lead to improved results for our data.

A possible issue can be seen in the model output for C_m. During stall onset, the model predicts a negative pitch moment, i.e., a pitch-down tendency that is not present in the data. Since the first action a pilot should take to recover from a stall is to reduce angle of attack, any errors in pitch moment are likely to affect the suitability of this model for use in stall recovery training in simulators.

A final validation check was done on the stall identification angle of attack. Since the model will be used to train pilots in recognizing a developing stall, it is extra relevant that the model output agrees with flight data around the angle of attack where the effects of stall begin to be significant. The values of the modeled and measured lift coefficient were compared at $\alpha = \alpha^*$. This was done for all maneuvers, and is shown in Figure 23. As is shown, the data points mostly lie on the diagonal, indicating that the model predicts the same lift at the stall identification angle of attack as measured in the data.

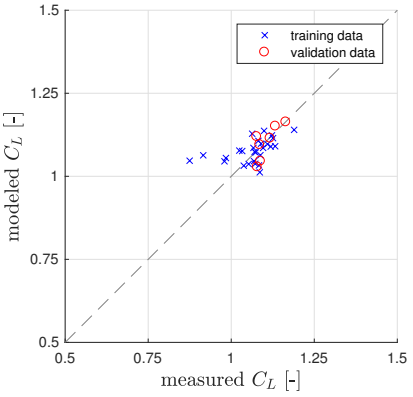

Figure 23. Comparison of C_L at the stall identification angle of attack $\alpha = \alpha^*$.

V. Discussion

This paper has presented a methodology for aerodynamic modeling of a Cessna Citation II, including the aerodynamic stall dynamics. It was applied to a series of flight data sets that were specifically collected for this purpose at an altitude of 5,500 meters. The obtained stall model shows very good agreement with the validation data. The discussion of these results is presented in this section, and is split into three parts. First, the resulting model itself will be discussed. Several potential model issues are covered, and the simulated model outputs are compared to those of other Citation II models. After that, the inclusion of dynamic effects in the stall model is considered. Finally, an exploration of the required effort to expand the current model to the full flight envelope is presented.

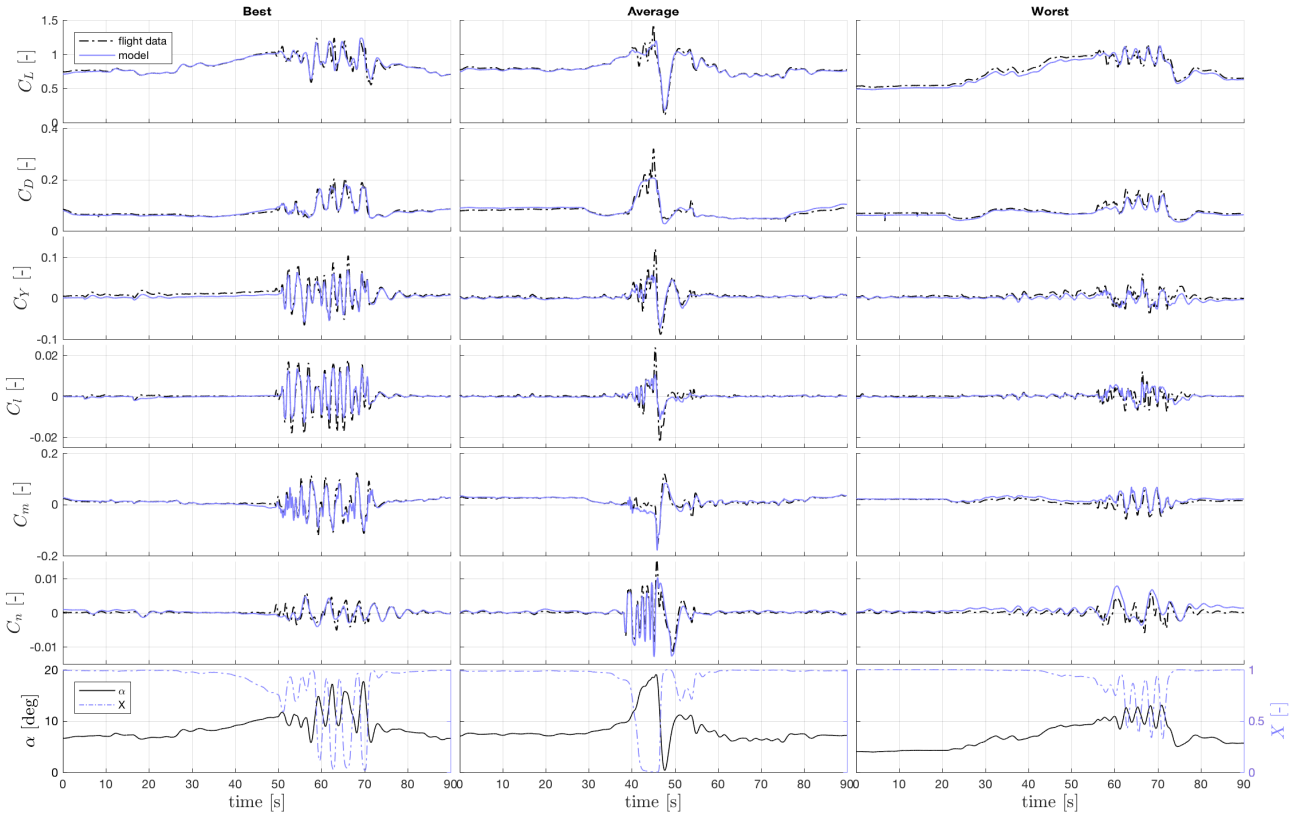

Figure 24. Selected plots from the 7 validation data sets, showing model output versus measured force and moment coefficients. Left column contains data set 12, which has the lowest MSE, middle is set 5, and right is set 22. In the bottom plot, angle of attack and the calculated flow separation point variable are shown.

1. Obtained Stall Model

The model structure that was selected in this research is well-supported by the flight data. The multivariate orthogonal function modeling algorithm provided good guidance in identifying and selecting effective model terms. However, there are a few noteworthy results that are discussed here.

First of all is the fact that no terms relating to pitch rate q are selected, while these are commonly found in models for C_L, C_D, and especially C_m. One explanation is that q really does not have an influence on the Citation II's stall dynamics, but since its regular flight envelope model *does* include q-terms,[23] this appears to be unlikely. A better explanation is that the contribution of q to the lift, drag, or pitch moment is small. Moreover, the measured values of q in the flight data are close to zero when the aircraft is not in stall. Hence, identifying these relatively small effects due to q during stalled flight conditions – where strong nonlinearities and (random) disturbances are present – is challenging. A potential remedy for this is to gather new flight tests, where a dynamic maneuver such as a 3-2-1-1 on the elevator is added just before the aircraft stalls.

Another aspect of the model structure that is noteworthy is that no changes in control effectiveness for the aileron and rudder were identified. In qualitative comments, the test pilots stated that the control response of the aircraft did not change too much during the stall. However, a similar effect as for the elevator was expected. Perhaps the current approach of using X to add effects to control effectiveness terms is unsuitable for the aileron or rudder. Alternatively, it could be that not enough data is available to identify these effects. Dynamic maneuvers such as a 3-2-1-1 using aileron or rudder, performed right before the stall will give a stronger reference point to compare the control performance inside the stall to.

Next, the fact that the thrust coefficient is used as a regressor for the models for C_m and C_D is uncommon. As is discussed in Appendix C, these terms are corrections for mismatches in the engine model.

A final note on the model structure is regarding the use of X as a regressor. In this research, it has been shown that it is beneficial to use X as (part of) a term in the lift, drag, and pitch moment coefficient stall models. Its use in the lift and drag models has been proposed by other research before,[13,18] but its use for modeling the reduction in elevator effectiveness is a novel contribution. Hence, given new flight data and/or better mathematical transformations, other uses of X are thought to be possible. For instance, the static pitch stability term C_{m_α} is expected to change during stall. However, it must be kept in mind that X is only a single variable used to describe all the flow separation phenomena around the entire aircraft. This obviously is a simplification of reality. From a system identification perspective, a simple model is actually desired, as long as it still leads to accurate results. Nevertheless, it might not be possible to explain all relevant stall-related effects on the flight dynamics using X.

The identified stall model is significant improvement compared to the previous Citation II stall model as well as its normal flight envelope model when simulating stall maneuvers. Table 8 shows the difference in average MSE over the 7 gathered validation data sets for all three of these models. Lateral model terms were not included in the previous stall model due to a lack of the side slip measurement. The new stall model achieves a much lower error for all model outputs. It is interesting to see that the normal flight envelope model actually achieved a lower error on the pitch moment coefficient fit than the previous stall model.

Table 8. Comparison of the newly developed stall model, the previous stall model, and the normal flight envelope model of the Citation II in terms of the average mean squared error on the 7 validation data sets gathered for this research.

	Current	*Previous stall model*[18]		*Normal flight envelope*[23]	
Model	**MSE**	**MSE**	**Difference**	**MSE**	**Difference**
C_L	1.45×10^{-3}	3.02×10^{-3}	+ 208%	3.35×10^{-2}	+2313%
C_D	6.72×10^{-5}	3.16×10^{-4}	+ 470%	1.38×10^{-3}	+2050%
C_Y	4.55×10^{-5}	*n/a*	*n/a*	2.47×10^{-4}	+ 543%
C_l	1.97×10^{-6}	*n/a*	*n/a*	1.30×10^{-5}	+ 662%
C_m	9.87×10^{-5}	2.89×10^{-3}	+2925%	7.84×10^{-4}	+ 795%
C_n	8.66×10^{-7}	*n/a*	*n/a*	1.61×10^{-5}	+1864%

Figure 25 visually compares the longitudinal model outputs of both these models, as well as the normal flight envelope Citation II model.[23] Figure 26 shows the lateral model outputs of just the new stall model alongside the regular flight envelope model. The improvement in model fit is illustrated clearly, especially for the drag and pitch moments. The previous stall model can be seen to experience a significant bias during most part of the pitch moment time trace, which explains the large difference in MSE for the previous stall model. Also, the normal flight envelope model can be seen lack the reduction in lift during stall.

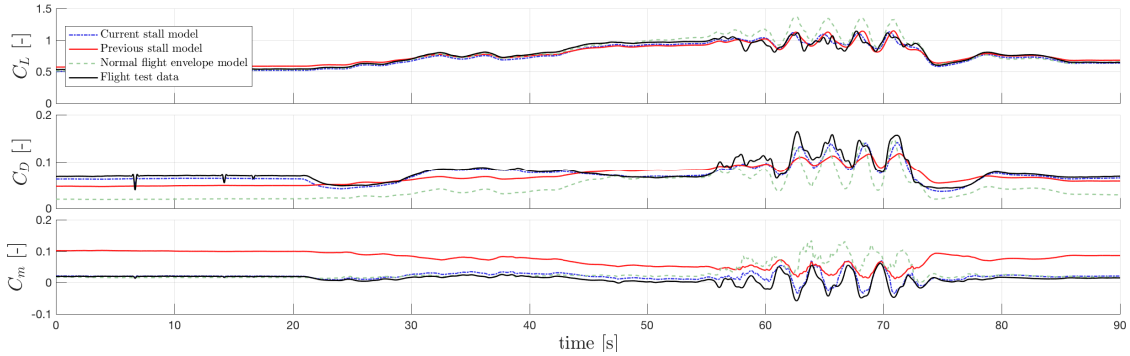

Figure 25. Comparison of longitudinal outputs of the newly-obtained stall model to the previous version's. Additionally, outputs of the normal flight envelope model are shown, which is a validated dynamics model for the Citation II. Data set 22 (validation) is shown.

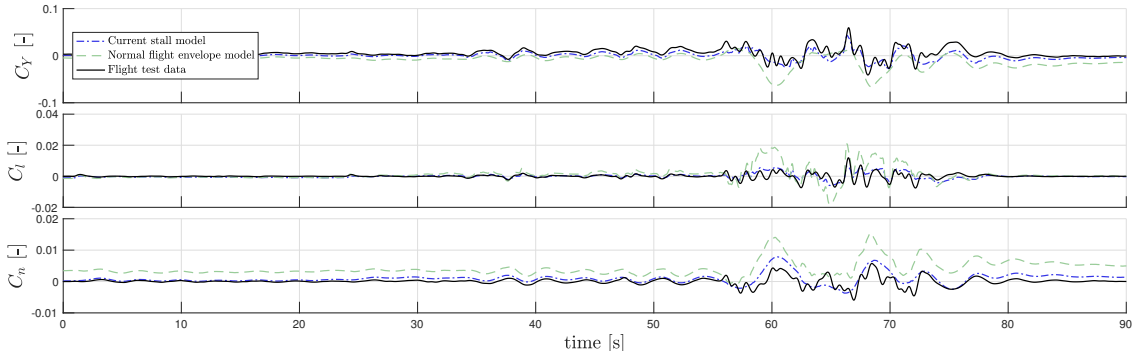

Figure 26. Comparison of lateral outputs of the obtained stall model with the outputs of the validated normal flight envelope model for the Citation II. Data set 22 (validation) is shown.

2. *Dynamic Stall Effects*

One of the goals of this research was to include dynamic effects of stall into the model. These effects are parametrized using τ_1 and τ_2. Including these terms into the model complicates both system identification as well as model evaluation, since an ODE needs to be solved to obtain X. Hence, it is sensible to review them: does the extra effort actually influence the model output in any significant way?

A simple test for this is to investigate what happens when either of these parameters is set equal to zero. The effect on the modeled lift coefficient of setting τ_1 equal to zero is shown in Figure 27. It is shown that due to the time delay parametrized by τ_1, the minimum value of X is larger, and therefore the maximum lift coefficient is higher than when τ_1 is neglected. As a result, the model provides a better match with the flight data. For τ_2, the change in model output is small. There is less than 1% difference in MSE and the difference with the current model output can hardly be seen in the time traces. From this result it seems likely that τ_2 can be neglected/set to zero in modeling the stall dynamics of a Citation II type aircraft, at the flight condition that was considered. This was to be expected, as the estimated value of τ_2 was already close to zero.

These results show that while the hysteresis effect, parametrized by τ_2 might not have a strong influence on model output, the dynamic time-delay effect by τ_1 is critical for a realistic model output.

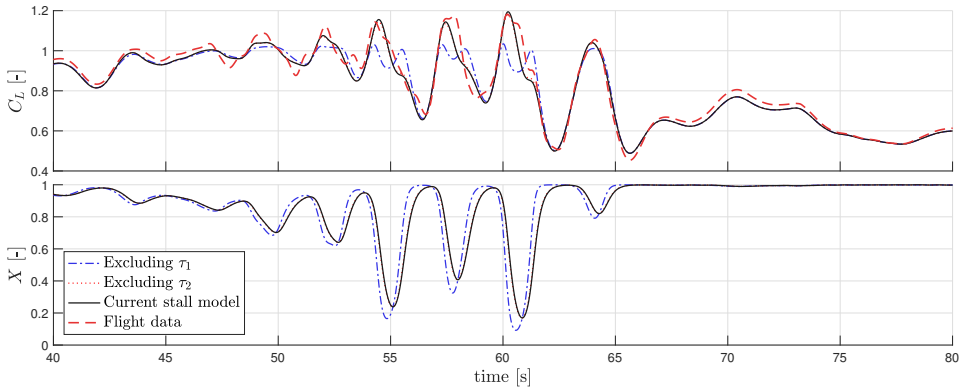

Figure 27. Illustration of the effect on model output by setting either τ_1 or τ_2 equal to zero. It is shown that the maximum achieved lift coefficient is decreased when $\tau_1 = 0$. The effect of $\tau_2 = 0$ is so small that it is indistinguishable from the current stall model.

3. *The Road to a Full-Envelope Stall Model*

The end goal of the research effort is to obtain a stall model that provides the most realistic simulator experience reasonably possible, for all flight conditions that are relevant for training scenarios. This model will then serve further research into what parts of such a stall model are relevant for effective training, and which are not. Before that is achieved, there are still many steps to take. The current stall model is only validated at an altitude of 5,500 meters, and has not yet been tested in a human-in-the-loop simulation. Regarding the research efforts that still are to be done, three major considerations are discussed here.

First of all, it is believed that the stall modeling methodology that was developed for this research will be a suitable tool for expanding the validated stall model envelope. It has been shown that Kirchoff's methodology can capture the relevant nonlinearities in a stall maneuver, and that both the model structure and parameters can be identified. The same procedure as was described should be repeated for other selected altitudes, and other flap and gear configurations. The model parameters can then be made functions of flight condition. This is a common practice in aerodynamic modeling, and was also applied for the normal flight envelope model of the Citation II from Reference 23. The stall model structures should ideally be the same at every flight condition. If terms need to be added or removed for different flight conditions, this will pose an additional challenge.

Secondly, new flight tests will have to be conducted. These should be planned based on what flight conditions are to be required during training scenarios. If only few and specific scenarios are foreseen, one could perhaps do with fewer (costly) flight tests than what would be required for a full flight envelope model. For this research, about 30 maneuvers were done at the same flight condition. This seems like a good number. Also the piloting technique that was used for this research was generally found to be effective. A good addition to the flight test maneuvers would be the inclusion of dynamic excitation *before* the aircraft stalls. For example, a sequence of 3-2-1-1s or doublets on all three control axes could be performed. This should facilitate identification of changes in control responses. Important is that the aircraft is sufficiently dynamically excited both in- and outside the stall, and that high enough angles of attack are reached. No clear differences were found between wings-level and accelerated stall maneuvers in terms of identifiability. All control surfaces, including rudder, should be used during the stall. Without rudder inputs, yaw moment identification is not possible.

Thirdly, since the model's goal is to provide the best simulator experience possible, it will be vital to actually put a human in the loop fly it. This should be done even before expanding the stall model to the full flight envelope. Current model development was solely guided by quality of fit metrics such as MSE, and by visually inspecting plots. These metrics might overlook properties of the model that are vital for a good simulator experience, or conversely: they might severely penalize some errors that are irrelevant for the intended purpose. Hence, early simulator experiments will help in steering the research focus to the most relevant issues.

VI. Conclusion

Using flight test data gathered specifically for this goal, a complete model of the stall dynamics of a Cessna Citation II is identified and validated around an altitude of 5,500 m, or 18,000 ft, in clean conditions. Overall, the model output shows very good agreement with flight data, especially during stalls.

Kirchoff's theory of flow separation is used as modeling principle, and is suitable for capturing the effects of stall on aircraft dynamics. Model structure selection is facilitated using a multivariate orthogonal function modeling method. Apart from modeling the effect on the lift, the flow separation point variable X is also used to capture the effect of stall on drag and elevator effectiveness. The latter of these additions is a novel approach of this research. Given the available data, X is not found to have an effect on the lateral dynamics (roll, yaw, lateral force) or aileron and rudder effectiveness.

The stall model parameters are estimated accurately. The flight data that was gathered includes the use of control surfaces and dynamic excitation during stall, and enables direct estimation of the stall model parameters. This is an improvement compared to previous research, which used data of only quasi-static stalls, and where the transient stall effects needed to be estimated indirectly, via the accelerations caused by the stall buffet.

In conclusion, the model identification methodology that is developed in this research is considered to be well-suited for identifying a stall model of a small business jet, like a Cessna Citation II. This methodology, as well as the

obtained model, will serve as the basis for future research, leading to better stall models and training programs, which will prepare pilots for real-life encounters with stall upsets.

References

[1]Boeing Commercial Airplanes, "Report: Statistical Summary of Commercial Jet Airplane Accidents, Worldwide Operations, 1959-2015," Tech. rep., 2015.

[2]Lambregts, A. A., Nesemeier, G., Newman, R. L., and Wilborn, J. E., "Airplane Upsets: Old Problem, New Issues," *AIAA Modeling and Simulation Technologies Conference and Exhibit*, American Institute of Aeronautics and Astronautics, Reston, Virigina, aug 2008.

[3]Crider, D. A., "The Need for Upset Recovery Training," *AIAA Modeling and Simulation Technologies Conference and Exhibit*, No. August, 2008.

[4]Federal Aviation Administration, "Advisory Circular 120-109A," 2015.

[5]Chambers, J. R. and Grafton, S. B., "Aerodynamic Characteristics of Airplanes at High Angles of Attack," *Journal of Aircraft*, Vol. 31, No. 5, 1977, pp. 1109–1115.

[6]Foster, J. V., Cunningham, K., and Fremaux, C. M., "Dynamics Modeling and Simulation of Large Transport Airplanes in Upset Conditions," *AIAA Guidance, Navigation, and Control Conference and Exhibit*, No. August, 2005.

[7]Murch, A. M. and Foster, J. V., "Recent NASA Research on Aerodynamic Modeling of Post- Stall and Spin Dynamics of Large Transport Airplanes," *45th AIAA Aerospace Sciences Meeting & Exhibit*, 2007.

[8]Abramov, N. B., Goman, M. G., and Khrabrov, A. N., "Aerodynamic Model of Transport Airplane in Extended Envelope for Simulation of Upset Recovery," *28th International Congess of the Aeronautical Sciences*, 2012.

[9]Groen, E. L., Ledegang, W., Field, J., Smaili, H., Roza, M., Fucke, L., Nooij, S. A. E., Goman, M. G., Mayrhofer, M., Zaichik, L., Grigoryev, M., and Biryukov, V., "SUPRA Enhanced Upset Recovery Simulation," *AIAA Modeling and Simulation Technologies Conference*, 2012.

[10]Goman, M. G. and Khrabrov, A. N., "State-space representation of aerodynamic characteristics of an aircraft at high angles of attack," *Astrodynamics Conference*, 1992.

[11]Fischenberg, D., "Identification of an Unsteady Aerodynamic Stall Model from Flight Test Data," 1995.

[12]Fischenberg, D. and Jategaonkar, R. V., "Identification of Aircraft Stall Behavior from Flight Test Data," *RTO SCI Symposium on System Identification for Integrated Aircraft Development and Flight Testing*, No. May, 1998.

[13]Dias, J. N., "Unsteady and Post-Stall Model Identification Using Dynamic Stall Maneuvers," , No. June, 2015, pp. 1–15.

[14]Da Ronch, A., Vallespin, D., Ghoreyshi, M., and Badcock, K. J., "Evaluation of Dynamic Derivatives Using Computational Fluid Dynamics," *AIAA Journal*, Vol. 50, No. 2, 2012, pp. 470–484.

[15]Nie, Y., Van Kampen, E., Chu, Q. P., Kier, T. M., and Looye, G., "Geometry Based Quick Aircraft Modeling Method for Upset Recovery Applications," *AIAA Modeling and Simulation Technologies Conference*, , No. January, 2015, pp. 1–16.

[16]Teng, T. T., Zhang, T. S., Liu, S., and Grant, P. R., "Representative Post-Stall Modelling of T-tailed Regional Jets and Turboprops for Upset Recovery Training," *AIAA Modeling and Simulation Technologies Conference*, , No. January, 2015.

[17]Schroeder, J. A., Bürki-Cohen, J., Shikany, D. A., Gingras, D. R., and Desrochers, P., "An Evaluation of Several Stall Models for Commercial Transport Training," *AIAA Modeling and Simulation Technology Conference*, No. January, 2014.

[18]van Horssen, L. J., Pool, D. M., and de Visser, C. C., "Aerodynamic Stall and Buffet Modeling for the Cessna Citation II based on Flight Test Data," *AIAA SciTech 2018, session: Modeling and Simulation of Air Vehicle Dynamics I*, 2018.

[19]Laban, M., *On-Line Aircraft Aerodynamic Model Identification*, Ph.D. thesis, Delft Univerity of Technology, 1994.

[20]Morelli, E. A., Cunningham, K., and Hill, M. A., "Global Aerodynamic Modeling for Stall/Upset Recovery Traning Using Efficient Piloted Flight Test Techniques," 2013.

[21]Norsett, S., Wanner, G., and Hairer, E., *Solving Ordinary Differential Equations I*, Vol. 8, 1993.

[22]Ljung, L., *System Identification: Theory for the User (Second Edition)*, 1999.

[23]van den Hoek, M. A., de Visser, C. C., and Pool, D. M., "Identification of a Cessna Citation II Model Based on Flight Test Data," *4th CEAS Specialist Conference on Guidance, Navigation & Control*, 2017.

[24]Dias, J. N., "High Angle of Attack Model Identification with Compressibility Effects," *AIAA Atmospheric Flight Mechanics Conference*, , No. January, 2015, pp. 1–15.

[25]Bonner, M. S. and Gingras, D. R., "Evaluation of the Navy's F/A-18A-D powered-approach aerodynamics model," *Modeling and Simulation Technologies Conference*, 1997.

[26]Leis, J. R. and Kramer, M. A., "The Simultaneous Solution and Sensitivity Analysis of Systems Described by Ordinary Differential Equations," *ACM Transactions on Mathematical Software (TOMS)*, Vol. 14, No. 1, 1988, pp. 45–60.

Appendices

A. Parameter Sensitivity of Solution of ODE

This Appendix presents the method used for computing the cost function gradient $\partial J(\theta, x)/\partial\theta$. Consider the example model structure from Equation 7, which results in the following parameter vector: $\theta = \begin{bmatrix}\tau_1 & \tau_2 & a_1 & \alpha^* & C_{L_0} & C_{L_\alpha} & C_{L_q}\end{bmatrix}^\mathsf{T}$.

The relevant equations are repeated for clarity:

$$J(\theta,x) = \tfrac{1}{N}\left(C_L - \hat{C}_L(\theta,x)\right)^{\mathsf{T}}\left(C_L - \hat{C}_L(\theta,x)\right) ,$$
$$\hat{C}_L(\theta,x) = C_{L_0} + C_{L_\alpha}\left(\tfrac{1+\sqrt{X}}{2}\right)^2\alpha + C_{L_q}\tfrac{q\bar{c}}{V} ,$$
$$\tau_1\tfrac{\mathrm{d}X}{\mathrm{d}t} + X = \tfrac{1}{2}\left(1 - \tanh\left[a_1\left(\alpha - \tau_2\dot{\alpha} - \alpha^*\right)\right]\right) .$$

The first four parameters in θ influence the cost function via X, the rest does not. As a result, the application of the chain rule requires a separate treatment of X-parameters and others:

$$\frac{\partial J(\theta,x)}{\partial\theta_i} = \begin{cases} \frac{\partial J}{\partial \hat{C}_L}\frac{\partial \hat{C}_L}{\partial X}\frac{\partial X}{\partial \theta_i} & \text{when} \quad \theta_i \in \{\tau_1\ \tau_2\ a_1\ \alpha^*\} \\ \frac{\partial J}{\partial \hat{C}_L}\frac{\partial \hat{C}_L}{\partial \theta_i} & \text{when} \quad \theta_i \in \{C_{L_0}\ C_{L_\alpha}\ C_{L_q}\} \end{cases} . \tag{21}$$

All the partial derivative terms in this equation are relatively straightforward to obtain using algebra, except for $\partial X/\partial\theta_i$. When using finite difference methods to compute the parameter sensitivity of a solution of an ODE (i.e., the flow separation point X), numerical issues can arise.[21] To avoid this, a different method is used instead.[26] First, Equation 2 is rewritten to the following form:

$$\tfrac{\mathrm{d}}{\mathrm{d}t}X(t,x,\theta) = \tfrac{1}{\tau_1}\left(-X + \tfrac{1}{2} - \tfrac{1}{2}\tanh\left[a_1\left(\alpha - \tau_2\dot{\alpha} - \alpha^*\right)\right]\right) \quad \text{with} \quad X(0,x,\theta) = X_0(x,\theta) . \tag{22}$$

X_0 is the static mapping from α to X, i.e., without considering dynamic effects. Equation 22 can be written as:

$$\tfrac{\mathrm{d}X(t,x,\theta)}{\mathrm{d}t} = G(X,t,x,\theta) . \tag{23}$$

Next, $\partial X/\partial\theta$, which is the partial derivative that we want to obtain, is defined as:

$$\tfrac{\partial X(t,x,\theta)}{\partial\theta} = S(t,x,\theta) . \tag{24}$$

When one takes the partial derivative of Equation 23 with respect to θ, the following result is obtained:

$$\tfrac{\partial}{\partial\theta}\tfrac{\mathrm{d}}{\mathrm{d}t}X(t,x,\theta) = \tfrac{\partial G(X,t,x,\theta)}{\partial X}\tfrac{\partial X(t,x,\theta)}{\partial\theta} + \tfrac{\partial G(X,t,x,\theta)}{\partial\theta} . \tag{25}$$

Substituting Equation 24 yields:

$$\tfrac{\mathrm{d}}{\mathrm{d}t}S(t,x,\theta) = \tfrac{\partial G(X,t,x,\theta)}{\partial X}S(t,x,\theta) + \tfrac{\partial G(X,t,x,\theta)}{\partial\theta} \quad \text{with} \quad S(0,x,\theta) = \mathbf{0} . \tag{26}$$

The terms $\partial G/\partial X$ and $\partial G/\partial\theta$ can be derived from Equation 22. A second ODE has been obtained, which can be solved numerically. The solution can be substituted into Equation 21 to complete the chain rule.

B. Results of Initial X-parameter Optimization

An important assumption is that the dependence of the optimal set of X-parameters on the selected C_L model structure is mild. When the optimization of the X-parameters is done using the initial model structure (as in Equation 7), then the results are as shown in Table 9. The parameters are clearly in the same order of magnitude, the assumption is concluded to hold.

C. Explanation for Including C_T As Regressor

The models for drag and pitch moment coefficient both contain the thrust coefficient C_T as a regressor term, since it was found that this has a strong beneficial effect on model quality. Since this might appear surprising, this Appendix presents the likely reason behind this.

First, recall that the aerodynamic force and moment coefficients, such as C_D and C_m, cannot be measured directly, but are determined based on other measurements. For this, it is required to have accurate knowledge of the engine

Table 9. Results of estimating the X-parameters using the initial model structure for C_L.

Parameter		Results				
Name	Unit	$\hat{\theta}$	Diff. w. final	θ_{lb}	θ_{ub}	$\sigma(\hat{\theta})$
τ_1	[s]	**0.4623**	+81.5%	0.001	2.00	0.4227
τ_2	[s]	**0.0212**	+20.5%	0.000	2.00	0.1049
a_1	[-]	**22.1161**	-20.1%	15.000	40.00	4.7636
α^*	[rad]	**0.2286**	+ 9.7%	0.100	0.35	0.0200

thrust. However, also the thrust cannot be measured directly. An engine model is used for computing the thrust based on signals that *are* measured, such as thrust lever setting, and atmospheric conditions. The Citation II is equipped with two Pratt & Whitney JT15D turbofans. The models that were used for these are included in the Delft University Aircraft Simulation Model and Analysis Tool (DASMAT).

It is clear that any errors in this engine model propagate into errors into the "measured" aerodynamic force and moment coefficients, and thus lead to changes in the identified model parameters. If the error in thrust would have been constant, only the bias term of the model would change. However, the thrust was not constant during the recorded stall maneuvers, which also led to a changing error in the engine thrust. As a result, the bias term cannot correct for this error. Since the thrust coefficient C_T is computed based on the same engine model, it contains the same error. Hence, because it is correlated with a pattern in the data that cannot be otherwise explained, it is beneficial to the model quality to include C_T as a regressor.

It is recommended to do research and improve the accuracy of the engine model. If that is successful, these thrust-related model terms should no longer be necessary, which would be an improvement to model simplicity.

D. Individual Model Term Contributions of C_Y, C_l, and C_n

The contributions of the individual model terms were shown in the main part of the paper only for the longitudinal model outputs (i.e., C_L, C_D, C_m). The same plots for the lateral model outputs are presented here in the Appendices, in Figures 28, 29, and 30.

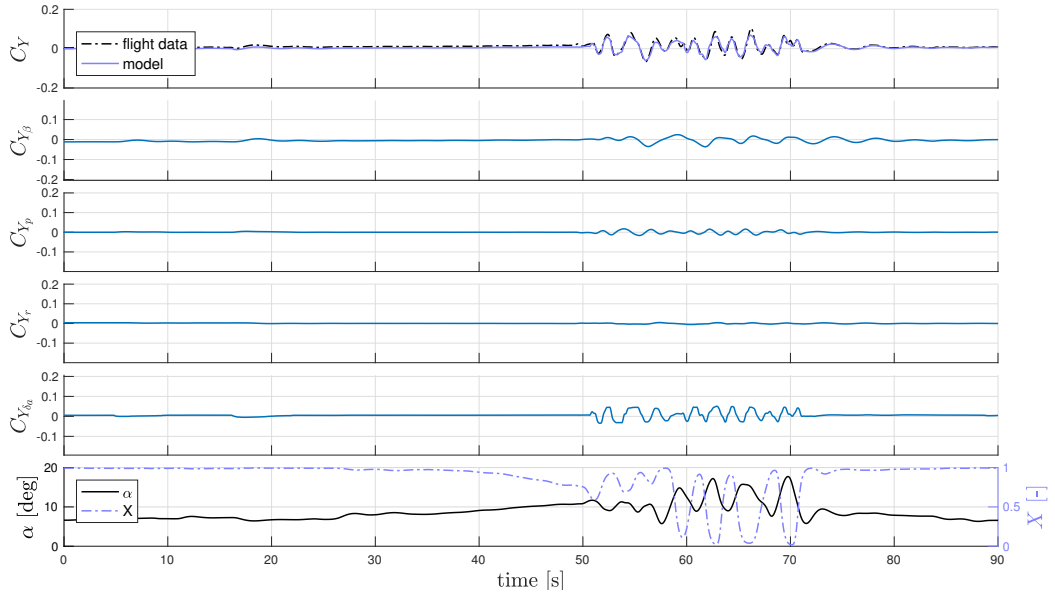

Figure 28. Example of the model term contributions of the lateral force model, example shown is data set 12 (validation).

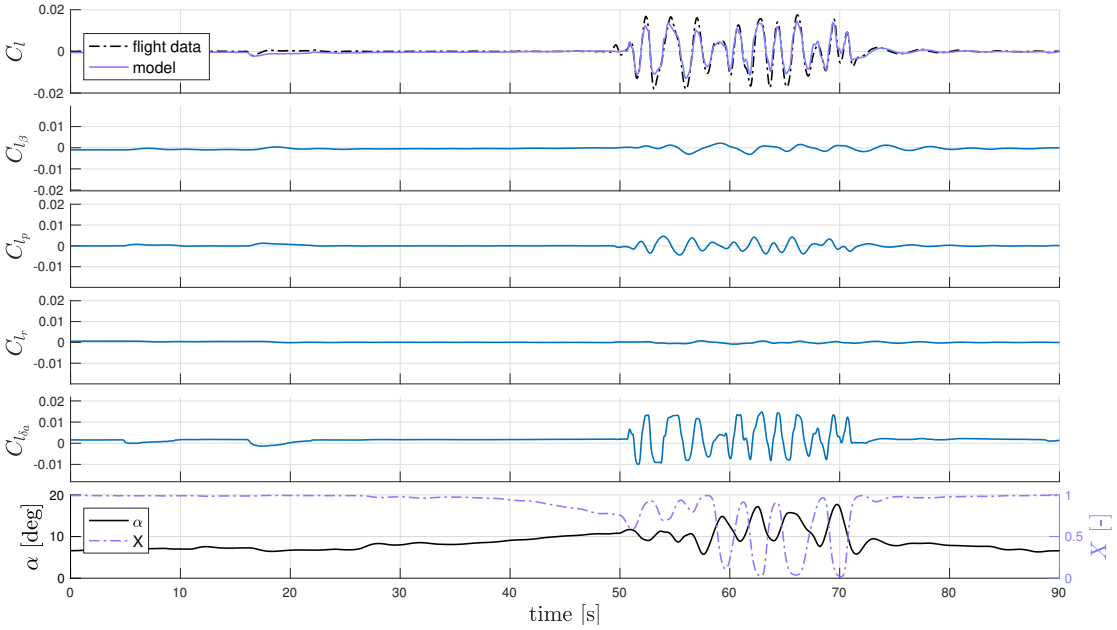

Figure 29. Example of the model term contributions of the roll moment model, example shown is data set 12 (validation).

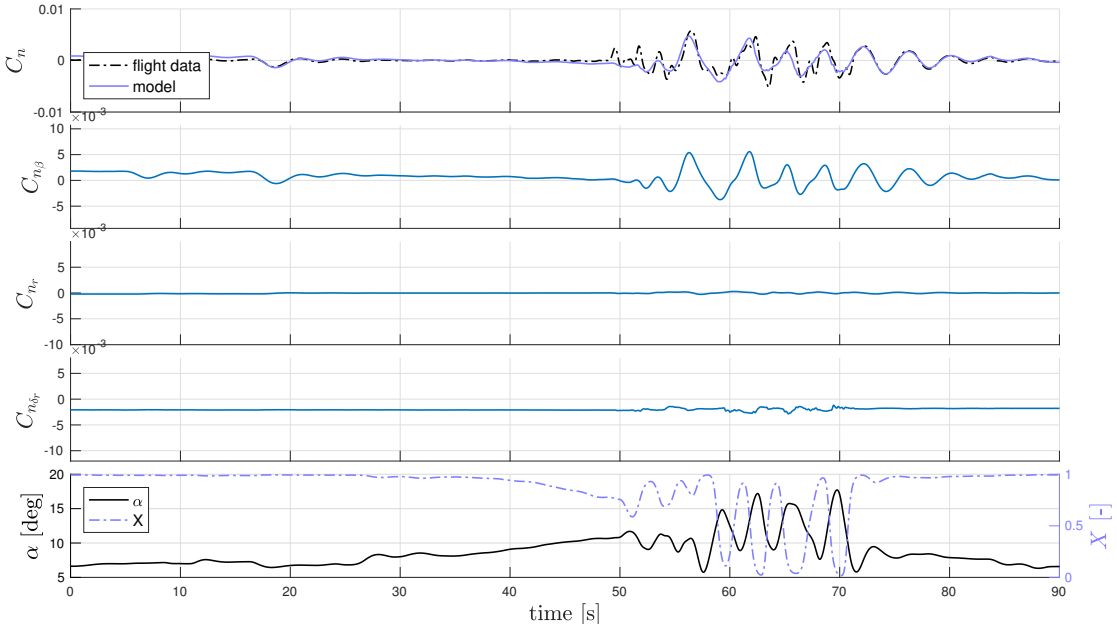

Figure 30. Example of the model term contributions of the yaw moment model, example shown is data set 12 (validation).

II

Preliminary Thesis Report

1 Introduction

Loss of control while in-flight (LOC-I) is usually defined as a significant deviation from the intended flight path, not resulting from a catastrophic system failure [34]. It can arise from a range of upset types, of which aerodynamic stall is a major candidate [38]. LOC-I currently is the largest category of fatal accidents in civil and general aviation, and the only one which is not decreasing over time [5]. Improving the type-specific stall recognition, prevention, and recovery training that pilots must receive is seen as a promising way of increasing aviation safety [11].

From March 2019, the FAA will require US airline pilots of following such stall training [20]. Due to the cost and safety issues of training in real aircraft, this will most likely take place in simulators. However, current flight simulation training devices (FSTDs) are generally not able to simulate aerodynamic stall due to limitations in their underlying flight dynamics models.

This gap has sparked new research in modeling aircraft dynamics at high angles of attack. In 2016, the FAA has released updated FTSD qualification requirements with respect to stall modeling [21]. Simulating a stall is challenging due to its highly nonlinear, unsteady, configuration-dependent, and fundamentally unpredictable nature [8]. The configuration dependence combined with FAA regulations requiring type-specific qualification indicate that a large amount of new stall models will be required by 2019. Current modeling methods rely on extensive flight test and/or wind tunnel measurement campaigns, involving large cost and complexity. This cost and complexity is seen as a barrier for the effective implementation of new pilot training.

To address these issues, a stall modeling task force was set up at the Control and Simulation department of the TU Delft Aerospace Engineering faculty. The group's goal is to develop a new method for creating stall models, that serve effective pilot stall training, at relatively low cost. The first step towards this goal is to develop a baseline stall model for the faculty's own Cessna Citation II aircraft from flight test data as a reference point. Developing such a baseline model will be the main goal of this thesis. A first effort in this area was already completed at the task force [56], this work builds on that.

Research Objective

The research objective of this thesis is formulated as: *"To identify, verify, and validate a stall model of the Cessna Citation II faculty aircraft that includes both longitudinal and lateral-directional dynamics, changes in control surface effectiveness, and dynamic effects, based on flight test data."*

This can be broken down into multiple sub-goals, which are easier to handle. The **sub-goals** of the thesis project are:

1. Gather flight data that enables the identification of the stall dynamics of a Cessna Citation II aircraft, including both longitudinal and lateral-directional terms, changes in control surface effectiveness, and unsteady effects, by designing and executing new flight tests.
2. Pre-process the flight data to obtain an optimal estimate of the aircraft state trajectory by adapting and applying an Unscented Kalman Filter, as described in [56].
3. Select a model structure that enables the representation of the desired stall characteristics, and whose parameters can be estimated with good accuracy given the available flight data.

4. Estimate the parameters of the selected model structure using a suitable parameter estimation method.
5. Verify and validate the identified stall model using flight data.
6. Integrate the newly developed stall model into the high-fidelity Citation II simulation tool DASMAT.

Research Question

The main research question of this thesis is fomulated as: *"How can a model of the stall behavior of a Cessna Citation II aircraft, including both longitudinal and lateral-directional dynamics, changes in control surface effectiveness, and dynamic effects, best be identified from flight test data?"*

Same as for the research goal, the research question can be broken down into smaller **sub-questions**. However, due to time constraints not all sub-goals of the thesis correspond to a sub-question, only those that are in the focus area.

1. What types of flight test maneuvers are suitable for identifying dynamic stall behavior, including control surface degradation?
2. What model structure is suitable for representing aircraft stall behavior, including both longitudinal and lateral-directional dynamics, changes in control surface effectiveness, and dynamic effects?
3. What parameter estimation techniques are suitable for accurately estimating the parameters of a non-linear stall model structure from flight data?

Methodology & Structure of This Report

As the main research goal of the work is to identify, verify, and validate a model, the steps that must be taken correspond to those of a general system identification framework. First, data needs to be gathered and possibly pre-processed. Then, a model structure must be chosen, and its parameters will be estimated. The result is then verified and validated, which might lead to re-visiting some of the earlier steps in case of errors. Finally, the model is implemented for the intended purpose. This structure is presented in block-diagram format in Figure 1.1. These steps correspond to the sub-goals of the thesis, and will be explained in more detail.

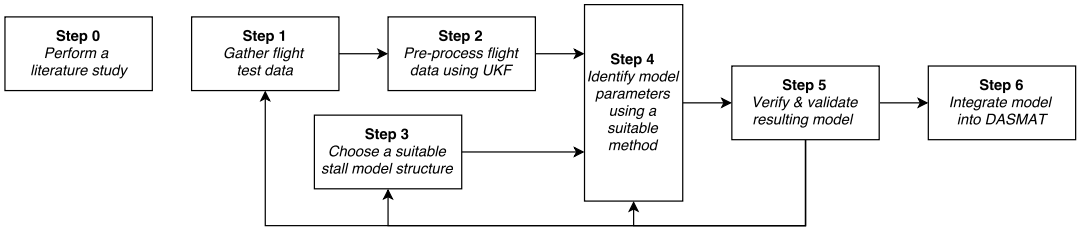

Figure 1.1: The structure of the proposed thesis research methodology

Step 0: Literature study The step that precedes the first step of the actual work is to get familiar with the body of knowledge already available on the topic of stall modeling. To that end, a literature survey was executed. Some general concepts, history, and prevailing methodologies found in stall modeling are presented in **chapter 2**.

Step 1: Gathering data The previous effort of identifying a Citation II stall model at DUT was based on a database of quasi-static stall maneuvers. This data lacked the availability of a side-slip measurement, and contained little excitation of control surfaces and dynamic terms, which prevented the identification of a full model. Therefore, new flight tests had to be be designed, planned, and executed. Details of the flight test vehicle, procedures, and maneuvers can be found in **chapter 3**.

Step 2: Pre-processing data The flight data contains measurement errors, so the real flight path of the aircraft is be unknown. To maximize the accuracy of the model, the flight data has been pre-processed to obtain the best estimate of this flight path. For this, the recommendations developed in [56] were followed

and an UKF was used. The mathematics and specific application of the UKF to this thesis are treated in **chapter 4**.

Step 3: Model structure selection A key step in system identification is to choose a suitable model structure. This is where the main focus of the thesis will be. This step involves a lot of engineering judgement, and is not a problem that can solved in closed form. **Chapter 5** presents the main building blocks from which the final stall model will be constructed.

Step 4: Parameter estimation Once the model structure is determined, its parameters must be estimated using (part of) the flight data. Both nonlinear and linear parameter optimization algorithms will be used in this thesis. Those algorithm, and the metrics used to evaluate model quality are covered in **chapter 6**.

Step 5: Verification & validation of results In order to finish the thesis work, the resulting model will have to be verified and validated. The current work has not yet reached this step, instead **chapter 7** covers an analysis of preliminary results.

Step 6: Integration As a final step in the thesis, the resulting model will be implemented in the DASMAT simulation framework used at the Control and Simulation department. DASMAT already includes many simulation models, such as a flight dynamics model for the conventional flight envelope, a thrust model, and a mass model. Moreover, it is used as an input for the department's research simulator SIMONA. This step is not yet covered by this report, and will be addressed in future updates.

2

Background & Literature Review

This chapter introduces the concept of aerodynamic stall. Next, it discusses recent regulatory developments that are relevant to the research. A list of properties which should be included in the modeling of stall is given, which represents the current industry best practices. Next is the main part of this chapter: a literature survey on the history and current state of the art in stall modeling. The chapter concludes with a short summary of the literature survey.

2.1. Aerodynamic Stall Definition

Physically, aerodynamic stall is a condition in which the flow (partially) separates from the wing of an aircraft, this phenomenon depends highly on angle of attack and Mach number. In practice, a wing is considered to be in the stall regime if its angle of attack is increased beyond the critical angle of attack (which corresponds to maximum lift). Figure 2.1 visualizes the stall progression of a typical wing and its effect on the lift it produces. Stall is characterized as highly nonlinear, unsteady, unpredictable, and configuration-dependent. For example, consider the effect of stalled wing wake on horizontal stabilizers, which is clearly dependent on aircraft geometry. Or, consider the effects of aerodynamic hysteresis on the flow field. These factors, and many others, make aerodynamic stall very challenging to predict and model accurately and effectively.

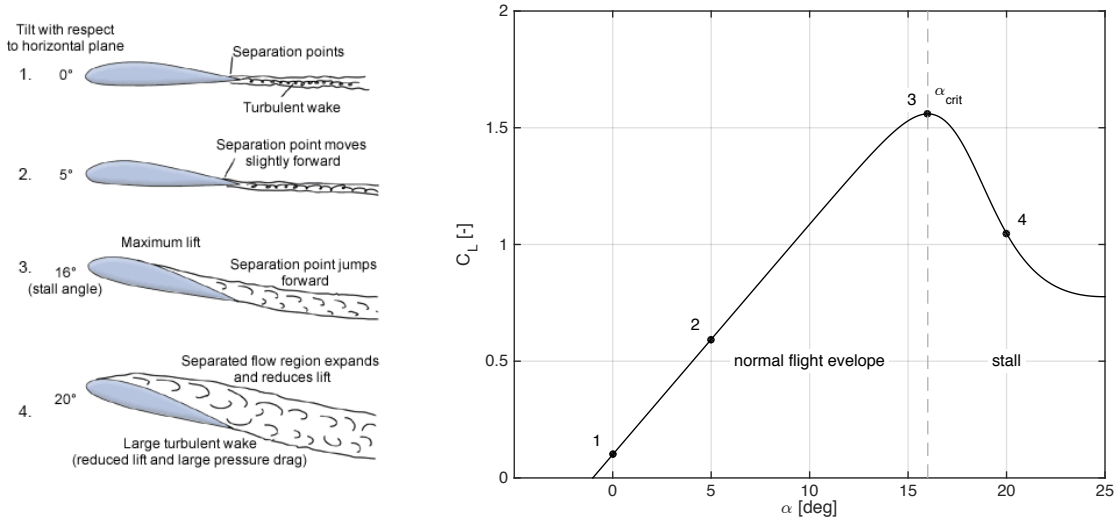

(a) Flow visualization

(b) Corresponding typica lift coefficient

Figure 2.1: Progression of trailing edge flow separation

Most wings of conventional aircraft have relatively thick and rough airfoils, resulting in a turbulent boundary layer. This type of wings, at regular angle of attack rates encountered during normal flight, experience

mainly trailing edge stall i.e separation initiates at the trailing edge and moves to the leading edge as angle of attack is increased [29].

2.2. New FAA Regulations Regarding Stall Modeling in FSTDs

In aircraft accident statistics, loss of control in-flight (LOC-I) is the number one category of fatalities in civil aviation. Figure 2.2 shows these statistics from 2006 through 2015. While new technologies have mitigated other accident categories such as controlled flight into terrain, or mid-air collisions, LOC-I has remained at a constant level. Aerodynamic stall is the biggest contributing factor to LOC-I [38], and is relevant in about 40% of cases.

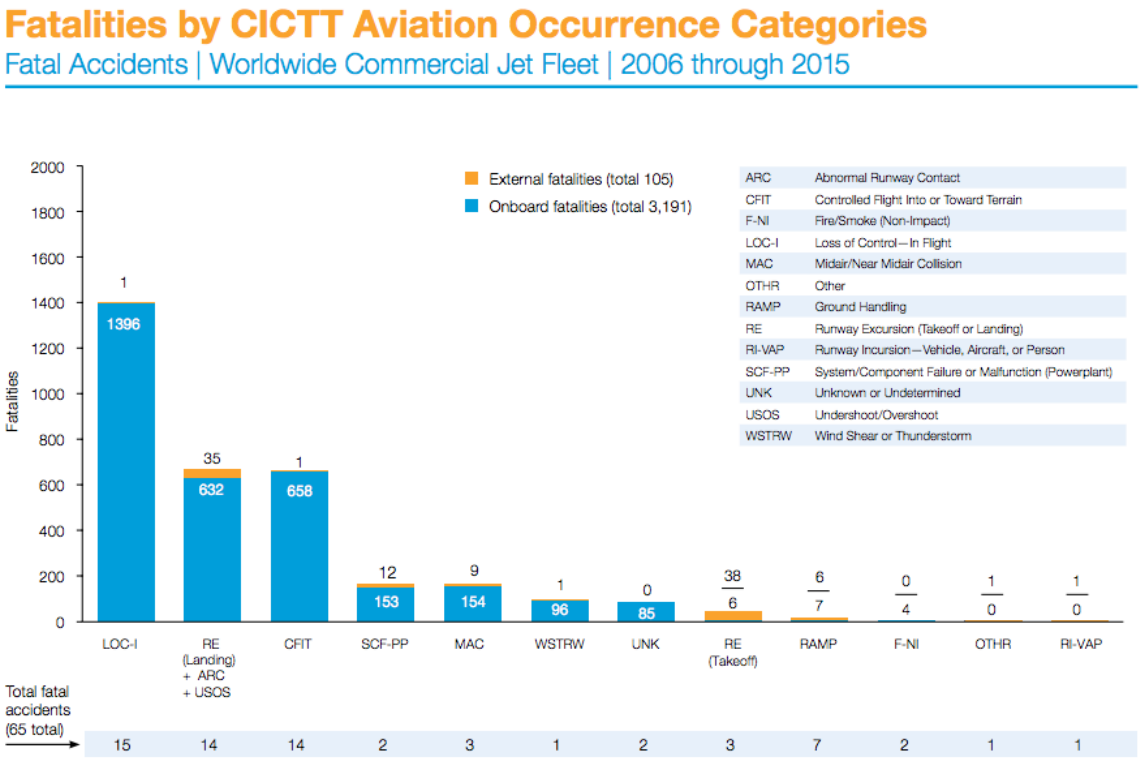

Figure 2.2: Statistics of civil aviation fatalities by category in 2006-2015, showing that LOC-I is the category that is biggest by far. Figure from [5].

As unfortunate as they are, these accidents have leant us valuable lessons. In many cases pilots did not follow the proper upset recovery procedures. Fatal accidents have resulted from upset situations from which recovery was likely to be possible. Therefore, improving pilot training is seen as an effective way to reduce LOC-I fatalities. The FAA has announced that from 2019 onwards, all civil aviation pilots need to be trained on how to properly recognize, prevent, and recover aerodynamic stall [20].

Because of cost and safety considerations, the new training will most likely take place in a flight simulation training devices (FSTDs). Current FSTDs generally cannot offer stall training. To address this, the FAA FTSD qualification requirements have also been updated [21]. According to the new additions to FAA Part 60, FTSDs should comply with the following points:

- The flight dynamics model should reflect the aircraft type-specific stall properties. These properties can be broken down into the list in section 2.3, not all properties will be equally relevant for all aircraft.
- The flight envelope of the dynamics model should enable the training tasks, with α-envelope being at least as big as the stall identification angle of attack + 10 degrees. The training tasks themselves are not defined in Part 60.
- During qualification, the simulator is evaluated using three types of stall maneuvers, i) wings-level (1g) stall entry, ii) stall entry in turning flight of >25 degrees bank (accelerated stall), and iii) stall entry in power-on conditions (only for propellor-driven aircraft).

- Each of these three maneuvers should be evaluated at least one of the following three flight conditions: a) high-altitude cruise near performance limit, in clean conditions, b) approach/landing conditions, with corresponding flaps and gear deployed, and c) second-stage climb, with different flap and gear settings than b.
- The simulated time histories are subject to a list of numerical tolerances compared to flight data. These tolerances hold up to but not beyond the stall angle of attack.
- Beyond the stall angle of attack, the time histories should be "of correct trend and magnitude" when compared to flight data.
- Separate requirements are put on the stall buffet model.
- Finally, the simulator should be subjectively rated by a subject-matter expert (SME) who is acceptable to the FAA. The SME should have extensive experience in stalling the real aircraft.

2.3. ICATEE List of Effects of Aerodynamic Stall

As can be imagined, the flow field around a complete aircraft at high angles of attack is highly complex. *Exactly* predicting and quantifying the *all* effects of a stall based on is not feasible with today's methods. However, several categories of effects are common, and give a good basis for modeling stall. The International Committee for Aviation Training in Extended Envelopes (ICATEE) has proposed a list of properties of aerodynamic stall to be modeled in future stall or post-stall flight models. These properties are listed here, and a short physical explanation is given. The characteristics of aircraft dynamics at high angles of attack are described in more detail in [8].

Degradation in lateral-directional stability Due to aerodynamic stall, static and dynamic lateral (roll motion) and directional (yaw motion) stability of the aircraft are negatively affected. This is one of the most dangerous aspects of a stall, since it can lead the aircraft to going into a spin motion from which it is hard to recover. There are numerous ways in which the lateral-directional stability is affected, some are explained here for illustrative purposes.

As can be seen in Figure 2.1, the derivative of the lift coefficient to the angle of attack C_{L_α} becomes negative in the α range following α_{crit}. This effect can make the roll damping C_{l_p} positive. In a roll the down-going wing experiences a higher local angle of attack. When $C_{L_\alpha} > 0$, this results in more lift for the down-going wing and thus a moment countering the roll motion. Hence the name, roll damping. In the stall regime, where $C_{L_\alpha} < 0$, this effect is reversed which can lead to large roll excursions.

A similar effect is seen on the effective dihedral C_{l_β}, which describes the roll response from sideslip angle. At a positive sideslip angle, the aircraft nose has rotated to the right. Due to the interaction of the wing and fuselage, the induced angle of attack on the right wing is increased. Now the sign of C_{L_α} again determines the type of response. For positive sideslip it is desirable to roll to the left, which only happens for $C_{L_\alpha} > 0$.

As a last example, the directional stability C_{n_β} can be greatly affected by stall effects. The two main contributors are the fuselage and vertical tail. Generally speaking, the fuselage has a destabilizing effect, and the tail a stabilizing one. If the vertical tail is inside a low-energy stalled wake, its effect can be greatly diminished, so that the fuselage effect can become dominating.

Degradation in control surface effectiveness At high angles of attack, turbulent or stalled wakes originating from wing, fuselage, engine, or others can impinge on the control surfaces, reducing their effectiveness. Needless to say, these effects are highly configuration-dependent. In extreme cases, control response can even be reversed. For example, consider a pilot who deflects his ailerons in order to initiate a left rolling motion while the aircraft is stalled. The right aileron then deflects downward, which can actually decrease lift due to the increase in local angle of attack. For the left wing the opposite can happen. This results in a right rolling motion, opposite to what was intended.

Changes in pitch stability For some aircraft configurations, entering a stall can result in an uncontrollable pitch-up motion. Obviously, this is highly undesirable; the first thing a pilot should do in a stall is unloading the wings by reducing angle of attack. Wings with high sweep are particularly prone to this issue. Typically, span-wise flow and upwash at the tip result in wing tips stalling first, which for swept wings moves the center of lift forward, potentially causing instability. This can be mitigated with wing fences (limit span-wise flow), wing twist (reduce the angle of attack near the tip), or increasing aspect ratio (relative move of aerodynamic center is smaller).

Another important contributor to pitch-up instability is the effect of the wing wake on the tail. The tail will move towards or away from the wing wake with changing angle of attack. The wake from an un-stalled wing will reduce the effective angle of attack due to downwash, reducing tail effectiveness. Much worse is the loss of dynamic pressure when the tail enters the wake of a stalled wing. T-tail aircraft are prone to this type of behavior. In extreme cases, it can lead to a second stable trim point at very high angle of attack. Combined with reduced elevator effectiveness, the pilot might not have enough control authority to pitch the aircraft out of the stall, a nasty situation to be in.

Stall buffet According to the Oxford dictionary, "to buffet" means "to strike repeatedly and violently", which is essentially what happens during stall and stall onset. Turbulent and separated flows impact on parts of the aircraft, resulting in significant vibrations that can be felt by pilot and passengers. It is one the most important cues that pilots use in evaluating the severity of the stalled flight condition, and therefore very important during stall training in the flight simulator [52].

Modeling the stall buffet consists of adding colored noise signals to the three orthogonal aircraft accelerations calculated by the flight dynamics when some threshold (e.g. angle of attack $\leq 10°$) is exceeded. The spectra of these noise signals can be obtained from flight test data. Since simulating stall buffet comes down to violently shaking your simulation equipment, the amplitude is often tuned down in real simulators to prevent fatigue damage to expensive equipment.

Unsteady and hysteresis effects Already in 1951, it was known that the angle of attack *rate* had a significant effect on the maximum lift a wing can produce due to flow circulation effects [25]. This effect is commonly called aerodynamic hysteresis. Furthermore, the process of flow separation is not instantaneous, hence it is subject to some dynamics. This can be imagined as that the flow needs some time to adjust after an abrupt upset. Studies have shown that including both these unsteady effects improves the model quality during dynamic maneuvers [22].

Un-commanded roll response requiring significant control deflection to counter Due to small asymmetries in geometry, propellors, atmospheric turbulences, or other disturbances; both wings never stall at exactly the same time. This creates a lift difference, resulting in a roll motion. The down-going wing then experiences a larger local angle of attack, which can deepen the local stall even further. This is called uncommanded roll-off, and occurs in each stall to greater or lesser extent. Some aircraft tend to roll in a specific direction during stall (especially propellor aircraft); others have more unpredictable behavior.

Apparent randomness or non-repeatability Because of the complex and unsteady nature of stall, small disturbances or imbalances can grow quickly and have significant effects. Such small disturbances are randomly present at all times in and around the aircraft; a prime example of this is atmospheric turbulence. This makes every stall maneuver unique in some way. This may have implications on the recovery strategy a pilot should apply: if two stall maneuvers can randomly turn out to be fundamentally different, then it may not make a lot of sense for the pilot to memorize a fixed set of actions as a recovery procedure. Instead, pilots could then be taught the underlying principles, and respond accordingly to the actual situation at hand.

Mach effects Mach number is one of the fundamental properties which a stall depends on. Due to changes in compressibility, the flow field around the wing changes. Moreover, local supersonic flows may occur during high subsonic speeds, which might drastically alter stall behavior. Generally, Mach effects are accounted for by gathering data (flight, wind tunnel, CFD) over a wide range of airspeeds, and letting the Mach number be an independent variable in the model.

2.4. A Literature Survey of Stall Modeling Research

The current section presents a literature survey of past and present research into understanding and modeling aircraft dynamics at high angles of attack. An attempt has been made to present it in chronological order, but some deviations from this are made for the sake of clarity. Next to that, parts of the section overlap with other chapter 5, but this was kept since it was the intention that this literature survey could be read as standalone.

2.4.1. Early Efforts

The early research into aircraft stability and control characteristics at high angles of attack started appearing in the 1950s and 1960s, with main contributions by NASA and the US air force [31], [7]. The majority of work considers fighter-type aircraft, which makes sense considering that it was (and still is) much more common for these aircraft to encounter the far reaches of their flight envelope. It is interesting to note that most early efforts focussed on investigating lateral-directional stability, as in [45] and [10], whereas in the period following the early efforts, the focus was on modeling longitudinal dynamics. A likely reason for this is that lateral-dynamic effects are much more complex to model mathematically, so any modeling effort would naturally begin with longitudinal terms. However, lateral-directional terms are most critical for flight safety, so gaining insights into physical flow phenomena causing instability and into configuration effects is valuable for the design of new aircraft. Some examples of design choices made for increasing directional stability at high angles of attack are given in [8].

In the 1970s, the first attempt at building a full aerodynamic model using flight test data is published in [18]. An important conclusion from this work was that due to the highly nonlinear nature of stall, experiment data does not generalize well to the entire flight envelope, so a lot of data is required for identifying a full model that is valid for the entire (extended) flight envelope. Around the same time, the same observations were made in a review of control and stability derivatives of an F-15 scaled model in [33]. In this technical note, the highly nonlinear effect of stall is visualized clearly by plots of control and stability derivatives versus either alpha or beta. Some examples are presented in Figure 2.3

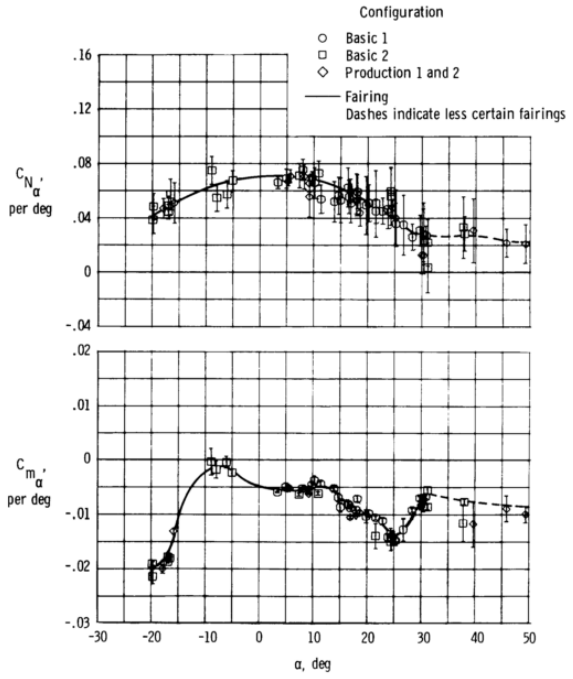

(a) Identified values of C_{N_α} and C_{m_α} plotted against α

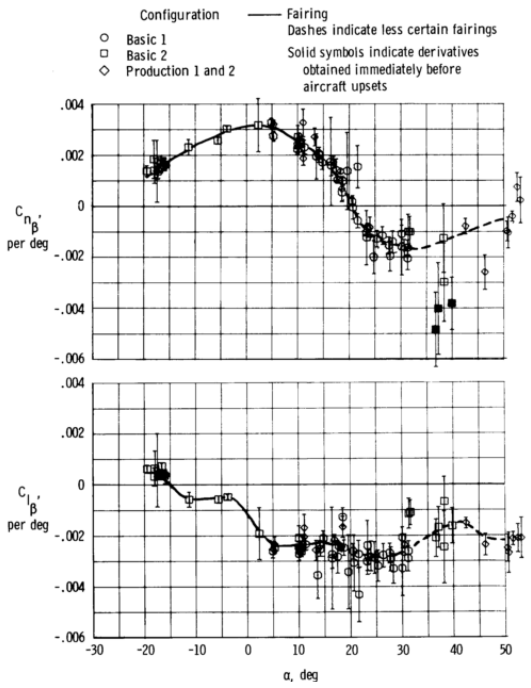

(b) Identified values of C_{n_β} and C_{l_β} plotted against α

Figure 2.3: Example figures from [33], illustrating the nonlinear nature of control and stability derivatives of a 3/8 scale model of an F-15

In the 1980s a move is seen to other aircraft types than fighters. In [9], a summary is given of research on stall and spin dynamics of general aviation aircraft, and in [54] a nonlinear model is given of a sailplane. The latter paper presents a modeling approach based on first partitioning flight test data based on alpha and beta, and then fitting a conventional linear-in-the-parameters-type polynomial model to each data bin. A work using a similar method is [4]. Although this data partitioning approach was succesful in explaining the large nonlinearities, data again proved to be a problem as each data bin should contain proper excitation of all aircraft states and control surfaces. Following the described period of early efforts, several distinct themes can be identified in the research into stall modeling.

2.4.2. Kirchoff's Theory of Flow Separation

The first attempt at describing the nonlinear, dynamic, and time-dependent phenomena caused by stall with a relatively simple model structure was published in [29] in the early 1990s. This research was inspired by previous work on rotorcraft propellor blades and is based on the assumption that the effects of flow separation on airfoil lift can be described by Kirchoff's theory of flow separation. This theory states that the relation between lift coefficient and the separation state of the flow X can be approximated by the nonlinear relation:

$$C_L = C_{L_\alpha}\left(\frac{1+\sqrt{X}}{2}\right)^2 \alpha \,. \tag{2.1}$$

X can take values on a range from 1 (flow fully attached) to 0 (flow fully separated), as is illustrated in Figure 2.4. The dynamics of X itself are also nonlinear and different for each aircraft configuration, but experiments have shown that they can be described by Equation 2.2, using only four parameters. These can be estimated from wind tunnel or flight test data. The dynamics are split in an unsteady part, with parameters τ_1 and τ_2, and an expression for the steady flow separation point. This model and its parameters, are explained in more detail in subsection 5.2.1.

$$\begin{aligned} \frac{dX}{dt} &= f(t, X, \alpha, \dot{\alpha}) \,. \\ \tau_1 \frac{dX}{dt} + X &= X_0(\alpha - \tau_2 \dot{\alpha}) \,. \\ X_0 &= \frac{1}{2}(1 - \tanh(a_1 \cdot (\alpha - \alpha^*))) \end{aligned} \tag{2.2}$$

In [22] the parameters of this model were estimated for two transport aircraft using flight data of quasi-steady and dynamic stall maneuvers. The model was then used to simulate the longitudinal dynamics of the aircraft during stall. A validation step showed good agreement between model output and flight data, especially when the parameters were estimated from dynamic stall maoeuvres. An extension to include lateral dynamics is presented in [53] and [23]. Basically, these papers separate the lift and drag contributions of the left and right wings to describe roll and yaw motions caused by flow separation. In recent years, [15] and [16] present another application of this method.

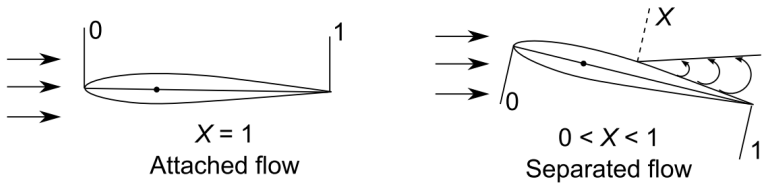

Figure 2.4: Illustration of internal variable X (figure from [15])

The power of this approach is that it effectively captures the nonlinear relation between α and C_L via the use of X. By doing this, prior knowledge is put into the model i.e. from years of wind tunnel research, it is known that the relation between flow separation point and lift is approximately as in Equations 2.1 and 2.2. Because of that, this method is physically meaningful and simple in the sense that it requires only four extra parameters to describe a complicated nonlinear mapping.

However, it is not the only way to capture this relation. Any nonlinear model with enough approximation power is theoretically able to do this, see for example the new developments in spline theory in [14]. Nevertheless, the question remains whether fitting such a model is feasible given the limited data available. Including as much previously available information in a modeling effort seems wise, which is an argument for using Kirchoff's theory. Furthermore, X could be used to help add new model terms that describe changes in stability or control surface effectiveness. So far, the models in [23] etc. did not contain any of these terms, which indicates possible areas of improvement.

Another issue, albeit perhaps a less relevant one, is that the current form of the model can never be valid for angles of attack in the very deep stall regime. Figure 2.5 shows that due to the definition in Equation 2.1,

once the flow is fully stalled i.e. $X = 0$, C_L becomes a nondecreasing function of α. This clearly is unphysical, so model is not valid for very high angles of attack, which might be an issue depending on the intended use of the model.

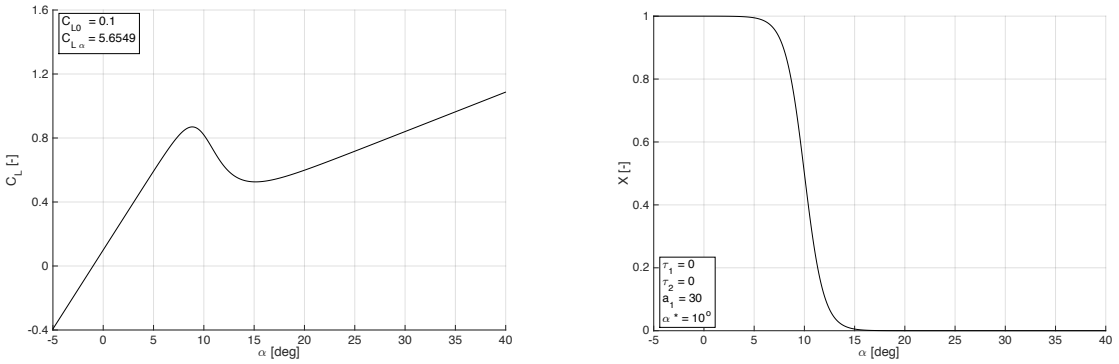

(a) Example lift coefficient

(b) Example flow separation variable

Figure 2.5: Illustration of non-physical behavior of the model based on Kirchoff's theory of flow separation.

2.4.3. Other Extensions to Aerodynamic Model Equations

As stated in the previous section, any model structure that has enough approximation power should be able to describe the high-angle-of-attack dynamics of any aircraft. In the research into Kirchoff's theory of flow separation, approximation power was gained by adding Equation 2.1 to the conventional aerodynamic model equations. However, other extensions are also possible. The conventional method is to use linear polynomials as the aerodynamic model equations for each flight condition, and make the parameters of these models depend on flight condition. Usually these models use only terms up to the first order Taylor series of the set of independent variables. For example, if C_m is to be modeled using only α, $\tilde{q}$, and δ_e in the pool of available explanatory variables, the model would be of the following form:

$$C_m = C_{m_0} + C_{m_\alpha}\alpha + C_{m_q}\tilde{q} + C_{m_{\delta_e}}\delta_e \tag{2.3}$$

Implicit in this model is the assumption that aerodynamic derivatives such as C_{m_α} are constant. Clearly, this only holds for limited ranges of α. By allowing higher order terms of the Taylor expansion to be included, nonlinearities and dependencies between explanatory variables can be explained. This can extend the range on which the model is valid. Consider the same example, but now allow the use of terms up to order two. The model would then take the form:

$$C_L = C_{m_0} + C_{m_\alpha}\alpha + C_{m_q}\tilde{q} + C_{m_{\delta_e}}\delta_e + C_{m_{\alpha^2}}\alpha^2 + C_{m_{q^2}}\tilde{q}^2 + C_{m_{\delta_e^2}}\delta_e^2 + C_{m_{\alpha q}}\alpha\tilde{q} + C_{m_{\alpha\delta_e}}\alpha\delta_e + C_{m_{q\delta_e}}\tilde{q}\delta_e \tag{2.4}$$

Of course, as the order of terms increases, the probability of a term (e.g. $\alpha\delta_e$) actually being useful in explaining the dynamics reduces. Selection of which model terms to include is a nontrivial task. In [41], this is addressed by orthogonalizing the model terms with respect to each other. The explanatory power of each model term can then be investigated independently, although the order of orthogonalization still influences the results.

In this paper, and in [36], another method is the addition of simple univariate spline functions of the explanatory variables into the pool of explanatory variables. An example spline function is given by:

$$(\alpha - \alpha_i)_+^m = \begin{cases} (\alpha - \alpha_i)^m & \text{if } \alpha > \alpha_i \\ 0 & \text{otherwise} \end{cases} \tag{2.5}$$

The terms in Equation 2.4 are global terms i.e. they cover the whole range of explanatory variables. Hence, it is not possible to make local adjustments without influencing the whole model domain, which is undesirable. This also makes it more likely that the model will require higher order terms to cope with strong local nonlinearities, also this leads to bad generalization behavior. By adding spline terms, the model can be adjusted locally without having to introduce higher order terms.

The downside of the method presented in this section is that it ignores previous knowledge, such as in Equations 2.1-2.2. Furthermore the current formulation does not contain unsteady effects, although these could potentially be added in the form:

$$\tau \frac{dC_m}{dt} + C_m = C_{m,\text{steady}}$$

where $C_{m,\text{st}}$ is for instance the right side of Equation 2.4. Another way of including time-dependent effects is to also include the time derivatives of the explanatory variables as candidate regressor, e.g. also train the model on terms such as $\dot{\alpha}$ and/or $\dot{\beta}$.

The method also has large potential benefits. The model form is linear in the parameters, which ensures finding a set of parameters that is globally optimal, and greatly speeds up the computational burden of parameter estimation. A second advantage is that the generation and selection of model terms can be fully automated if the candidate pool, maximum model order, and some threshold of explanatory performance are set. In conclusion, this method is a more general approach than using Kirchoff's theory of flow separation. Combinations of both methods might offer benefits.

2.4.4. Application of Fighter Methods to Civil Aircraft

In 1998, the Commercial Aviation Safety Team (CAST) was founded in the USA with the goal of reducing aviation fatalities by 80% in 10 years. To achieve this, the NASA Aviation Safety Program (AvSP) was launched in 2000, a partnership between the Federal Aviation Authority (FAA), Department of Defence (DoD), and aviation industry. As part of the AvSP, research has been done to develop aerodynamic modeling methods for the dynamics of large transport airliners in upset conditions. This has led to a series of publications, see [6], [12], [24], [43], and [44].

Traditional methods for modeling the dynamics of civil aircraft are based on obtaining static effects via wind tunnel tests, and dynamic effects via small-amplitude flight test maneuvers. These models are normally only validated for the normal flight envelope, but accident investigations showed this is often exceeded during loss-of-control events. The conclusion was that traditional models were not suitable for predicting post-stall and spin dynamics. After analyzing loss-of-control motions of civil aircraft, it was found that they were more similar to those of high-performance aircraft (i.e. fighters) than previously thought. This led to methods designed for the latter, which had been successful at describing fighter spin dynamics for many years, being also applied to civil aircraft.

The methods derived from those of high-performance aircraft are based on extensive wind tunnel testing. Like traditional methods, static effects are also found from static wind tunnel tests. However, dynamic effects are identified differently. An important assumption is that data from rotary balance tests, and forced oscillation test can be combined vectorially to obtain the total dynamic response. Even though these two tests are fundamentally different, and this combination poses numerous challenges, good results have been obtained.

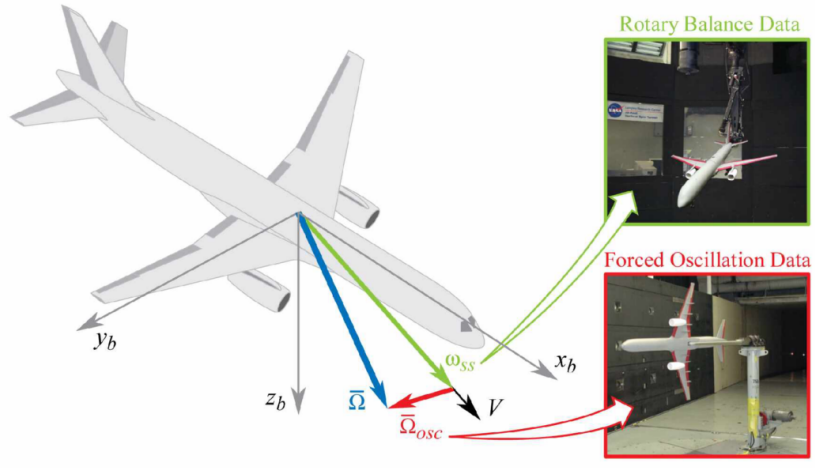

Figure 2.6: Decomposition of total aircraft angular rate vector into steady-state and oscillatory components (figure from [44])

Data from the rotary balance tests represent aircraft responses during coordinated turns, in which the vector of rotation lies close to the velocity vector. Rotary balance tests do exactly this: an aircraft model is

moved with a rotation vector that is parallel to the free stream velocity. Angle of attack/sideslip, rotation rate, and control surface deflections are varied. The associated rotation is called the steady-state rotation ω_{ss}.

Forced oscillation tests involve moving the model in a sinusoidal way along its body pitch, roll, and yaw axes, and represent dynamic responses from uncoordinated turns. Angle of attack/sideslip, oscillation amplitude/frequency, and possibly control surface deflections are varied. The associated rotation is called the oscillatory rotation ω_{osc}. See Figure 2.6 for an illustration of how the total aircraft angular rate vector can be factorized into ω_{ss} and ω_{osc}.

The databases which result from these tests are combined by factoring the total aircraft rotation vector into a steady-state rotation ω_{ss} and an oscillatory rotation $\omega_{\text{osc}} = \begin{bmatrix} p_{\text{osc}} & q_{\text{osc}} & r_{\text{osc}} \end{bmatrix}^T$. This results in the following model structure:

$$\begin{aligned} C_i &= C_{i,\text{static}}(\alpha,\beta) + \Delta C_{i,\delta}(\alpha,\beta,\delta) + \Delta C_{i,q_{\text{osc}}}(\alpha,q_{osc}) + \Delta C_{i,\omega_{\text{ss}}}(\alpha,\beta,\omega_{\text{ss}}) \\ C_j &= C_{j,\text{static}}(\alpha,\beta) + \Delta C_{j,\delta}(\alpha,\beta,\delta) + \Delta C_{j,p_{\text{osc}}}(\alpha,p_{\text{osc}}) + C_{j,r_{\text{osc}}}(\alpha,r_{\text{osc}}) + \Delta C_{j,\omega_{\text{ss}}}(\alpha,\beta,\omega_{\text{ss}}) \end{aligned} \tag{2.6}$$

where $i = N,T,m$, $j = Y,l,n$, and $\delta = [\delta_a \;\; \delta_e \;\; \delta_r]^T$. Factoring out the aircraft rotation vector into a steady-state and an oscillatory rotation is non-trivial, and can be done in infinitely many ways. There are several proposed methods to do this, these are explained in detail in [44], where it is also shown that each leads to different predicted spin dynamics. As an example, the so-called "direct resolution" method is given in Equation 2.7. Direct resolution is considered one of the simplest mechanization methods.

$$\begin{aligned} \omega_{ss} &= p_b\cos\alpha\cos\beta + q_b\sin\beta + r_b\sin\alpha\cos\beta \\ p_{osc} &= p_b - \omega_{ss}\cos\alpha\cos\beta \\ q_{osc} &= q_b - \omega_{ss}\sin\beta \\ r_{osc} &= r_b - \omega_{ss}\sin\alpha\cos\beta \end{aligned} \tag{2.7}$$

An approach essentially equivalent as described here was taken by the European SUPRA project (Simulation of Upset Recovery in Aviation). SUPRA was part of the 7th European Framework Programme and ran from 2009 to 2012. Its goal was to enhance flight simulation capabilities for upset recovery training of large civil aircraft by improving 1) aerodynamic modeling capabilities in the envelope beyond stall [2], [3], [1]; and 2) motion cueing solutions for motion-base simulators [30], [48]. The final report summary can be found in [19] (unfortunately, the project website supra.aero is offline).

The SUPRA project added on the stall modeling work done at NASA mainly in two ways. First, it adds unsteady aerodynamics terms to the model using a simple additional term. Second, it uses complementary CFD analysis to generate more data and help in verifying model output.

2.4.5. Founding of ICATEE

In 2009, the Royal Aeronautical Society hosted a conference fully devoted to high angle-of-attack flight dynamics modeling titled "Flight Simulation – Towards the Edge of the Envelope". It was clear that there was a growing need for better upset prevention and recovery training, and thus more research into this area. An international working group was formed to specifically address this issue: the **International Committee for Aviation Training in Extended Envelopes (ICATEE)**. The group is chaired by Dr. Sunjoo Advani, and currently has about eighty members including airframe manufacturers, airlines, authorities, simulator manufacturers, training providers, and research institutes. Section 2.3 presents the list of properties of aerodynamic stall that the ICATEE recommends to include in a model. These recommendations have been taken over in the new regulations by the FAA.

2.4.6. Bihrle Applied Research

One name that pops up frequently when reading literature on modeling aerodynamic stall is the one of Bihrle Applied Research (BAR), the research company of Bill Bihrle Jr. Early work done by BAR considered the use of simulation as a support tool for high-angle-of-attack flight testing [51] and explains the process of augmentating the aerodynamic database of high performance fighter-type aircraft [50], [35], [17]. First, these papers conclude that it is possible to augment existing aerodynamic models that are only valid for the normal flight envelope, and that the updated model output can have a high correlation with test data. Second, they show that gathering aerodynamic data for the extended (post-stall) flight envelope in wind tunnel experiments is a good approach.

Later papers approach the problem of modeling stall and post-stall aircraft behavior more from the perspective of pilot training. Reference [26] describes the problems with the current FSTDs relating to stall and how to address them. In [28] an argument is made for updating regulations, as it is shown that the problems with FSTDs can directly be related to the FAA and JAR requirements of that time.

A recent paper from 2012 [27] is a summary of all this. It builds the case why high-angle-of-attack aerodynamics cannot be represented using conventional linear modeling methods, using several examples. It then goes on to argue that in order to represent the stall dynamics with high fidelity, the advanced nonlinear modeling used for fighter aircraft is needed. They also argue that for this modeling method to work, wind tunnel test campaigns are needed.

Finally, in [27] the (now updated) FAA regulations are considered. These require that aircraft responses should be "of correct trend and magnitude", as evaluated by a subject matter expert, which already gives some leeway. Next, the evaluation of correctness is done based on several pre-defined maneuvers, which can be found in the Qualification Test Guide (QTG). These maneuvers only cover a limited part of the flight envelope. This means that by regulation, the quality of the entire simulator stall dynamics model is evaluated subjectively on only a small part of the envelope. While making the qualification process easier, this does raise the question on whether it results in adequate simulators. This question is left unanswered; and is also one of the motivating factors of the current research.

2.4.7. Recent Developments

In recent years, the interest in stall modeling has gained momentum, likely due to the upcoming regulations stating that pilots must receive simulator stall training. What can be seen is that research has become more diverse, and attempts to take a more pragmatic approach, i.e. the focus lies on developing a stall model of sufficient fidelity for simulator-based stall training, with a minimum of resources. This section briefly addresses several of these new efforts.

In [13] dynamic stability derivatives up to very large angles of attack are determined used CFD analysis. They claim a good agreement with experimental data. The potential upsides of accurate CFD procedures are obvious: full-scale geometries can be tested, no safety issues, and significantly lower costs.

The training aspect of stall modeling is covered in [52]. It explains research into the effect of stall model fidelity on pilot training. Even though a large group of participants was evaluated, there were not many differences in training caused by varying model fidelity. The experiment also included a surprise stall scenario, and despite being briefed on the correct recovery procedure short beforehand, only a quarter of test subjects strictly followed the proper procedures. This finding once again emphasizes the need for proper stall training.

Two works of generating stall models based on aircraft geometry are given in [46] and [55]. The first uses an empirical approach based on aircraft geometry to arrive at a base model, and uses vortex-lattice methods to enhance it. The second work focusses on post-stall modeling of a T-tailed regional jet or turboprop based on configuration. Tools such as these could offer a simple and quick method of arriving at a basic model, which might already be sufficient for pilot training.

2.5. Chapter Summary

Aerodynamic stall is a highly nonlinear, unsteady flight condition and is currently one of the most important contributors to fatalities in civil aviation. To address this, new regulations have been announced: all US commercial pilots need to receive stall training from 2019 onwards. Training is expected to take place in flight simulation training devices (FSTDs). As current FTSDs do not support stall simulation, this is an open research field. The International Committee for Aviation Training in Extended Envelopes (ICATEE) has proposed a list of stall properties that FSTDs should be able to replicate, depending on aircraft type.

1. Degradation in static/dynamic lateral-directional stability
2. Degradation in control surface effectiveness (pitch, yaw, roll)
3. Changes in pitch stability
4. Stall buffet
5. Unsteady and hysteresis effects
6. Un-commanded roll response
7. Apparent randomness
8. Mach effects

The current state of the art in modeling high-angle-of-attack aircraft dynamics is based on experience with modeling fighter aircraft spin dynamics. This approach heavily relies on extensive wind tunnel testing

campaigns. A second approach lies closer to traditional aerodynamic modeling. It attempts to explain the nonlinearities caused by stall by adding terms based on Kirchoff's theory of flow separation. Alternatives or extensions of this second method lie in adding additional terms which are combinations of explanatory variables or simple splines.

While having very accurate models will always help in some way, the question remains what level of fidelity is needed for effective pilot training. So far, the investigated effect of model fidelity level on training is not clear yet. Recent stall modeling developments show a more pragmatic approach, attempting to quickly and cheaply arrive at a basic model.

3

Flight Test Experiments

The current chapter describes the flight test experiments that were conducted to gather the data used in this thesis. First, the test aircraft and its systems are shown. After that, the flight test design is explained. Last, some notes and visualizations of the results of the flight tests are given.

Figure 3.1: A picture of the PH-LAB laboratory aircraft of DUT and NLR, note that the air data boom is not installed in this picture

3.1. Test Aircraft and FTIS

Delft University of Technology and the Netherlands Aerospace Laboratory (NLR) collaboratively own a Cessna Citation II, with registration code PH-LAB, to execute flight tests that support their research goals. It is is business jet type aircraft with un-swept wings, twin fuselage-mounted jet engines, and a cruciform tail (i.e. the horizontal tail intersects the vertical tail somewhat in the middle). Figure 3.1 gives an impression of what the aircraft looks like. Figure 3.2 shows the aircraft schematically, and Table 3.1 presents the aircraft dimensions and mass properties in more detail.

Table 3.1: Mass & dimensions

Dimensions	
b	15.9 m
$\bar{c}$	2.09 m
S	30.0 m^2
Mass and inertia	
m	4,157 kg
I_{xx}	12,392 kgm^2
I_{yy}	31,501 kgm^2
I_{zz}	41,908 kgm^2
I_{xz}	2,252.2 kgm^2

The PH-LAB is equipped with an advanced flight test instrumentation system (FTIS) that has available a range of sensors signals and logs them in a data file during flight. Additionally, an air data boom with an α and β-vane was installed on the nose of the aircraft. The dimensions of the air data boom vanes are given in Table 3.3. A procedure is available that calculates the c.g. location based on weight balance tests, payload

mass, and fuel burn. The end result of all this, is that obtaining calibrated measurements from flight tests is quite user-friendly, and less prone to errors. Table 3.2 lists all measured signals that were used.

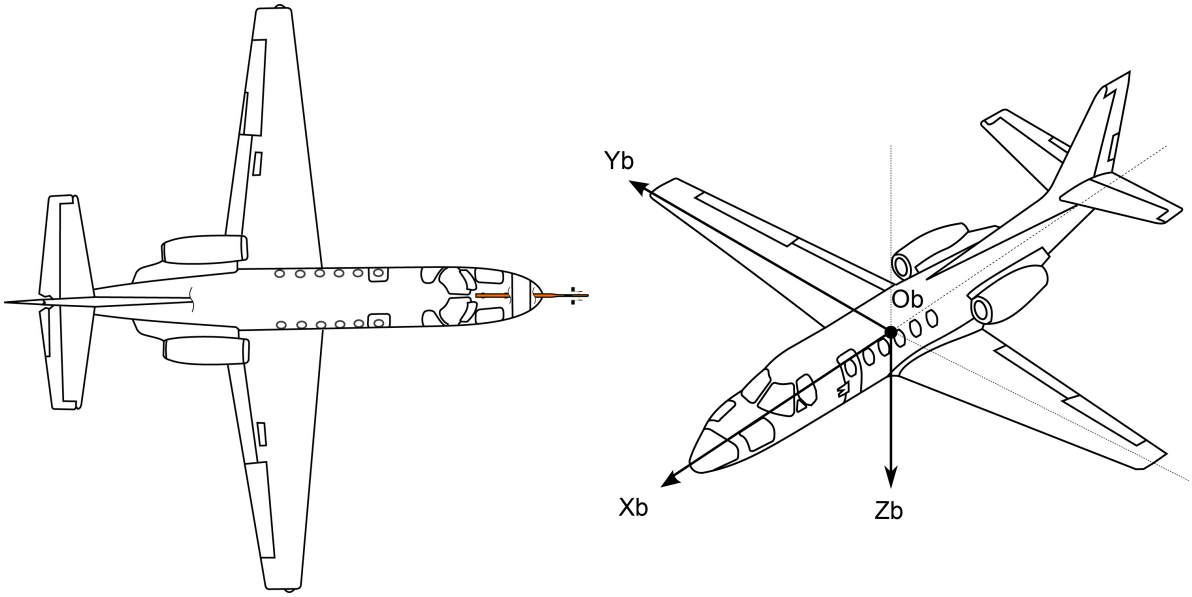

Figure 3.2: Schematic views of the PH-LAB, including the body-fixed reference frame axes definition

3.2. Flight Test Design

This section presents flight tests themselves, starting with a description of their objective; i.e. what would be desirable if safety, cost, and time were no constraints. Next, the maneuvers themselves are briefly described. For more details on the flight test procedures, please refer to Appendix D, where one of the flight test cards that was used is included as an example.

3.2.1. Objectives For Flight Tests

The flight test objectives were mainly based on two sources. First, previous experience at the research group with stall modeling led to a series of recommendations. This prior modeling effort used a set of recorded stall maneuvers, which was already available. This data was not gathered with the goal of stall modeling, so it was not ideal. The most important recommendations were: i) the availability of a sideslip measurement to explain lateral effects, ii) to record dynamic stall maneuvers, and iii) to excite control surfaces to investigate reduced control effectiveness during stall.

The second source is the FAA simulator qualification requirements document [21]. These provide guidance on what properties of stalls are to be included in a stall model. Next to that, this document explains in detail which maneuvers need to be evaluated during the qualification process. Including this type of maneuver in the flight tests makes sense, as it enables the (partial) validation of the model according to FAA standards.

When the objectives from above two sources are combined, in the ideal case the flight tests would satisfy the following list of requirements.

- Fly two types of stall maneuvers, namely:
  1. **wing-level (1g) stalls**
  2. **accelerated stalls** (bank angle of > 25 deg)
- Fly each of these two stall maneuvers in three conditions:
  1. **high altitude** (near performance limit altitude, clean)
  2. **approach/landing** (corresponding flaps, gear down)
  3. **second-stage climb** (flaps other than approach/landing, gear up)
- Dynamically excite the aircraft, such that transient and unsteady effects can be estimated from the data, and such that variables that normally are highly correlated (such as $\dot{\alpha}$ and q) are sufficiently uncoupled.

- Have an accurate measurement of all relevant state and input signals, including angle of attack and angle of sideslip.
- Both before and during stall, sufficiently excite control surfaces δ_a, δ_e, and δ_r, and combinations of these in an uncorrelated way.
- Ensure that the flight envelope is sufficiently covered by the recorded maneuvers so that the model can be identified and validated for all relevant flight conditions.
- Gather sufficient repetitions of each maneuver such that model overfitting is no problem and enough data is left for model validation.

3.2.2. Maneuver Descriptions

After discussing the above desires with the test pilots of the PH-LAB, two types of maneuvers were prepared. Each could then be executed with or without perturbations on the control inputs, and at different flight conditions. The following paragraphs explain the maneuvers and their execution. Due to cost and time constraints, it was decided to execute all maneuvers in clean conditions. Please see Appendix D for an example flight test card.

Wing-level (1g) stall This maneuver consists of establishing trimmed, level flight, and reducing airspeed at 1 kts/s until the aircraft stalls. The pilot then attempts to hold the stall for a few moments, before recovering.

Accelerated stall at 30 or 45 deg bank After establishing trimmed and level flight, the pilot rolls the aircraft to the desired bank angle and applies pitch up to maintain altitude. After that, airspeed is reduced at 1 kts/s until the aircraft stalls. Bank angles of 30 and 45 deg correspond to 1.1g and 1.4g respectively.

Control surface perturbations (AKA "wiggle") During some of the maneuvers, the pilots applied semi-random perturbations to the controls. Based on the maneuver description in [41], the objective of these perturbations was to apply as wide a frequency spectrum as possible, and with amplitudes such that the aircraft attitude does divert too much from the desired stall condition. During flight, a practical way to implement this was to let one pilot control the elevators by holding on to the steering column, and the other pilot controlled ailerons and rudder. This reduced individual pilot workload, and increased the likelihood that the control signals were uncorrelated with each other.

Table 3.2: Measured signals in-flight

Signal name	Update [Hz]	σ^2 (var)	Unit	Source
x	1.0	1.1e-2	m	GPS
y	1.0	1.1e-0	m	GPS
h	1.0	2.2e-2	m	GPS
$\dot{x}$	1.0	2.3e-5	m/s	GPS
$\dot{y}$	1.0	2.4e-5	m/s	GPS
$\dot{h}$	1.0	1.0e-4	m/s	GPS
ϕ	52.1	1.6e-4	deg	AHRS
θ	52.1	2.6e-5	deg	AHRS
ψ	52.1	1.1e-4	deg	AHRS
V_{TAS}	16.0	4.8e-2	kt/s	DADC
α_v	100.0	2.5e-2	deg	synchro
β_v	100.0	1.2e-2	deg	synchro
A_x	52.1	3.9e-5	m/s^2	AHRS
A_y	52.1	3.8e-4	m/s^2	AHRS
A_z	52.1	2.7e-3	m/s^2	AHRS
p	52.1	5.2e-2	deg/s	AHRS
q	52.1	8.5e-3	deg/s	AHRS
r	52.1	3.1e-3	deg/s	AHRS
δ_a	100.0	8.1e-4	deg	synchro
δ_e	100.0	8.2e-3	deg	synchro
δ_r	100.0	2.3e-3	deg	synchro

Table 3.3: Air data boom dimensions w.r.t. datum line

Dimension	Description	Dimension [inch]
x_α	x-position of α vane	-27.5
z_α	z-position of α vane	128.5
x_β	x-position of β vane	-16.3
z_β	z-position of β vane	128.5

3.3. Notes on the Flight Tests

In total, data was recorded of 37 stall maneuvers, of which 34 were in clean conditions. About half the maneuvers were wing-level (1g) stalls, the rest were accelerated. During flight it became clear that if the pilots were to keep the aircraft stalled for more than a moment, control surface deflections are always necessary. Therefore, the distinction between "wiggle" and "no wiggle" is not clear-cut: all stalls contained some control surface deflections. This was not seen as a problem, as this only increased the information contained in the data sets.

Furthermore, the stall behavior of the Cessna Citation II that was seen during the flight tests was generally considered very benign and forgiving by all persons on board. It required significant excitation of control surfaces to keep it in the stall, as the aircraft had a strong tendency to restore itself. Also while in stall, there there was enough time and control surface effectiveness to control the aircraft.

4

Flight Path Reconstruction

The current chapter describes the flight path reconstruction (FPR) techniques used in this thesis. The work builds further on previous research done at Delft University of Technology, in the sense that the Unscented Kalman Filter (UKF) implementation of [56] is used, with small adaptations. Flight path reconstruction is necessary since not all aircraft states needed for the parameter estimation can be measured directly. Moreover, those variables that *can* be measured are subject to sensor bias and noise. FPR aims to address these issues; by combining several measurements with knowledge of the system dynamics, a better estimate of the aircraft states can be obtained.

First the implementation of the UKF is described. Next, the full navigation and observation equations that describe the system dynamics and measurement prediction are given. After that it is shown that some states need to be removed due to observability issues. Finally, some preliminary results are given to indicate the quality of the FPR.

4.1. Unscented Kalman Filter

The Kalman filter is a widely-used method for reconstructing the aircraft state history from raw flight data. Its basic idea is to recursively provide an optimal state estimate based on the previous estimate, knowledge of the system dynamics, and the current output measurement. There are other methods for FPR, each has certain strengths. Moreover, there are multiple variations of the Kalman filter. Making a choice from all these is not an easy task. In [56] a thorough analysis of multiple methods for FPR is presented, and the UKF is appointed as best option. In this research, that recommendation is followed since the flight test vehicle is the same, so repeating the analysis would lead to double work. This also led to more time being available for other parts of this thesis, e.g. gathering more data via flight tests, implementing new parameter estimation methods, and validating the choice of model structure.

4.1.1. UKF Implementation

The UKF is a variation of the Kalman filter that is based on the idea of creating a set of so-called sigma points $\mathcal{X}$ in the state space around the current state estimate, and propagating these through the navigation and observation equations to obtain the required information on the innovation and cross covariances.

To implement the UKF, the state vector $\mathbf{x}_k$ is appended with the process noise variables $\mathbf{v}_k$ and observation noise variables $\mathbf{w}_k$ to obtain the **augmented** state vector $\mathbf{x}_k^a = \left[\mathbf{x}_k^\top \; \mathbf{v}_k^\top \; \mathbf{w}_k^\top\right]^\top$. The estimate for the augmented state vector, which has length L, is given by:

$$\hat{\mathbf{x}}_{k,k}^a = E\left\{\mathbf{x}_{k,k}^a\right\} = \left[\hat{\mathbf{x}}_k^\top \; \mathbf{0} \; \mathbf{0}\right]^\top \; . \tag{4.1}$$

Due to the assumption that the noise can be described by zero-mean Gaussian random variables, the expected value of the noise vectors is zero. The corresponding augmented covariance matrix is given by:

$$P_{k,k}^a = E\left\{\mathbf{x}_{k,k}^a - \hat{\mathbf{x}}_{k,k}^a\right\} = \begin{bmatrix} P_{k,k} & 0 & 0 \\ 0 & Q & 0 \\ 0 & 0 & R \end{bmatrix} , \tag{4.2}$$

where Q and R are the process and observation noise covariance matrices, respectively. The set of sigma points based on $\hat{\mathbf{x}}^a_{k,k}$ and $P^a_{k,k}$ is called the augmented set of sigma points, and is constructed as:

$$\begin{aligned}
\mathcal{X}^a_0 &= \hat{\mathbf{x}}^a_{k,k}\,, \\
\mathcal{X}^a_i &= \hat{\mathbf{x}}^a_{k,k} + \left(\sqrt{(L+\lambda)\,P^a_{k,k}}\right)_i \qquad i = 1,\,2,\,\ldots,\,L\,, \\
\mathcal{X}^a_i &= \hat{\mathbf{x}}^a_{k,k} - \left(\sqrt{(L+\lambda)\,P^a_{k,k}}\right)_{i-L} \qquad i = L+1,\,L+2,\,\ldots,\,2L\,.
\end{aligned} \tag{4.3}$$

The notation $(\cdot)_i$ indicates the i^{th} column of a certain matrix. Again, L is the dimension of $\hat{\mathbf{x}}^a_{k,k}$. λ is a scaling parameter defined as:

$$\lambda = \alpha^2\,(L+\kappa) - L\,. \tag{4.4}$$

Parameters α and κ are also scaling parameters to set the spread of the sigma points around the mean, $\alpha \in [0,\,1]$ and κ such that $\lambda \neq 0$. Another important notion is that each sigma point (i.e. each column in $\mathcal{X}^a_{k,k}$) has two corresponding weights. One set, denoted by $(\cdot)^{(m)}$, is used for calculating the new state estimate; as this is calculated by taking the weighted *mean* of the transformed sigma points. The other, denoted by $(\cdot)^{(c)}$, is for obtaining the updated *covariance* matrices. These weights are defined as:

$$\begin{aligned}
W^{(m)}_0 &= \lambda\,/\,(L+\lambda)\,, \\
W^{(m)}_i &= \lambda\,/\,(L+\lambda) \qquad\qquad i = 1,\,2,\,\ldots,\,2L\,,
\end{aligned} \tag{4.5}$$

and:

$$\begin{aligned}
W^{(c)}_0 &= \lambda\,/\,(L+\lambda) + \left(1-\alpha^2+\beta\right)\,, \\
W^{(c)}_i &= W^{(m)}_i \qquad\qquad i = 1,\,2,\,\ldots,\,2L\,.
\end{aligned} \tag{4.6}$$

β is a (non-negative) tuning parameter; for Gaussian distributions, $\beta = 2$ is optimal. The set of augmented sigma points $\mathcal{X}^a_{k,k}$ can be split between those points corresponding to the state, those corresponding to the process noise variables, and those corresponding to the observation noise variables:

$$\mathcal{X}^a_{k,k} = \left[\left(\mathcal{X}^{\mathbf{x}}_{k,k}\right)^\top \left(\mathcal{X}^{\mathbf{v}}_{k,k}\right)^\top \left(\mathcal{X}^{\mathbf{w}}_{k,k}\right)^\top\right]^\top\,. \tag{4.7}$$

Once the augmented sigma points are calculated, those that belong to the state are transformed through the navigation equation f, after which the predicted state estimate and predicted state covariance can be calculated using the sigma weights:

$$\mathcal{X}^{\mathbf{x}}_{k+1,k} = \mathcal{X}^{\mathbf{x}}_{k,k} + \int_{t_k}^{t_{k+1}} f\left(\mathcal{X}^{\mathbf{x}}_{k,k},\,\mathbf{u}_k,\,\mathcal{X}^{\mathbf{v}}_{k,k}\right) dt\,. \tag{4.8}$$

$$\hat{\mathbf{x}}_{k+1,k} = \sum_{i=0}^{2L} W^{(m)}_i \left(\mathcal{X}^{\mathbf{x}}_{k+1,k}\right)_i\,. \tag{4.9}$$

$$P_{k+1,k} = \sum_{i=0}^{2L} W^{(c)}_i \left[\left(\mathcal{X}^{\mathbf{x}}_{k+1,k}\right)_i - \hat{\mathbf{x}}_{k+1,k}\right]\left[\left(\mathcal{X}^{\mathbf{x}}_{k+1,k}\right)_i - \hat{\mathbf{x}}_{k+1,k}\right]^\top\,. \tag{4.10}$$

Here, $\mathbf{u}_k$ denotes the input at time k. Next, the set $\mathcal{X}^{\mathbf{x}}_{k+1,k}$ is transformed a second time; now through the observation equation h, after which the measurement prediction $\hat{\mathbf{y}}_{k+1,k}$ is calculated similar to the state prediction.

$$\mathcal{Y}_{k+1,k} = h\left(\mathcal{X}^{\mathbf{x}}_{k+1,k},\,\mathbf{u}_k,\,\mathcal{X}^{\mathbf{w}}_{k,k}\right)\,. \tag{4.11}$$

$$\hat{\mathbf{y}}_{k+1,k} = \sum_{i=0}^{2L} W^{(m)}_i \left(\mathcal{Y}_{k+1,k}\right)_i\,. \tag{4.12}$$

Now that the measurement prediction is made, the innovation covariance P_{yy} and cross covariance P_{xy} matrices can be obtained.

$$P_{yy} = \sum_{i=0}^{2L} W^{(c)}_i \left[\left(\mathcal{Y}_{k+1,k}\right)_i - \hat{\mathbf{y}}_{k+1,k}\right]\left[\left(\mathcal{Y}_{k+1,k}\right)_i - \hat{\mathbf{y}}_{k+1,k}\right]^\top\,. \tag{4.13}$$

$$P_{xy} = \sum_{i=0}^{2L} W^{(c)}_i \left[\left(\mathcal{X}^{\mathbf{x}}_{k+1,k}\right)_i - \hat{\mathbf{x}}_{k+1,k}\right]\left[\left(\mathcal{Y}_{k+1,k}\right)_i - \hat{\mathbf{y}}_{k+1,k}\right]^\top\,. \tag{4.14}$$

Using the covariance matrices, the Kalman gain K_{k+1} can be calculated, and the state and covariance matrix predictions can be updated using the latest measurement $\mathbf{y}_{k+1}$.

$$K_{k+1} = P_{xy} P_{yy}^{-1} . \tag{4.15}$$

$$\hat{\mathbf{x}}_{k+1,k+1} = \hat{\mathbf{x}}_{k+1,k} + K_{k+1}\left(\mathbf{y}_{k+1} - \hat{\mathbf{y}}_{k+1,k}\right) . \tag{4.16}$$

$$P_{k+1,k+1} = P_{k+1,k} - K_{k+1} P_{yy} K_{k+1}^{\top} . \tag{4.17}$$

This concludes a single time step, after which the index k is advanced by one, and the process is repeated. Like all Kalman filters, the UKF requires the user to initialize the state and covariance matrix. Ideally, the state is initialized close to its optimally estimated value, and the covariance matrix is sufficiently large such that divergence is avoided. One of the advantages of the UKF is that it is relatively robust to such errors.

4.1.2. UKF Parameters

For clarity, the tuning parameter values used for the implementation of the UKF in this work are listed in Table 4.1.

Table 4.1: UKF parameters used for the FPR in this thesis.

Parameter	Allowable range	Chosen value
α	[0, 1]	0.3
κ	$\neq \left(\frac{1}{\alpha^2} - 1\right) L$	0
β	[0, inf)	2

4.2. Navigation Equation

As stated above, the Kalman filtering technique requires knowledge of the system dynamics and the relation between state and measured signals. The navigation equation contains the former. This section will present the state variables required to describe the system, and their dynamics equations.

4.2.1. Position, Velocity, Attitude

The "core" of the aircraft state is position, velocity, and attitude. The position in the Earth-centered Earth-fixed (ECEF) reference frame (x_E, y_E, z_E) is governed by:

$$\dot{x}_E = [u\cos\theta + (v\sin\phi + w\cos\phi)\sin\theta]\cos\psi - (v\cos\phi - w\sin\phi)\sin\psi + W_{xE} \tag{4.18}$$

$$\dot{y}_E = [u\cos\theta + (v\sin\phi + w\cos\phi)\sin\theta]\sin\psi + (v\cos\phi - w\sin\phi)\cos\psi + W_{yE} \tag{4.19}$$

$$\dot{z}_E = -u\sin\theta + (v\sin\phi + w\cos\phi)\cos\theta + W_{zE} \tag{4.20}$$

The change of body velocities of the aircraft (u, v, w):

$$\dot{u} = (A_x - \lambda_x - w_x) - g_0\sin\theta - (q - \lambda_q - w_q)w + (r - \lambda_r - w_r)v \tag{4.21}$$

$$\dot{v} = (A_y - \lambda_y - w_y) + g_0\cos\theta\sin\phi - (r - \lambda_r - w_r)u + (p - \lambda_p - w_p)w \tag{4.22}$$

$$\dot{w} = (A_z - \lambda_z - w_z) + g_0\cos\theta\cos\phi - (p - \lambda_p - w_p)v + (q - \lambda_q - w_q)u \tag{4.23}$$

where $g_0 = 9.08665$ [m/s] is the gravitational acceleration. The dynamics of the Euler attitude angles (ϕ, θ, ψ):

$$\dot{\phi} = (p - \lambda_p - w_p) + (q - \lambda_q - w_q)\sin\phi\tan\theta + (r - \lambda_r - w_r)\cos\phi\tan\theta \tag{4.24}$$

$$\dot{\theta} = (q - \lambda_q - w_q)\cos\phi - (r - \lambda_r - w_r)\sin\phi \tag{4.25}$$

$$\dot{\psi} = (q - \lambda_q - w_q)\frac{\sin\phi}{\cos\theta} + (r - \lambda_r - w_r)\frac{\cos\phi}{\cos\theta} \tag{4.26}$$

In above equations (W_{xE}, W_{zE}, W_{zE}) are the estimated wind velocities. Next, (A_x, A_y, A_z) and (p, q, r) are the measured body accelerations and rotation rates. These measurements will be contaminated with bias and noise. Variables (λ_x, λ_y, λ_z) and (λ_p, λ_q, λ_r) are the estimated sensor biases, and (w_x, w_y, w_z) and (w_p, w_q, w_r) are the sensor noise variables. A correction for the bias is included to improve accuracy. Also, the effect of noise is explicitly included, as it is required by the formulation of the UKF.

4.2.2. Wind, IMU Sensor Biases

It is assumed that the biases present in the measurement signals of the IMU are constant, therefore their dynamics are simply:

$$\dot{\lambda}_x = 0 \tag{4.27}$$
$$\dot{\lambda}_y = 0 \tag{4.28}$$
$$\dot{\lambda}_z = 0 \tag{4.29}$$
$$\dot{\lambda}_p = 0 \tag{4.30}$$
$$\dot{\lambda}_q = 0 \tag{4.31}$$
$$\dot{\lambda}_r = 0 \tag{4.32}$$

The wind velocities are assumed to be a random walk, i.e. they are expected to meander (slowly) over time.

$$\dot{W}_{xE} = 0.01\, w_N \tag{4.33}$$
$$\dot{W}_{yE} = 0.01\, w_N \tag{4.34}$$
$$\dot{W}_{zE} = 0.01\, w_N \tag{4.35}$$

where w_N is a standard normally distributed random variable. The constant 0.01 was determined in [56] to yield good results.

4.2.3. Air Data Boom Vane Parameters

The last variables to be added to the state vector are several air data boom vane parameters. These vanes measure the direction of the *local* flow ($u_\mathrm{v},\ v_\mathrm{v},\ w_\mathrm{v}$) at the vane position, which is different from the flow direction ($u,\ v,\ w$) at the aircraft center of gravity. There are two main sources for this error: *i)* aircraft induced flow effects and *ii)* flow velocity components induced by aircraft body rotations.

The following relations are an approximation of the air data boom vane angles that includes these two perturbation effects [37]:

$$\alpha_\mathrm{v} = \operatorname{atan}\left(\frac{w_\mathrm{v}}{u_\mathrm{v}}\right) \approx (1 + C_{\alpha_\mathrm{up}}) \operatorname{atan}\left(\frac{w}{u}\right) - \frac{x_{\mathrm{v}_\alpha}(q - \lambda_q - w_q)}{u} + C_{\alpha_0}$$
$$\beta_\mathrm{v} = \operatorname{atan}\left(\frac{v_\mathrm{v}}{u_\mathrm{v}}\right) \approx (1 + C_{\beta_\mathrm{si}}) \operatorname{atan}\left(\frac{v}{u}\right) + \frac{x_{\mathrm{v}_\beta}(r - \lambda_r - w_r)}{u} - \frac{z_{\mathrm{v}_\beta}(p - \lambda_p - w_p)}{u} + C_{\beta_0}$$

Where x_{v_α}, x_{v_β}, and z_{v_β} are x, z offset length of the α and β vanes, respectively, compared to the aircraft c.g. which can be reconstructed since the c.g. location is available. C_{α_up}, C_{β_si}, C_{α_0}, and C_{β_0} are parameters that describe the aircraft induced flow effects (and possibly also account for any measurement biases). As can be seen, the induced flow is modeled as a linear function of angle of attack or flank angle, which obviously is an approximation of the real, much more complex aerodynamic effects.

From previous experience, it was found the up- and sidewash coefficients vary over time, so they too were modeled as random walks. The bias terms were assumed to be constant, hence:

$$\dot{C}_{\alpha_\mathrm{up}} = 0.01\, w_N \tfrac{\pi}{180} \tag{4.36}$$
$$\dot{C}_{\beta_\mathrm{si}} = 0.01\, w_N \tfrac{\pi}{180} \tag{4.37}$$
$$\dot{C}_{\alpha_0} = 0 \tag{4.38}$$
$$\dot{C}_{\beta_0} = 0 \tag{4.39}$$

Adding extra states makes the system harder to observe, and might result in bad convergence of the state estimate. Therefore it seems desirable to experimentally obtain fixed values for these parameters, and treat them as true constants. However, determining the values of these parameters experimentally beforehand is also a difficult task, and might be dependent on the way the boom is installed, or other day-to-day variations. Therefore, it is chosen to let the Kalman filter estimate their values. The observability analysis is described in section 4.4.

4.2.4. Full Navigation Equation

To summarize, the complete navigation equation is repeated in Equation 4.40. As will be seen in section 4.4, there will be some adjustments following the observability analysis.

$$\dot{\mathbf{x}} = f(\mathbf{x}(t),\, \mathbf{u}(t),\, \mathbf{w}(t)) \tag{4.40}$$

$$\dot{\mathbf{x}} = \begin{bmatrix}
[u\cos\theta + (v\sin\phi + w\cos\phi)\sin\theta]\cos\psi - (v\cos\phi - w\sin\phi)\sin\psi + W_{xE} \\
[u\cos\theta + (v\sin\phi + w\cos\phi)\sin\theta]\sin\psi + (v\cos\phi - w\sin\phi)\cos\psi + W_{yE} \\
-u\sin\theta + (v\sin\phi + w\cos\phi)\cos\theta + W_{zE} \\
(A_x - \lambda_x - w_x) - g\sin\theta - (q - \lambda_q - w_q)w + (r - \lambda_r - w_r)v \\
(A_y - \lambda_y - w_y) + g\cos\theta\sin\phi - (r - \lambda_r - w_r)u + (p - \lambda_p - w_p)w \\
(A_z - \lambda_z - w_z) + g\cos\theta\cos\phi - (p - \lambda_p - w_p)v + (q - \lambda_q - w_q)u \\
(p - \lambda_p - w_p) + (q - \lambda_q - w_q)\sin\phi\tan\theta + (r - \lambda_r - w_r)\cos\phi\tan\theta \\
(q - \lambda_q - w_q)\cos\phi - (r - \lambda_r - w_r)\sin\phi \\
(q - \lambda_q - w_q)\frac{\sin\phi}{\cos\theta} + (r - \lambda_r - w_r)\frac{\cos\phi}{\cos\theta} \\
\mathbf{0_{6\times 1}} \\
0.01\,w_N \\
0.01\,w_N \\
0.01\,w_N \\
0.01\,w_N \frac{\pi}{180} \\
0.01\,w_N \frac{\pi}{180} \\
\mathbf{0_{2\times 1}}
\end{bmatrix} \tag{4.41}$$

where the state vector is:

$$\mathbf{x} = [x\ \ y\ \ z\ \ u\ \ v\ \ w\ \ \phi\ \ \theta\ \ \psi\ \ \lambda_x\ \ \lambda_y\ \ \lambda_z\ \ \lambda_p\ \ \lambda_q\ \ \lambda_r\ W_{xE}\ \ W_{yE}\ \ W_{zE}\ \ C_{\alpha_{\text{up}}}\ \ C_{\beta_{\text{up}}}\ \ C_{\alpha_0}\ \ C_{\beta_0}]^\top \tag{4.42}$$

the input vector:

$$\mathbf{u} = [A_x \quad A_y \quad A_z \quad p \quad q \quad r]^\top \tag{4.43}$$

and the process noise vector:

$$\mathbf{w} = [w_x \quad w_y \quad w_z \quad w_p \quad w_q \quad w_r]^\top \tag{4.44}$$

4.3. Observation Equation

In an ideal case, all state variables can be measured directly. Unfortunately, this is not always the case, but the measured variables do hold a relation to the states of interest. The observation equation captures this relation, and enables the Kalman filter to use the measurements to correct the current best state estimate.

4.3.1. Position Measurements

Using GPS, the position and velocity in the ECEF reference frame are measured. The aircraft position state is also defined in the ECEF frame so a direct measurement is available:

$$x_{\text{GPS}} = x + v_{x_{\text{GPS}}} \tag{4.45}$$
$$y_{\text{GPS}} = y + v_{y_{\text{GPS}}} \tag{4.46}$$
$$z_{\text{GPS}} = -z + v_{y_{\text{GPS}}} \tag{4.47}$$

To relate the body velocities to the ECEF velocity, a transformation is needed in order to predict the measurement. This results in the following observation equations:

$$\dot{x}_{\text{GPS}} = [u\cos\theta + (v\sin\phi + w\cos\phi)\sin\theta]\cos\psi - (v\cos\phi - w\sin\phi)\sin\psi + W_{xE} + v_{\dot{x}_{\text{GPS}}} \tag{4.48}$$
$$\dot{y}_{\text{GPS}} = [u\cos\theta + (v\sin\phi + w\cos\phi)\sin\theta]\sin\psi + (v\cos\phi - w\sin\phi)\cos\psi + W_{yE} + v_{\dot{y}_{\text{GPS}}} \tag{4.49}$$
$$\dot{z}_{\text{GPS}} = u\sin\theta - (v\sin\phi + w\cos\phi)\cos\theta + W_{zE} + v_{\dot{z}_{\text{GPS}}} \tag{4.50}$$

4.3.2. Attitude Measurements

The body attitude is measured directly by the attitude and heading reference system (AHRS), which results in the simple equations:

$$\phi_{\text{AHRS}} = \phi + v_{\phi_{\text{AHRS}}} \tag{4.51}$$

$$\theta_{\text{AHRS}} = \theta + v_{\theta_{\text{AHRS}}} \tag{4.52}$$

$$\psi_{\text{AHRS}} = \psi + v_{\psi_{\text{AHRS}}} \tag{4.53}$$

The AHRS also measures the body accelerations and rotation rates, but these are not included in the observation equation. They are included in the Kalman filter by using them as inputs to the navigation equation.

4.3.3. Air Data Measurements

The test vehicle is equipped with a digital air data computer (DADC) that can output a pressure altitude and total airspeed signal. Since GPS is used for the altitude, only the total airspeed measurement is used:

$$V_{\text{TAS}} = \sqrt{u^2 + v^2 + w^2} + v_{TAS_{\text{DADC}}} \tag{4.54}$$

Finally, the air data boom vanes measure the local direction of the flow at the location of the boom. Note that the boom β-vane does not measure the angle of sideslip, but an angle that shall in the rest of this thesis be called *flank angle*. This angle is related to the angle of sideslip via the relation $\tan\beta = \tan\beta_{\text{fl}}\cos\alpha$. Also henceforth, β_{v} denotes the flank angle measured by the boom. The observation equations for the boom vane angles are:

$$\alpha_{\text{v}} = (1 + C_{\alpha_{\text{up}}})\,\text{atan}\left(\frac{w}{u}\right) - \frac{x_{\text{v}_\alpha}(q - \lambda_q - w_q)}{u} + C_{\alpha_0} + v_{\alpha_{\text{boom}}} \tag{4.55}$$

$$\beta_{\text{v}} = (1 + C_{\beta_{\text{si}}})\,\text{atan}\left(\frac{v}{u}\right) + \frac{x_{\text{v}_\beta}(r - \lambda_r - w_r)}{u} - \frac{z_{\text{v}_\beta}(p - \lambda_p - w_p)}{u} + C_{\beta_0} + v_{\beta_{\text{boom}}} \tag{4.56}$$

4.3.4. Full Observation Equation

The complete vector containing all measurement variables used in the UKF implementation is given by Equation 4.59. Note the addition

$$\mathbf{y} = h(\mathbf{x}(t),\, \mathbf{u}(t),\, \mathbf{v}(t)) \tag{4.57}$$

$$\mathbf{y} = \begin{bmatrix}
x + v_{x_{\text{GPS}}} \\
y + v_{y_{\text{GPS}}} \\
-z + v_{z_{\text{GPS}}} \\
[u\cos\theta + (v\sin\phi + w\cos\phi)\sin\theta]\cos\psi - (v\cos\phi - w\sin\phi)\sin\psi + W_{xE} + v_{\dot{x}_{\text{GPS}}} \\
[u\cos\theta + (v\sin\phi + w\cos\phi)\sin\theta]\sin\psi + (v\cos\phi - w\sin\phi)\cos\psi + W_{yE} + v_{\dot{y}_{\text{GPS}}} \\
u\sin\theta - (v\sin\phi + w\cos\phi)\cos\theta + W_{zE} + v_{\dot{z}_{\text{GPS}}} \\
\phi + v_{\phi_{\text{AHRS}}} \\
\theta + v_{\theta_{\text{AHRS}}} \\
\psi + v_{\psi_{\text{AHRS}}} \\
\sqrt{u^2 + v^2 + w^2} + v_{TAS_{\text{DADC}}} \\
(1 + C_{\alpha_{\text{up}}})\,\text{atan}\left(\frac{w}{u}\right) - \frac{x_{\text{v}_\alpha}(q - \lambda_q - w_q)}{u} + C_{\alpha_0} + v_{\alpha_{\text{boom}}} \\
(1 + C_{\beta_{\text{si}}})\,\text{atan}\left(\frac{v}{u}\right) + \frac{x_{\text{v}_\beta}(r - \lambda_r - w_r)}{u} - \frac{z_{\text{v}_\beta}(p - \lambda_p - w_p)}{u} + C_{\beta_0} + v_{\beta_{\text{boom}}}
\end{bmatrix} \tag{4.58}$$

where the measurement vector is:

$$\mathbf{y} = [x_{\text{GPS}} \quad y_{\text{GPS}} \quad z_{\text{GPS}} \quad \dot{x}_{\text{GPS}} \quad \dot{y}_{\text{GPS}} \quad \dot{z}_{\text{GPS}} \quad \phi_{\text{AHRS}} \quad \theta_{\text{AHRS}} \quad \psi_{\text{AHRS}} \quad V_{\text{TAS}} \quad \alpha_{\text{v,boom}} \quad \beta_{\text{v,boom}}]^\top \tag{4.59}$$

the input vector:

$$\mathbf{u} = [A_x \quad A_y \quad A_z \quad p \quad q \quad r]^\top \tag{4.60}$$

and the measurement noise vector:

$$\mathbf{v} = [v_{x_{\text{GPS}}} \quad v_{y_{\text{GPS}}} \quad v_{z_{\text{GPS}}} \quad v_{\dot{x}_{\text{GPS}}} \quad v_{\dot{y}_{\text{GPS}}} \quad v_{\dot{z}_{\text{GPS}}} \quad v_{\phi_{\text{AHRS}}} \quad v_{\theta_{\text{AHRS}}} \quad v_{\psi_{\text{AHRS}}} \quad v_{TAS_{\text{DADC}}} \quad v_{\alpha_{\text{boom}}} \quad v_{\beta_{\text{boom}}}]^\top \tag{4.61}$$

4.4. Observability and Final System

For a Kalman filter to function properly, it is important that the system described by Equation 4.40 and Equation 4.57 is fully observable: observability is a necessary condition for convergence of the state estimate. Unfortunately, the considered system is nonlinear, which makes a *global* observability analysis difficult. *Local* observability, on the other hand, can be shown quite easily using a method from [58] that was implemented by [14]. Subsection 4.4.1 will show that the system is indeed locally observable. Unfortunately, this does not guarantee good performance of the Kalman filter. Subsection 4.4.2 takes a more practical approach by simply attempting to apply the Kalman filter to one of the available data sets, and investigating the convergence properties of the result. There it will be seen that some of the states had to be removed.

4.4.1. Local Observability Analysis

Proving local nonlinear observability can be done with relatively little effort, as is shown in [32] and [58]. Using Lie derivatives, an observability matrix $\mathcal{O}(x)$ can be constructed in a way that is comparable to the analysis done for linear systems. If the rank of $\mathcal{O}(x_{\text{test}})$ is equal to the dimension of the state vector x, the system is said to be locally observable at x_{test}.

The Lie derivative of a system with state equation $f(x)$ and output equation $h(x)$ is noted and defined as follows:

$$L_f h(x) = \frac{\partial h(x)}{\partial x} f(x) \tag{4.62}$$

where $\frac{\partial h(x)}{\partial x}$ denotes the Jacobian of $h(x)$ with respect to x. Using a recursive series of n Lie derivatives, where n is the dimension of x, the observability matrix $\mathcal{O}(x)$ can be constructed:

$$\mathcal{O}(x) = \begin{bmatrix} L_f^0 h(x) \\ L_f^1 h(x) \\ L_f^2 h(x) \\ \vdots \\ L_f^{n-1} h(x) \end{bmatrix} = \begin{bmatrix} \frac{\partial h(x)}{\partial x} \\ L_f h(x) \\ L_f L_f h(x) \\ \vdots \\ L_f \left(L_f^{n-2} h(x) \right) \end{bmatrix} \tag{4.63}$$

The MATLAB code written by [14], which included symbolic derivations of the observability matrix, was adjusted to the current case. Since significantly reduced the probability of errors compared to doing these derivations by hand. Next, the numeric values for any state can be substituted, and the rank of the matrix can be determined. A number of example states were uniformly sampled from the range presented in Table 4.2 (all values are in SI units), and all were subjected to the observability test.

Table 4.2: The range from which the random states were sampled for the local observability analysis.

	x	y	z	u	v	w	ϕ	θ	ψ	λ_x	λ_y	λ_z
lower	0	0	-8000	50	0	-10	0	-1.5	0	-0.5	-0.5	-0.5
upper	0	0	0	200	20	40	1.5	1.5	2π	0.5	0.5	0.5
	λ_p	λ_q	λ_r	W_{xe}	W_{ye}	W_{ze}	$C_{\alpha_{\text{up}}}$	$C_{\beta_{\text{si}}}$	C_{α_0}	C_{β_0}		
lower	-0.5	-0.5	-0.5	0	0	-10	0	0	-1	-1		
upper	0.5	0.5	0.5	20	20	10	0.5	0.5	1	1		

In total, 100 states were sampled and tested, and **all tested states turned out to be fully observable**. However, this does not prove general observability. The chosen range of states does not cover all states possible in real flight, just a subset that was estimated to be representative of the conventional flight envelope. Also, since the state is of high dimension ($n = 24$), the chosen subset will tend to be sparsely populated, even if many more states are evaluated. And next, even if two states that are relatively close to each other are shown to be observable, it is not guaranteed that the state space in between also is (although it is quite likely). All in all, it is a good sign that the evaluated states are observable, yet the true test is in applying the current system and Kalman filter algorithm to a real data set.

4.4.2. State Covergence On a Real Data Set

A more practical approach to observability is to apply the Kalman filter to a data set and investigate the convergence behaviour of the estimated states. In previous section it appeared as if the system is indeed observ-

able, but again this does not guarantee good convergence of state estimates.

The Kalman filter was run on a data set of an accelerated stall maneuver, initiated from a coordinated turn at approximately 30° bank. Three sets of initial conditions were used. The first was chosen such that it was reasonably close to the expected state. The other were set either much too low or much too high. If the system has good convergence properties, all three initial conditions should converge reasonably quickly to the same state estimate. Failure to do so indicates problems. Figure 4.2 and 4.3 present the state convergence results.

It can be seen that several states are not converging well. However, not all states that currently are converging badly need to be removed: one "bad" state might cause "good" states to fail to converge. Since there are many interconnections in the system it is not straightforward to say which states are causing the problems. First of all, W_{zE} was removed from the system. The vertical wind component is generally very small, in the order of magnitude of 0.1 to 0.2 m/s [42]. Therefore, removing it should have only a small effect on the estimation of $\dot{z}_{\text{GPS}}$, but it will make estimating the other wind velocity components easier.

Next, C_{α_0} was removed. It converges badly, and it is clearly visible in Figure 4.1 that it is strongly negatively correlated with $C_{\alpha_{\text{up}}}$. This makes sense, as they can both describe a bias in α-measurements, so an increase in one parameter leads to a reduction in the other. Finally, both $C_{\beta_{\text{si}}}$ and C_{β_0} were dropped, as they led to large uncertainties in the estimated value of β. An attempt was made to remove only one of these, but in both cases the resulting system performance was still bad. After these changes, the resulting system offered good and reliable convergence behavior.

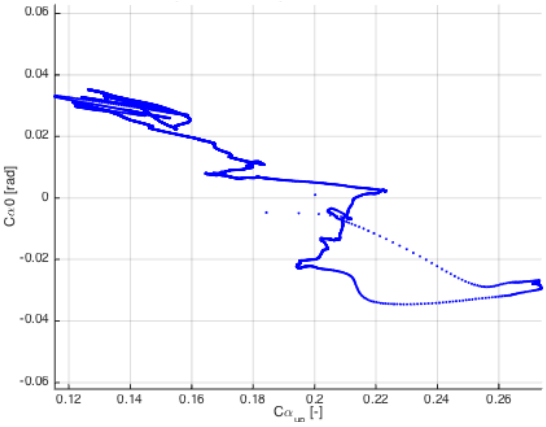

Figure 4.1: Plot of $C_{\alpha_{\text{up}}}$ vs. C_{α_0} showing strong negative correlation (cor = -0.936)

4.4.3. Final System

To conclude this section, the final system used in the Unscented Kalman Filter is repeated here. The system attempts to obtain an estimate for the state:

$$\mathbf{x} = [x \;\; y \;\; z \;\; u \;\; v \;\; w \;\; \phi \;\; \theta \;\; \psi \;\; \lambda_x \;\; \lambda_y \;\; \lambda_z \;\; \lambda_p \;\; \lambda_q \;\; \lambda_r \;\; W_{xE} \;\; W_{yE} \;\; C_{\alpha_{\text{up}}}]^\top \tag{4.64}$$

based on the measurement:

$$\mathbf{y} = [x_{\text{GPS}} \;\; y_{\text{GPS}} \;\; z_{\text{GPS}} \;\; \dot{x}_{\text{GPS}} \;\; \dot{y}_{\text{GPS}} \;\; \dot{z}_{\text{GPS}} \;\; \phi_{\text{AHRS}} \;\; \theta_{\text{AHRS}} \;\; \psi_{\text{AHRS}} \;\; V_{\text{TAS}} \;\; \alpha_{\text{v,boom}} \;\; \beta_{\text{v,boom}}]^\top \tag{4.65}$$

and the input:

$$\mathbf{u} = [A_x \quad A_y \quad A_z \quad p \quad q \quad r]^\top. \tag{4.66}$$

Furthermore, it is influenced by process noise:

$$\mathbf{w} = [w_x \quad w_y \quad w_z \quad w_p \quad w_q \quad w_r]^\top \tag{4.67}$$

and measurement noise:

$$\mathbf{v} = [v_{x_{\text{GPS}}} \;\; v_{y_{\text{GPS}}} \;\; v_{z_{\text{GPS}}} \;\; v_{\dot{x}_{\text{GPS}}} \;\; v_{\dot{y}_{\text{GPS}}} \;\; v_{\dot{z}_{\text{GPS}}} \;\; v_{\phi_{\text{AHRS}}} \;\; v_{\theta_{\text{AHRS}}} \;\; v_{\psi_{\text{AHRS}}} \;\; v_{TAS_{\text{DADC}}} \;\; v_{\alpha_{\text{boom}}} \;\; v_{\beta_{\text{boom}}}]^\top \tag{4.68}$$

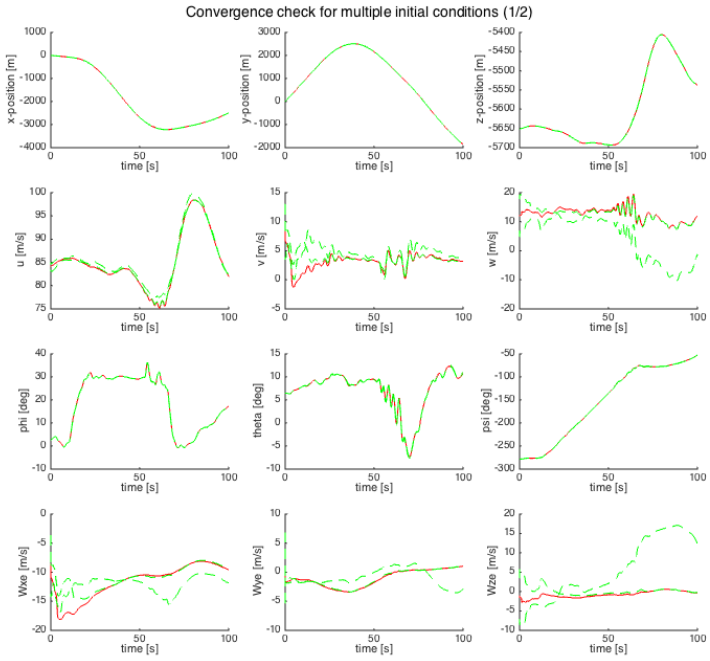

Figure 4.2: Convergence of state (1/2) using the full KF system. Three initial conditions were used: one expected to lie close to the correct state (red) and high/low estimates (greens). The body velocities v and w, and all wind velocity components are converging badly.

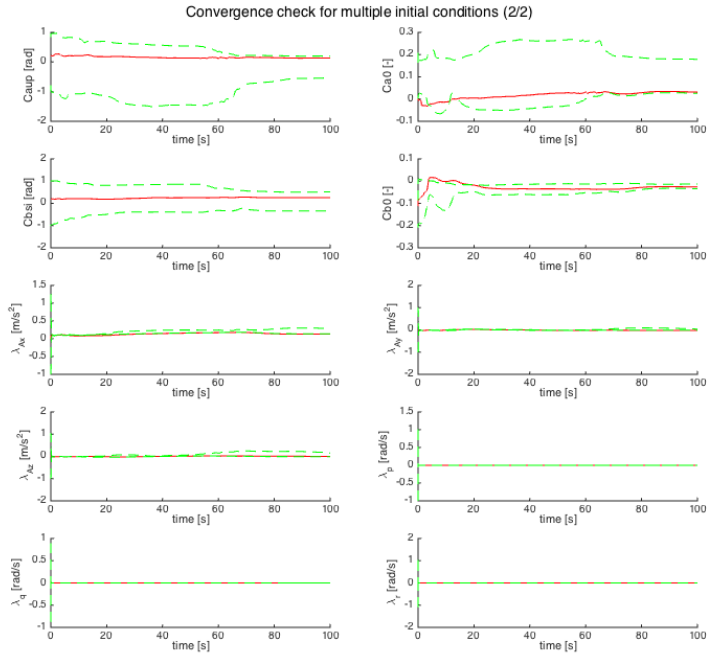

Figure 4.3: Convergence of state (2/2) using the full KF system. Three initial conditions were used: one expected to lie close to the correct state (red) and high/low estimates (greens). The states $C_{\alpha_{\text{up}}}$ and C_{α_0} appear to be negatively correlated; both $C_{\beta_{\text{si}}}$ and C_{β_0} converge badly.

The navigation equation f is:

$$\dot{\mathbf{x}} = f(\mathbf{x}(t),\, \mathbf{u}(t),\, \mathbf{w}(t)) \tag{4.69}$$

$$\dot{\mathbf{x}} = \begin{bmatrix} [u\cos\theta + (v\sin\phi + w\cos\phi)\sin\theta]\cos\psi - (v\cos\phi - w\sin\phi)\sin\psi + W_{xE} \\ [u\cos\theta + (v\sin\phi + w\cos\phi)\sin\theta]\sin\psi + (v\cos\phi - w\sin\phi)\cos\psi + W_{yE} \\ -u\sin\theta + (v\sin\phi + w\cos\phi)\cos\theta + W_{zE} \\ (A_x - \lambda_x - w_x) - g\sin\theta - (q - \lambda_q - w_q)w + (r - \lambda_r - w_r)v \\ (A_y - \lambda_y - w_y) + g\cos\theta\sin\phi - (r - \lambda_r - w_r)u + (p - \lambda_p - w_p)w \\ (A_z - \lambda_z - w_z) + g\cos\theta\cos\phi - (p - \lambda_p - w_p)v + (q - \lambda_q - w_q)u \\ (p - \lambda_p - w_p) + (q - \lambda_q - w_q)\sin\phi\tan\theta + (r - \lambda_r - w_r)\cos\phi\tan\theta \\ (q - \lambda_q - w_q)\cos\phi - (r - \lambda_r - w_r)\sin\phi \\ (q - \lambda_q - w_q)\frac{\sin\phi}{\cos\theta} + (r - \lambda_r - w_r)\frac{\cos\phi}{\cos\theta} \\ \mathbf{0_{6\times 1}} \\ 0.01\, w_r \\ 0.01\, w_r \\ 0.01\frac{\pi}{180} w_r \end{bmatrix} \tag{4.70}$$

and the measurement equation is given by:

$$\mathbf{y} = h(\mathbf{x}(t),\, \mathbf{u}(t),\, \mathbf{v}(t)) \tag{4.71}$$

$$\mathbf{y} = \begin{bmatrix} x + v_{x_{\text{GPS}}} \\ y + v_{y_{\text{GPS}}} \\ -z + v_{z_{\text{GPS}}} \\ [u\cos\theta + (v\sin\phi + w\cos\phi)\sin\theta]\cos\psi - (v\cos\phi - w\sin\phi)\sin\psi + W_{xE} + v_{\dot{x}_{\text{GPS}}} \\ [u\cos\theta + (v\sin\phi + w\cos\phi)\sin\theta]\sin\psi + (v\cos\phi - w\sin\phi)\cos\psi + W_{yE} + v_{\dot{y}_{\text{GPS}}} \\ u\sin\theta - (v\sin\phi + w\cos\phi)\cos\theta + W_{zE} + v_{\dot{z}_{\text{GPS}}} \\ \phi + v_{\phi_{\text{AHRS}}} \\ \theta + v_{\theta_{\text{AHRS}}} \\ \psi + v_{\psi_{\text{AHRS}}} \\ \sqrt{u^2 + v^2 + w^2} + v_{TAS_{\text{DADC}}} \\ (1 + C_{\alpha_{\text{up}}})\,\text{atan}\left(\frac{w}{u}\right) - \frac{x_{v_\alpha}(q - \lambda_q - w_q)}{u} + C_{\alpha_0} + v_{\alpha_{\text{boom}}} \\ (1 + C_{\beta_{\text{si}}})\,\text{atan}\left(\frac{v}{u}\right) + \frac{x_{v_\beta}(r - \lambda_r - w_r)}{u} - \frac{z_{v_\beta}(p - \lambda_p - w_p)}{u} + C_{\beta_0} + v_{\beta_{\text{boom}}} \end{bmatrix} \tag{4.72}$$

4.5. Example of UKF Performance on Data

To give an impression of the performance of the UKF algorithm combined with the system described in this chapter, Figures 4.4 to 4.6 offer a illustrative overview of the results. Plots for the states that were left out were intentionally left blank to show that they were dropped from the original system.

On the scale that is shown, the states estimates have very narrow confidence bounds, which indicates good performance. In Figure 4.5 it can be seen that the bias terms converge to steady values. Next, the measurement innovations are also generally within their uncertainty bounds. Finally, no strange or unexpected behavior is seen anywhere. It is therefore concluded that the current filter approach works well for the data sets that were gathered. The described filter was applied to all the gathered test data.

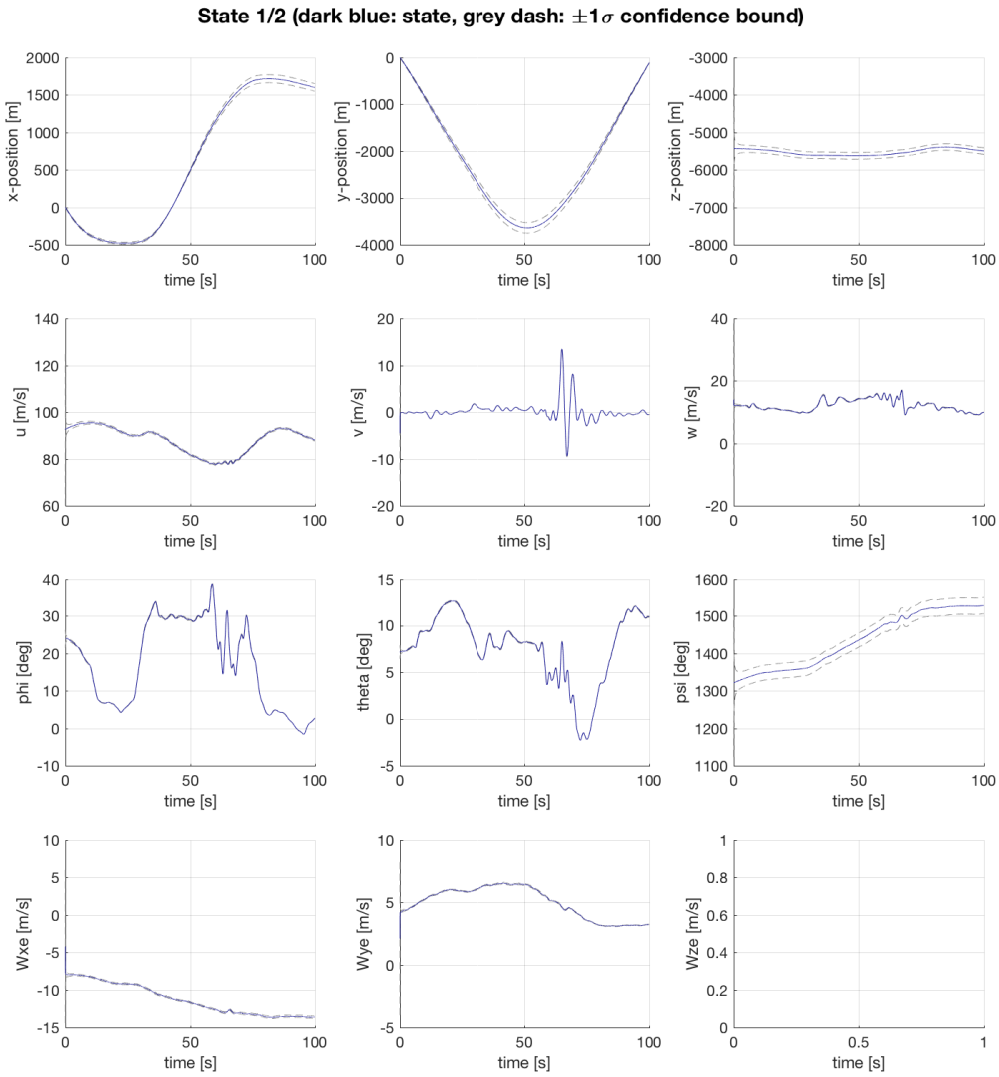

Figure 4.4: Reconstructed aircraft states (1/2) of an accelerated stall maneuver (and recovery), initiated at approximately 30 deg bank

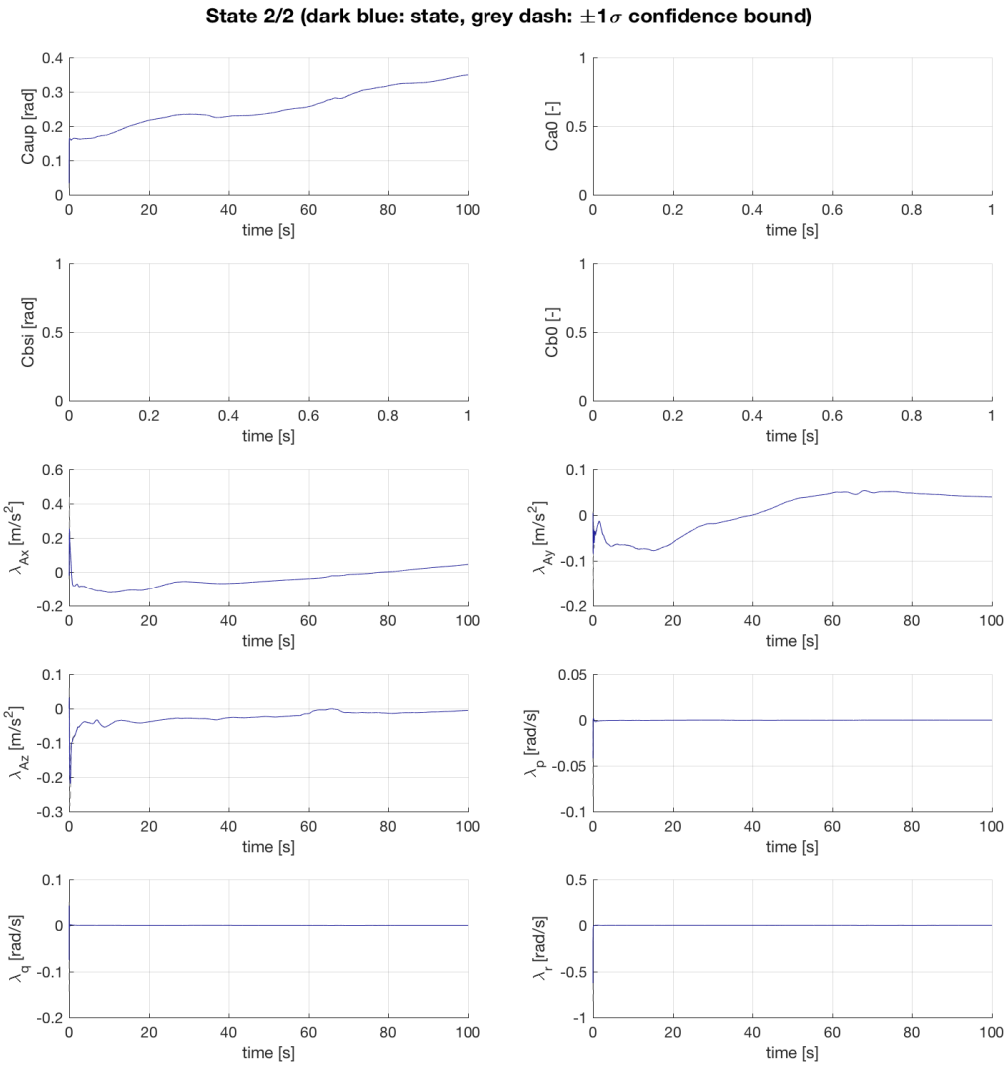

Figure 4.5: Reconstructed aircraft states (2/2) of an accelerated stall maneuver (and recovery), initiated at approximately 30 deg bank

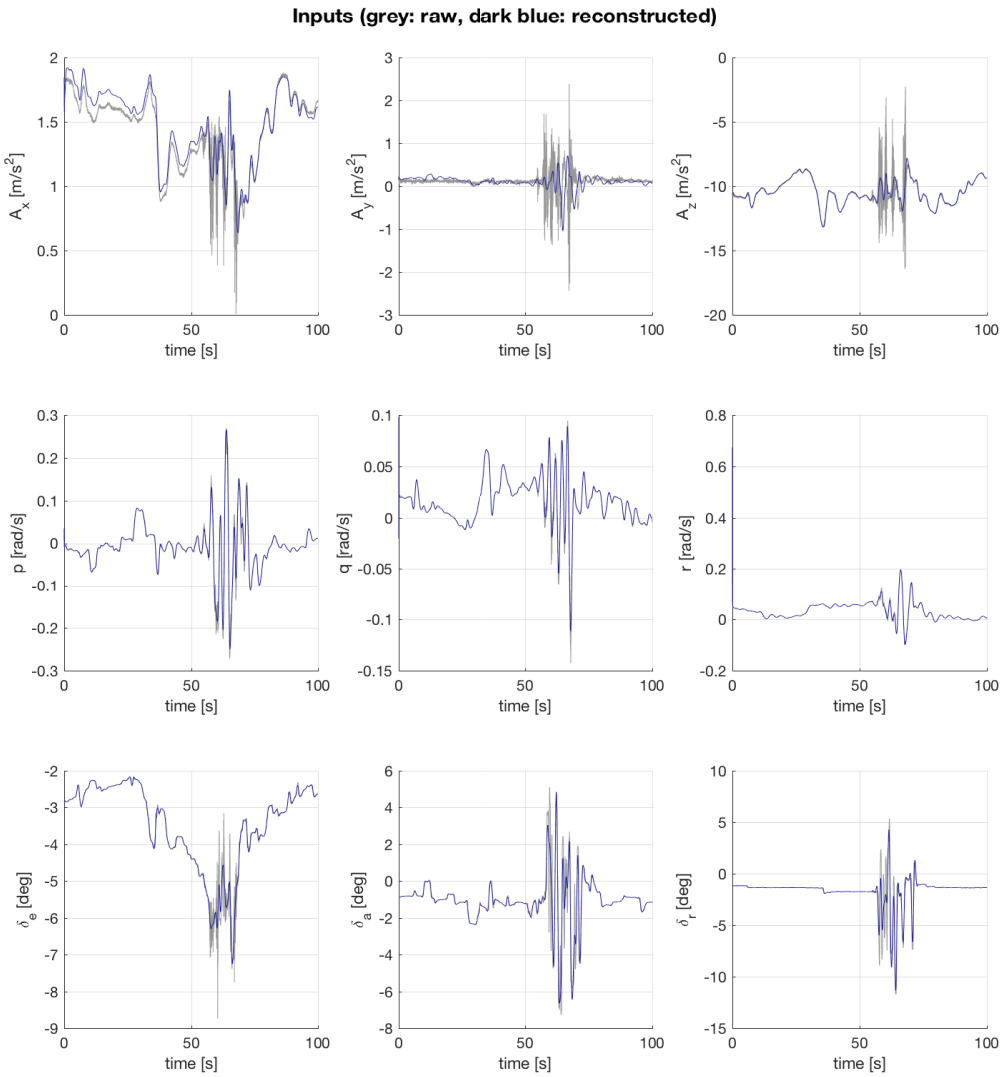

Figure 4.6: Measured (raw) and reconstructed signals that function as input to the Kalman filter; the reconstructed acceleration signals have been corrected with the bias terms

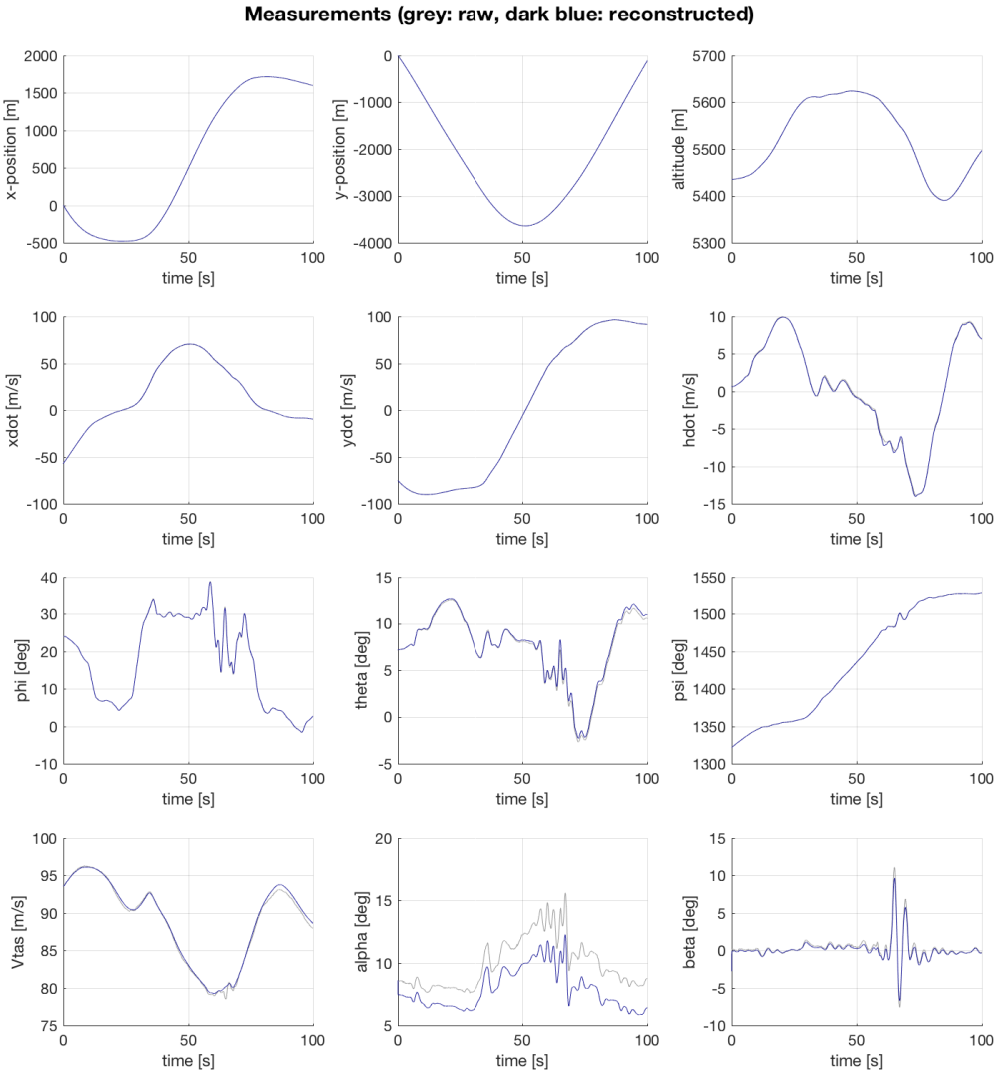

Figure 4.7: Measured (raw) and reconstructed signals that appear in the output vector of the Kalman filter

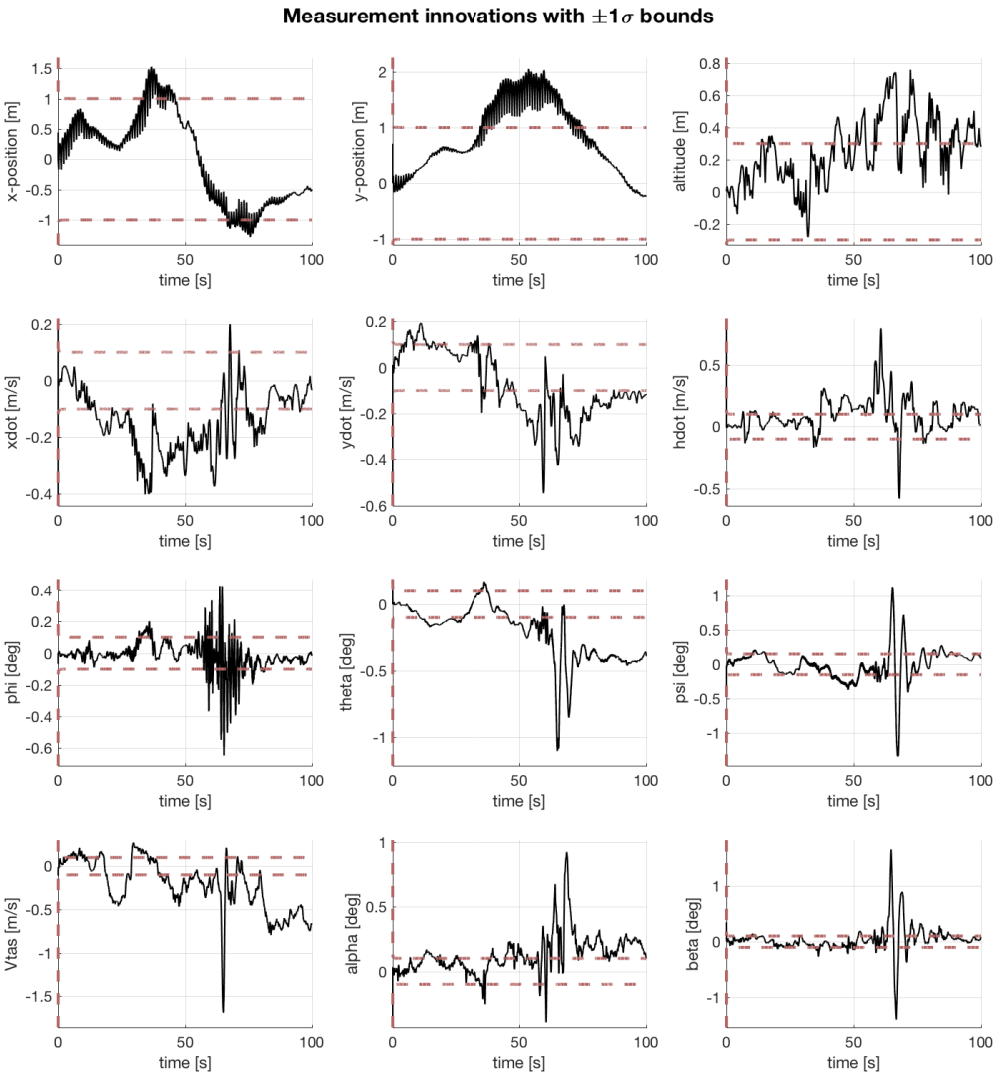

Figure 4.8: Innovations of the signals that appear in the output vector of the Kalman filter, along with $\pm 1\sigma$ bounds; where σ is the square root of the diagonal elements of the estimated covariance matrix

5

Stall Model Structure

In modeling aircraft dynamics, the goal is to provide a solution for the equations of motion, which govern the rate of change of the aircraft velocity components and angular rates. These equations of motion are generally understood very well. To illustrate this, consider the (common) analysis case where an aircraft that is: rigid, of constant mass, symmetric in the XZ-plane, and ignoring rotating masses; which flies over flat and non-rotating Earth. The equations of motion (EOM) that result from these assumptions, defined in the aircraft body frame of reference, are:

$$m \begin{bmatrix} \dot{u} + qw - rv \\ \dot{v} + ru - pw \\ \dot{w} + pv - qu \end{bmatrix} = mg_0 \begin{bmatrix} -\sin\theta \\ \sin\phi\cos\theta \\ \cos\phi\sin\theta \end{bmatrix} + \begin{bmatrix} X \\ Y \\ Z \end{bmatrix} \tag{5.1}$$

$$\begin{bmatrix} I_{xx} & 0 & I_{xz} \\ 0 & I_{yy} & 0 \\ -I_{xz} & 0 & I_{xz} \end{bmatrix} \begin{bmatrix} \dot{p} \\ \dot{q} \\ \dot{r} \end{bmatrix} = \begin{bmatrix} l \\ m \\ n \end{bmatrix} - \begin{bmatrix} p \\ q \\ r \end{bmatrix} \times \begin{bmatrix} I_{xx} & 0 & I_{xz} \\ 0 & I_{yy} & 0 \\ -I_{xz} & 0 & I_{xz} \end{bmatrix} \begin{bmatrix} p \\ q \\ r \end{bmatrix} \tag{5.2}$$

Where X, Y, Z are the body axis components of the total aerodynamic force acting on the aircraft, and l, m, n are the moments. Once these are known, solving the EOM is quite straightforward. It is clear that identifying models for these six forces and moments, which are called the **aerodynamic model equations**, is the major challenge and focus in modeling aircraft motion.

This chapter will start with a background on the conventional expressions of these aerodynamic model equations as linear polynomials of the aircraft state and control surface deflections. Next, several additions to this approach that enable the modeling of the effects of separated flow are discussed. Finally, the modeling methodology for stall buffet is presented.

5.1. Conventional Aerodynamic Model Equations

It is customary to express the aerodynamic model equations in non-dimensional form. In this way, they do not depend on dynamic pressure, hence the model parameters are easier to compare between different flight conditions and aircraft. Moreover, under a number of reasonable assumptions (e.g. sub-sonic flight, aircraft is much more dense than surrounding air) the equations can be written as functions of just the incidence angles of the incoming air and their rates of change ($\alpha, \beta, \dot{\alpha}, \dot{\beta}$), the body angular rates (p, q, r), and the control surface deflections (δ). In system identification, such variables are called the independent variables (IVs).

$$C_i = C_i(\alpha, \beta, p, q, r, \dot{\alpha}, \dot{\beta}, \delta) \tag{5.3}$$

Here, $i = L, D, Y, l, m, n$.[1] For conventional aircraft, δ contains aileron, elevator, and rudder deflections, but advanced control effectors, flaps, slats, and trim deflections could be included as well. Although the true interaction between aircraft body and the flow field around it is incredibly complex, the conventional

[1] The choice for $i = X, Y, Z, l, m, n$ is also common, although this thesis the former is chosen. Conversion between the two can be done with a simple transformation.

method is to simplify the dimensionless aerodynamic model equations as a first order Taylor expansion about a certain trim condition, for example:

$$C_L = C_{L_0} + C_{L_\alpha}\Delta\alpha + C_{L_\beta}\Delta\beta + C_{L_p}\frac{\Delta pb}{2V} + C_{L_q}\frac{\Delta q\bar{c}}{V} + \ldots + C_{L_{\delta_a}}\Delta\delta_a + C_{L_{\delta_e}}\Delta\delta_e + C_{L_{\delta_r}}\Delta\delta_r \tag{5.4}$$

Here $\bar{c}$ and b are the mean aerodynamic chord length and wing span respectively, and are chosen as the characteristic lengths for longitudinal and lateral model terms. The Δ-notation denotes deviations from a trim condition i.e. $\Delta\alpha = \alpha - \alpha_0$. In Equation 5.4 the parameters are the partial derivatives of the force or moment coefficients. Partial derivatives with respect to states are called *stability derivatives*, whereas partial derivatives with respect to control surface deflections are called *control derivatives*. To illustrate their definitions:

$$C_{L_\alpha} = \frac{\partial C_L}{\partial \alpha}\Big|_0, \qquad C_{L_p} = \frac{2V}{b}\frac{\partial C_L}{\partial p}\Big|_0, \qquad C_{L_q} = \frac{V}{\bar{c}}\frac{\partial C_L}{\partial q}\Big|_0, \qquad C_{L_{\delta_a}} = \frac{\partial C_L}{\partial \delta_a}\Big|_0, \qquad \text{etc.}$$

Final common assumptions are that the longitudinal and lateral terms are uncoupled, and the control surface deflections only influence the moment equations. Note that these assumptions do not hold for all cases, especially for large incidence angles and control surface deflections they are not likely to be correct!

From here onwards, the notation is simplified: when states are written with a tilde, the non-dimensional state is meant (e.g. $\tilde{q} = \frac{q\bar{c}}{V}$), and the Δ-notation is dropped. This leads to the following (exemplary) form of the aerodynamic model equations:

$$\begin{aligned}
C_L &= C_{L_0} + C_{L_\alpha}\alpha + C_{L_q}\tilde{q} + C_{L_{\dot{\alpha}}}\dot{\alpha} \\
C_D &= C_{D_0} + C_{D_\alpha}\alpha + C_{D_q}\tilde{q} + C_{D_{\dot{\alpha}}}\dot{\alpha} \\
C_Y &= C_{Y_0} + C_{Y_\beta}\beta + C_{Y_p}\tilde{p} + C_{Y_r}\tilde{r} + C_{Y_{\dot{\beta}}}\dot{\beta} \\
C_l &= C_{l_0} + C_{l_\beta}\beta + C_{l_p}\tilde{p} + C_{l_r}\tilde{r} + C_{l_{\dot{\beta}}}\dot{\beta} + C_{l_{\delta_a}}\delta_a + C_{l_{\delta_r}}\delta_r \\
C_m &= C_{m_0} + C_{m_\alpha}\alpha + C_{m_q}\tilde{q} + C_{m_{\dot{\alpha}}}\dot{\alpha} + C_{m_{\delta_e}}\delta_e \\
C_n &= C_{n_0} + C_{n_\beta}\beta + C_{n_p}\tilde{p} + C_{n_r}\tilde{r} + C_{n_{\dot{\beta}}}\dot{\beta} + C_{n_{\delta_a}}\delta_a + C_{n_{\delta_r}}\delta_r
\end{aligned}$$

Again, this model structure is but one of many possibilities. Which terms to include is determined on a case-by-case basis. In many cases, for example, it will be found that q and $\dot{\alpha}$ are not sufficiently de-correlated to include both terms, in which case one of them is usually dropped.

Because of the assumptions made, this model structure is only valid close to the trimmed flight condition at which its parameters were identified[2]. A global aerodynamic model, which is valid for all flight conditions of interest, is obtained by estimating the model parameters for many different trimmed flight conditions. Then, the found model parameters are generalized as functions of the flight condition variables. This makes it possible to interpolate between, or extrapolate, the estimated parameter values.

To estimate the parameters, data is required. This can come from wind tunnel experiments, flight test experiments, or analytic methods (i.e. CFD). It is common to use wind tunnel tests to estimate the so-called static terms (e.g. C_{L_0}, C_{m_α}), and flight tests for the dynamic terms (e.g. C_{L_q}). While this method has been proven to be effective, one can imagine that lots of tests are required to sufficiently cover the flight envelope of interest.

Another downside of this method, which is especially relevant for stall modeling, is that when the nonlinearities in aircraft response become stronger, the validity range of the conventional model structure becomes more narrow. This could be remedied by estimating the model parameters on a finer partitioning of the flight envelope, but this only adds to the already challenging and expensive effort of gathering data. Furthermore, since stall is a unsteady flight condition, trimming the aircraft in a stall is extremely challenging, which basically makes flight tests impossible.

It can therefore be concluded that the conventional modeling approach is not very suitable for stall modeling, and that more advanced model structures are necessary. The next section will explore several extensions that can be made to the linear model structure, which increase the approximation power of the aerodynamic model equations.

[2]The flight condition can be defined by variables like α, β, M, h, but other choices are also possible

5.2. Extensions to the Conventional Aerodynamic Model Equations

There is a theoretically infinitely large set of model terms that can be added to the aerodynamic model equations, but only a few will be considered in this section. Increasing approximation power is a good step if the model is not able to describe the patterns in the data that is used for estimating its parameters (i.e. the training data). In such a case, the model is said to have high *bias*. The model from section 5.1 has relatively low approximation power, but since only small ranges of the linear flight envelope are used as training data, the complexity of the patterns between input and output is relatively low. When larger ranges of the (possibly nonlinear parts of the) flight envelope are considered, adding extra model terms is a good approach.

However, adding more model terms is not always a good step. This cannot be seen if the model quality is only evaluated based on the training data: adding more terms will always result in a equally good or better training fit. In contrast, when comparing model output to a separate data set, which was not used for training (i.e. validation data), there comes a point where adding more model terms leads to an decrease in quality. When this occurs, the model is said to suffer from high *variance*.

The objective in model structure selection is to minimize both bias and variance, whilst keeping the model as simple as possible. This is a task which requires a lot of creativity and engineering judgement. This section will present several building blocks with which a suitable model structure can be created.

5.2.1. Terms Based on Kirchoff's Theory of Flow Separation

When modeling any phenomenon, taking into account as much prior knowledge as possible is generally a good idea. In [29], this is exactly what was done. The authors derived a relation between angle of attack and lift of an airfoil, based on Kirchoff's theory of flow separation, and expanded the aerodynamic model with an expression for this.

The central idea is to add an internal variable X that describes the flow separation point. X can range from 0 to 1, and is illustrated in Figure 5.1. The effect of X on the lift of the airfoil/wing can be described by Equation 5.5, and the dynamics of X have been experimentally determined to be describable by Equation 5.6.

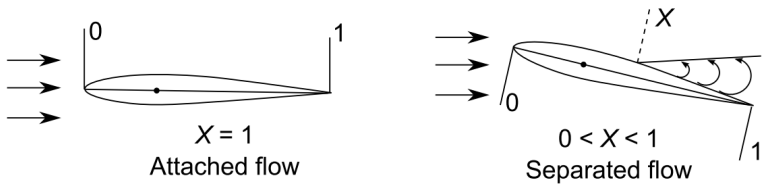

Figure 5.1: Illustration of internal variable X (figure from [15])

$$C_L = C_{L_\alpha}\left(\frac{1+\sqrt{X}}{2}\right)^2 \alpha \tag{5.5}$$

$$\tau_1 \frac{dX}{dt} + X = \frac{1}{2}\left[1 - \tanh\left(a_1 \cdot (\alpha - \tau_2 \dot{\alpha} - \alpha^*)\right)\right] \tag{5.6}$$

As can be seen, the dynamics of X depend on four parameters $(\tau_1, \tau_2, a_1, \alpha^*)$, which can be interpreted physically. A description of this interpretation will be given, in addition to plots of the effect of varying these parameters.

- τ_1 describes the time dependency of the flow condition. One can imagine that after an abrupt flow disturbance, like a gust of turbulence, the flow needs some time to readjust to the new conditions. This is modeled as a first-order differential equation. The effect of varying τ_1 is shown in Figure 5.2.

- τ_2 describes the effect of hysteresis, i.e. the dependency on rate of change of angle of attack $\dot{\alpha}$. Due to circulation and boundary layer effects, the result is that for positive $\dot{\alpha}$ the separation point moves to higher angle of attack. The opposite also happens: for negative $\dot{\alpha}$ the reattachment point is shifted to a lower angle of attack. The effect of varying τ_2 is shown in Figure 5.3.

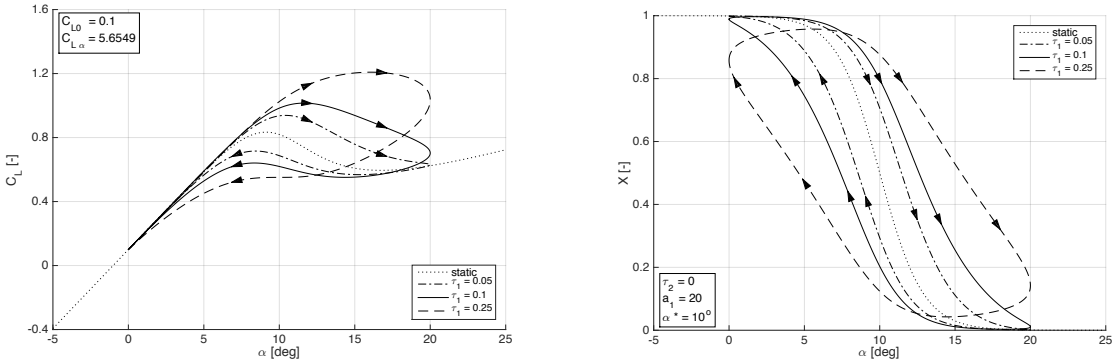

(a) Lift coefficient **(b)** Flow separation variable

Figure 5.2: Effect of varying τ_1 on unsteady flow separation point and lift coefficient (adapted from [56]), forced oscillation $\alpha(t) = 10° + 10°\cos\left(\frac{2\pi t}{2} + \pi\right)$

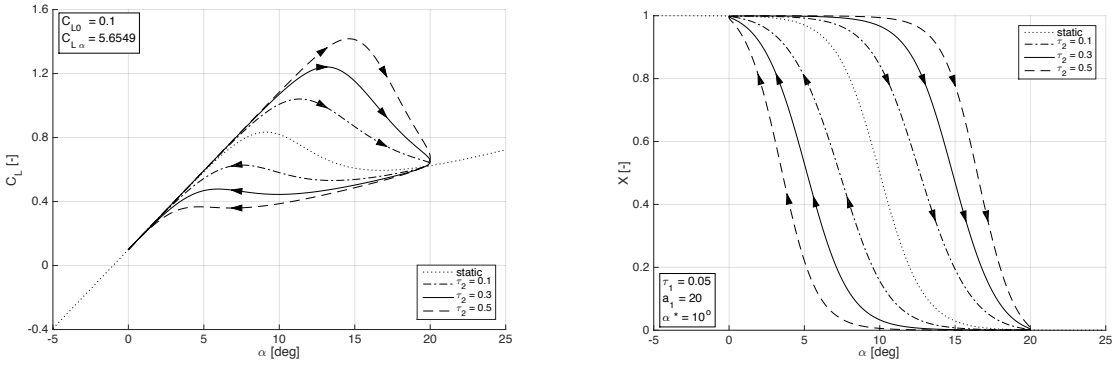

(a) Lift coefficient **(b)** Flow separation variable

Figure 5.3: Effect of varying τ_2 on unsteady flow separation point and lift coefficient (adapted from [56]), forced oscillation $\alpha(t) = 10° + 10°\cos\left(\frac{2\pi t}{2} + \pi\right)$

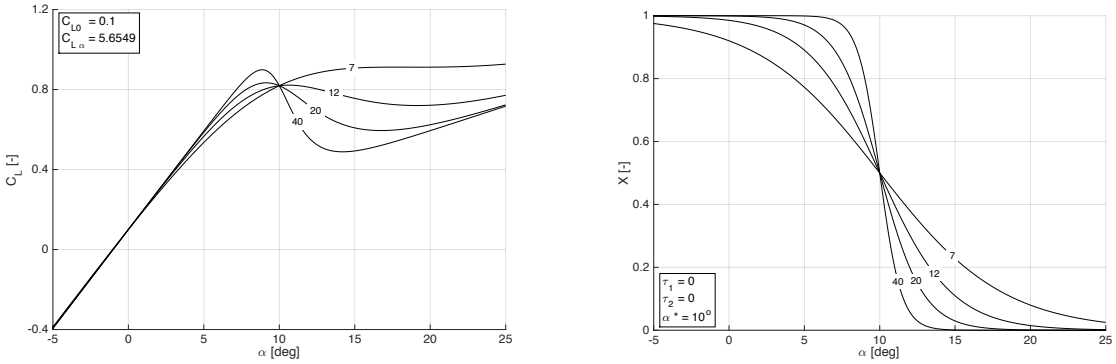

(a) Lift coefficient **(b)** Flow separation variable

Figure 5.4: Effect of varying a_1 on static flow separation point and lift coefficient (adapted from [56])

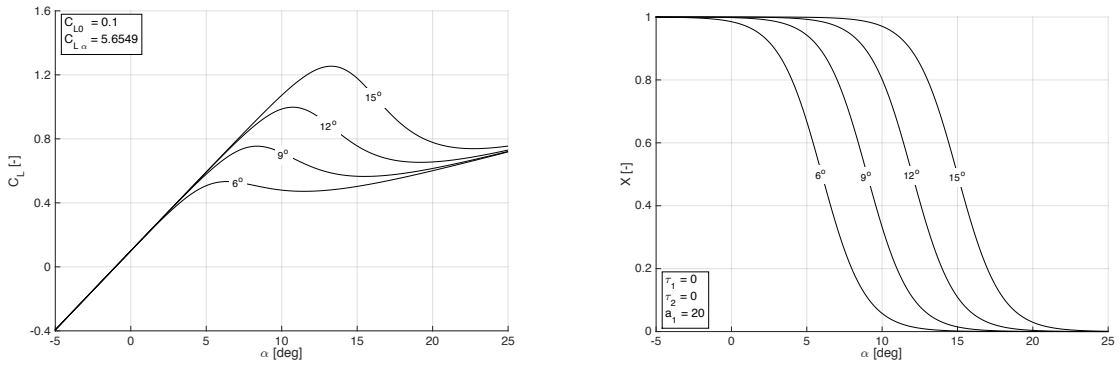

(a) Lift coefficient

(b) Flow separation variable

Figure 5.5: Effect of varying α^* on static flow separation point and lift coefficient (adapted from [56])

- $\mathbf{a_1}$ is a shape parameter determining the abruptness of the transition into a stalled state. The effect of varying a_1 is shown in Figure 5.4.
- α^* is a scheduling parameter that can shift the turning point to higher or lower angle of attack. It is straightforward to show that when $\alpha = \alpha^*$, then $X = 0.5$ i.e. the flow separation point lies between leading and trailing edges. The effect of varying α^* is shown in Figure 5.5.

A strong advantage of this model structure is that it is able to describe the unsteady, nonlinear relation between lift and angle of attack, and only uses four parameters to do so. Furthermore, it has been shown that the parameters can be estimated from flight data. A downside is that this turns the parameter estimation into a nonlinear optimization problem. Because of this, finding the set of globally optimal parameters is no longer guaranteed, and the optimization becomes computationally much more expensive. Parameter estimation techniques will be discussed in chapter 6.

The theory is explicit in its effect on the aircraft lift; the effect on other forces and the moments is not as clear. However, it can with relatively little effort be adapted to also describe other effects of a stall. An obvious first step is to use the internal variable X, or its derivative $\dot{X}$, as an IV. For example, adding a term:

$$C_{D_X}(1-X) \tag{5.7}$$

to the drag equation adds a term that, as the wing progresses into stall, linearly increases C_D (or decreases, depending on the sign). Such terms can be added to the other aerodynamic model equations as well.

Finally, asymmetric effects can be described by computing X for left and right wing separately. These can differ due to e.g. roll and/or yaw motion, which can cause differences in local angle of attack. Then, a term such as:

$$[(C_Z)_R - (C_Z)_L]\,\Delta y\,, \tag{5.8}$$

which describes an induced roll moment can be added. Δy denotes the effective lever arm between left and right wing, which introduces another unknown parameter which must be estimated from the data. Other lateral-directional effects can be included in a similar manner.

Overall, Kirchoff's theory of flow separation offers a strong basis for modeling the effects of aerodynamic stall. The effect on lift has been derived from both theory and empirical observations, and has been shown to be effective at explaining flight data. By determining a flow separation variable X, new model terms are made possible.

5.2.2. Higher Order Polynomial Terms

A straightforward extension to the conventional aerodynamic model equations is to relax the assumption that only first order Taylor expansion terms are used. It takes but little extra effort to include higher order terms like α^2 or $\alpha\beta$ into the set of independent variables. See for example the model for C_L based on α and q where terms up to order 2 are used:

$$C_L = C_{X_0} + C_{L_\alpha}\alpha + C_{L_q}\tilde{q} + C_{L_{\alpha^2}}\alpha^2 + C_{L_{q^2}}\tilde{q}^2 + C_{L_{\alpha q}}\alpha\tilde{q} \tag{5.9}$$

This is a good method for including (mild) nonlinearities and phenomena that result from the coupling of states and/or control inputs. Additionally, the parameter estimation problem is still linear.

There is no theoretical limitation to the maximum order or terms that are included. In practice, however, high-order polynomials generally suffer from two main issues. First, they are quite prone to have high variance, i.e. the models have a bad fit on validation data compared to training data. Next, they do not generalize well outside of the data range used for training. These effects are well-understood in literature. The result is that it is rare to encounter terms of higher order than, say, 3.

5.2.3. Univariate Splines of State Variables

A technique that has the advantages of polynomials, but does not suffer from the same downsides, is the use of spline functions. A spline is a function that is defined locally, and thus has to fit only a small subpart of the training data. This will reduce the complexity of the patterns in the data, and thus will reduce the required model order. Multiple splines can be combined to cover a larger (or the whole) state and input space. Continuity between the splines can be mathematically ensured.

Splines are very suitable for representing local variations in the training data. An example of local variations might be a variation in $C_{m_{\delta_e}}$ with α: once the angle of attack increases beyond a certain threshold value, the horizontal stabilizer might be in the main wing wake. This could create a strong local change in $C_{m_{\delta_e}}$. A formulation for a univariate spline, as given in [41], is:

$$(x - x_i)_+^m = \begin{cases} 0 & \text{when } x < x_i \\ (x - x_i)^m & \text{when } x > x_i. \end{cases} \tag{5.10}$$

The variable x could represent any of the aircraft state or control inputs. Choosing the partitioning of these input variables, i.e. setting x_i correctly, is a task left to the engineer designing the model structure.

Terms such as described in Equation 5.10 can be combined with each other and "normal" state and input variables in the same way as described in subsection 5.2.2, which gives a lot of freedom to the designer. Furthermore, also these spline terms result in a model structure that is linear in the parameters.

5.2.4. Other Model Extensions

The model terms mentioned in this chapter so far have mostly been quite simple. It is possible, even likely, that more elaborate terms with complexity comparable to Equation 5.5 will be good additions to the model. By choosing specific functions of IVs as model terms, one is already injecting information into the model, which is very benificial if these functions correspond well to reality. Badly chosen expressions will not likely be of any value, hence careful thought should be put into them.

Without a thorough theoretical or empirical analysis, it is difficult to derive useful model terms. However, as long as the model terms remain linear in the parameters, a "brute force" type approach could provide a good strategy. Based on some intuition (e.g. that the rudder effectiveness should decrease with X) one can propose a set of model expressions (square root, logarithmic, rational, combinations of these, etc.), and test each of them on the data.

In this approach lies the risk of ending up on a "treasure hunt" to finding ever more complex and obscure model terms that improve the fit. To avoid this, it is wise to apply the famous principle of "Occam's razor", which loosely states that when one must decide between multiple solutions that offer the same or very similar performance, the simplest one is often the best. Including regularization, which will be discussed in chapter 6, is another way of preventing excessive model terms.

5.3. Buffet Model

Stall buffet is a clearly noticeable vibration caused by the separation of the flow around the airframe. It is one of the most important queues for pilots to recognize a stall situation, and therefore vital to include it during stall simulation.

Previous research into the buffet in longitudinal and lateral body axes found that the dominant frequencies of the vibrations were much larger than those of the aircraft dynamics. This makes it possible to model the aircraft dynamics and buffet independently. It was shown that the power spectrum of the stall buffet S_{yy} can be modeled as a white noise signal that is passed through a shaping filter

$$S_{yy} = \left|H(j\omega)\right|^2 S_{uu}. \tag{5.11}$$

In [56], the shaping filter is composed of the sum of one or more second-order band-pass filters, which can be written as

$$H(j\omega) = \frac{H_0\ \omega_0^2}{(j\omega)^2 + \frac{\omega_0}{Q_0} j\omega + \omega_0^2}\ . \tag{5.12}$$

Creating a buffet model based in this approach can be reduced to three problems. First, the dominant frequency peaks must be identified in each of the three aircraft body axis. Second, the average amplitude or power of the buffet signals must be determined. Thirdly, some threshold from which the buffet is engaged must be defined, potentially with some scaling in the amplitude. Likely candidates for a threshold function are fixed values of α, or X.

All these can be identified from flight data. Separating the dynamics and buffet signals can be done using simple high- or low-pass filters since these two responses are sufficiently separated in the frequency domain.

5.4. Merging the Stall Model with the Regular Aerodynamic Model

A topic that has not been considered so far, but which is very important, is the merging of the stall model with the aerodynamic model for the "regular" flight envelope. These two models have some overlap, but at some condition a transition needs to be made between them. Although a final solution for merging the models can only be implemented when the stall model is nearing completion, already some thoughts can be shared. In general, there are three important considerations.

First of all is the point or region of transition. At some point or over some region of flight condition, the output of the current model should be replaced by the other. This transition should be triggered by some variable(s) that is/are available in the simulation. An obvious candidate would be angle of attack α, but other (and combinations of) variables are worth considering as well.

Second is the shape of the transition. Potential options are a "hard" transition, which instantaneously switches between the output of the two models, or a sigmoidal transition, which is a more smooth transition. The exact shape of such a transition can and should be modified to deliver satisfactory results.

Third, care should be taken that the outputs of both models agree to at least a reasonable degree in their transition areas. For example, the major control and stability derivatives should have the same sign, and comparable magnitude. This will likely be the hardest consideration to implement, because the two models are structured differently and might make use of different aircraft states. One way of preventing a large mismatch between model outputs is to fit the stall model on a wider range of flight condition that just the stall alone. In that way, the stall model will be forced to agree more with the regular flight envelope. Of course, this will have implications on the stall model structure. One could consider the resulting model to be an intermediate variant between "local" and "global".

5.5. Chapter Conclusion

A major part of modeling aircraft dynamics is identifying models for the aerodynamic model equations, which describe the six aerodynamic forces and moments acting on the airframe. The conventional approach is to express these as linear models of the aircraft states and pilot control inputs, containing only first order Taylor expansion terms. Due to the highly nonlinear nature of stall, this approach only works well in the flight domain below the stall angle of attack.

To include the effects of aerodynamic stall, several types of extensions to the aerodynamic model equations can be made. Kirchoff's theory of flow separation adequately describes the nonlinear, unsteady relation between α and C_L using only four extra parameters. Other options are to include higher-order Taylor terms, spline functions, or other transformations of state and/or input variables. The goal in model structure selection is to minimize both *variance* and *bias*, whilst keeping the model as simple as possible.

The stall buffet can be modeled independently of the aircraft dynamics. It can be represented by passing a white noise signal through a shaping filter. The parameters of the shaping filter and a threshold rule for the buffet can be identified from flight data.

6

Parameter Estimation

Once a model structure has been defined, the next task is to estimate its parameters. To do so, a cost or objective function must be defined. Next, an algorithm or method for finding the optimum of this cost function must be chosen. Afterwards, the resulting parameters can be analyzed to judge the quality of the model. This chapter introduces the methods that make this possible.

First, the metrics and methods for evaluating model quality are presented. After that, nonlinear and linear parameter estimation algorithms are treated separately. Some special considerations that are specific to the current stall modeling task are given wherever they arise. The chapter ends with a brief conclusion on the most promising method for the case of stall modeling.

6.1. Evaluating Model Fit Quality

Metrics that measure the quality of a model fit are important tools that aid engineering judgement. Moreover, parameter optimization requires an optimization objective, or cost function, which should be a numerical measure describing model fit. This section presents several tools that will be used to analyze the model quality.

6.1.1. Mean Squared Error

This popular choice for cost function is aptly named, as describes the average value of the mismatch between model output and measurement squared.

$$\mathrm{MSE} = \frac{1}{N}\sum_{k=1}^{N}(z_k - \hat{z}_k)^2 \ , \tag{6.1}$$

where N is the amount of data points, z_k denotes the k-th sample of the measured output, and $\hat{z}_k$ the corresponding model output. Since the aerodynamic model equations provide six outputs, the MSE is averaged over all of them, regardless of the absolute size.

6.1.2. Variance Accounted For

In contrast to the MSE, which is a measure of the absolute difference between model output and measurement, the variance accounted for (VAF) is a relative measure of fit, since it is scaled with the size of the measured variable.

$$\mathrm{VAF} = 100\% \times \left(1 - \frac{\Sigma_{k=1}^{N}(z_k - \hat{z}_k)^2}{\Sigma_{k=1}^{N} z_k^2}\right) . \tag{6.2}$$

As can be seen from its definition, the upper limit of the VAF is 100%, but it can take any negative value.

6.1.3. Regularization

Regularization refers to a range of techniques to prevent models having a high variance problem. It is especially relevant in cases where models with very high approximation power are used, such as the neural

networks in machine learning. It can be seen as adding a penalty for model complexity in the objective function of an optimization problem, e.g.

$$J(\theta) = \text{MSE}(\theta) + \lambda P(\theta) \,. \tag{6.3}$$

Here, J is the cost function value, θ is the parameter vector, P is some regularization penalty function, and λ is a scaling parameter. Common choices for P are either a fixed penalty per parameter, or the sum of the squared parameter values. Note that metrics such as Equation 6.1 or 6.2 only evaluate the parameter estimation problem, whereas Equation 6.3 entails both the tasks of model structure selection, as well as parameter estimation. In this sense, regularization can be seen as a generalization of the goodness of fit metric.

In the current case, regularization will be most useful in deciding whether or not to add a new model term. It provides a numerical judgement for decisions such as "Should I add this model term if it improves the objective by only 1% ?"

6.1.4. Parameter Correlations

When the model parameters are estimated on multiple data sets, it is possible to investigate the correlation of their variations between data sets:

$$C(\theta) = \text{cor}(\Theta) \,, \tag{6.4}$$

where Θ is a $(d \times p)$ matrix containing the d estimates of the p parameters. When C_{ij} is "close to 1" (or to -1), this indicates that parameters θ_i and θ_j are describing the same phenomena in the data, which could mean there are redundancies in the model. In such cases it might be wise to drop one of the model terms corresponding to these parameters.

Of course, the definition of "close to 1" is subject to interpretation. A common test is to regard correlations higher than 0.9 as problematic [36]. One should also take care in interpreting the results when d is low, since the computed correlation value is an estimate of the true correlations.

6.1.5. Cramèr-Rao Lower Bounds

If changing a model parameter results in no change in cost function value, one can imagine that it is impossible to obtain a meaningful estimate of its value. The Cramèr-Rao Lower Bound (CRLB) is a measure for the sensitivity of a model's output with respect to its parameters. Furthermore, it is a theoretical lower limit on the accuracy of the parameter estimates i.e.

$$\text{var}(\theta) \geq \text{CRLB} \,. \tag{6.5}$$

The CRLB can be computed as the inverse of the Fisher information matrix M: CLRB = M^{-1}. A good approximation of M can be obtained by

$$M(\theta, x) \approx \sum_{k=1}^{N} \nabla_\theta \hat{z}_k(\theta, x)^T R^{-1} \nabla_\theta \hat{z}_k(\theta, x) \,, \tag{6.6}$$

where $\hat{z}_k$ is the k-th time sample from $\hat{z}$, the $(m \times N)$ model output, θ is the $(p \times 1)$ parameter vector, and x is the $(n \times N)$ model input. Hence, the model has n inputs, p parameter, m outputs, and is evaluated at N time samples. The notation ∇_θ denotes the gradient of the model output with respect to θ, hence $\nabla_\theta \hat{z}_k$ is an $(m \times p)$ matrix. Finally, R is a scaling factor. In many cases, the choice is $R = \text{cov}(\hat{z} - z)$, the $(m \times m)$ prediction error covariance matrix. Note that for single-output models, such an R is equal to the mean squared error. From Equation 6.6 it is clear that M and thus the Cramèr-Rao Lower Bounds depend on the model input, output, as well as the estimated parameter values.

Theoretically, the variance of the estimated values of the parameters should tend towards the CRLB as the number of estimates increases. In practice, the observed variance in parameter values often is multiple times greater. In [40], the likely cause for this mismatch is traced back to a key assumption in the determination of M. By using R^{-1} as a scaling factor, the power spectrum of the model residuals is assumed to be uniform up to the Nyquist frequency. In reality, the noise power is significantly colored. Taking this effect into account requires careful analysis of the model residuals, and complicates the calculation of the bounds significantly. The authors of [40] propose alternative methods which provide a better representation of reality, but the results should still be reviewed with caution.

Nevertheless, while the CRLB might not necessarily be a good measure of the absolute parameter estimation accuracy, it does provide information of the relative accuracy. Several types of flight test maneuvers were used, and each was executed by a human pilot, causing variations between the data sets. Knowledge of

which maneuvers provide more information is valuable for future research, and the CRLB are a useful metric for such an analysis.

6.2. Nonlinear Parameter Estimation

Parameter estimation is the task of finding the best parameters given a parametrized model structure, and a set of data. The goal is to minimize a cost objective (or maximize a value objective) by changing the parameters. In cases where the cost function is a nonlinear function of the model parameters, the estimation problem is said to be nonlinear. This is the case when model terms such as in subsection 5.2.1 are used.

Nonlinear optimization is a challenging research field by itself, on which a lot of theory has been written, see for instance [47]. It is beyond the scope of this thesis to formally derive or even properly explain the nonlinear optimization algorithms presented here. Instead, use will be made of existing implementations of such solvers, particularly those available in MATLAB and its Optimization Toolbox.

A list of available algorithms will be given in subsection 6.2.1. Many of these algorithms depend on (estimates of) the gradient of the cost function with respect to the model parameters. The model terms defined in subsection 5.2.1 requires the solution of an ODE. Obtaining an estimate of the sensitivity of a solution of an ODE to its parameters is numerically challenging. Subsection 6.2.2 describes a technique that is numerically more stable that finite differences.

6.2.1. Nonlinear Optimization in MATLAB

MATLAB as multiple built-in algorithms that can be used for finding the minimum of any nonlinear function. Each will differ in computational effectiveness, accuracy, and tendency to get stuck in local optima. The most straightforward method of finding the most suitable algorithm is simply to try them all. Since they are all available in MATLAB, this will not require a lot of development effort. The best candidate can then be selected and used for obtaining the final results.

Dealing with local optima The possibility of ending in a local optimum is inevitable in any nonlinear optimization. A good approach to mitigate this risk is to randomly generate a large set of initial conditions from which the optimization is run. After this, the result with the lowest cost function is assumed to be the global optimum. Issues like finding two optima that have nearly the same associated cost value can still arise. In the end, engineering judgement is the final test.

Limiting the search space In order to speed up the search, and to exclude any unfeasible results, it is wise to apply constraints to the parameter space wherever possible. For instance, from experience it is known that C_{L_α} should be about 2π. It is reasonable to constrain its value to the range, say, [0 10]. Here, the use of dimensionless coefficients shows its worth, as the parameter values should all be with the same order of magnitude.

Gradient-based Algorithms MATLAB employs a range of well-known optimization algorithms that make use of the gradient of a cost function w.r.t. its parameters. Detailed backgrounds on these algorithms can be found in [47]. The following algorithms are available:

- Interior Point
- Active Set
- Sequential Quadratic Programming
- Trust Region Reflective
- Levenberg-Marquardt

Implementing these can be done either using the functions `fmincon` or `lsqnonlin`. These differ in the required formatting of the cost function, and not all algorithms are available to both. Setting the desired algorithm can be done in the options struct generated by `optimset`.

When the gradient is not explicitly provided, the solvers will automatically attempt to estimate it using finite difference methods. These can be one-sided or two-sided.

$$\nabla_\theta J(\theta) \approx \frac{J(\theta+\Delta\theta)-J(\theta)}{\Delta\theta} \tag{6.7}$$

$$\nabla_\theta J(\theta) \approx \frac{J(\theta+\Delta\theta)-J(\theta-\Delta\theta)}{2\Delta\theta} \tag{6.8}$$

The perturbation $\Delta\theta$ must be chosen small enough to prevent the influence of nonlinearities in J, but large enough to prevent numerical issues. MATLAB will choose $\Delta\theta$ itself. If the estimate of the gradient is not accurate, it is likely that the optimization will not perform well. Using finite differences to obtain the gradient of the solution of an ODE to its parameters is especially prone to numerical errors [49].

Gradient-free Algorithms In cases where the gradient is not known, or when it simply is not feasible to estimate it, gradient-free algorithms can provide a solution. Two that are built into MATLAB, and which can be called by `patternsearch` and `fminsearch` functions:

- Nelder-Mead Simplex
- Pattern Search

6.2.2. Parameter Sensitivity of the Solution of an ODE

Using finite difference methods to estimate the gradient of a model with respect to its parameters is known to suffer from numerical issues when the model is governed by an ODE [49]. In some cases, a numerical estimate of the parameter sensitivity can be obtained simultaneous with the solution of the ODE [39]. The use of the internal flow separation point variable X is such a case.

Consider an example system governed by the ordinary differential equation

$$\frac{d}{dt}y(t,x,\theta) = G(y,t,x,\theta) \qquad \text{with} \qquad y(0,x,\theta) = y_0\,; \tag{6.9}$$

where t is time, x system input, and θ the parameters. The sensitivity of the solution y of the system to θ can be written as

$$\frac{\partial}{\partial\theta}y(t,x,\theta) = S(y,t,x,\theta)\,. \tag{6.10}$$

Differentiation of Equation 6.9 with respect to θ results in another ODE that governs the first-order parameter sensitivity.

$$\frac{d}{dt}S(y,t,x,\theta) = \frac{\partial G(y,t,x,\theta)}{\partial y}S(y,t,x,\theta) + \frac{\partial G(y,t,x,\theta)}{\partial\theta}\,. \tag{6.11}$$

The initial conditions of $S_{ij} = 1$ if $\theta_j = y_i^O$, and zero otherwise (which is the case in the current application). This ODE can be solved using the same numerical methods as the original ODE. Doing so results in a much more accurate estimate of the parameter sensitivity than using finite differences [49].

This result can be used to find the parameter sensitivity of the cost function to the model parameters. A distinction between parameters must be made: those that govern the dynamics of X, and other parameters. The first category contains τ_1, τ_2, a_1, and α^*. In order to illustrate this example, assume that the model only simulates the lift coefficient. For the first category of parameters, the chain rule states

$$\frac{\partial J}{\partial\theta} = \frac{\partial J}{\partial C_L}\frac{\partial C_L}{\partial X}\frac{\partial X}{\partial\theta}\,. \tag{6.12}$$

The first two terms on the right hand side are straightforward to obtain; the last term can be computed using the method presented in this section. For the other parameter category, the result is the much simpler

$$\frac{\partial J}{\partial\theta} = \frac{\partial J}{\partial C_L}\frac{\partial C_L}{\partial\theta}\,. \tag{6.13}$$

6.3. Linear Parameter Estimation

Very efficient and effective methods exist for estimating the optimal parameters of linear systems. Contrary to nonlinear parameter estimation, finding a global optimum can be guaranteed, and their computational demand is generally much lower. This makes it desirable to only apply nonlinear optimization where it is absolutely necessary.

The stall model structure proposed in chapter 5 is made nonlinear via the use of the flow separation point parameter X. Note that if the parameters of X are assumed to be fixed, the remaining problem is linear, and thus can be solver much more efficiently. This could potentially greatly increase the accuracy and speed with which the optimization is done. However, by doing this one makes the implicit assumption that the parameters of X are independent of the other parameters. As long as the dependence is not too strong, the

gains from the more efficient estimation method could very well outweigh the error made by ignoring this relation.

It is not possible to estimate just the parameters of X by themselves, as the flow separation point is not measured. The most obvious solution for this is to estimate the parameters of X based on the lift coefficient. This makes sense, as Kirchoff's theory is defined for the relation between α and C_L. This approach will be implemented and the resulting parameter estimates will be compared to other approaches, where all model parameters (i.e. not just those belonging to X first, then the rest) are optimized simultaneously.

Once X is fixed, it can be added to the set of independent variables, which are also called regression variables. The model output $\hat{y}$ can then be written as

$$\hat{y}(\theta) = A\theta \tag{6.14}$$

in which A is the matrix of regression variables, and θ the vector of parameters. The goal of parameter estimation is to minimize a cost function that penalizes the remnant between model output and measured variables:

$$\hat{\theta} = \arg\min_{\theta} J(\theta) \,. \tag{6.15}$$

Using a quadratic cost function results in the maximum likelihood estimate for $\hat{\theta}$. The derivation of the well-known ordinary least-squares (OLS) algorithm follows from setting the derivative of the cost function to the parameters to zero, and is as follows:

$$J(\theta) = \tfrac{1}{2}\left(y - \hat{y}(\theta)\right)^T \left(y - \hat{y}(\theta)\right) \tag{6.16}$$

$$J(\theta) = \tfrac{1}{2}\left(y - A\theta\right)^T \left(y - A\theta\right) \tag{6.17}$$

$$\frac{\partial J(\hat{\theta})}{\partial \theta} = 0 \quad \longleftrightarrow \quad -A^T(y - A\hat{\theta}) = 0 \tag{6.18}$$

$$A^T A\hat{\theta} = A^T y \tag{6.19}$$

$$\hat{\theta} = \left[A^T A\right]^{-1} A^T y \,. \tag{6.20}$$

It has been proven that OLS leads to the maximum likelihood estimate (MLE) under the assumption that the remnant samples $\epsilon = y - \hat{y}$ are normally distributed. If they only includes sensor noise, this is a reasonable assumption. However, if the remnant also includes a significant modeling error contribution, OLS might not yield the best results. In such cases, more advanced MLE methods such as weighted least-squares (WLS) could be applied.

6.4. Chapter Conclusion

This chapter has presented the methods that will be used for solving the parameter estimation problem, and analyzing the results. Due to the use of X, at least part of the parameter optimization is nonlinear. All parameters can be solved for simultaneously by any nonlinear optimizer.

Alternatively, by estimating the parameters that determine X first using the measured values of C_L, the remaining problem can be solved using linear methods. When the solving for the optimal X-parameters is done using gradient-based methods, the gradient can be obtained more accurately that from finite differences by applying the theory from subsection 6.2.2.

The results of these different approaches can be compared using engineering judgement and the metrics and methods from section 6.1. The best method will be selected and used for estimating the final model parameters.

7

Preliminary Results

This chapter presents the process and result of fitting a preliminary model structure on the newly gathered flight data sets. This preliminary model structure was selected based on a combination of conventions found in literature, and intuition. It was not expected that this would result in a perfect model, or even a particularly good one, yet undertaking this effort was a valuable step in the research. The reasons for this are threefold. First, it tests if Kirchoff's theory is at least a reasonable choice for stall modeling. Secondly, it gives insight into the accuracy with which the model parameters can be estimated from the data; this is informative of both the flight data quality as well as the parameter estimation method. Thirdly, it enables the identification of problems and guides the direction of further thesis work.

First, the approach taken to estimate the parameters is explained. This approach was implemented in MATLAB and applied to all the training test data. Next, the resulting parameter values are investigated. To get a feeling for the model quality, two time histories of model output are compared to measured data: one from the training data, and one from the validation data. Finally, a brief sensitivity analysis is presented. This chapter does not end with a conclusions section, this is postponed to chapter 8, where the conclusions regarding the preliminary results are combined with conclusions on the other aspects of the thesis work so far.

7.1. Model Identification Approach

This section describes the process of selecting a model structure, and then fitting it to the newly gathered flight data. Of the 34 new flight data sets, 26 were selected as training data. This corresponds to about 75% of the total. The remaining 8 data sets were used for validating the model. The sets were selected such that both maneuver types (longitudinal and accelerated stalls) were present in the training as well as the validation sets.

7.1.1. Selected Model Structure

The preliminary model structure was selected based on conventions found in literature and intuition. A formal substantiation of the choices made was left to later stages of the thesis work, as at this time the goal was not to create the perfect stall model, but to gain experience with the process of parameter estimation and its issues.

Kirchoff's model term was implemented into the C_L-equation. The equation governing the dynamics of X was included was well. A static and a q-term were also added, which made the model for C_L essentially the same as those found in literature, in which good results are claimed. If Kirchoff's theory is indeed a good model structure for stall modeling, the fit for C_L should at least be reasonable.

For the other force and moment equations, the most intuitive terms were added. It was assumed that the longitudinal and lateral-directional dynamics are uncoupled. All equations include a static term, an α or β-term, and relevant dynamic stability terms. Control derivative terms were added to the moment equations. Finally, linear terms depending on X were included in both the drag and pitch moment equations, as this was a common choice in literature. The effect of stall on asymmetric model terms was less clear, so a X-term was not added. The resulting model structure was:

$$
\begin{aligned}
&\tau_1 \tfrac{dX}{dt} + X = \tfrac{1}{2}\left[1 - \tanh\left(a_1(\alpha - \tau_2\dot{\alpha} - \alpha^*)\right)\right] \\
&C_L = C_{L_0} + C_{L_\alpha}\left\{\tfrac{1+\sqrt{X}}{2}\right\}^2 \alpha + C_{L_q}\tilde{q} \\
&C_D = C_{D_0} + C_{D_\alpha}\alpha + C_{D_q}\tilde{q} + C_{D_X}(1-X) \\
&C_Y = C_{Y_0} + C_{Y_\beta}\beta + C_{Y_p}\tilde{p} + C_{Y_r}\tilde{r} \\
&C_l = C_{l_0} + C_{l_\beta}\beta + C_{l_p}\tilde{p} + C_{l_r}\tilde{r} + C_{l_{\delta_a}}\delta_a \\
&C_m = C_{m_0} + C_{m_\alpha}\alpha + C_{m_q}\tilde{q} + C_{m_X}(1-X) + C_{m_{\delta_e}}\delta_e \\
&C_n = C_{n_0} + C_{n_\beta}\beta + C_{n_p}\tilde{p} + C_{n_r}\tilde{r} + C_{n_{\delta_r}}\delta_r \ .
\end{aligned}
\tag{7.1}
$$

7.1.2. Cost Function & Solver Algorithm

The mean squared error (MSE) between the measured coefficients and model output was used as cost function. Since the model generates six outputs, the MSE is averaged over all of them. The interior point algorithm, implemented by `fmincon`, was selected as solver. For each training data set, 500 parameter sets were randomly sampled from the parameter space defined in Table 7.1. The cost value associated with these conditions were evaluated, and the 30 best were used as initial conditions for the optimization, which was then run.

The optimization was automatically stopped when the cost value had converged to within specified tolerance. Other stopping criteria were: the step parameters had become sufficiently small, or after 150 iterations, or when a single iteration took longer than 1.0 second. Most iterations were finished in the order of 0.1 to 0.2 seconds on the computer that was used, yet it turned out that some combinations of training data and parameters resulted in numerical difficulties, which led to much longer computation times. Most optimizations converged to a steady value before the other stopping criteria were active, hence stopping some optimization attempts early was not seen as a big problem, while it saved a lot of computation time.

Table 7.1: Upper and lower bounds of the 30 model parameters, all are dimensionless except τ_1, τ_2 [s], and α^* [rad]

parameter	lb	ub	parameter	lb	ub
τ_1	0.001	6.0	C_{l_0}	-1.5	0.5
τ_2	0.0	6.0	C_{l_β}	-0.5	0.5
a_1	0.0	80.0	C_{l_p}	-1.0	1.0
α^*	0.0	0.5	C_{l_r}	-1.0	1.0
C_{L_0}	0.1	0.6	$C_{l_{\delta_a}}$	-2.0	2.0
C_{L_α}	0.0	10.0	C_{m_0}	-0.5	0.5
C_{L_q}	-2.0	5.0	C_{m_α}	-1.0	1.0
C_{D_0}	-1.0	1.0	C_{m_q}	-1.0	1.0
C_{D_α}	-1.0	1.0	C_{m_X}	-1.0	1.0
C_{D_q}	-1.0	1.0	$C_{m_{\delta_e}}$	-2.0	2.0
C_{D_X}	-1.0	1.0	C_{n_0}	-0.5	0.5
C_{Y_0}	-0.5	0.5	C_{n_β}	-0.5	0.5
C_{Y_β}	-1.0	1.0	C_{n_p}	-0.5	0.5
C_{Y_p}	-1.0	1.0	C_{n_r}	-0.5	0.5
C_{Y_r}	-1.0	1.0	$C_{n_{\delta_r}}$	-1.0	1.0

7.2. Estimated Parameter Values

A set of parameters was estimated for each training set. To gain insight into the accuracy of the estimates, the parameter value results are presented in two ways. First, they are given as function of flight condition. This is presented in the form of a plot of estimated parameter values versus altitude. Second, the correlations between the estimated parameter values are presented, this time in the form of a table.

7.2.1. As Function of Flight Condition

Figures 7.1 to 7.7 present plots of the estimated parameter values versus the flight condition. The plots are organized by model equation, i.e. X-parameters are separate, C_L-parameters are separate, etc. For each

parameter, a linear fit through the data points is presented.

The flight condition is assumed to be completely defined by altitude h alone. A common choice for defining flight condition in literature is to use α, β, M, and h. Only the last of these variables was used. The goal of the stall modeling is to lose the parameter dependence on α and β; the model structure should be able to describe the effect of (relatively large) variations in these variables. It should therefore be no longer necessary to include them in the flight condition description. The Mach dependence was dropped because all stalls were flown at approximately the same speed, which made it very hard to derive a relation. An alternative for using h is to use the Reynolds number, this will be investigated during later stages.

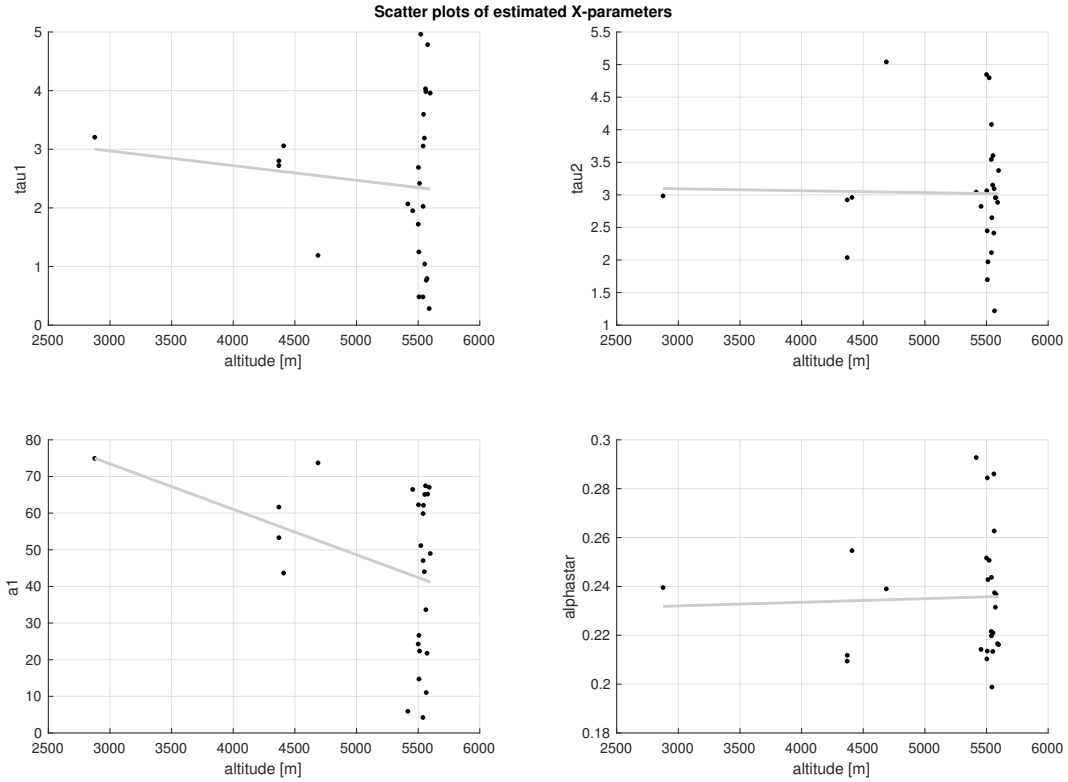

Figure 7.1: Plots of the estimated X-parameter values versus average altitude h during the stall maneuver, with linear trend lines fitted to them

Overall, is clear that fitting a line through the data points does not make a lot of sense. Since most stalls were recorded around 5500 m altitude, the slope of the trend line is strongly influenced by the few stalls at lower altitudes. Since the variance in the parameter estimates is still significant, this makes it impossible to derive conclusions on the real relation between parameters and altitude. It seems wise to lose the altitude dependence of the parameters, and consider them constants, due to lack of data.

In Figure 7.1, it can be seen that there is quite a large spread in the estimated X-parameter values. The estimated values of τ_1, τ_2, and a_1 are spread over almost the complete allowed range. The estimate of α^* is the only one which shows some measure of accuracy, its average value is about 0.25 radians, which corresponds to a stall angle of about 14°, which seems reasonable.

For the modeled force equation parameters from Figures 7.2 to 7.4, the spread is generally lower than for the X-parameters, but it still is significant. From an analysis of the theory of flight dynamics modeling, it is possible to construct some prior expectations on the value (or at least: the sign) of the model parameters. Several of the parameters showed results that were inconsistent with these expectations. Some estimates of C_{D_α}, C_{D_q} and C_{D_X} were negative, while an increase in drag physically makes much more sense when these regression values increase. Finally, some estimates of C_{Y_β} were positive, this also contrasts intuition. In general, if the sign of a parameter estimate varies between data sets, this is usually an indication of bad accuracy. Next to that, some parameters (like C_{L_q}) show a large scatter, which also indicates bad accuracy.

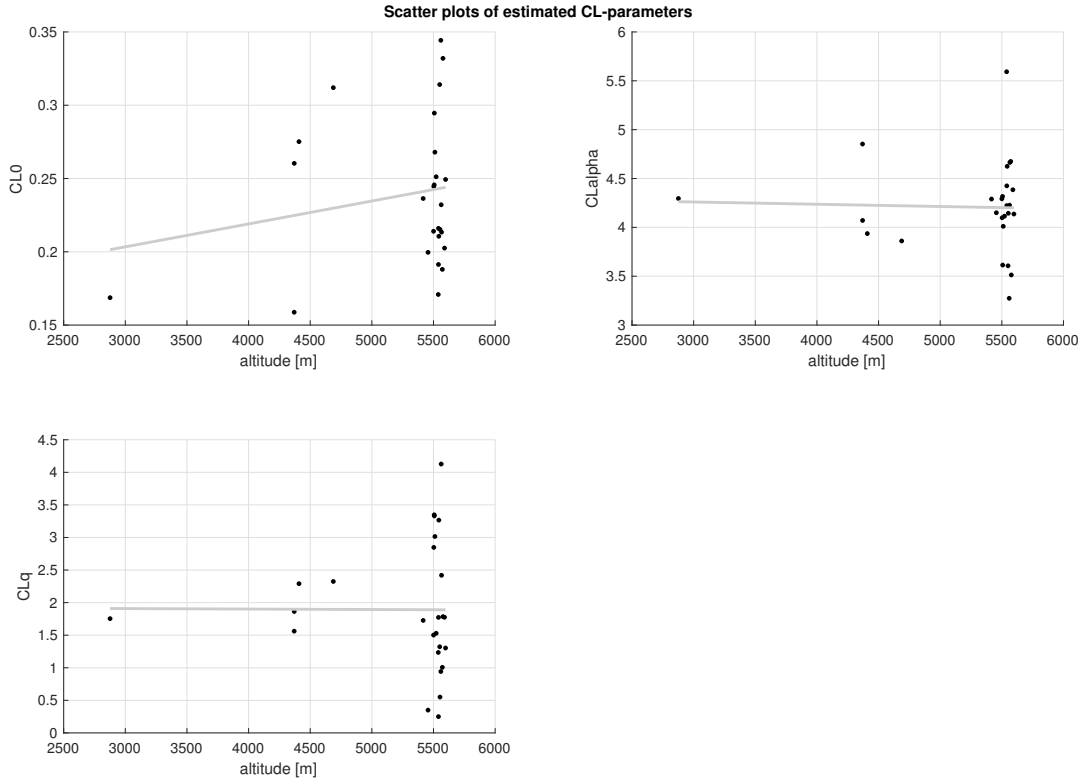

Figure 7.2: Plots of the estimated C_L-parameter values versus average altitude h during the stall maneuver, with linear trend lines fitted to them

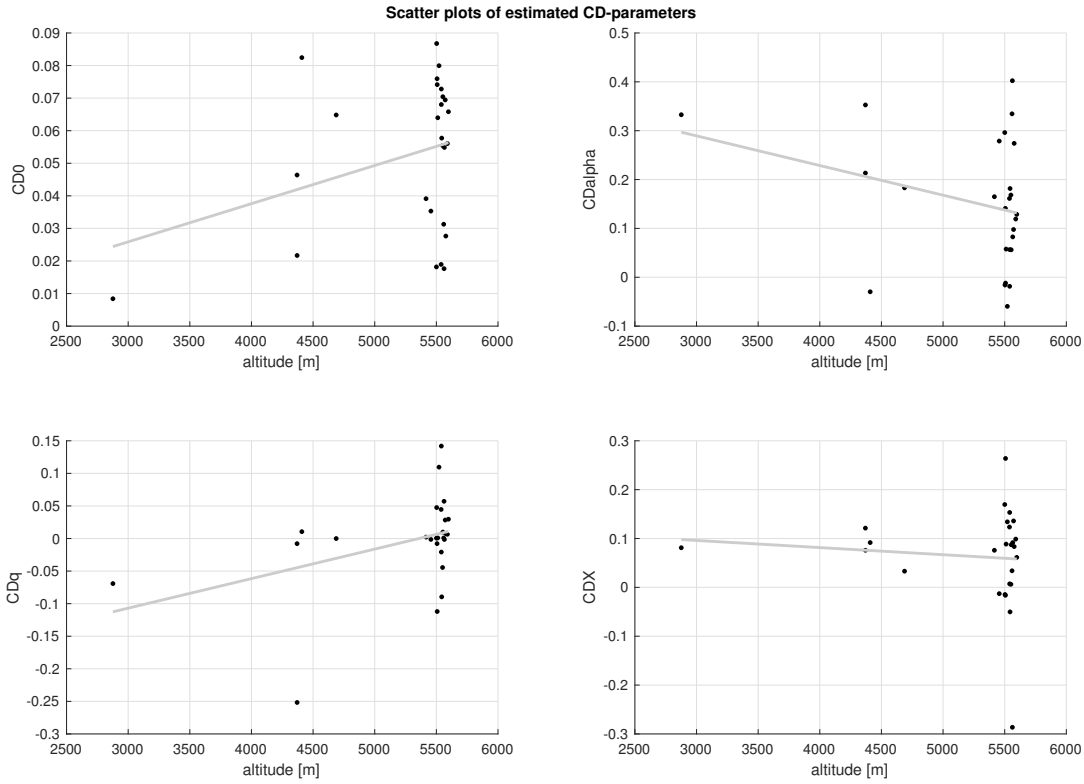

Figure 7.3: Plots of the estimated C_D-parameter values versus average altitude h during the stall maneuver, with linear trend lines fitted to them

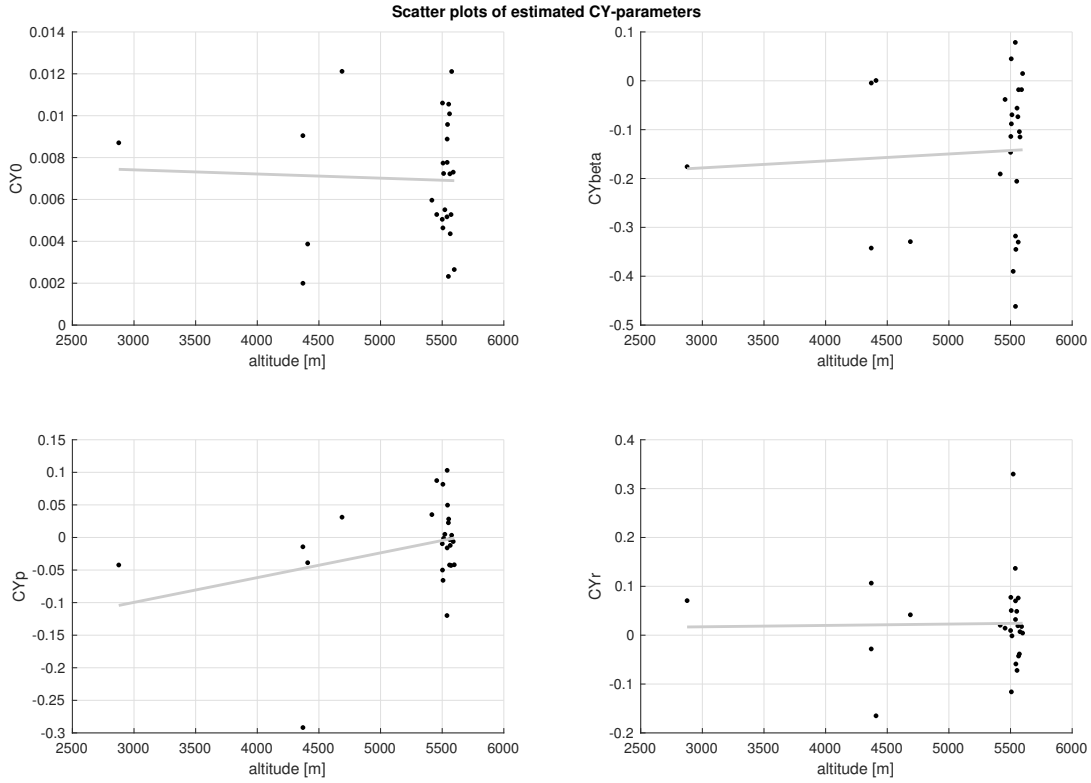

Figure 7.4: Plots of the estimated C_Y-parameter values versus average altitude h during the stall maneuver, with linear trend lines fitted to them

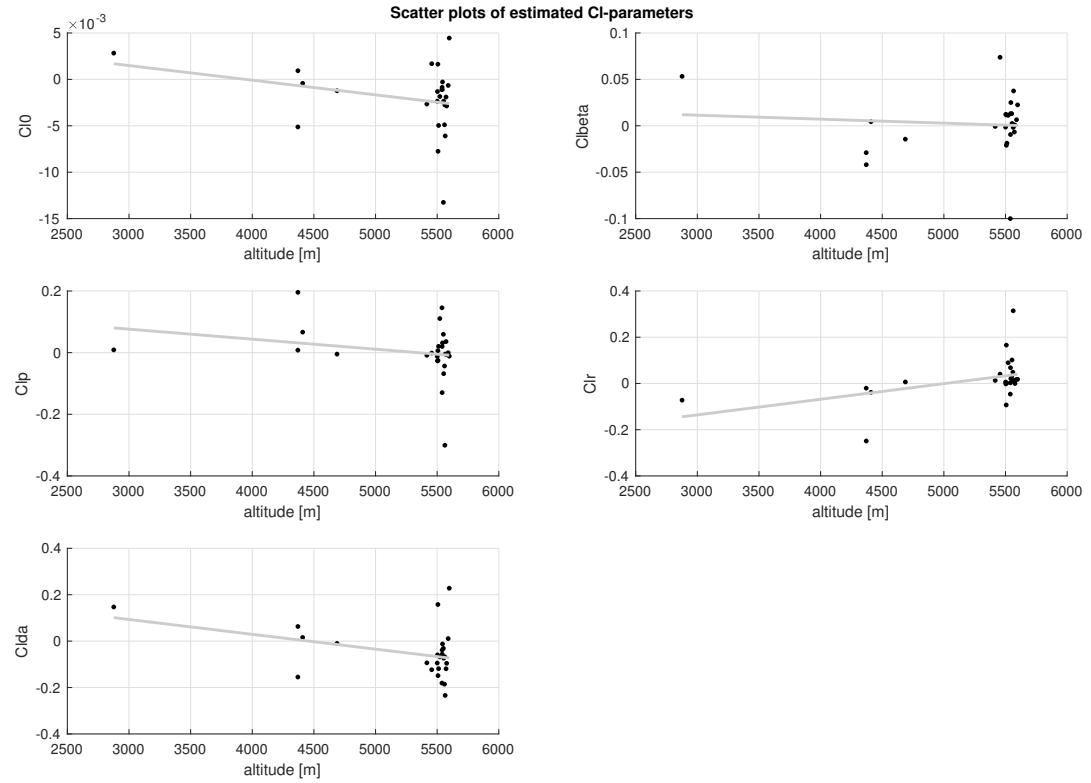

Figure 7.5: Plots of the estimated C_l-parameter values versus average altitude h during the stall maneuver, with linear trend lines fitted to them

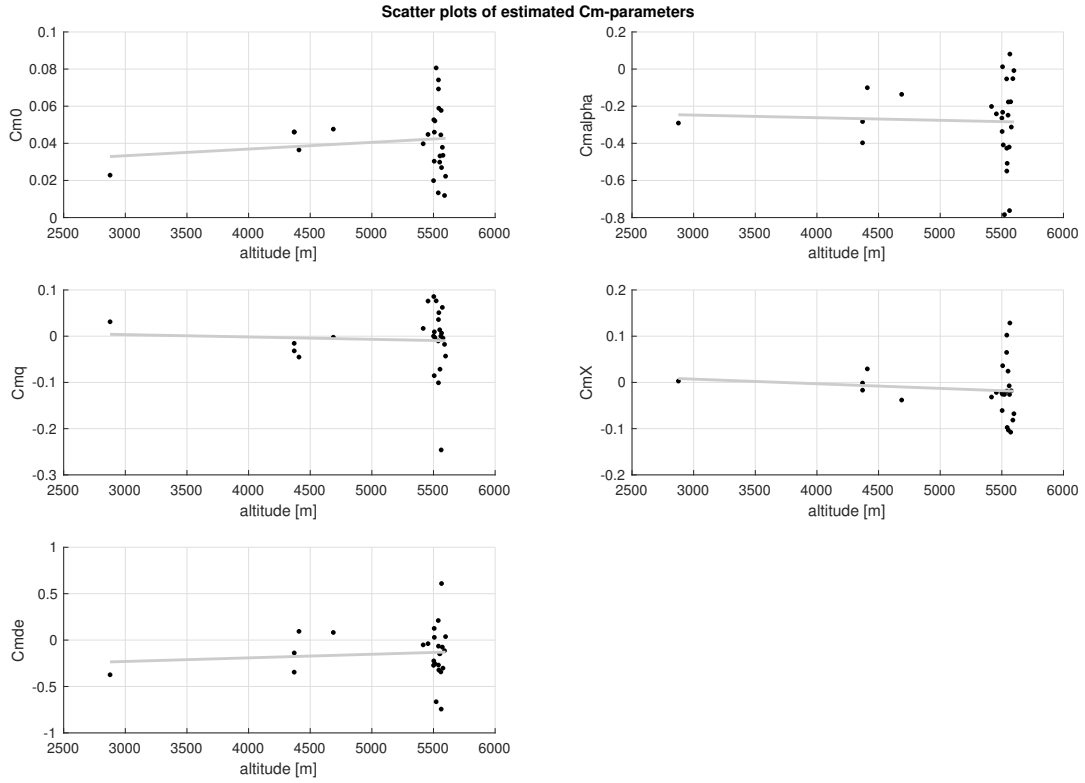

Figure 7.6: Plots of the estimated C_m-parameter values versus average altitude h during the stall maneuver, with linear trend lines fitted to them

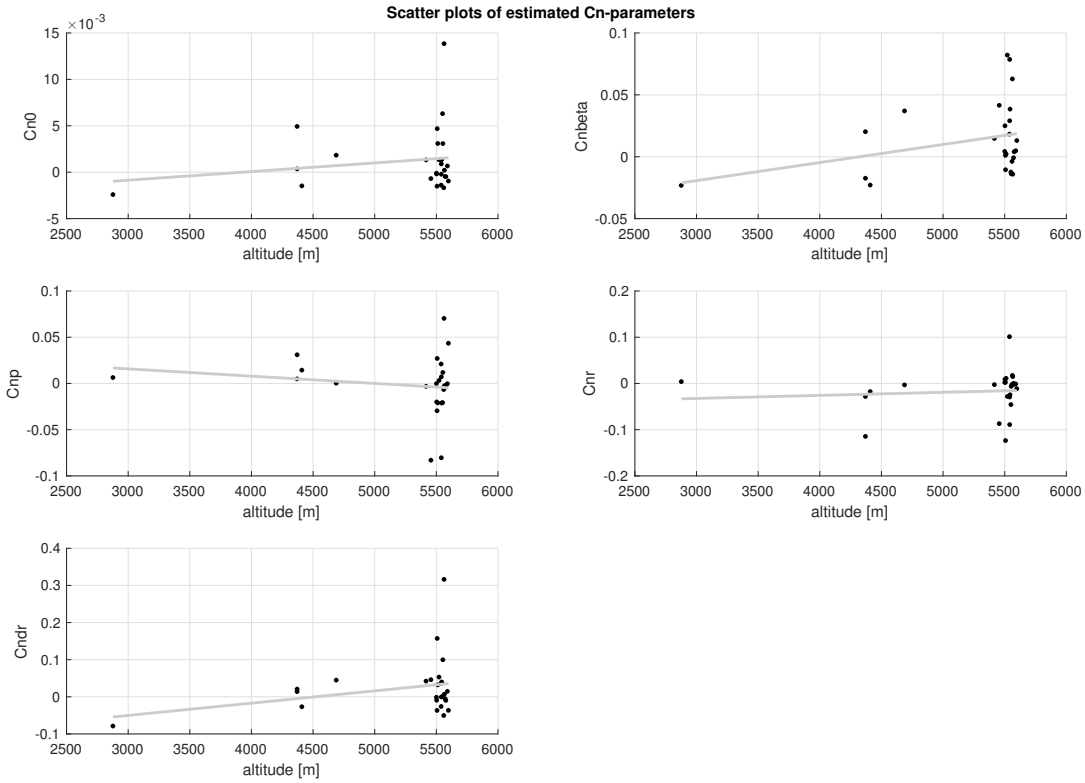

Figure 7.7: Plots of the estimated C_n-parameter values versus average altitude h during the stall maneuver, with linear trend lines fitted to them

For the modeled moment equation parameters, shown in Figures 7.5 to 7.7, one very clear observation can be made. The estimated values of the dynamic damping terms (C_{l_p} C_{m_q} C_{n_r}) as well as the control effectiveness terms ($C_{l_{\delta_a}}$ $C_{m_{\delta_e}}$ $C_{n_{\delta_r}}$) are approximately zero: some estimates are positive, some are negative. Under normal flight conditions, one would expect these derivatives to have a clear positive or negative value. Changes in the sign during flight has a strong effect on flight dynamics.

It is possible that exactly this has happened, that during stall the sign of these terms changes. The data sets contain portions of both "normal" as well as stalled flight, but the model has only one parameter to describe both parts. The optimal value is then likely to be around zero. Unfortunately, this will result in a bad description of both flight conditions. It would be interesting to see what happens if the model is given more freedom to vary the dynamic damping and control response as the aircraft progresses into stall. New model terms could enable such freedom.

Overall, what is clear is that the variance of the parameter estimates is significant, and that some results are not in line with expectation. Large or unexpected variations in parameter estimates on training data can be a symptom of several underlying problems. First, it can arise from modeling error. This is likely if the model cannot represent the features in the data. The changing sign of the control effectiveness terms could be an example of this.

Second, it is possible that the data is not informative enough. This can arise from a range of causes: the flight test maneuver flown, flight instrumentation calibration errors or noise, or errors in the flight path reconstruction. Of these, the first is most likely, as the sensors and Kalman filter methods are the result of careful development, yet all these reasons deserve looking into.

The final possible error source is the optimization method. Currently, `fmincon` is tasked with optimizing all 30 parameters simultaneously, which means that the search space is of high dimension. It is probable that on at least several of the data sets the optimum was not found. Other issues could be that the cost function is not sensitive to parameter changes, or that the estimation of the sensitivity cannot be determined accurately.

7.2.2. Parameter Correlations

Table 7.3 presents the correlations between the model parameters. Since large absolute correlation values are indicative of modeling or data issues, correlations larger than 0.7 have been highlighted. Judging what is "too large" of a correlation factor is subject to debate, but 0.9 is a common threshold. For more convenient referencing, the largest correlation values (i.e. those >0.7) have been repeated in Table 7.2.

Table 7.2: Largest absolute parameter correlation values (repeated from Table 7.3)

θ_1	θ_2	cor
C_{L_0}	C_{L_α}	-0.86
C_{D_0}	C_{D_α}	-0.88
C_{m_0}	C_{m_α}	-0.79
C_{m_α}	$C_{m_{\delta_e}}$	0.87
C_{n_0}	$C_{n_{\delta_r}}$	0.87
C_{l_r}	C_{l_p}	-0.73
C_{m_0}	C_{Y_β}	-0.73
C_{m_α}	C_{Y_β}	0.75
C_{l_r}	$C_{n_{\delta_r}}$	0.75

C_{L_0} and C_{L_α}, C_{D_0} and C_{D_α} as well as C_{m_0} and C_{m_α} are significantly negatively correlated. Apparently it is difficult for the optimization to distinguish between a static effect and the influence of α. Most of the flight data (approach to stall, stall recovery) is within a narrow range of α-values, which might be a reason for this. However, since during the stall several large α-excitation have been achieved, it was expected that the correlation would have been lower.

The second strong correlation is between C_{m_α} and $C_{m_{\delta_e}}$. A possible explanation for this is a strong correlation between α and δ_e. This explanation is feasible, as during the entry into stall the angle of attack increase is achieved by increasing the elevator input. This corresponds to a large fraction of the time of the recorded maneuvers.

Along the yaw axis, C_{n_0} and $C_{n_{\delta_r}}$ show a large positive correlation. It is not quite clear what is the cause of this, since one would expect C_{n_0} to be zero for an aircraft that is nearly symmetric along the XZ-plane. For many maneuvers, the rudder input was not actively used, and thus close to zero. Small static rudder effects may thus have been attributed to both of these parameters.

Next, C_{l_p} and C_{l_r} are negatively correlated. This means that as the roll damping term becomes larger (i.e. less negative), the term for roll moment due to yaw becomes smaller. This can easily happen in roll and yaw motions are strongly correlated during the maneuvers.

The rest of the correlations are less obvious to explain, as they consider derivatives of different forces/moments to different variables. Of course, their correlations could be a coincidence, but it is likely that each of them is influenced by the fact that the aircraft has stalled during the test flight maneuver. Hence, their correlations are expected to arise from several different flow phenomena that all arise from the stall condition. This is a flag for that more model terms are needed to explain the difference under stalled flight.

7.3. Time-History Comparisons

To illustrate the model fit quality in a more intuitive way, this section presents time-history comparisons of the data and model output. Both a training data example and a validation data example are shown.

7.3.1. Training Data Example

The training set with the lowest mean squared error is presented in Figure 7.8. Due to the nonlinear solver method that is used, many optimization attempts do not end up in the global optimum. The result is a modeling error that is not entirely due to the model structure. Hence, showing the result with the lowest error is most illustrative of the model approximation power of the model structure. It must be noted that this approach can only be used when it is reasonable to assume that the model will suffer from *bias* (i.e. the approximation power is expected to be too low). Due to the structure of Equation 7.1 and the estimated parameter values, this was deemed appropriate in this case.

The plot shows the control surface deflections, the model values of the flow point separation parameter X, and the comparisons of the six aerodynamic forces and moments acting on the aircraft. The maximum angle of attack recorded during the maneuver was about 19°.

Considering the modeled force equations, it was expected beforehand that at least the lift coefficient should show a reasonable fit, since Kirchoff's theory was developed for modeling the effect on airfoil lift. Figure 7.8 shows that this was correct, both C_L and drag coefficient C_D are represented quite well. The model output follows the general trend of the measured data closely, during both stall and the regular flight regime. However, there is some oscillatory behavior during the stall around $t = 38$ seconds that the model cannot reproduce. Furthermore, the model output for the lateral force C_Y is clearly lacking, and is around zero during the entire maneuver.

The modeled moment equations show a less adequate fit than the forces. For all moments, some type of response can be seen during the stall. However, the model cannot track the oscillations in the data. For C_m and C_n at least the phase response is in accordance; for the roll moment C_l the derivative model response is at some points of opposite sign compared to the measurements. It is clear that the models for the moments need a lot of work.

7.3.2. Validation Data Example

A better indication of overall model quality is obtained when investigating the model output compared to a validation data set. To generate the validation data, the altitude of the flight maneuver was used to look up the model parameter values from the fitted linear trend lines in Figures 7.2 to 7.7. The results is shown in Figure 7.9.

The validation data plot has the same structure as the training data plot. The type of stall performed here was different compared to the one shown in Figure 7.8: the Citation II was stalled multiple times. This can be seen from the variation of X, and in the oscillations of C_L. Eight validation data sets were available, one of them was chosen that contained excitations in all control surfaces. When observed visually, all validation data plots were of similar quality.

The lift coefficient again shows a reasonable fit. Some phase lag is seen, the model response is slightly slower than the measured response. The fact that the results agree quite well is a good indication that the model structure is indeed suitable for simulating aerodynamic stall.

It is interesting to observe that the fits for C_l and C_n appear to be *better* than in the training data. A conclusive reason for this could not be found, but it appears that the parameters found during model training are far from optimal. The plots for C_D, C_Y, and C_m show that the fitting quality is not good, and a lot of work still needs to be done.

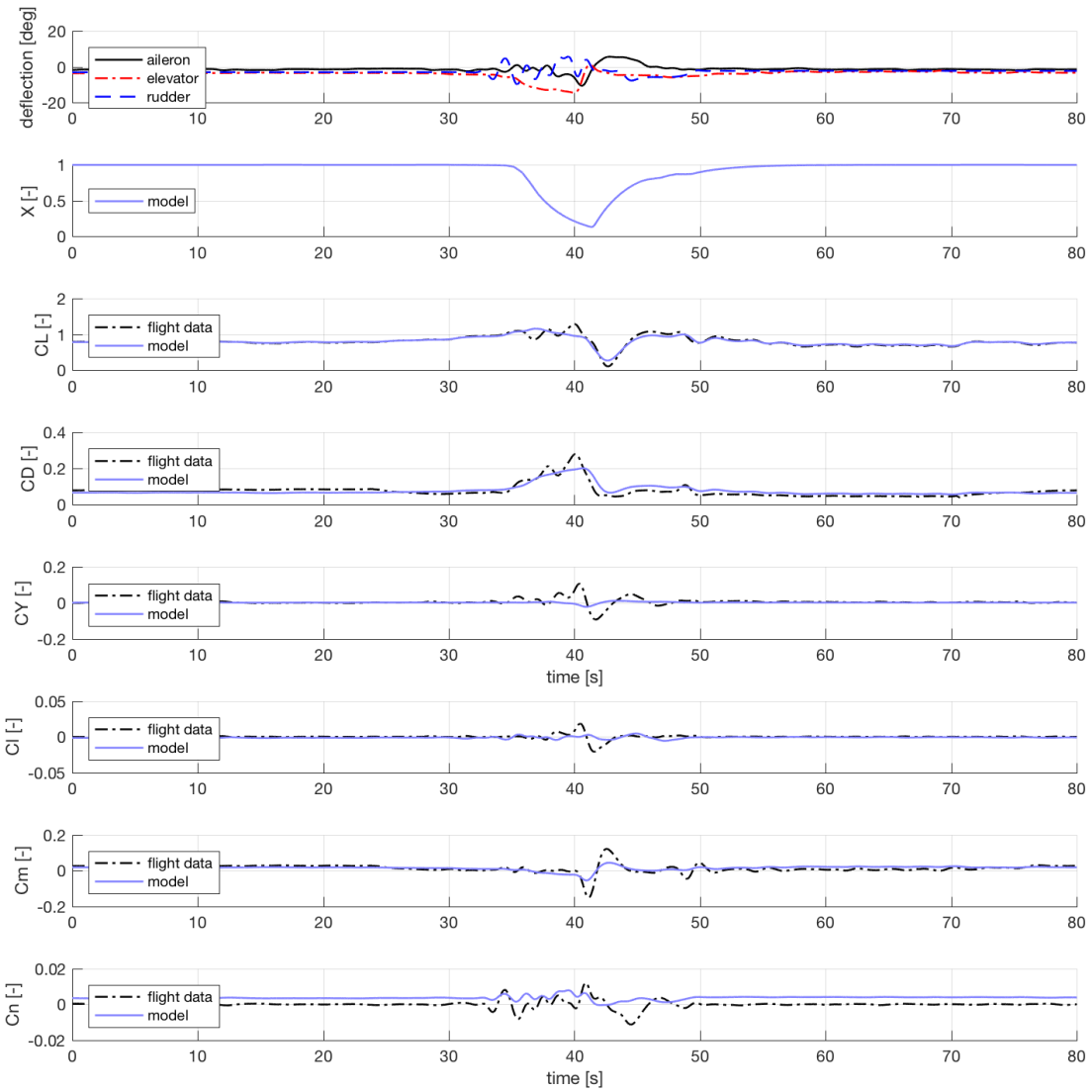

Figure 7.8: Time history comparison of **training data** versus model output, the best training result was selected with MSE=$6.6087e-4$

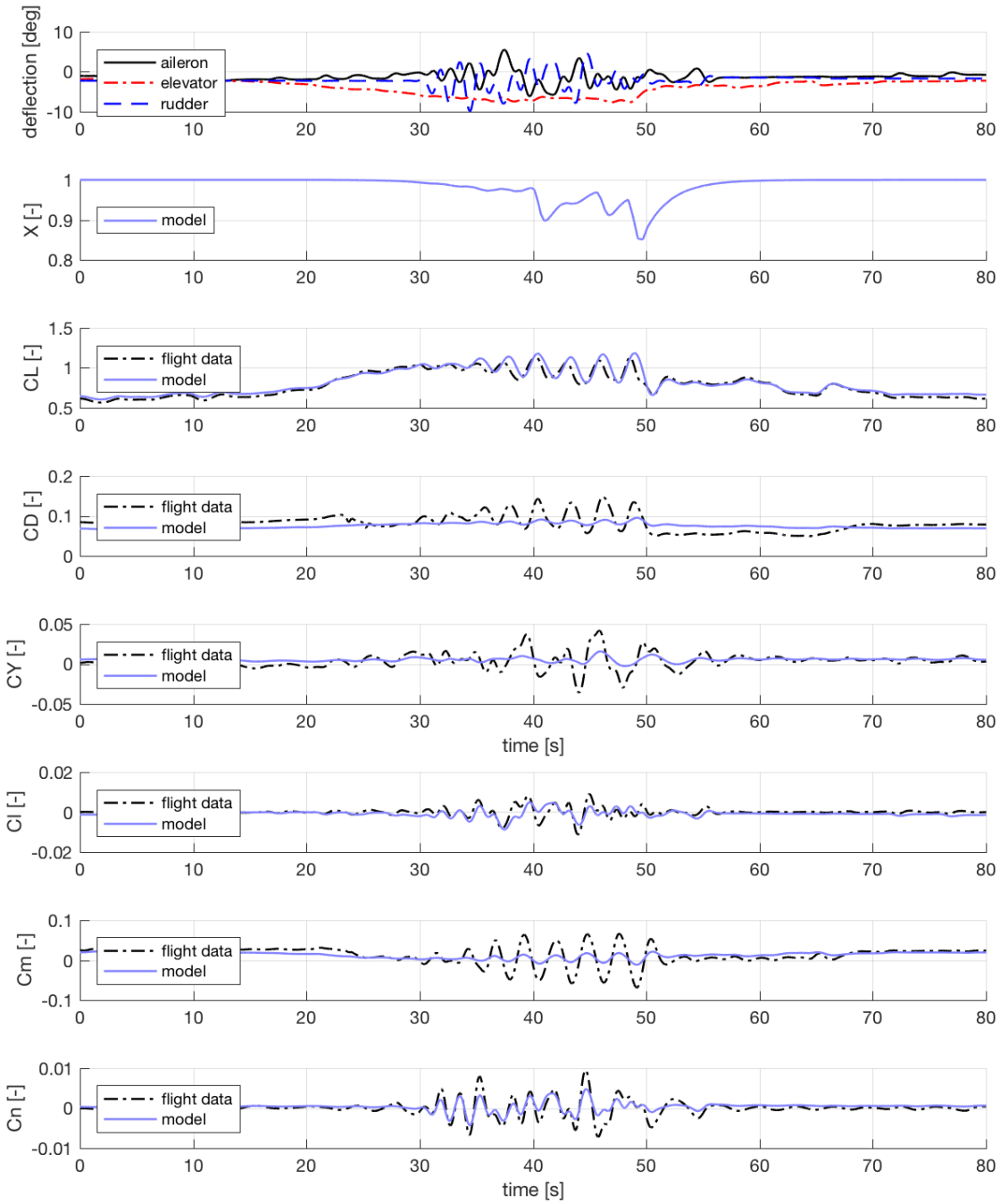

Figure 7.9: Time history comparison of **validation data** versus model output

7.4. Sensitivity Analysis

One possible reason for the large observed variance in the estimated parameter values is that the model fit quality might be insensitive to changes in parameter values. A sensitivity analysis offers more insight into such issues, which is why one was performed. The result shown here is the sensitivity of the parameters on the same training data set as displayed in Figure 7.8.

It is expected that during future research, only the parameters of X are solved using the nonlinear optimization, based on the measured C_L signals. After that, all other model parameters can be solved using linear methods, which are guaranteed to find the global optimum. Hence, at this point only the X and C_L-parameter sensitivity is of interest.

To perform the sensitivity analysis, each parameter of interest was varied over a range around its current value in small steps. At each step, the VAF was computed as a measure for model fit. An advantage of the VAF for this purpose is that it is a normalized metric. All other parameters were kept fixed at their respective optimally estimated values. Because of the model nonlinearity, the parameter sensitivity may depend on the values themselves. Moreover, note that cross-dependencies between multiple parameters cannot be investigated in this way.

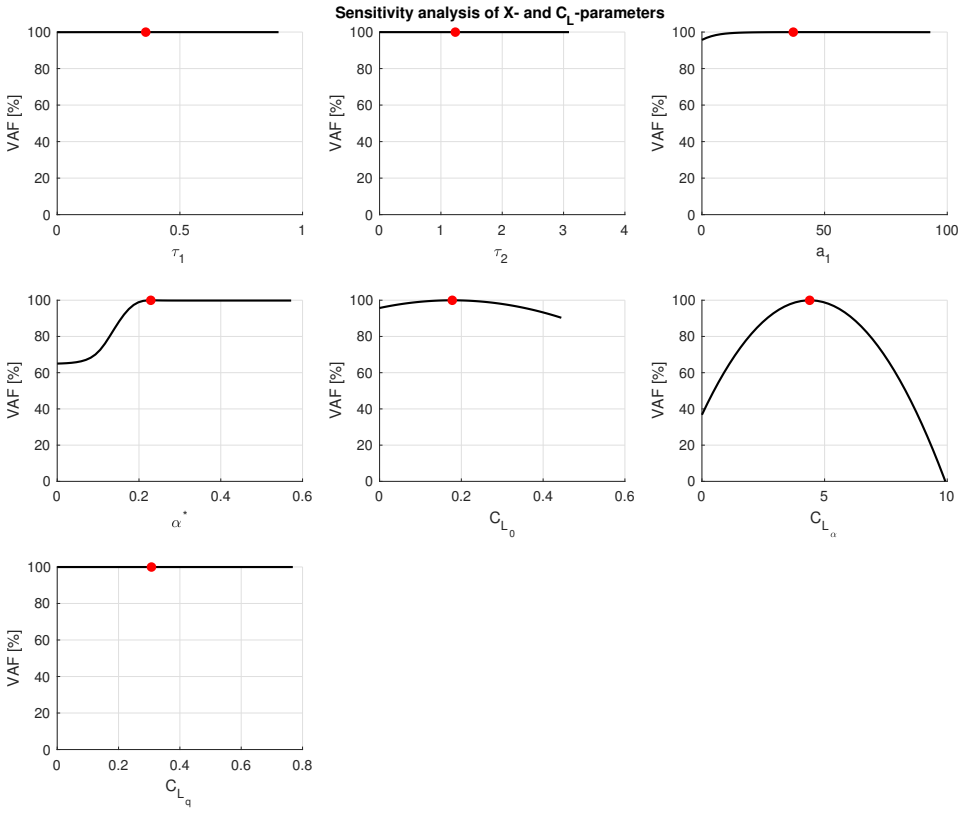

Figure 7.10: Sensitivity analysis of X and C_L-parameters, red dot indicates estimated optimal parameter value, same dataset as the one presented in Figure 7.8

It is clear from Figure 7.10 that the sensitivity of the X-parameters is very low, possibly with the exception of α^*. Furthermore, it appears as if C_{L_q} is difficult to estimate. Which might indicate that it is not necessary to include this model term.

Overall, it can be concluded that whilst the stall model structure using Kirchoff's theory of flow separation enables modeling of the aircraft lift during aerodynamic stall, the associated parameter estimation is a challenging task.

Table 7.3: Correlations between the estimates of the model parameters on the 26 training data sets, absolute correlation values larger than 0.7 have been highlighted

	τ_1	τ_2	a_1	α^*	C_{L_0}	C_{L_α}	C_{L_q}	C_{D_0}	C_{D_α}	C_{D_q}	C_{D_X}	C_{Y_0}	C_{Y_β}	C_{Y_p}	C_{Y_r}	C_{l_0}	C_{l_β}	C_{l_p}	C_{l_r}	$C_{l_{\delta_a}}$	C_{m_0}	C_{m_α}	C_{m_q}	C_{m_X}	$C_{m_{\delta_e}}$	C_{n_0}	C_{n_β}	C_{n_p}	C_{n_r}	$C_{n_{\delta_r}}$
τ_1	1.00	0.17	0.41	0.06	0.34	-0.40	0.06	-0.14	0.24	0.06	-0.33	0.09	-0.37	0.03	0.32	0.07	0.26	-0.07	0.11	0.23	0.43	-0.63	-0.08	-0.05	-0.64	0.11	0.28	0.15	-0.11	-0.01
τ_2		1.00	0.26	-0.06	-0.05	0.06	-0.21	-0.01	0.02	0.31	0.07	0.17	-0.33	0.27	0.39	0.20	-0.06	0.07	0.15	0.15	0.06	-0.17	-0.03	-0.19	-0.28	-0.08	0.34	0.17	0.18	-0.02
a_1			1.00	-0.37	0.10	-0.35	-0.24	0.01	0.20	-0.08	-0.19	0.51	-0.28	0.13	0.08	0.29	0.40	-0.05	-0.08	0.33	0.20	-0.25	0.10	-0.32	-0.39	-0.15	0.13	-0.16	-0.25	-0.17
α^*				1.00	0.39	-0.40	0.10	-0.14	0.01	0.16	0.13	0.09	-0.09	-0.03	-0.07	-0.27	-0.09	-0.32	0.40	-0.34	0.13	-0.20	-0.09	0.19	-0.14	0.16	-0.01	0.21	0.02	0.29
C_{L_0}					1.00	-0.86	0.18	0.14	0.02	-0.12	-0.06	0.12	0.08	-0.07	-0.06	-0.38	-0.03	-0.02	0.08	0.00	0.10	-0.04	-0.01	0.00	-0.05	0.20	-0.16	0.06	-0.18	0.04
C_{L_α}						1.00	-0.05	-0.13	-0.06	0.15	0.06	-0.19	0.04	-0.06	0.13	0.28	-0.31	0.20	-0.17	-0.11	-0.20	0.18	-0.01	0.11	0.25	-0.19	0.16	0.06	0.43	-0.09
C_{L_q}							1.00	0.11	0.01	-0.24	-0.32	0.09	-0.02	0.03	-0.13	-0.09	-0.04	-0.22	0.23	0.12	0.12	-0.12	-0.39	0.08	-0.06	0.43	-0.03	0.39	0.04	0.42
C_{D_0}								1.00	-0.88	0.29	0.18	0.04	-0.10	0.30	-0.17	-0.07	0.11	0.04	0.11	0.10	0.36	0.08	0.19	-0.15	0.22	-0.13	0.14	-0.23	-0.19	-0.03
C_{D_α}									1.00	-0.38	-0.40	0.02	0.06	-0.18	0.08	0.12	0.05	-0.15	-0.09	0.07	-0.29	-0.09	-0.30	-0.06	-0.28	0.21	-0.13	0.21	0.06	0.08
C_{D_q}										1.00	-0.19	0.17	-0.28	0.45	0.26	0.04	0.05	-0.43	0.43	-0.20	0.19	-0.21	0.03	-0.09	-0.16	-0.14	0.58	-0.24	0.54	0.06
C_{D_X}											1.00	-0.06	0.23	-0.19	-0.16	-0.13	-0.24	0.58	-0.30	-0.19	-0.21	0.35	0.42	0.25	0.36	-0.50	-0.40	0.02	-0.22	-0.43
C_{Y_0}												1.00	-0.39	0.32	-0.10	-0.01	0.02	-0.38	0.28	-0.23	0.27	-0.29	0.04	-0.21	-0.30	-0.08	0.20	-0.09	0.13	0.12
C_{Y_β}													1.00	-0.33	-0.29	0.16	-0.09	0.34	-0.36	0.09	-0.73	0.75	-0.03	0.07	0.58	-0.30	-0.70	0.15	0.17	-0.34
C_{Y_p}														1.00	-0.14	-0.06	0.54	-0.39	0.46	-0.04	0.17	-0.08	-0.05	-0.04	-0.03	-0.11	0.31	-0.41	0.06	0.08
C_{Y_r}															1.00	0.16	-0.13	0.19	-0.07	0.10	0.31	-0.44	0.12	0.01	-0.41	0.08	0.55	-0.02	0.15	-0.01
C_{l_0}																1.00	0.19	0.07	-0.32	0.60	-0.05	0.12	-0.04	-0.33	0.00	-0.41	0.18	0.00	0.09	-0.24
C_{l_β}																	1.00	-0.26	0.16	0.27	0.07	-0.02	0.18	-0.11	-0.05	-0.16	0.02	-0.36	-0.26	-0.09
C_{l_p}																		1.00	-0.73	0.09	-0.19	0.32	0.48	0.17	0.34	-0.45	-0.34	-0.05	-0.14	-0.62
C_{l_r}																			1.00	-0.33	0.29	-0.43	-0.36	-0.04	-0.35	0.54	0.40	0.24	0.02	0.75
$C_{l_{\delta_a}}$																				1.00	-0.15	0.17	-0.20	-0.32	-0.06	-0.10	-0.10	0.15	-0.11	-0.25
C_{m_0}																					1.00	-0.79	0.05	-0.01	-0.48	0.28	0.69	-0.22	-0.41	0.37
C_{m_α}																						1.00	0.07	0.13	0.87	-0.44	-0.66	0.01	0.18	-0.47
C_{m_q}																							1.00	-0.15	0.11	-0.54	0.02	-0.60	-0.08	-0.50
C_{m_X}																								1.00	0.42	-0.06	-0.16	0.08	-0.09	-0.11
$C_{m_{\delta_e}}$																									1.00	-0.39	-0.46	-0.10	0.06	-0.36
C_{n_0}																										1.00	0.21	0.40	-0.20	0.87
C_{n_β}																											1.00	-0.24	0.03	0.40
C_{n_p}																												1.00	0.12	0.33
C_{n_r}																													1.00	-0.18
$C_{n_{\delta_r}}$																														1.00

8

Conclusion & Outlook

This chapter concludes the preliminary thesis report. It is structured in two parts. First the conclusions that have followed from the past months of thesis work are presented. These are connected to the research questions as much as possible. The second part of this chapter presents what actions and research still needs to be performed during the remainder of the thesis work.

8.1. Conclusion

A conclusive answer to the main research question cannot be given yet. However, the findings in this preliminary thesis report allow for some statements to be made which already constrain the solution space of the sub-questions. The sub-questions are repeated here, along with the findings so far.

1. *What types of flight test maneuvers are suitable for identifying dynamic stall behavior, including control surface degradation?*

- 34 new stall maneuvers were gathered, including the measurements of a boom-mounted α- and β-vane. Additionally, a database of about 80 recorded stall maneuvers, which do not include this boom data, exists. Comparison of the reconstructed state trajectories between the two databases showed that from the old data, the longitudinal states could potentially still be used, under some conditions. The lateral-directional states, β in particular, could not be accurately reconstructed with a lacking boom signal.
- The amount of test data gathered so far does not seem sufficient to make a stall model that is valid for the entire operational altitude envelope. Instead, the final model will likely be constrained to around 5500 m altitude (FL180), since most new test data was gathered at that condition.
- Two types of new flight test maneuvers were gathered: longitudinal (1g) and accelerated (1.1g or 1.4g). Moreover, there was significant variation between the recorded maneuvers in terms control surface excitation (choice of control, amplitude, frequency). It was not yet possible to analyze the relation between these types of maneuvers and the resulting model quality, as the current stall model is not yet of sufficient fidelity for this.

2. *What model structure is suitable for representing aircraft stall behavior, including both longitudinal and lateral-directional dynamics, changes in control surface effectiveness, and dynamic effects?*

- In literature, two main stall modeling methods can be found. The first is derived from methods developed originally for fighter aircraft, and is heavily based on wind tunnel tests. The second method is derived from semi-empirical knowledge on the lift of a stalled airfoil, and builds on Kirchoff's theory of flow separation. It has been shown that its parameters can be estimated from flight data.
- Given the current availability of flight test data, the considerable cost and complexity of executing wind tunnel tests, and prior experience with Kirchoff's method, the fighter method is not feasible for the current research.

- The current preliminary results, which follow from a naive approach, indicate that modeling the lift coefficient during aerodynamic stall using Kirchoff's method is a promising approach. This confirms what could be found in literature.
- The results of the models for the other forces and the moments indicate that the preliminary model structure did not offer adequate approximation power. As a result, these models still need a lot of work.

3. *What parameter estimation techniques are suitable for accurately estimating the parameters of a nonlinear stall model structure from flight data?*

- Estimating the X-parameters is a challenging task with the methods that have been applied so far. A large variance in the estimated values can be seen. The presence of local optima is very likely. The model output is not very sensitive to changes in the X-parameters. Moreover, the finite difference methods used internally by MATLAB's gradient-based numerical optimization algorithms do not give robust results as X is governed by an ODE.
- Estimating the other model parameters shows similar difficulties as the X-parameters, albeit slightly less severe. An important realization was that for a wide range of model structures, and once the X-parameters are fixed, the rest of the model parameters can be solved using the familiar least-squares methods. Doing so would give an incredible boost to the speed and convenience of estimating these parameters.
- Large parts of the model are the same as a conventional aerodynamic modeling approach, which describes the flight dynamics of the Citation II in the regular flight envelope. Such a model already exists, so prior knowledge on these parameters that coincide is available.

Other conclusions

- The recommendation from [56] to use an Unscented Kalman Filter for flight path reconstruction appears to lead to correct results. Also when the UKF was modified to include the new boom signals, the results were as expected.

8.2. Outlook For Remainder of the Thesis

From the conclusions and experience of thesis work so far, a general approach for the rest of the thesis work was derived. In broad terms, the work will mainly involve iterations between implementing better parameter estimation methods and adjusting the stall model structure.

However, a list of more specific adjustments or topics that can be investigated was gathered. This section presents this list, with the elements roughly ordered in a logical order of execution. Obviously, it is not expected to be conclusive, and only represents the best ideas during the writing of this report.

- The first action will be to implement the numerical method for computing the parameter gradient of an ODE, as described in chapter 6, and use this to explicitly supply MATLAB's nonlinear solvers with the cost function gradient. This should improve the algorithms' performance.
- Next, the effect of the resampling of the AHRS output signals will be investigated. The AHRS has an update rate of 19.2 ms, whereas all flight data is re-sampled to 100 Hz, or 10 ms. This resampling might result in large numerical jumps in the body specific force or rotations signals. The effect of this on the data is not understood yet.
- For the preliminary results, the interior point algorithm was used for estimating the optimal parameter values. MATLAB offers several other gradient-based algorithms; each has different performance and robustness. A straightforward comparison of these will be done to investigate any noticeable difference in practicality and results.
- So far, only gradient-based algorithms have be used for the nonlinear optimization, yet numerically estimating the gradient is difficult and complex. Gradient-free algorithms exist, and are available within MATLAB's Optimization toolbox. Also their performance will be investigated, preferably alongside the gradient-based algorithms.
- The "old" flight test data, i.e. the data without air data boom, will be included in the parameter estimation effort for the longitudinal model terms wherever possible, especially the C_L case. Differences between the old and new data estimates will be closely monitored, as it is not clear yet whether including the old flight data indeed leads to an increase in model quality.

- An explicit analysis into the effect of the data on the resulting model quality will be done. This includes comparing the old and new data, but also comparing between the maneuver types within the new data. This analysis could result into valuable insights that guide further flight test experiments.
- An attempt will be made to estimate the X-parameters first, using only the measured lift coefficient signals. In this, the assumption is made that these X-parameters are independent of the other parameters. For this to be successful, it should be made sufficiently plausible that the X-parameters can be accurately be described as a function of flight condition.
- If it is possible to fix the X-parameters, linear methods will be implemented for the remainder of the parameter estimation task.
- New candidate model terms will be proposed for all aerodynamic model equations. These terms can include: X, $\dot{X}$, other aircraft states or control signals, simple splines, (polynomial) functions, or combinations of these. All these terms will then be evaluated: do they improve the model fidelity enough to justify the added model complexity?
- The current stall buffet model will be investigated and compared to the new flight test data. If necessary, an update will be made.
- Special care must be taken to merge the newly developed stall model and the "regular" aerodynamic model of the Citation II. The envelopes of these models overlap, and some way of switching between them is required. Moreover, the output of the two models should agree to a reasonable level in the transition area, i.e. the simulated response should at least have the same sign, and preferably also approximately the same magnitude.
- To include prior knowledge of the flight dynamics model of the Citation II, Bayesian parameter estimation techniques can be used. Such methods are fundamentally different from the MLE-based methods that implemented so far, their implementation is quite complex, and will require a significant effort time-wise. Therefore, doing this might not be worth it in the limited time available.
- The resulting stall model will be integrated into DASMAT, which will enable the use of the model in the SIMONA research simulator. Experiencing the result of the simulated stall in a full-motion simulator will help in identifying the model's strong and weak points.
- The last planned step of the thesis is to compare the model output to the FAA FTSD qualification requirements. The regulations clearly specify a set of maneuvers for which the performance of the flight dynamics model must be evaluated. Besides the numerical tolerances, the evaluation also contains a subjective part, which might not be feasible yet to evaluate.

Bibliography

[1] N. B. Abramov, M. G. Goman, and A. N. Khrabrov. Aerodynamic Model of Transport Airplane in Extended Envelope for Simulation of Upset Recovery. In *Royal Aeronautical Society Aerodynamics Conference*, number July, 2010. URL http://www.icas-proceedings.net/ICAS2012/PAPERS/770.PDF.

[2] N. B. Abramov, M. G. Goman, and A. N. Khrabrov. Aerodynamic Model of Transport Airplane in Extended Envelope for Simulation of Upset Recovery. In *28th International Congess of the Aeronautical Sciences*, 2012. URL http://www.icas-proceedings.net/ICAS2012/PAPERS/770.PDF.

[3] N. B. Abramov, M. G. Goman, A. N. Khrabrov, E. N. Kolesnikov, L. Fucke, B. Soemarwoto, and H. Smaili. Pushing Ahead - SUPRA Airplane Model for Upset Recovery. In *AIAA Modeling and Simulation Technologies Conference*, number August, 2012. ISBN 9781624101830. doi: 10.2514/6.2012-4631.

[4] J. Batterson and V. Klein. Partitioning of flight data for aerodynamic modeling of aircraft at high angles of attack. *14th Atmospheric Flight Mechanics Conference*, 26(4):334–339, 1987. ISSN 00218669. doi: doi:10.2514/6.1987-2621.

[5] Boeing Commercial Airplanes. Report: Statistical Summary of Commercial Jet Airplane Accidents, Worldwide Operations, 1959-2015. Technical report, 2015. URL http://www.boeing.com/resources/boeingdotcom/company/about{_}bca/pdf/statsum.pdf.

[6] J. M. Brandon, J. V. Foster, G. H. Shah, W. Gato, and J. E. Wilborn. Comparison of Rolling Moment Characteristics During Roll Oscillations for a Low and a High Aspect Ratio Configuration. In *AIAA Atmospheric Flight Mechanics Conference and Exhibit*, number August, 2004. ISBN 978-1-62410-072-7. doi: 10.2514/6.2004-5273. URL http://arc.aiaa.org/doi/abs/10.2514/6.2004-5273.

[7] J. R. Chambers and E. L. Anglin. NASA Technical Note D-5361: Analysis of Lateral-Directional Stability Characteristics of a Twin-Jet Fighter Airplane at High Angles of Attack, 1969.

[8] J. R. Chambers and S. B. Grafton. Aerodynamic Characteristics of Airplanes at High Angles of Attack. *Journal of Aircraft*, 31(5):1109–1115, 1977.

[9] J. R. Chambers and H. P Stough. Summary of NASA Stall/Spin Research for General Aviation Configurations. *AIAA General Aviation Technology Conference*, (86), 1986.

[10] P. L. Coe, A. B. Gruhum, and J. R. Chambers. NASA Technical Note D-7972: Summary of Information on Low-Speed Lateral-Directional Derivatives Due to Rate of Change of Sideslip, 1975.

[11] D. A. Crider. The Need for Upset Recovery Training. In *AIAA Modeling and Simulation Technologies Conference and Exhibit*, number August, 2008. ISBN 9781600869624. doi: AIAA-2008-6864.

[12] K. Cunningham, J. V. Foster, G. H. Shah, E. C. Stewart, R. N. Ventura, R. A. Rivers, J. E. Wilborn, and W. Gato. Simulation Study of Flap Effects on a Commercial Transport Airplane in Upset Conditions. In *AIAA Atmospheric Flight Mechanics Conference and Exhibit*, number August, 2005. ISBN 156347736X. doi: AIAA-2005-5908.

[13] A. Da Ronch, D. Vallespin, M. Ghoreyshi, and K. J. Badcock. Evaluation of Dynamic Derivatives Using Computational Fluid Dynamics. *AIAA Journal*, 50(2):470–484, 2012. ISSN 0001-1452. doi: 10.2514/1.J051304.

[14] C. C. de Visser. *Global Nonlinear Model Identification with Multivariate Splines*. PhD thesis, Delft University of Technology, 2011.

[15] J. N. Dias. High Angle of Attack Model Identification with Compressibility Effects. *AIAA Atmospheric Flight Mechanics Conference*, (January):1–15, 2015. doi: 10.2514/6.2015-1477. URL http://arc.aiaa.org/doi/10.2514/6.2015-1477.

[16] J. N. Dias. Unsteady and Post-Stall Model Identification Using Dynamic Stall Maneuvers. (June):1–15, 2015. doi: 10.2514/6.2015-2705.

[17] E.G. Dickes, J.N. Ralston, and K. Lawson. Application Of Large-Angle Data For Flight Simulation. In *AIAA Modeling and Simulation Technologies Conference and Exhibit*, number August, 2000. doi: doi: 10.2514/6.2000-4584.

[18] B.J. Eulrich and N.C. Weingarten. Identification and Correlation of the F-4E Post-Stall Aerodynamic Stability and Control Characteristics From Existing Test Data, 1973.

[19] European Commission. SUPRA Report Summary. pages 1–12, 2013. URL `http://cordis.europa.eu/result/rcn/56069{_}en.html`.

[20] Federal Aviation Administration. Advisory Circular 120-109A, 2015. ISSN 0047-2875. URL `https://www.faa.gov/documentLibrary/media/Advisory{_}Circular/AC{_}120-109A.pdf`.

[21] Federal Aviation Administration. 14 CFR Part 60, 2016. URL `https://www.faa.gov/about/initiatives/nsp/media/14CFR60{_}Searchable{_}Version.pdf`.

[22] D. Fischenberg. Identification of an Unsteady Aerodynamic Stall Model from Flight Test Data. 1995.

[23] D. Fischenberg and R. V. Jategaonkar. Identification of Aircraft Stall Behavior from Flight Test Data. In *RTO SCI Symposium on System Identification for Integrated Aircraft Development and Flight Testing*, number May, 1998. URL `http://www.dtic.mil/cgi-bin/GetTRDoc?AD=ADA361699{#}page=228`.

[24] J. V. Foster, K. Cunningham, and C. M. Fremaux. Dynamics Modeling and Simulation of Large Transport Airplanes in Upset Conditions. In *AIAA Guidance, Navigation, and Control Conference and Exhibit*, number August, 2005. ISBN 978-1-62410-056-7. doi: AIAA-2005-5933. URL `http://arc.aiaa.org/doi/pdf/10.2514/6.2005-5933`.

[25] B.L. Gadeberg. NACA Technical Note 2525: The Effect of Rate of Change of Angle of Attack on the Maximum Lift Coefficient, 1951.

[26] D. R. Gingras and J. N. Ralston. Aerodynamics Modeling for Upset Training. *AIAA Modeling and Simulation Technologies Conference and Exhibit*, (August), 2008.

[27] D. R. Gingras and J. N. Ralston. Aerodynamics Modelling for Training on the Edge of the Flight Envelope. *Aeronautical Journal*, 116(1175):67–86, 2012. ISSN 00019240.

[28] D. R. Gingras, J. N. Ralston, and C. A. Wilkening. Improvement of Stall-Regime Aerodynamics Modeling for Aircraft Training Simulations. *AIAA Modeling and Simulation Technologies Conference*, (August), 2010. doi: doi:10.2514/6.2010-7793. URL `http://arc.aiaa.org/doi/pdf/10.2514/6.2010-7793`.

[29] M. G. Goman and A. N. Khrabrov. State-space representation of aerodynamic characteristics of an aircraft at high angles of attack. In *Astrodynamics Conference*, 1992. doi: 10.2514/6.1992-4651.

[30] E. L. Groen, W. Ledegang, J. Field, H. Smaili, M. Roza, L. Fucke, S. A. E. Nooij, M. G. Goman, M. Mayrhofer, L. Zaichik, M. Grigoryev, and V. Biryukov. SUPRA – Enhanced Upset Recovery Simulation. In *AIAA Modeling and Simulation Technologies Conference*, 2012.

[31] D.E. Hewes. NASA Memo 5-20-59L: Low-Subsonic Measurements of the Static and Oscillatory Lateral Stability Derivatives of a Sweptback-Wing Airplane Configuration at AOA from -10 to 90 deg, 1959.

[32] M. Hwang and J.H. Seinfeld. Observability of Nonlinear Systems. *Journal of Optimization Theory and Applications*, 10(2), 1972.

[33] K.W. Iliff, R.E. Maine, and M.F. Shafer. NASA Technical Note D-8136: Subsonic Stability and Control Derivatives for an Unpowered, Removely Piloted 3/8-Scale F-15 Airplane Model Obtained from Flight Test, 1976.

[34] S.R. Jacobson. Aircraft Loss of Control Causal Factors and Mitigation Challenges. In *AIAA Guidance, Navigation, and Control Conference*, pages 1–59, 2010. ISBN 978-1-60086-962-4. doi: 10.2514/6.2010-8007. URL `papers2://publication/uuid/D78999A0-9BA0-4720-A2CE-BB2777112613`.

[35] J. Kay, J.N. Ralston, and S.F. Lash. Development of Non-Linear, Low-Speed Aerodynamic Model for the F-16 VISTA. In *22nd Atmospheric Flight Mechanics Conference*, 1997.

[36] V. Klein and E. A. Morelli. *Aircraft System Identification: Theory and Practice*. 2006. ISBN 1563478323. doi: ISBN1-56347-832-3.

[37] M. Laban. *On-Line Aircraft Aerodynamic Model Identification*. PhD thesis, Delft Univerity of Technology, 1994.

[38] A. A. Lambregts, G. Nesemeier, R. L. Newman, and J. E. Wilborn. Airplane Upsets: Old Problem, New Issues. In *AIAA Modeling and Simulation Technologies Conference and Exhibit*, Reston, Virigina, aug 2008. American Institute of Aeronautics and Astronautics. ISBN 978-1-62410-000-0. doi: 10.2514/6.2008-6867. URL http://arc.aiaa.org/doi/10.2514/6.2008-6867.

[39] J. R. Leis and M. A. Kramer. The Simultaneous Solution and Sensitivity Analysis of Systems Described by Ordinary Differential Equations. *ACM Transactions on Mathematical Software (TOMS)*, 14(1):45–60, 1988. ISSN 15577295. doi: 10.1145/42288.46156. URL http://dl.acm.org/citation.cfm?id=46156.

[40] R.E. Maine and K.W. Iliff. Use of Cramer-Rao Bounds on Flight Data with Colored Residuals. *Journal of Guidance, Control, and Dynamics*, 4(2):207–213, 1981. ISSN 0731-5090. doi: 10.2514/3.56073.

[41] E. A. Morelli, K. Cunningham, and M. A. Hill. Global Aerodynamic Modeling for Stall/Upset Recovery Traning Using Efficient Piloted Flight Test Techniques. 2013.

[42] J. A. Mulder, J. K. Sridhar, and J. H. Breeman. AGARD Identification of Dynamic Systems - Applications to Aircraft Part 2: Nonlinear Analysis and Manoeuvre Design, 1994.

[43] A. M. Murch. *Aerodynamic Modeling of Post-Stall and Spin Dynamics of Large Transport Airplanes*. PhD thesis, Georgia Institude of Technology, 2007.

[44] A. M. Murch and J. V. Foster. Recent NASA Research on Aerodynamic Modeling of Post- Stall and Spin Dynamics of Large Transport Airplanes. *45th AIAA Aerospace Sciences Meeting & Exhibit*, 2007.

[45] L.T. Nguyen. NASA Technical Note D-7739: Evaluation of Importance of Lateral Acceleration Derivatives in Extraction of Lateral-Directional Derivatives at High Angles of Attack, 1974.

[46] Y. Nie, E. Van Kampen, Q. P. Chu, T. M. Kier, and G. Looye. Geometry Based Quick Aircraft Modeling Method for Upset Recovery Applications. *AIAA Modeling and Simulation Technologies Conference*, (January):1–16, 2015. doi: 10.2514/6.2015-2034. URL http://arc.aiaa.org/doi/abs/10.2514/6.2015-2034.

[47] J. Nocedal and S.J. Wright. *Numerical Optimization (2nd Ed.)*. 2006. ISBN 9780387303031. doi: 10.1002/lsm.21040.

[48] S. A. E. Nooij, M. Wentink, H. Smaili, L. Zaichik, and E. L. Groen. Motion Simulation of Transport Aircraft in Extended Envelopes: Test Pilot Assessment. In *AIAA Modeling and Simulation Technologies Conference*, 2012. doi: 10.2514/1.G001790.

[49] S.P. Norsett, G. Wanner, and E. Hairer. *Solving Ordinary Differential Equations I*, volume 8. 1993. ISBN 9783540566700. doi: 10.1007/978-3-540-78862-1. URL http://www.springerlink.com/index/10.1007/978-3-540-78862-1.

[50] M.J. O'Rourke, J.N. Ralston, J.W. Bell, and S.F. Lash. PC-based simulation of the F-16/MATV. In *Modeling and Simulation Technologies Conference*, pages 481–489, 1997. doi: 10.2514/6.1997-3728. URL http://arc.aiaa.org/doi/10.2514/6.1997-3728.

[51] J.N. Ralston and J. Kay. The Utilization of High Fidelity Simulation in the Support of High Angle of Attack Flight Testing. In *NASA High Angle-of-Attack Technology Conference*, 1996.

[52] J. A. Schroeder, J. Bürki-Cohen, D. A. Shikany, D. R. Gingras, and P. Desrochers. An Evaluation of Several Stall Models for Commercial Transport Training. In *AIAA Modeling and Simulation Technology Conference*, number January, 2014. ISBN 9781624102974. doi: doi:10.2514/6.2014-1002.

[53] J. Singh and R.V. Jategaonkar. Identification of Lateral-Directional Behavior in Stall from Flight Data. *Journal of Aircraft*, 33(3):627–630, 1996.

[54] R.F. Stengel and M. Sri-Jayantha. Determination of Nonlinear Aerodynamic Coefficients Using the Estimation-Before-Modeling Method. *Journal of Aircraft*, 25(9), 1987.

[55] T. T Teng, T. S. Zhang, S. Liu, and P. R. Grant. Representative Post-Stall Modelling of T-tailed Regional Jets and Turboprops for Upset Recovery Training. *AIAA Modeling and Simulation Technologies Conference*, (January), 2015.

[56] L. J. Van Horssen. Aerodynamic Stall Modeling for the Cessna Citation II based on Flight Test Data, 2016.

[57] L. J. van Horssen, D. M. Pool, and C. C. de Visser. Aerodynamic Stall and Buffet Modeling for the Cessna Citation II based on Flight Test Data. In *AIAA SciTech 2018, session: Modeling and Simulation of Air Vehicle Dynamics I*, 2018.

[58] B.L. Walcott, M.J. Corless, and S.H. Zak. Comparative study of non-linear state-observation techniques. *International Journal of Control*, 45(6):2109–2132, 1987. ISSN 0020-7179. doi: 10.1080/00207178708933870. URL http://www.tandfonline.com/doi/abs/10.1080/00207178708933870.

III

Appendices to Preliminary Thesis Report

A

AHRS Data Corrections

In order to be able to apply flight path reconstruction successfully, accurate information of the aircraft body accelerations is needed. For the flight test data used in this thesis, output signals of the AHRS were used for this. However, several values in these signals were unexpected, and led to diverging Kalman filter results in some cases. These findings sparked a closer examination of any pre-processing of the AHRS signals done by the sensor itself. The result of this was the conclusion that before accounting for the effect of gravity, a correction applied by the AHRS had to be undone.

First the conversion from specific force to acceleration is given. Next, the conversion from raw AHRS data to specific force is presented. To arrive at this second conversion, the correction done inside of the sensor is derived from an example flight data set. Lastly, the complete correction method for transforming the AHRS signals to body accelerations is given.

Table A.1: Definition of signal notations in this appendix

Signal	Symbol(s)
AHRS output	A_x, A_y, A_z
Body specific force	S_x, S_y, S_z
Body acceleration	a_x, a_y, a_z

A.1. Specific Force to Acceleration

First, consider the difference between the AHRS output signals, body specific force signals, and body acceleration signals. The notation that is used **in this appendix** is defined in Table A.1.

Due to the presence of gravity, accelerations cannot be measured directly. Instead, accelerometers measure specific force. Body accelerations can be computed from this by taking out the effect of gravity, for which the body attitude has to be known. The magnitude of the gravitational acceleration is assumed to be $g_0 = 9.80665\ \mathrm{ms}^{-2}$. The conversion from specific force to body accelerations is:

$$\begin{aligned} a_x &= S_x - g_0 \sin\theta \\ a_y &= S_y + g_0 \sin\phi\cos\theta \\ a_z &= S_z + g_0 \cos\phi\cos\theta\ . \end{aligned} \tag{A.1}$$

A.2. AHRS Output to Specific Force

It was expected that the AHRS output would be equal to the specific force. Hence, any mismatches between these are likely due to internal pre-processing done by the sensor. One possibility is that the AHRS fuses several measurements and already applies the correction to take out the influence of gravity. Alternatively, some other signal manipulation might have been applied.

It is challenging to reverse-engineer what is going on inside the sensor, since only the sensor measurement is available. Luckily, common sense, combined with the fact that the gravitational acceleration points

(approximately) vertically down and is about $g_0 = 9.80665\ \text{ms}^{-2}$, provides clues. An example of the raw AHRS output is given in Figure A.1.

It can be clearly seen that already some correction for gravity is done in the z-axis. The first part of the data (i.e up until t is about 10 seconds) is of steady and level flight conditions. During that time the value of A_z is close to zero. One would have expected the value to be about $-g_0$ because the body z-axis is (nearly) aligned with the local vertical. Hence, one possibility is that the AHRS has already added a correction term $g_0 \cos\phi \cos\theta$, and fully corrects for the gravity. Another possibility is simply that g_0 has been added to the signal.

However, from Figure A.1 it can be seen that is not likely that the gravity has been fully corrected for. Between 20 to about 50 seconds, the aircraft is in a coordinated turn at 30 degrees bank angle. As such, the aircraft is experiencing a lateral acceleration i.e. a_y is non-zero. A_y is zero during this coordinated turn, which corresponds to a measurement of specific force, not acceleration. Thus, A_y has not received any pre-processing.

Secondly, A_x shows a steady, positive value for the most part of the maneuver. In contrast, Figure A.1 also shows that during the first 40 or so seconds, the airspeed is approximately constant. The most sensible explanation for this is that A_x represents specific force, so no pre-processing was applied to A_x.

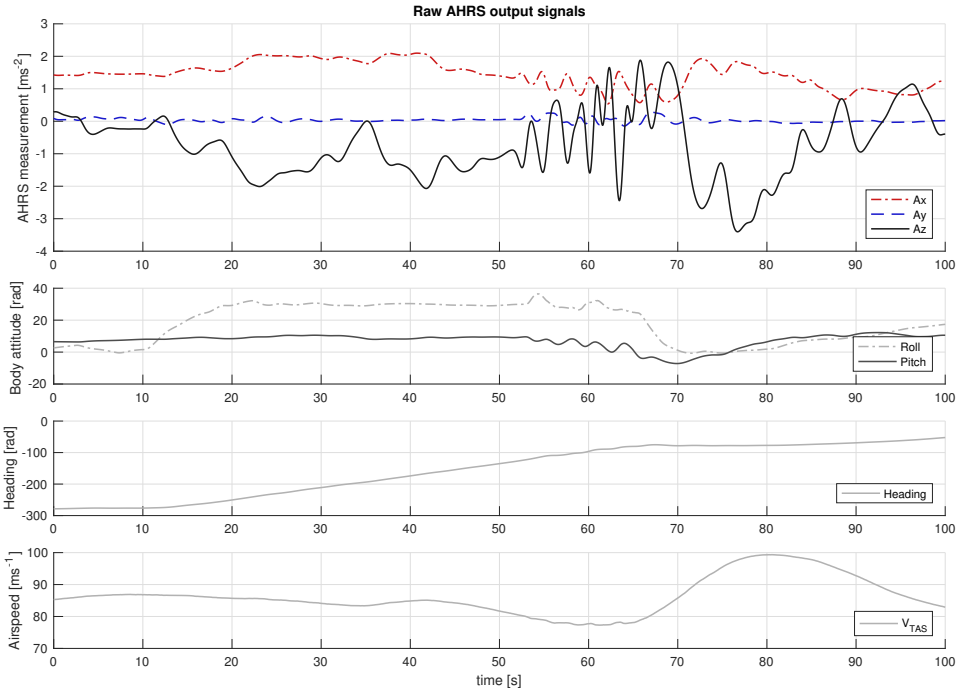

Figure A.1: Plot of raw AHRS output of an accelerated stall maneuver, including plots of the aircraft attitude and airspeed

To summarize, no pre-processing is done inside the AHRS for x and y directions. A_x and A_y represent specific force, or S_x and S_y. A correction is made for A_z. The most sensible option is to assume that g_0 was added to the signal, otherwise the Euclidean norm of the AHRS signal is a function of body attitude due to the correction factor. In equations, the following correction must be made to convert the AHRS output into specific force:

$$\begin{aligned} S_x &= A_x \\ S_y &= A_y \\ S_z &= A_z - g_0\ . \end{aligned} \tag{A.2}$$

This does leave the fact that such a correction makes no physical sense. A potential explanation for why the manufacturers of the sensor did choose to apply it was found in the documentation of the sensor. This revealed that the data bus was encoded to represent a valid data range of about $\pm 40\ \text{ms}^{-2}$. Applying the mentioned correction shifts A_z more to the zero point, which increases the freedom in the data range for representing dynamic maneuvers.

A.3. Complete Correction Method

When Equations A.1 and A.2 are combined, the complete correction that needs to be applied to the AHRS signals in order to obtain body accelerations is given in Equation A.3. To illustrate the correctness of this method, consider the same example data set as was used for Figure A.1. The results are presented in Figure A.2.

$$\begin{aligned} a_x &= A_x - g_0 \sin\theta \\ a_y &= A_y + g_0 \sin\phi\cos\theta \\ a_z &= A_z + g_0 \left(\cos\phi\cos\theta - 1\right) . \end{aligned} \tag{A.3}$$

The results now make a lot more sense. There is a clear correlation between a_y and a_z which one would expect to see while in a coordinated turn. Furthermore, when the airspeed does not change the signal a_x now is approximately zero, as it should be. The current method was concluded to be correct, and was applied inside the Kalman filter to obtain the body acceleration signals.

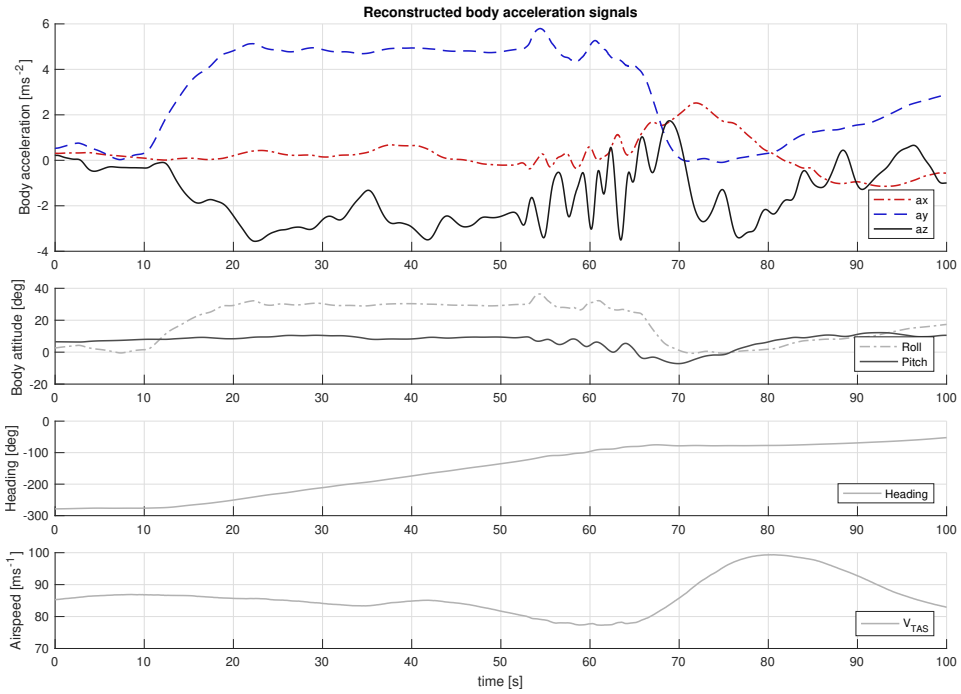

Figure A.2: Plot of reconstructed body acceleration signals during an accelerated stall maneuver, including plots of the aircraft attitude and airspeed

B

Usability of Old Flight Data

This Appendix investigates the effect on the reconstructed aircraft state trajectory of removing the air data boom signals. First, the analysis method is explained. After that, the results are presented. The Appendix ends with a discussion which results in the following conclusion: the old data cannot be used for lateral model terms as β cannot be reconstructed accurately without boom signals. For longitudinal model terms, the old data could potentially used under some conditions: the reconstruction of α is only accurate when no significant lateral motions are present anywhere in the recorded data set.

B.1. Analysis Method

Prior to the start of this thesis, data has been gathered of about 80 stall maneuvers, which were performed during the practical of the Flight Dynamics course. This data differs from the newly gathered stall data in two important ways. First of all, the old data solely consists of quasi-static longitudinal stall maneuvers, and does not include significant control surface excitations. This makes the old data less informative of the dynamic properties of aerodynamic stall.

Secondly, during the old flight tests, an air data boom was not installed. This means that instead of the boom α-vane, the fuselage-mounted α-vane had to be used, and a sideslip measurement was not present. In order to compare the effect of the lack of air data boom signals, one of the new flight test maneuvers was taken as an analysis case. Then, two different Kalman filters were run on the data. In this way, only the relevant differences are observed between the two approaches.

New Kalman Filter The first Kalman filter makes use of the boom data, and serves as baseline. This filter is the same one as described in chapter 4 of this report.

- Used α-signal: from air data boom, added in observation equation.
- Used β-signal: from air data boom, added in observation equation.

Old Kalman Filter The second Kalman filter does not make use of the boom signals, and represents the case where these signals are unavailable. The old stall data uses the body α-vane. A special approach was implemented to account for the viscous damping in this sensor, but it was unclear what level of accuracy could be obtained. Furthermore, a measurement of the sideslip was lacking entirely. The incidence angles are important inputs for the flight path reconstruction. Since a sideslip measurement was lacking, a pseudo-β was used instead, which essentially is a white noise signal of predefined intensity.

- Used α-signal: from body vane, added in navigation equation.
- Used β-signal: pseudo-β, added in observation equation.

B.2. Results

The complete results of both flight path reconstruction algorithms are presented in Figures B.2 to B.5. Since the old data only contains longitudinal maneuvers, a longitudinal stall maneuver was selected as the analysis case.

The main difference between the two Kalman filters lies in the α and β-signals which are used; a more detailed plot of the reconstructed flow incidence angles is presented in Figure B.1. Another reason for highlighting these these two signals is that they are extremely important for the fitting of the aerodynamic model.

In all plots, the results from the new filter, which uses the new data, is colored blue. The old filter, which uses the equivalent of the old data, is colored green. The raw data is only added for illustrative purposes, and is grey. The next section discusses the differences present in the data.

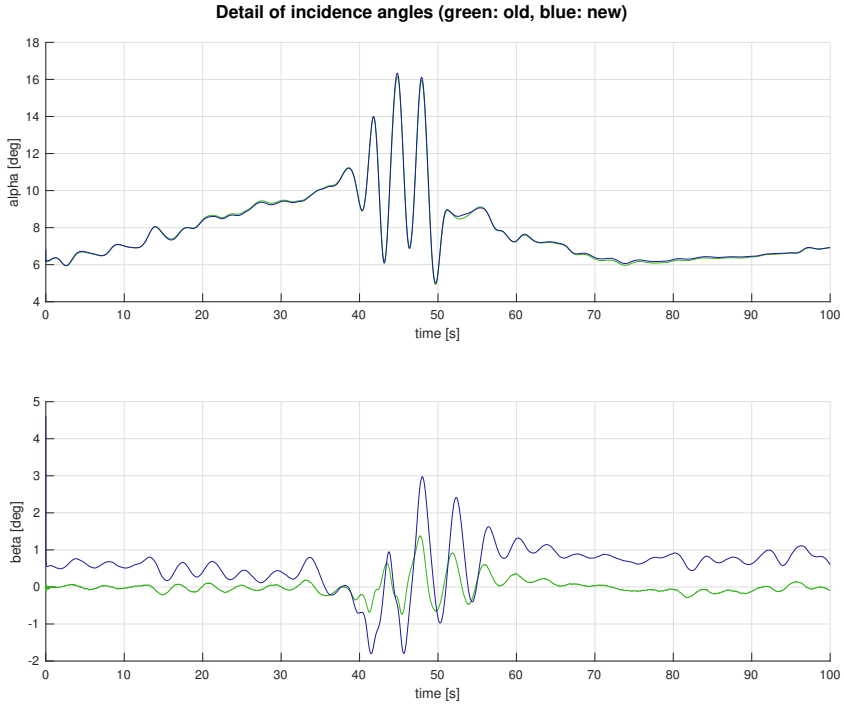

Figure B.1: Detailed comparison of the flow incidence angles α and β for a longitudinal stall maneuver

B.3. Discussion

In interpreting the results, the output of the new Kalman filter is regarded as the baseline. Although the boom vanes signals are inevitably contaminated by errors and noise, they are the best source of information available.

The reconstructed angle of attack is a close match; there is a small error during the dynamic parts (i.e. where the stall actually occurs) of the maneuver. Overall, from this plot it appears as if the reconstruction of α based on the old data is accurate. However, the observed errors are larger while a significant sideslip occurs. It appears that during assymmetric motions, the lack of a sideslip measurement also influences the angle of attack measurement. This could cause issues when some lateral motions are included in the old data, which could happen e.g. by accident or because of roll-off due to the stall.

To further investigate this potential problem, please see Figure B.6 and B.7. These shows the same detailed plots of α and β as in Figure B.1, but now for a dataset that starts with a coordinated turn. Because the old Kalman filter has issues with reconstructing lateral maneuvers, an error builds up during the initial part of the data set, from which it does not fully recover. The result of this is a significant error in α. Further analysis has shown that during accelerated stall maneuvers, the old Kalman filter fails to reconstruct α with meaningful accuracy. Because α is such an important variable, this discrepancy will influence any modeling effort. It is clear that a lot of care needs to be taken when using the old data.

Conversely, the reconstructed angle of sideslip does not match well. It is clear that using a pseudo-β signal leads to a significant underestimate of the true angle of sideslip. This makes sense, as one is telling the Kalman filter at every time that the expected value of β is zero, which is clearly not true during stall maneuvers (or motions like a coordinated turn).

Looking at the rest of the results, the main differences are in the body velocity components u, w, v, the estimated wind velocities W_{xe}, W_{ye}, and the accelerometer bias terms λ_{Ax}, λ_{Ay} λ_{Az}. Finally, $C_{\alpha_{\text{up}}}$ shows an

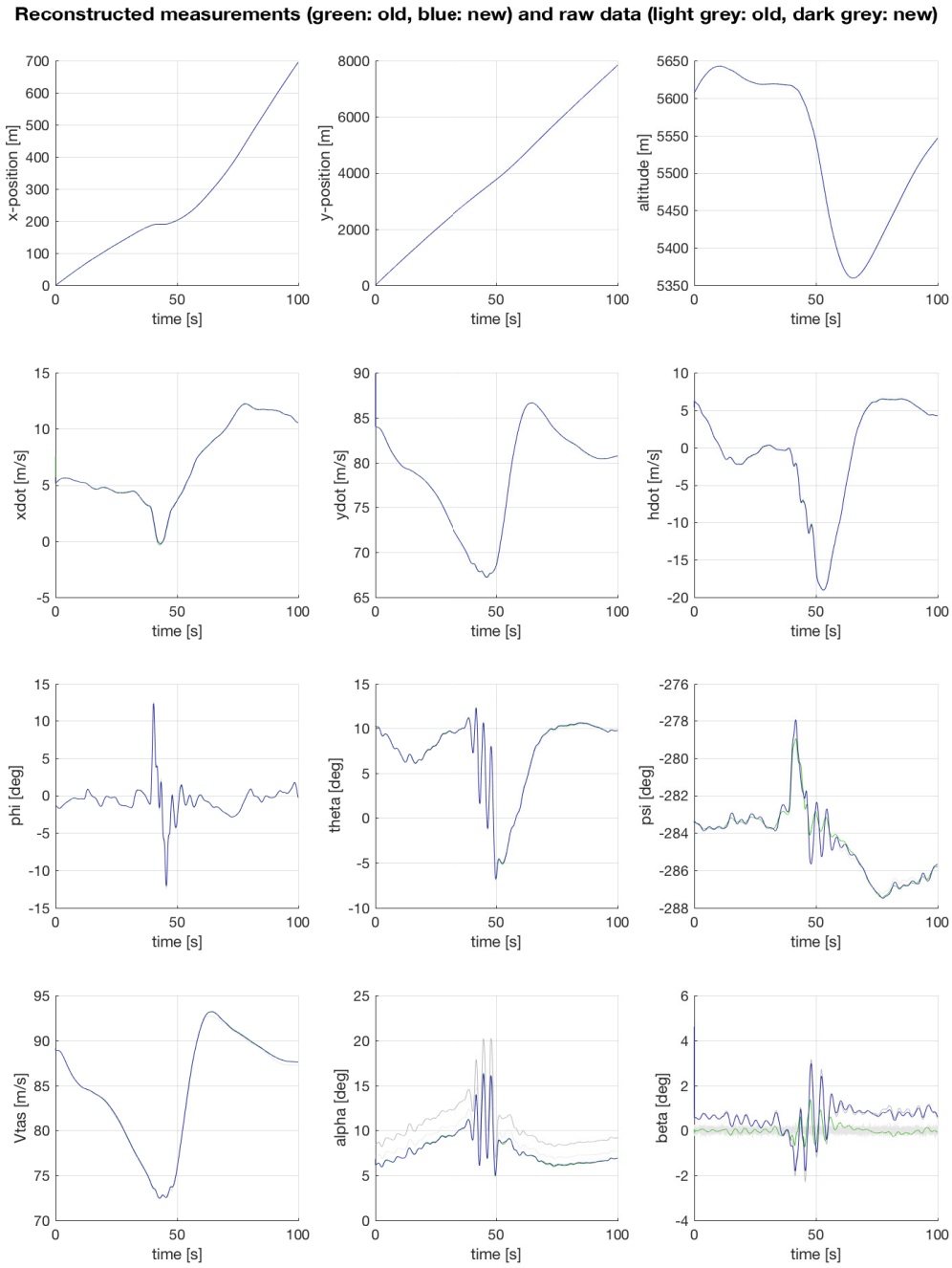

Figure B.2: Comparison of reconstructed measured signals between the old and new data sets

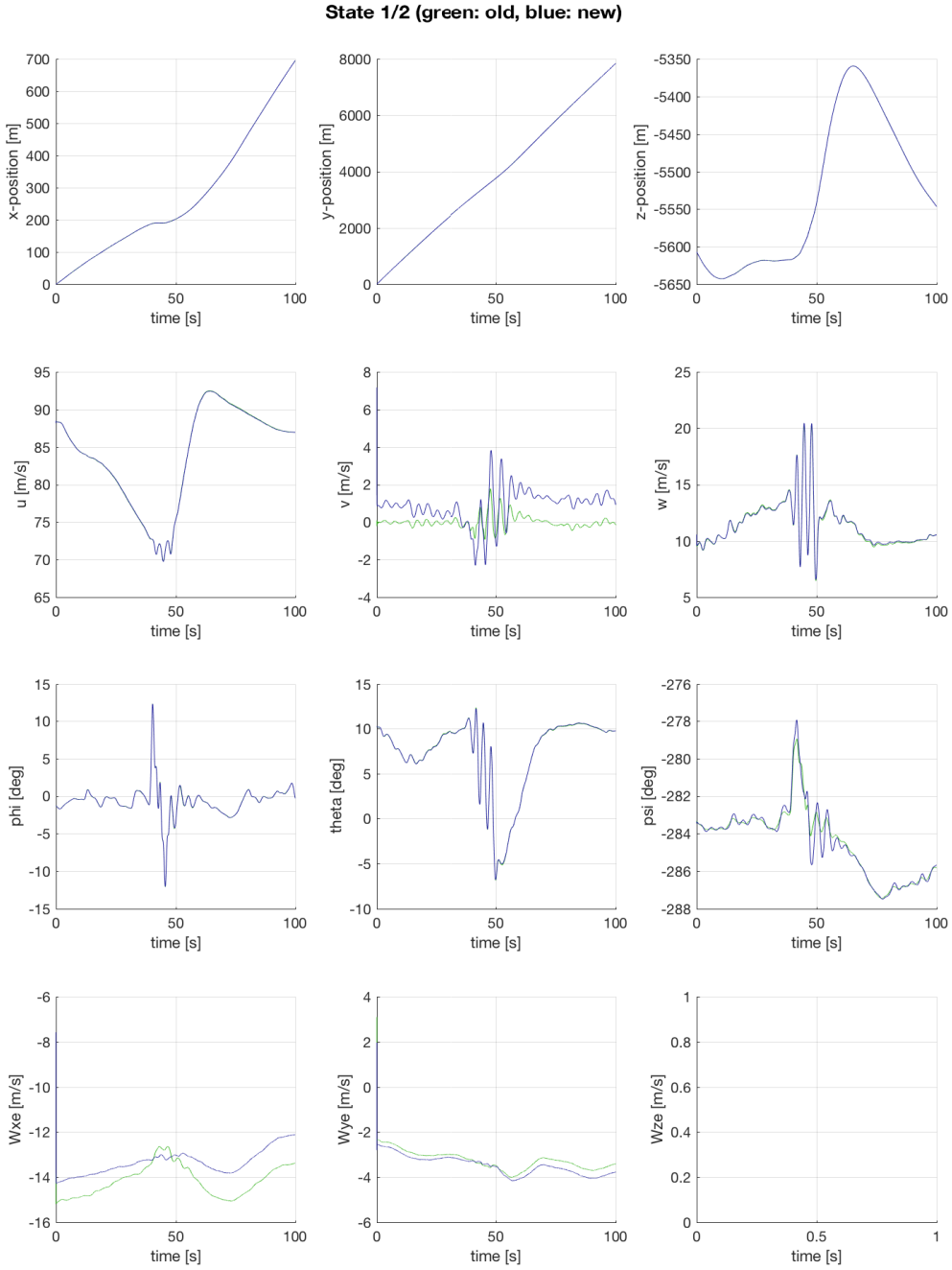

Figure B.3: Comparison of reconstructed state signals (1/2) between the old and new data sets

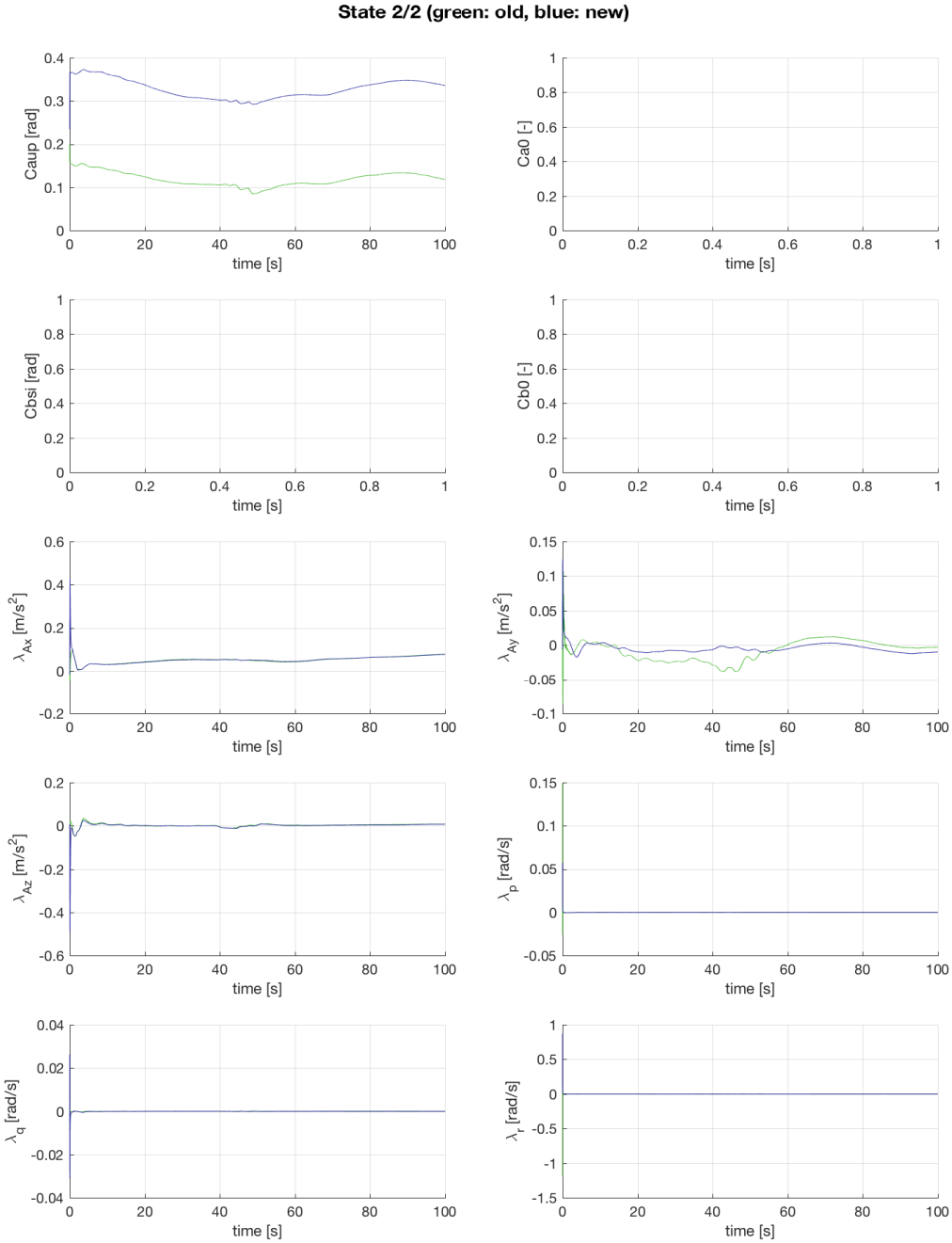

Figure B.4: Comparison of reconstructed state signals (2/2) between the old and new data sets

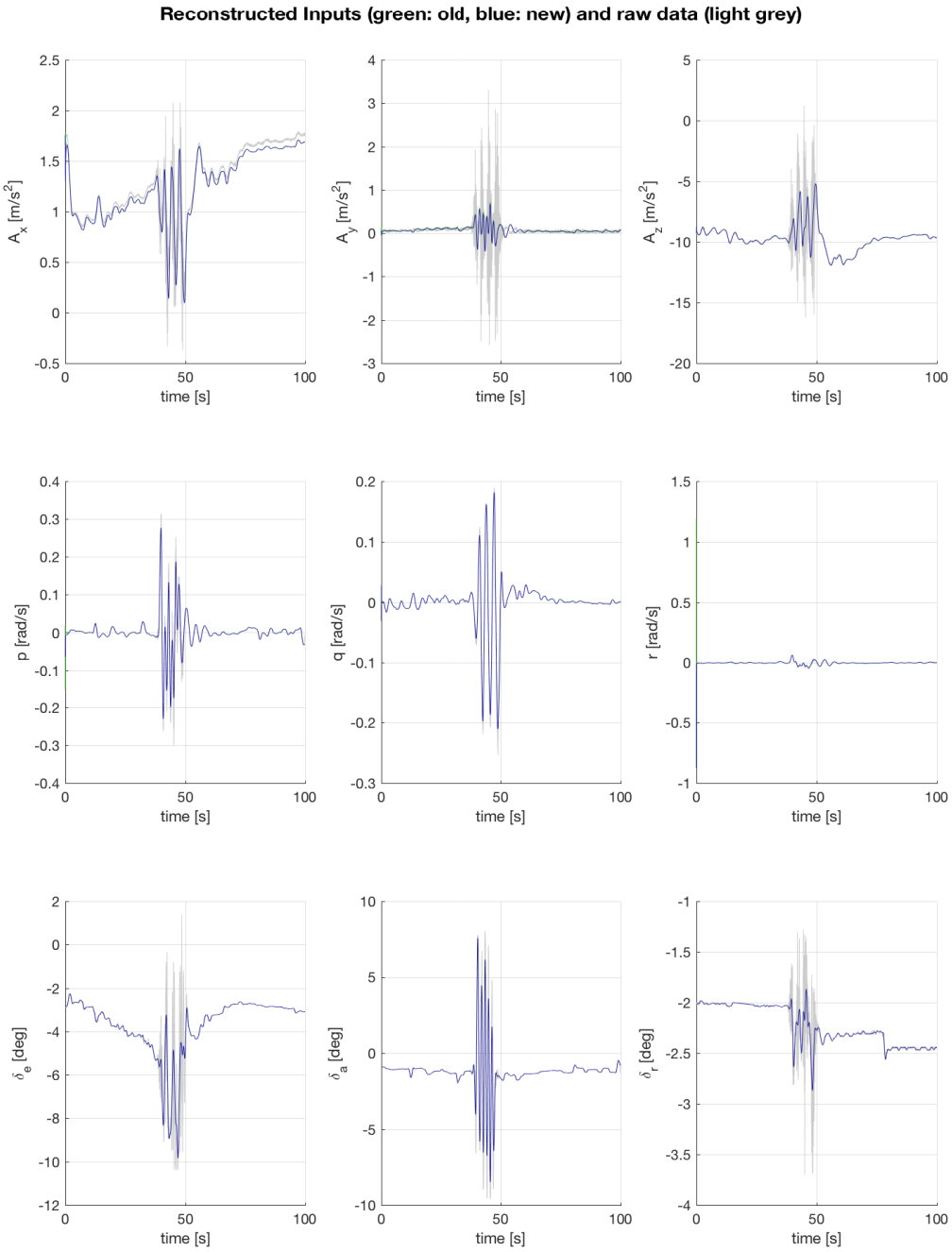

Figure B.5: Comparison of reconstructed input signals between the old and new data sets

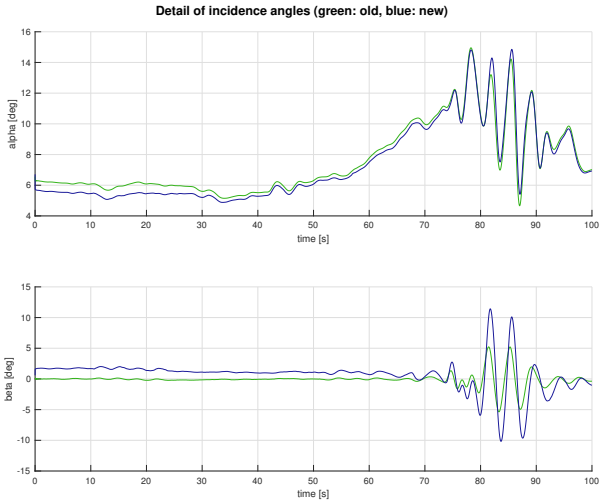

Figure B.6: Analysis plot of a second **stall maneuver starting from a lateral motion**, detailed comparison of the flow incidence angles α and β

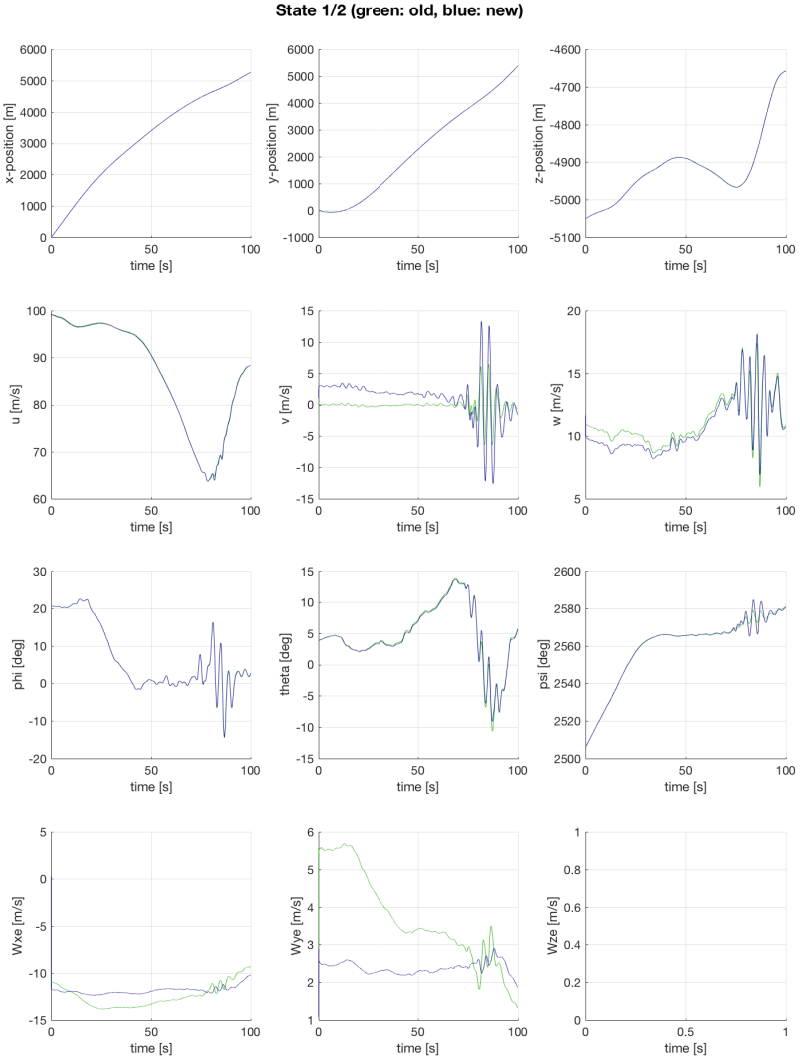

Figure B.7: Part of the reconstructed state signals (1/2) of a second **stall maneuver starting from a lateral motion**

offset, but this was to be expected since a different α-vane was used. None of these signals are used as regression variables, so these differences are much less relevant than any discrepancies in α and β.

To summarize, the old data cannot be used for modeling the lateral model terms, as the reconstructed sideslip is not accurate. For the longitudinal state reconstruction: it appears that α is only accurate when there are no asymmetric maneuvers present anywhere in the data set. Hence, a lot of care should be taken when using the old data. A manual inspection of each of the data sets will be necessary to ensure that no such lateral maneuvers are present.

There remain some troubling issues. First of all, even when a manual check has been done of all data to prevent unwanted maneuvers, it will still be impossible to check the accuracy of the reconstructed signals. Secondly, although is it known that α is an essential state variable for the modeling effort, it is not clear how big of a problem it is when there are small errors. The question then is: does the inclusion of extra data, which is known to have some issues, improve the resulting model quality or decrease it? Such questions will have to be addressed ad hoc during the actual modeling effort itself.

C

Vibrations in the Air Data Boom

The air data boom installed on the nose of the aircraft is not completely rigid. During the flight tests, this could clearly be seen from the cockpit window as mechanical vibrations; especially during the stall buffet. Due to the up- and downward motion of the tip of this boom, the measurements of α and β are influenced. In [37], a more formal analysis of this issue is treated. In this thesis, the issue will be tackled pragmatically.

First, an estimate of the power spectrum of the boom α-signal is given. From that, a filtering strategy was derived, which was applied to the data. To illustrate the result of the filtering, a time-history plot is presented.

C.1. Power Spectral Density Estimate of Vibrations

A power spectral density (PSD) estimate is informative of what the boom vibrations look like in the frequency domain. From the flight tests, it was observed that the boom exhibited what appeared to be harmonic excitations. One would thus expect a clear peak in the power spectrum at some frequency. Ideally such a peak is far away from the frequencies at which the aircraft dynamics themselves have power.

A PSD estimate $S_{\bar{u}\bar{u}}(\omega)$ of a random signal $\bar{u}(t)$ is obtained as

$$S_{\bar{u}\bar{u}} = \frac{1}{2T}|U(\omega)|^2 \tag{C.1}$$

where T is the length of the data sample in seconds, and $U(\omega)$ can be obtained using the Fast-Fourier Transform routine in MATLAB. If the power is converted into dB/Hz, the result is Figure C.1

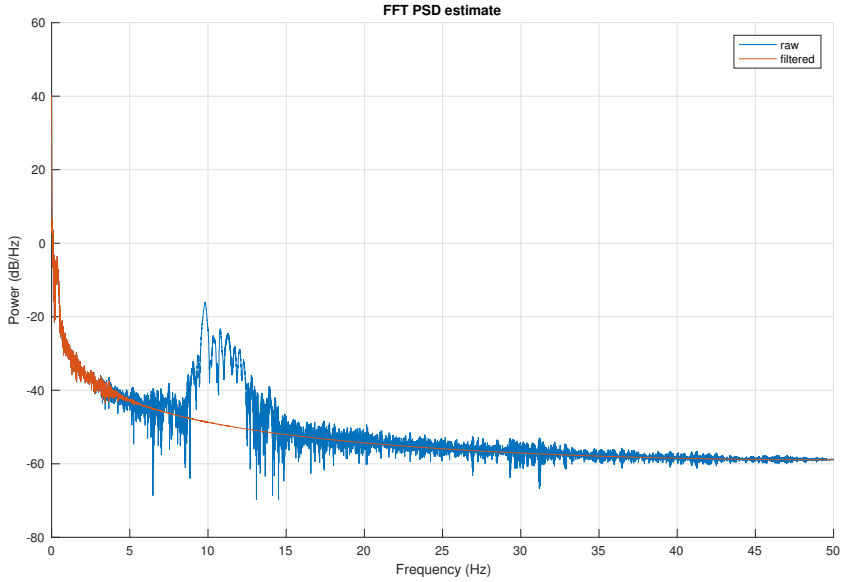

Figure C.1: Power spectral density estimate of the boom α-signal, both before and after the filtering procedure

A clear peak can be seen around 10 Hz, which corresponds to the mechanical vibrations. Moreover, while it is challenging to exactly define the break frequency of the frequency response of the aircraft dynamics, it is reasonable to assume that it is between 1 and 4 Hz. As a result, the vibrations and aircraft dynamics are clearly separated in the frequency domain.

C.2. Filtering the Vibrations

A Butterworth type of filter of order four was selected for getting rid of the vibrations in the data. To preserve as much of the aircraft dynamics as possible, the cut-off frequency was set at 4 Hz. The result of this is in the frequency domain is presented in Figure C.1. The peak has been completely removed, while keeping the spectrum below 4 Hz intact.

To illustrate the effect in the time domain, Figure C.2 shows a sub-selection of the dataset used for this analysis. It could be cross-checked with the A_z-signal that the stall buffet first occurred around 45 seconds. The vibrations are completely removed by the filtering procedure.

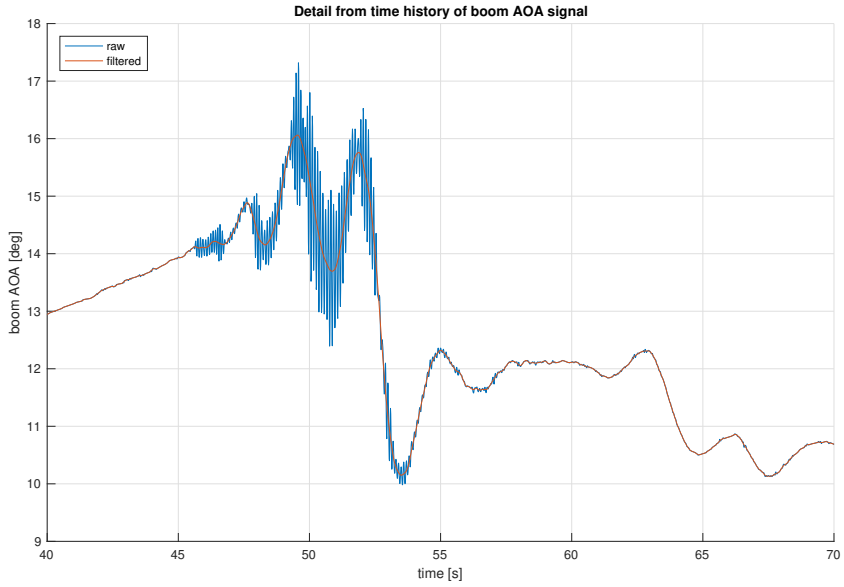

Figure C.2: Detail of the time history of the boom α-signal, both before and after the filtering procedure

The current analysis is only for the α-signal, but the conclusions hold for the boom β-signal; the same filter is applied. The main difference between them is the total power in the signal and the vibrations specifically: typically β is much smaller, and the intensity of the buffet vibrations are much lower in y-direction. All of the boom α and β-signals are filtered with the described procedure before applying the Kalman filters.

D

Example Flight Test Card

Below, an example flight test card was included to illustrate the procedures that were used during the flight tests.

TU Delft Flight Department

FLIGHT TEST CARD

PROJECT	:	Dynamic Stall Modeling for the Cessna Citation II
TEST CARD NUMBER	:	1a
SUBJECT	:	Control effectiveness during stall
REFERENCE	:	
NOTES	:	
EST. DURATION OF TEST POINT	:	120 seconds
HAZARD CATEGORY	:	~~ROUTINE~~ / LOW / ~~MEDIUM~~ / ~~HIGH~~

INITIAL CONDITIONS

ALT/FL	:	As required	ENGINE SETTING	:	As required
IAS	:	As required	FLAP SETTING	:	UP
MACH	:	As required	LANDING GEAR	:	Up
MASS	:		OTHER	:	NO-ICING Conditions ANTI-ICE OFF
C.G.	:				

EXPERIMENT PROCEDURE — **REC. NRS**

	Maneuver	ALT/FL	Flap setting	Landing gear
☐	Wing level stall (1g) + control wiggle	FL150-FL200	Clean	Up
☐	Accelerated stall @ 30 deg bank	FL150-FL200	Clean	Up
☐	Accelerated stall @ 45 deg bank	FL150-FL200	Clean	Up

	Maneuver	ALT/FL	Flap setting	Landing gear
☐	Wing level stall (1g) + control wiggle	FL110-FL150	Clean	Up
☐	Accelerated stall @ 30 deg bank	FL110-FL150	Clean	Up
☐	Accelerated stall @ 45 deg bank	FL110-FL150	Clean	Up

Note 1: See test card 2 for procedures for chosen maneuvers.

EXPERIMENT PROCEDURE	**REC. NRS**
WINGS LEVEL 1-G STALL 1. Set max N1 values on box 2. perform the pre-stall items of the Slow Flight/Stalls checklist 3. clean stalls NOT in icing conditions. If A/I ON: observe minimum N2 of 65% 4. minimum altitude 4000 ft AGL, anticipate loss of 1000 ft 5. No stalls above FL250 crew coordination: 6. all selections by PNF on command of PF 7. controls and thrustlevers by PF The recommended stalling exercise goes as follows: 8. thrustlevers to 50% N1 one by one 9. extend speedbrakes 10. do not trim below green speed reference 11. slowing through green speed reference: retract speedbrakes 12. recovery at stall: set 90% N1 13. pitch attitude 2.5° below horizon 14. speed 120 KIAS: climb to original level 15. accelerate and perform after-stall checks (in a series of exercises, after stall checks may be delayed until after the last exercise). 16. Establish trimmed level flight Extra for these tests: 17. Confirmation: “data tag activated” 18. Reduce airspeed with ~1 kts/sec 19. Maintain stall for 1 second 20. Recover 21. Confirmation: “data tag ended” 22. PNF checks slip indicator and altitude and if necessary notifies the PF ***** Perturbations … - excite both elevator and ailerons, **no rudder** - do not result in large a/c attitude excitations(max ±5 degrees) - are as random and uncorrelated as possible - cover as wide a frequency range as possible	

Accelerated stall @ 30 or 45 deg bank procedure:

1. Set max N1 values on box
2. perform the pre-stall items of the Slow Flight/Stalls checklist
3. clean stalls NOT in icing conditions. If A/I ON: observe minimum N2 of 65%
4. minimum altitude 4000 ft AGL, anticipate loss of 1000 ft
5. No stalls above FL250

crew coordination:

6. all selections by PNF on command of PF
7. controls and thrustlevers by PF

The recommended stalling exercise goes as follows:

8. thrustlevers to 50% N1 one by one
9. extend speedbrakes
10. do not trim below green speed reference
11. slowing through green speed reference: retract speedbrakes
12. recovery at stall: set 90% N1
13. pitch attitude 2.5° below horizon
14. speed 120 KIAS: climb to original level
15. accelerate and perform after-stall checks (in a series of exercises, after stall checks may be delayed until after the last exercise).
16. Establish trimmed level flight

Extra for these tests:

17. Confirmation: "data tag activated"
18. Bank to 30 or 45 degrees
19. Establish level turn
20. Reduce airspeed with ~1 kts/sec
21. Maintain stall for 1 second
22. Recover
23. Confirmation: "data tag ended"
24. PNF checks slip indicator and altitude and if necessary notifies the PF

***** Perturbations …

- excite both elevator and ailerons, **no rudder**
- do not result in large a/c attitude excitations (max ± 5 degrees)
- are as random and uncorrelated as possible
- cover as wide a frequency range as possible

IV

Appendices to Final Report

E

Time History Plots of All Flight Data Sets

This appendix contains the time history plots of all of the 34 data sets that were gathered, as well as the model outputs. All force (C_L, C_D, C_Y) and moment (C_l, C_m, C_n) outputs are shown, alongside the two most crucial inputs: α and X. Table E.1 lists which data sets were used training, and which for validation.

Table E.1: List of all gathered data sets, showing whether they were a wings-level or accelerated stall, and wheter they were used as training (T) or validation (V) data.

Set	Type	Use	Set	Type	Use	Set	Type	Use	Set	Type	Use
1	wings-level	T	10	wings-level	T	19	accelerated	T	28	accelerated	T
2	wings-level	T	11	wings-level	T	20	accelerated	T	29	accelerated	T
3	wings-level	T	12	wings-level	V	21	accelerated	T	30	accelerated	T
4	wings-level	T	13	wings-level	T	22	accelerated	V	31	accelerated	T
5	wings-level	V	14	wings-level	T	23	accelerated	V	32	accelerated	T
6	wings-level	T	15	accelerated	T	24	accelerated	T	33	wings-level	T
7	wings-level	V	16	accelerated	V	25	accelerated	V	34	wings-level	T
8	wings-level	T	17	accelerated	T	26	accelerated	T			
9	wings-level	T	18	accelerated	T	27	accelerated	T			

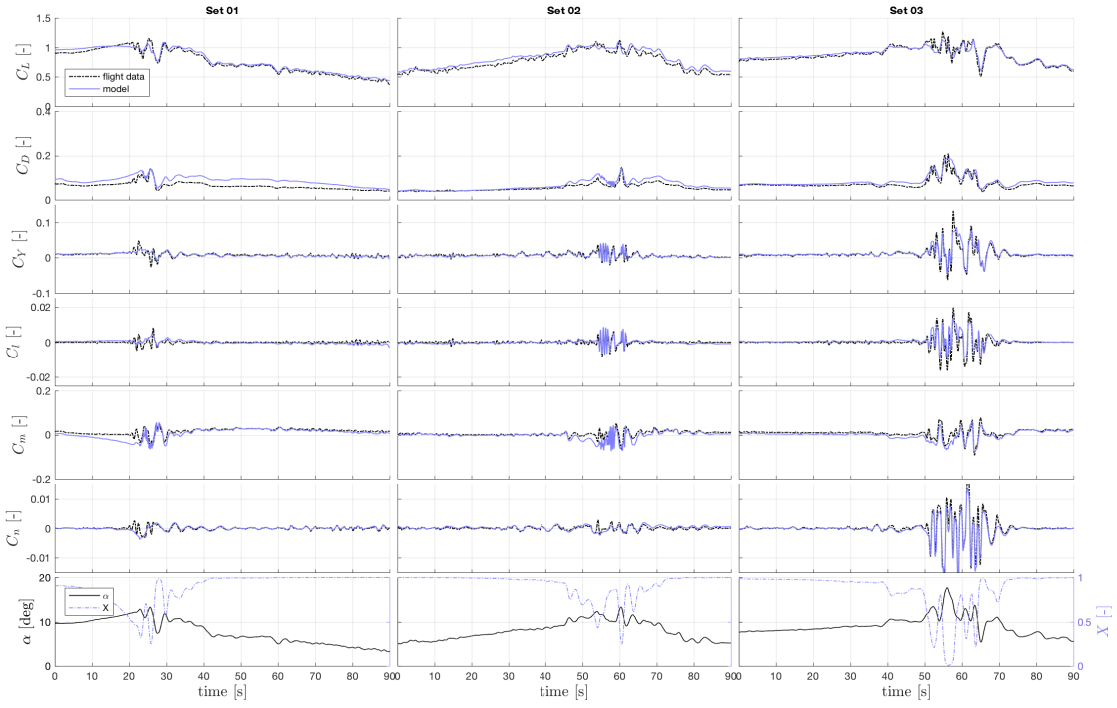

Figure E.1: Time history plots of training sets 1, 2, and 3.

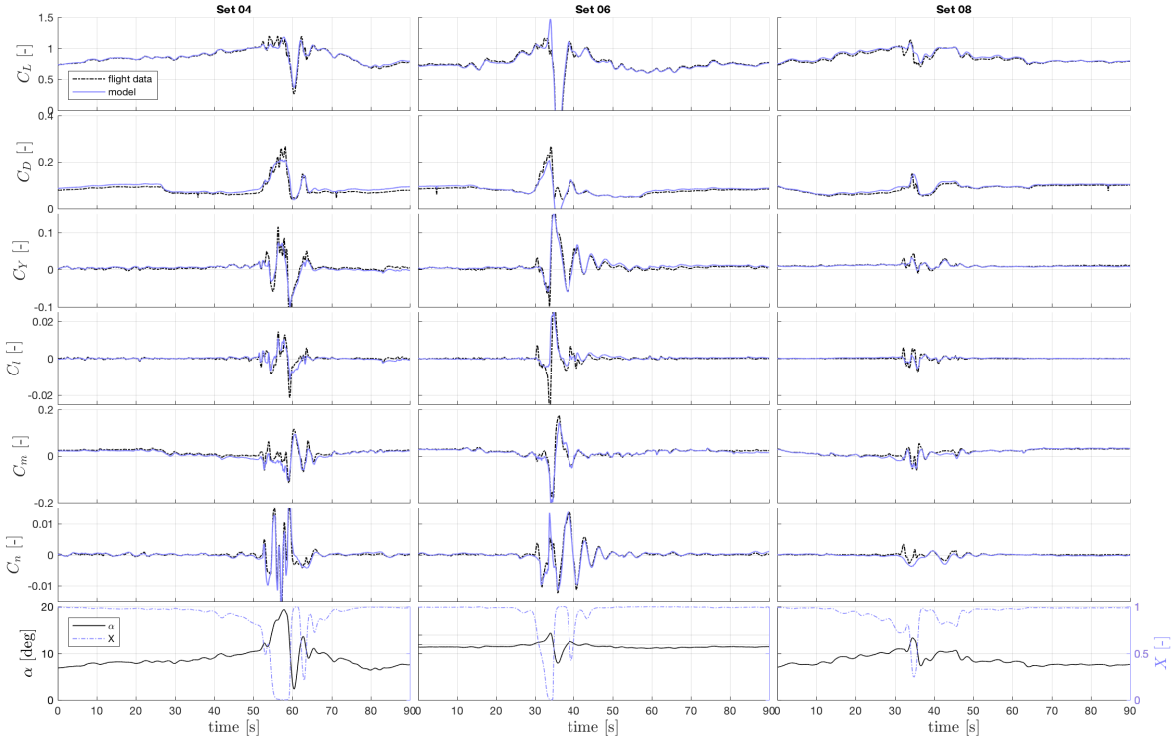

Figure E.2: Time history plots of training sets 4, 6, and 8.

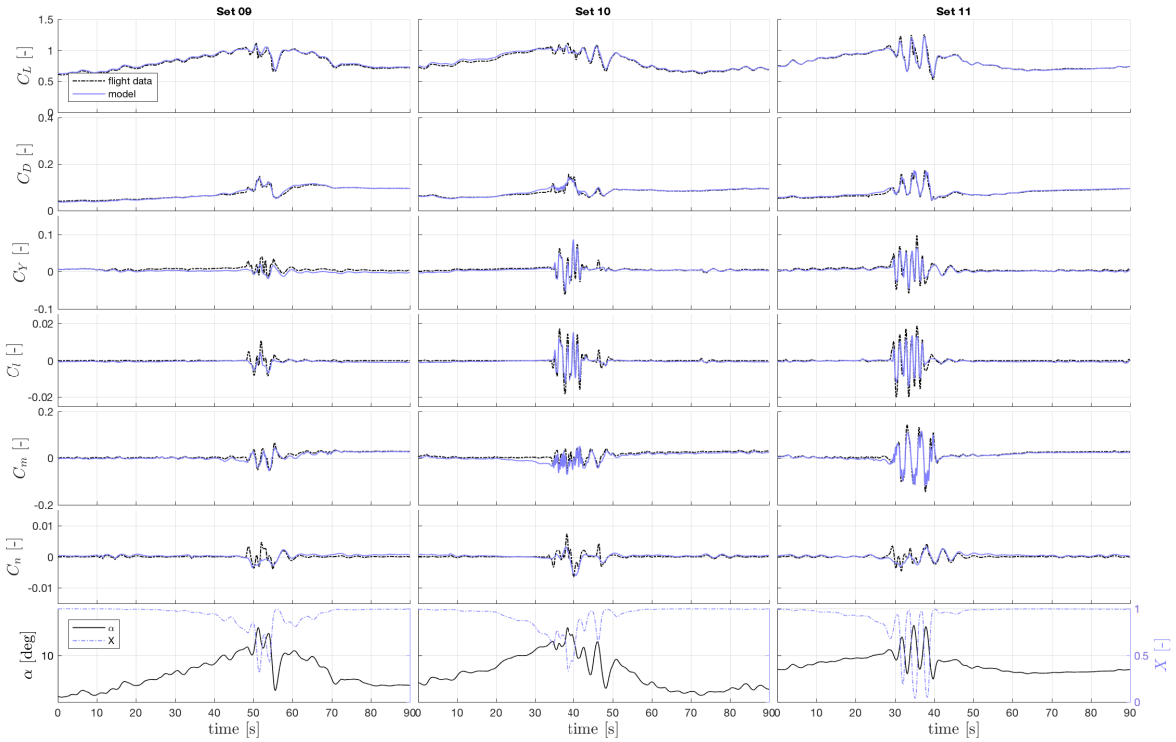

Figure E.3: Time history plots of training sets 9, 10, and 11.

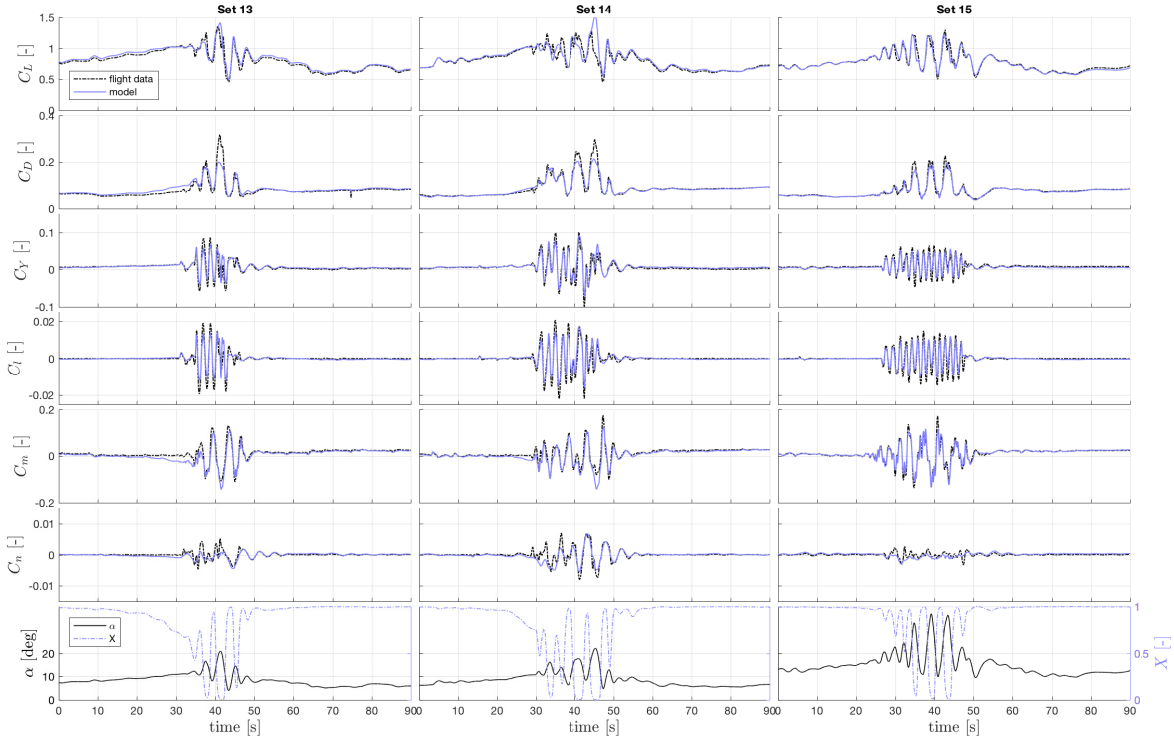

Figure E.4: Time history plots of training sets 13, 14, and 15.

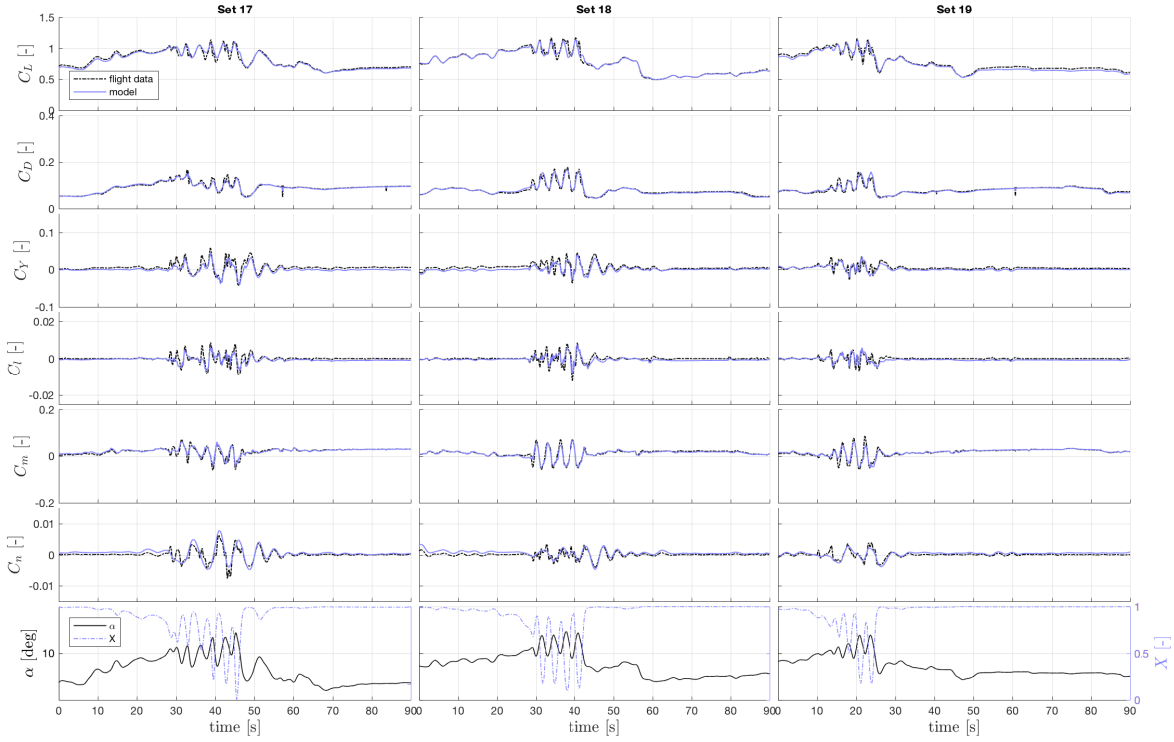

Figure E.5: Time history plots of training sets 17, 18, and 19.

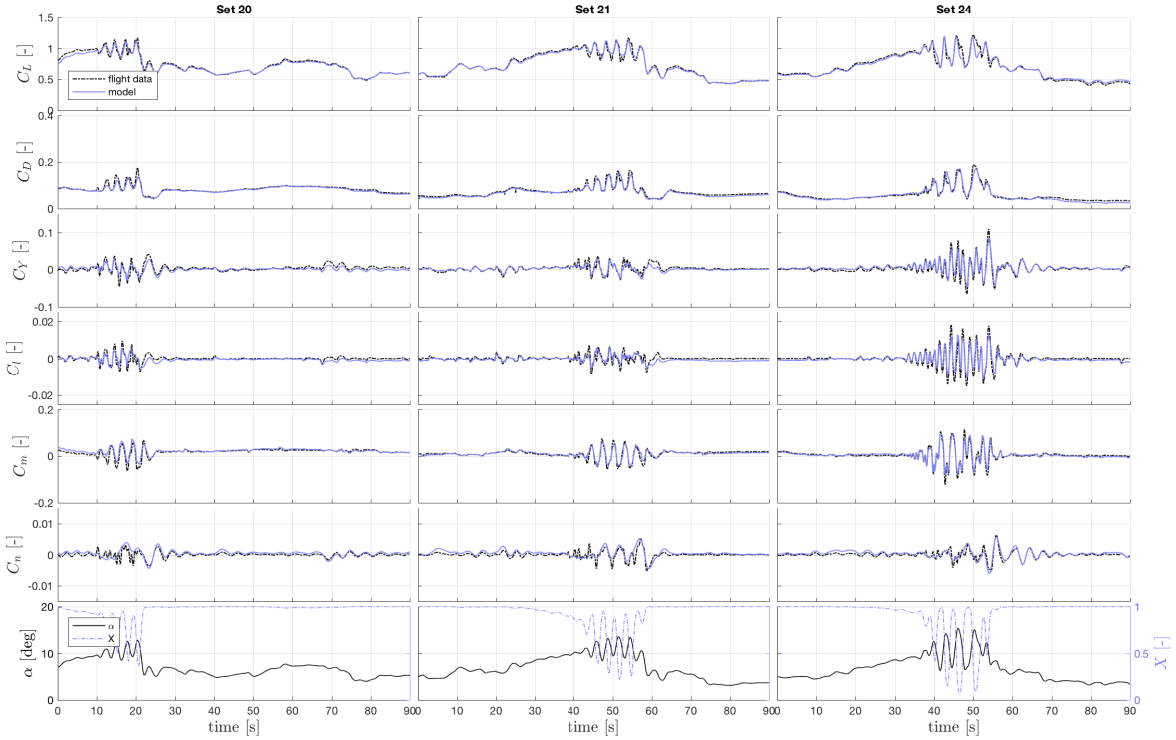

Figure E.6: Time history plots of training sets 20, 21, and 24.

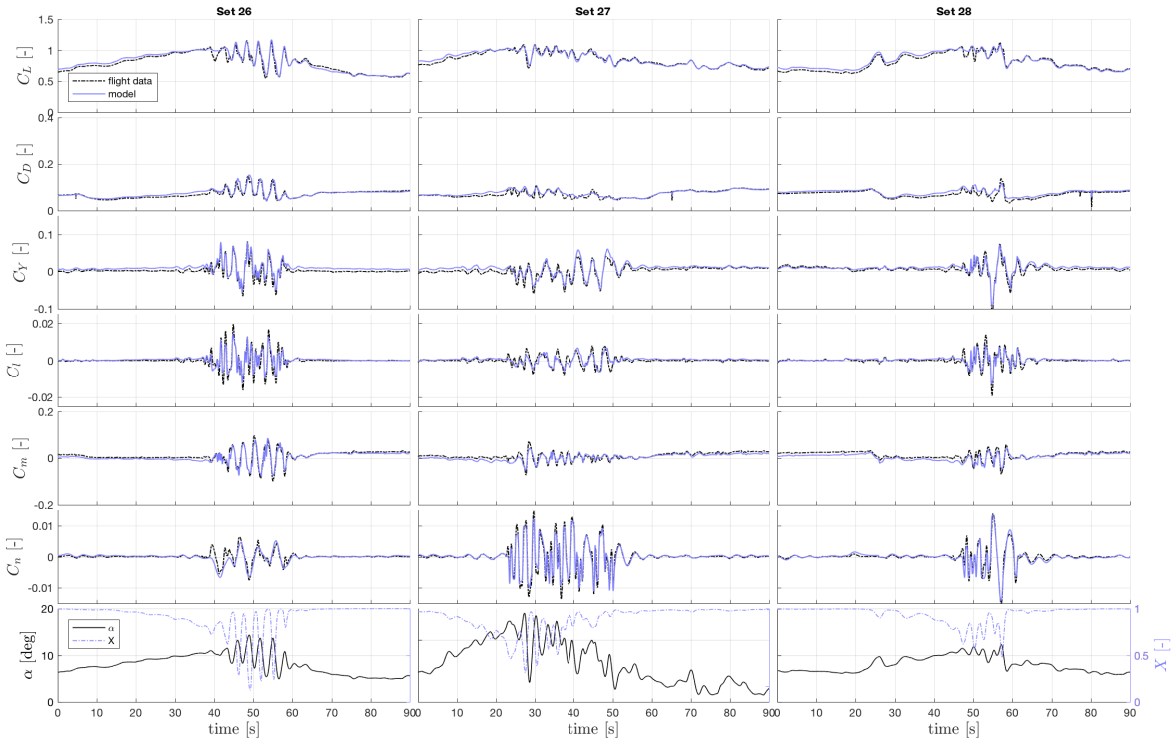

Figure E.7: Time history plots of training sets 26, 27, and 28.

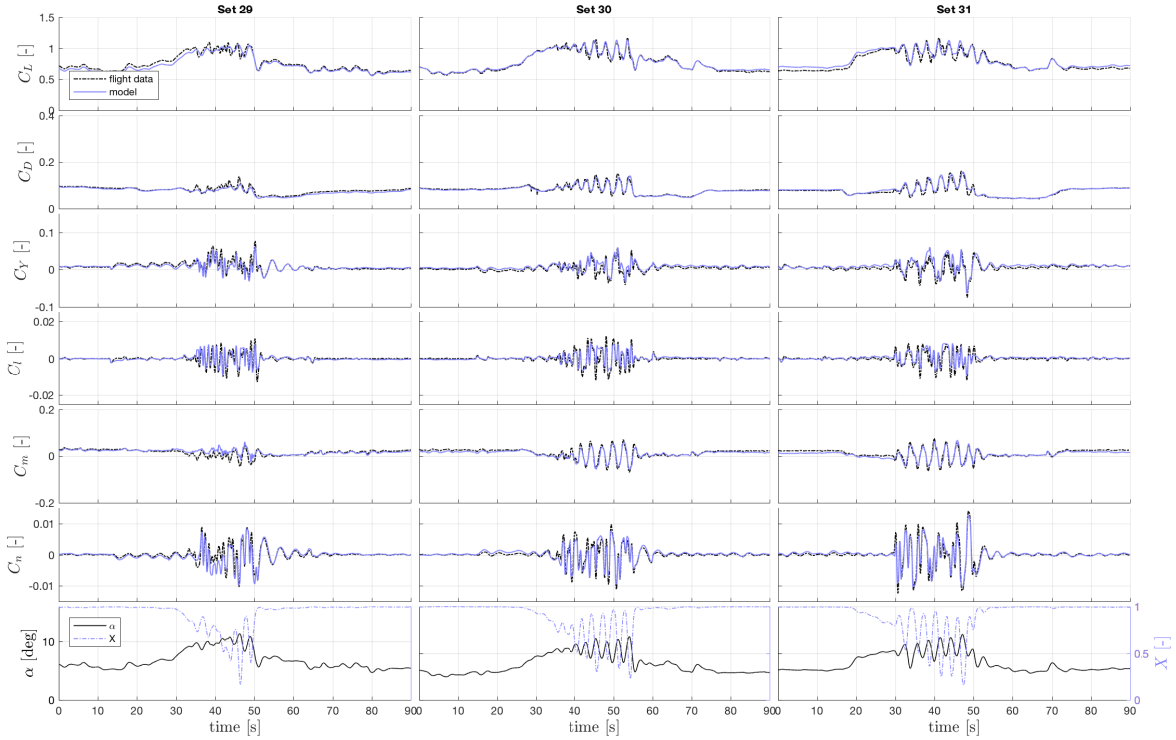

Figure E.8: Time history plots of training sets 29, 30, and 31.

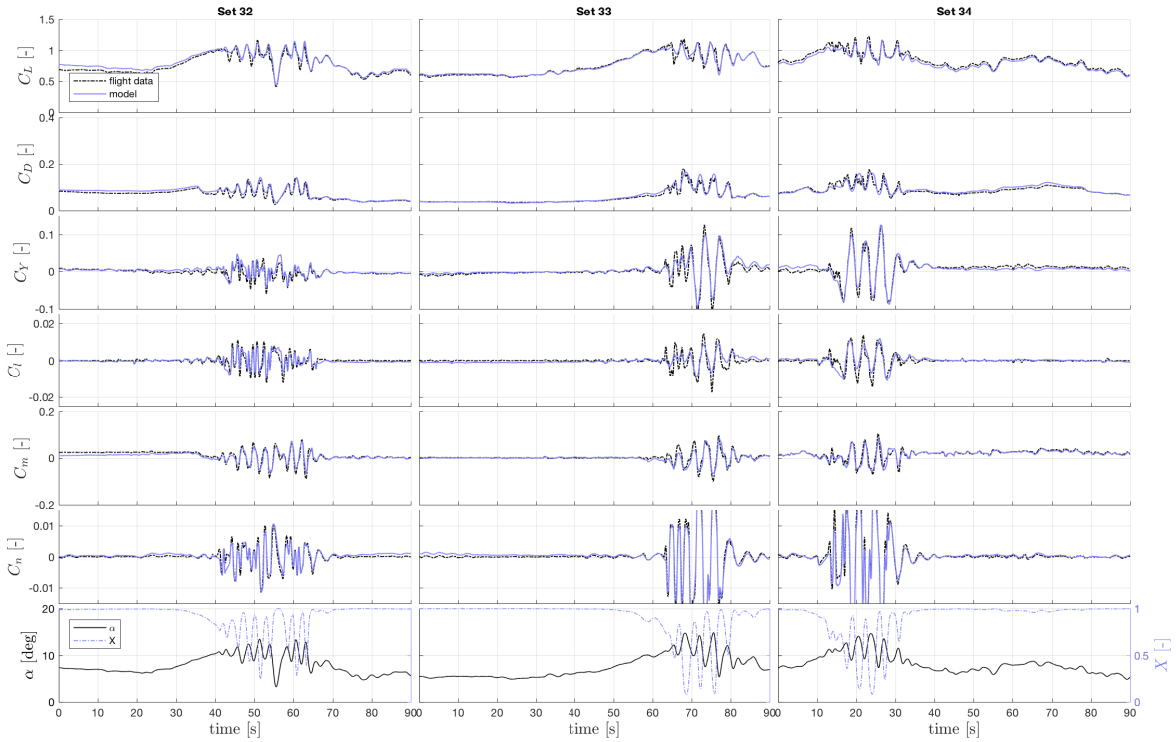

Figure E.9: Time history plots of training sets 32, 33, and 34.

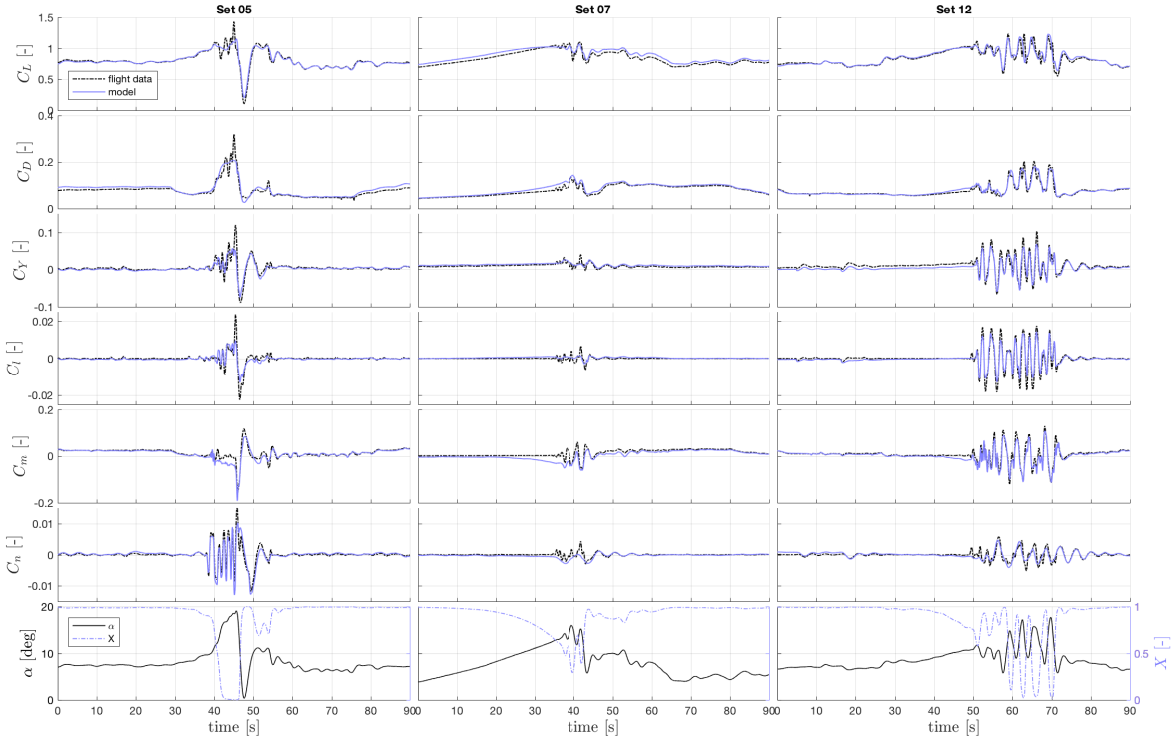

Figure E.10: Time history plots of validation sets 5, 7, and 12.

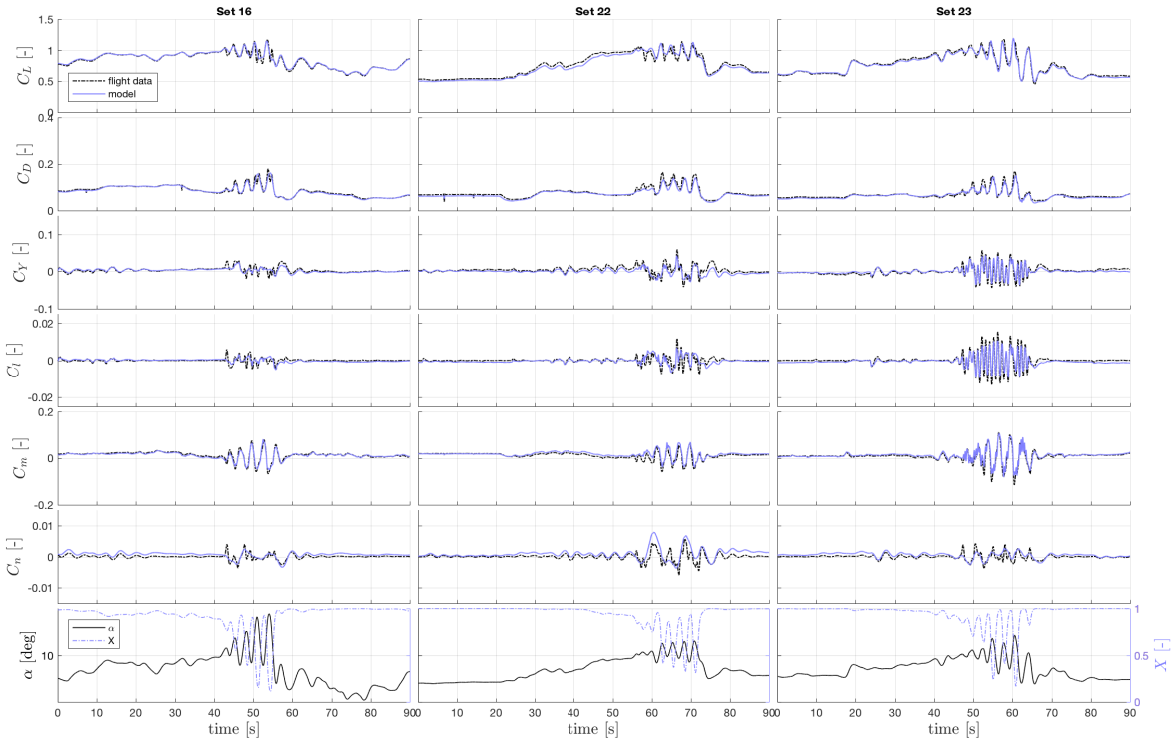

Figure E.11: Time history plots of validation sets 16, 22, and 23.

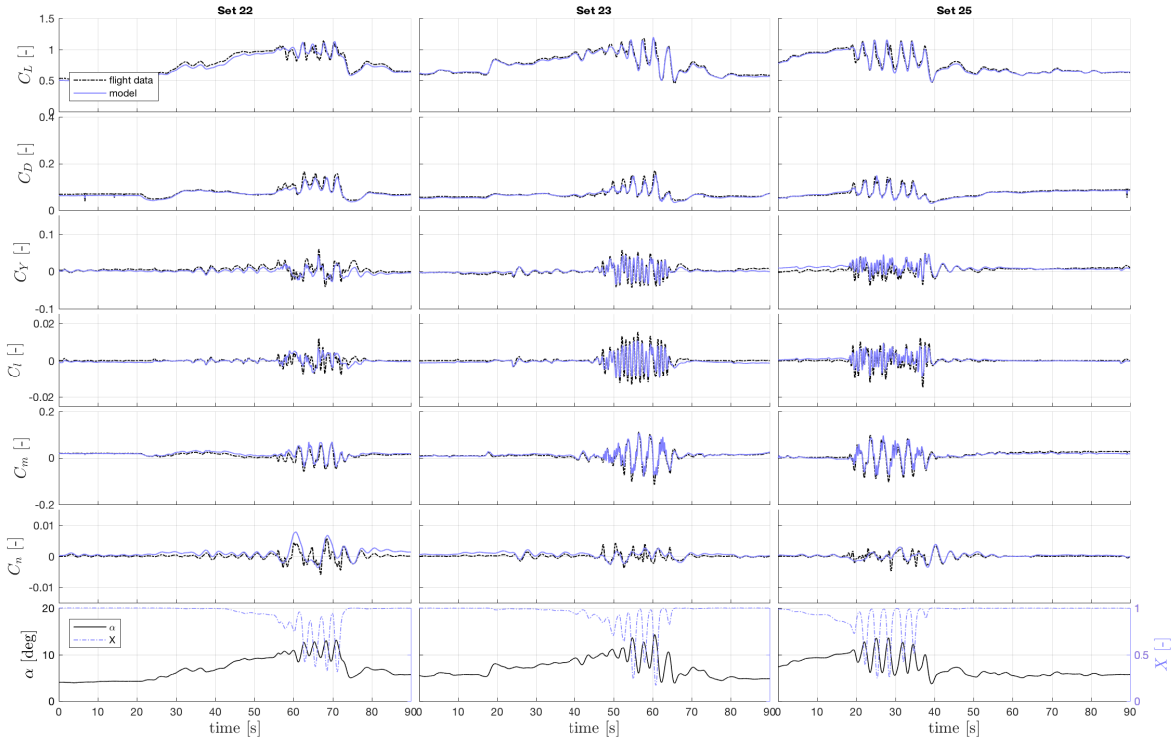

Figure E.12: Time history plots of validation sets 22, and 23, which are repeated from previous figure and 25.

F

Analysis of Flight Test Maneuver Effectiveness

During the flight tests performed for this research, two types of stalls were flown: wings-level symmetric stalls, and accelerated stalls. Next to that, there were differences between the degree to which the control surfaces were used during the maneuvers, especially for the rudder. Finally, because the maneuvers were executed by human pilots, there was natural variation between the maneuvers. If a link can be found between certain characteristics of the flight test maneuvers and the quality of the model that can be estimated from them, this would be very helpful in planning new flight tests. This Appendix presents the results of an analysis into this topic.

F.1. Methodology & Results

To perform such an analysis, two issues need to be solved. First of all, how can the characteristics (i.e. properties) of the flight test maneuvers be quantified? Secondly, how can the quality of the model that can be estimated from this maneuver be quantified (i.e. metrics)? Especially this second issue is complex, since the quality of the model depends on many factors, including the parameter estimation method, the selected model structure, and of course all other data sets. A list of the properties and quality metrics that were used is shown in Table F.1.

Since it was not clear which properties and metrics would be related, if any, it was chosen to evaluate all possible combinations. This led to a great number of plots, which will be presented in Figures F.1 to F.7. The plots are split between the X-parameters, C_L-parameters, C_D-parameters, and so on.

Interpreting the results, several observations can be made. First of all, no clear difference between wings-level and accelerated stall maneuvers can be seen. Secondly, the properties that have visibly most consistent relation with the metrics are the maximum angle of attack, and the RMS of the body rotation rates. Thirdly, the negative effect on C_n-model quality of the lack of rudder excitation in some of the data sets can be seen. Finally, the CRLB of the X-parameters, especially those of τ_1 and τ_2 appear to benefit from stronger excitation of X and q.

The mean squared error does not seem to be an effective metric. Generally, it is shown that the MSE increases when the excitation of the aircraft (i.e. RMS of body rotations) increases. However, this excitation can be both because of pilot inputs, as well as because of stall-related disturbances. This latter part is unlikely to be captured by the model, and thus leads to an increase in MSE. However, these disturbances can probably not be avoided if high angles of attack are to be achieved, since this leads to stall.

F.2. Conclusions

The following conclusions can be made based on the results of the analysis. They are certainly not surprising, but they deserve to be re-stated.

- It is beneficial to achieve a angle of attack that is as high as possible.
- All control surfaces, including the rudder, should be excited during stall.
- Larger dynamic excitation (i.e. in p, q, r) lead to better identifiable model parameters.

Table F.1: List of the properties and metrics that were used in the analysis if flight test maneuver effectiveness.

Type	Name	Unit	Description
Property	maneuver type	-	Categorical variable, either 1 (wings-level) or 2 (accelerated)
Property	TIS	s	Time in stall, amount of seconds during data set when $X < 0.9$
Property	$\alpha_{\max}$	rad	Maximum achieved angle of attack during maneuver
Property	X_{RMS}	-	RMS of X-signal
Property	$\delta_{a,\text{RMS}}$	rad	RMS of δ_a-signal
Property	$\delta_{e,\text{RMS}}$	rad	RMS of δ_e-signal
Property	$\delta_{r,\text{RMS}}$	rad	RMS of δ_r-signal
Property	p_{RMS}	rad/s	RMS of p-signal
Property	q_{RMS}	rad/s	RMS of q-signal
Property	r_{RMS}	rad/s	RMS of r-signal
Property	α_{RMS}	rad/s	RMS of α-signal
Property	β_{RMS}	rad/s	RMS of β-signal
Metric	MSE of $\mathbf{y}_i$	-	Mean squared error of model output $\mathbf{y}_i$ with respect to measured signal $\mathbf{y}$. This is done for all six outputs.
Metric	CRLB of θ_i	div.	Cramèr-Rao lower bound of parameter θ_i. This is computed for all of the parameters included in the model.

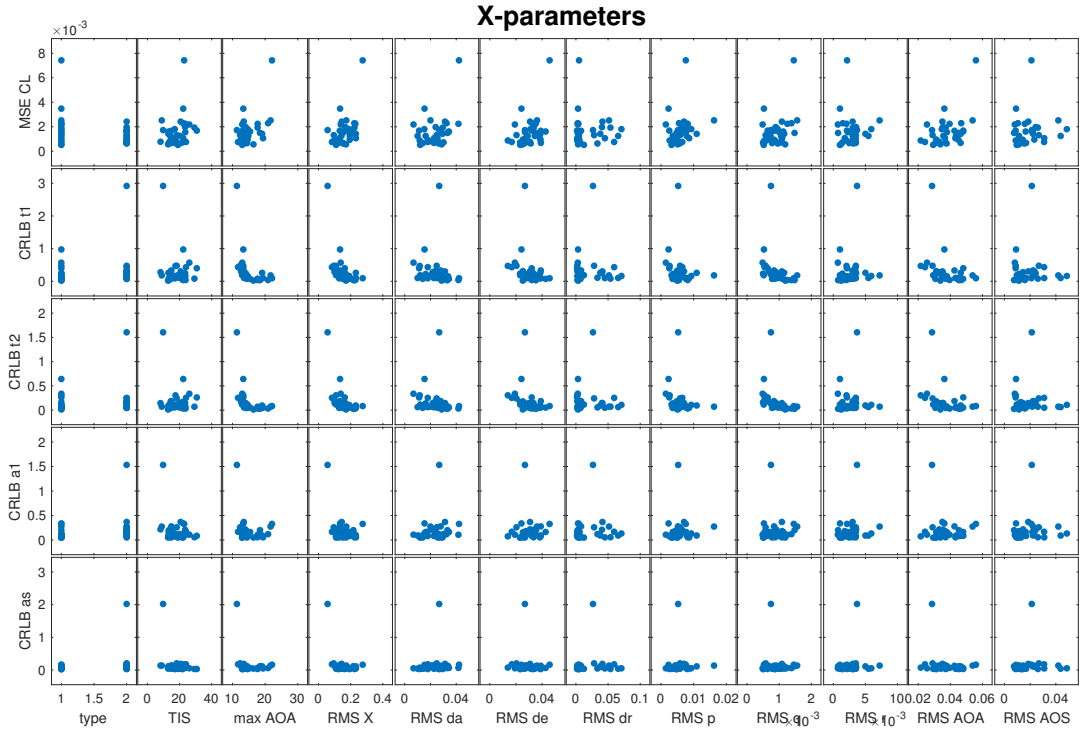

Figure F.1: Flight test maneuver analysis plots for the X-parameters.

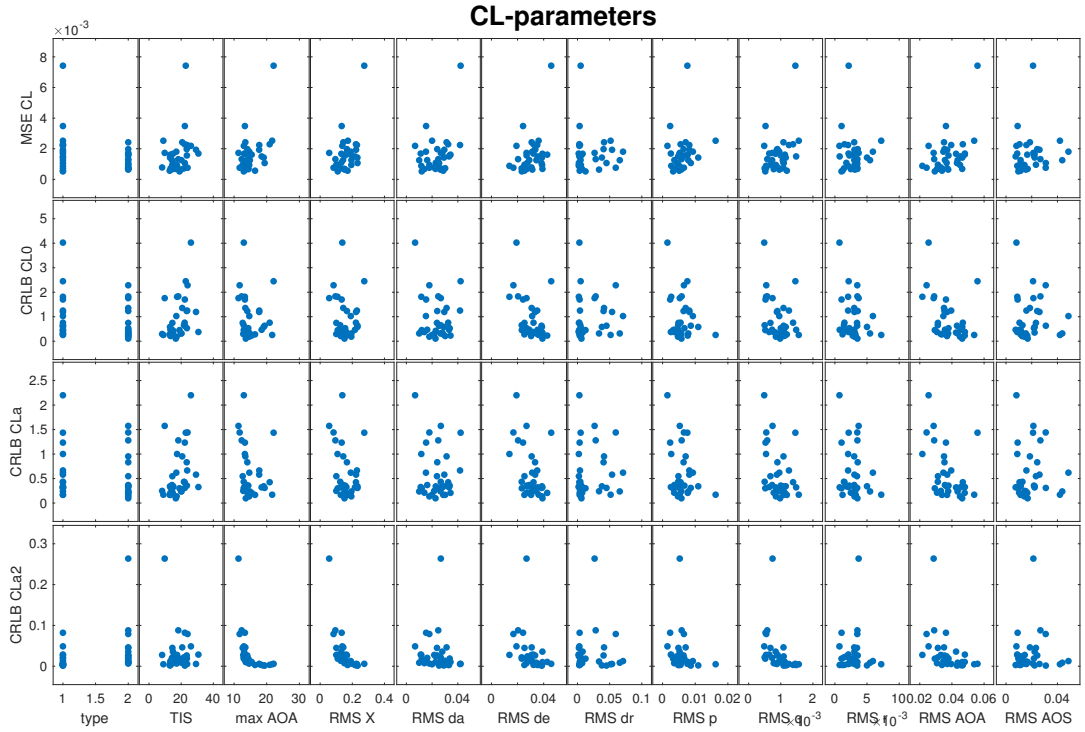

Figure F.2: Flight test maneuver analysis plots for the C_L-parameters.

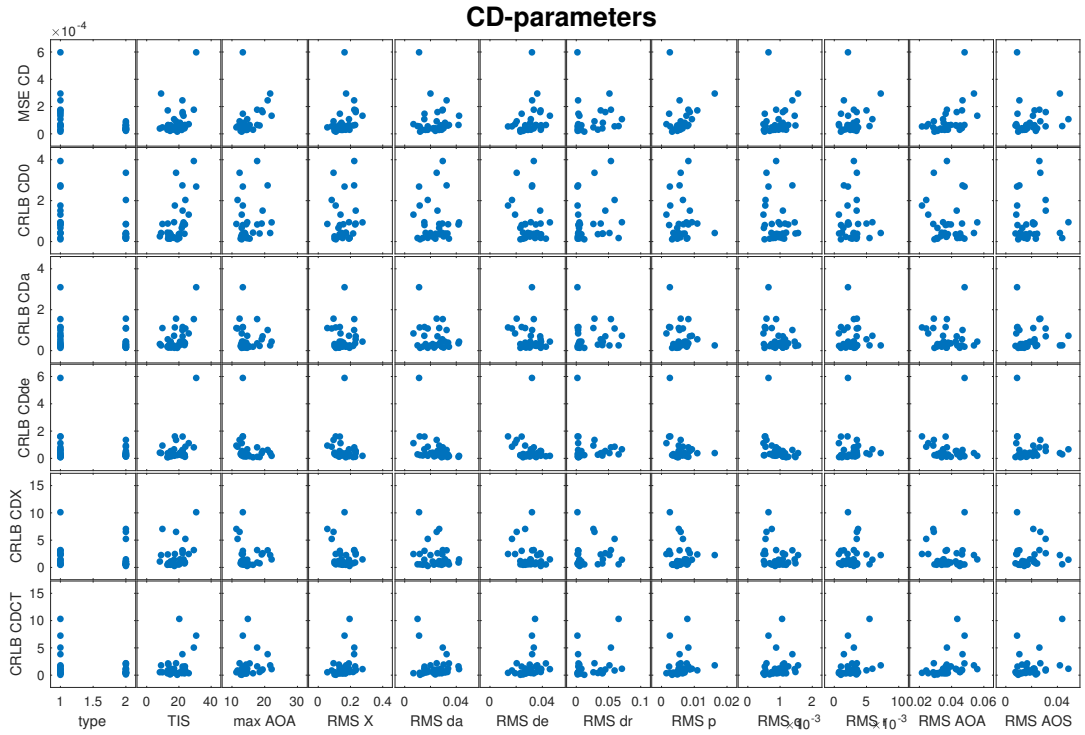

Figure F.3: Flight test maneuver analysis plots for the C_D-parameters.

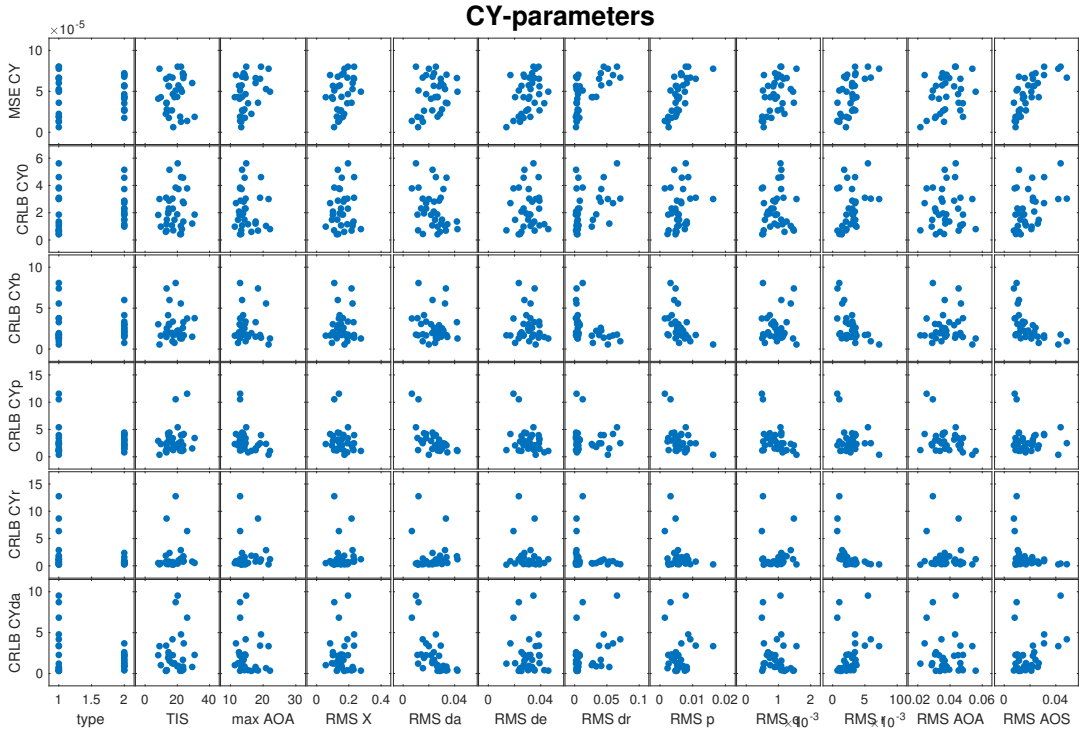

Figure F.4: Flight test maneuver analysis plots for the C_Y-parameters.

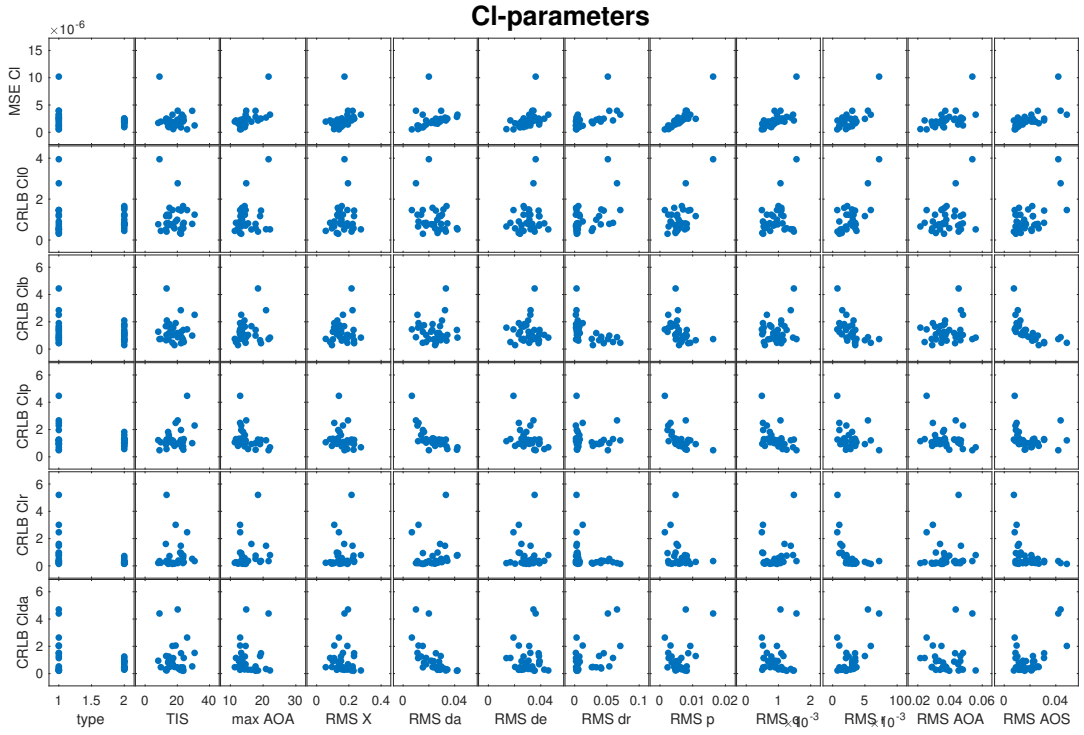

Figure F.5: Flight test maneuver analysis plots for the C_l-parameters.

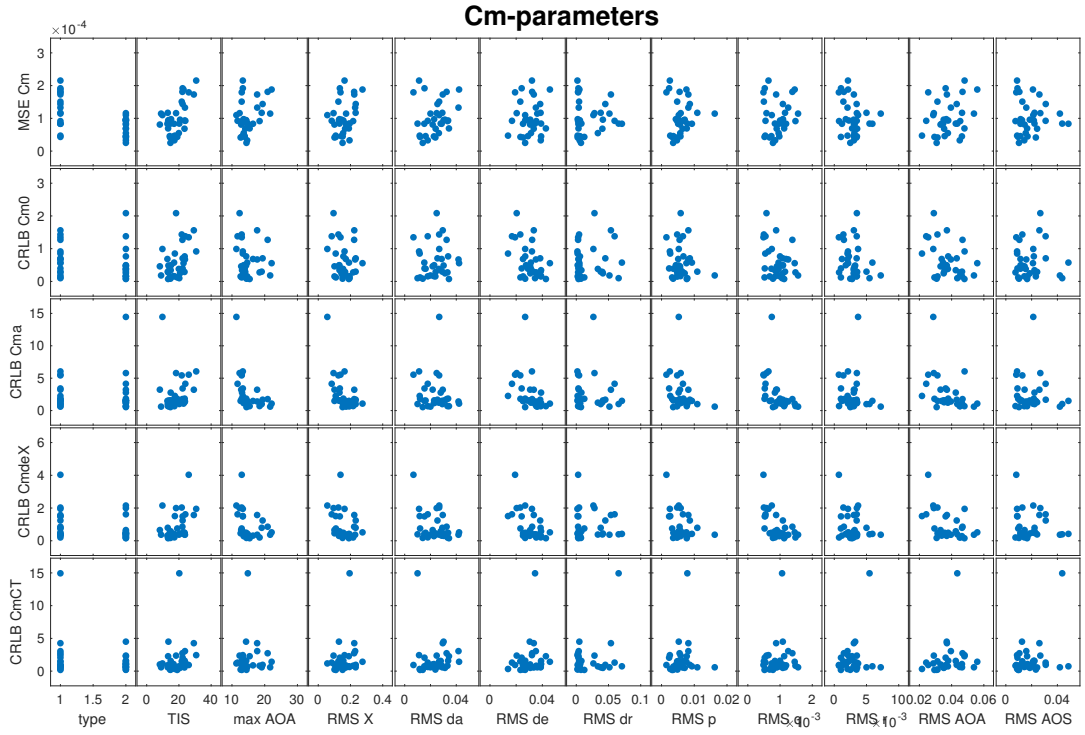

Figure F.6: Flight test maneuver analysis plots for the C_m-parameters.

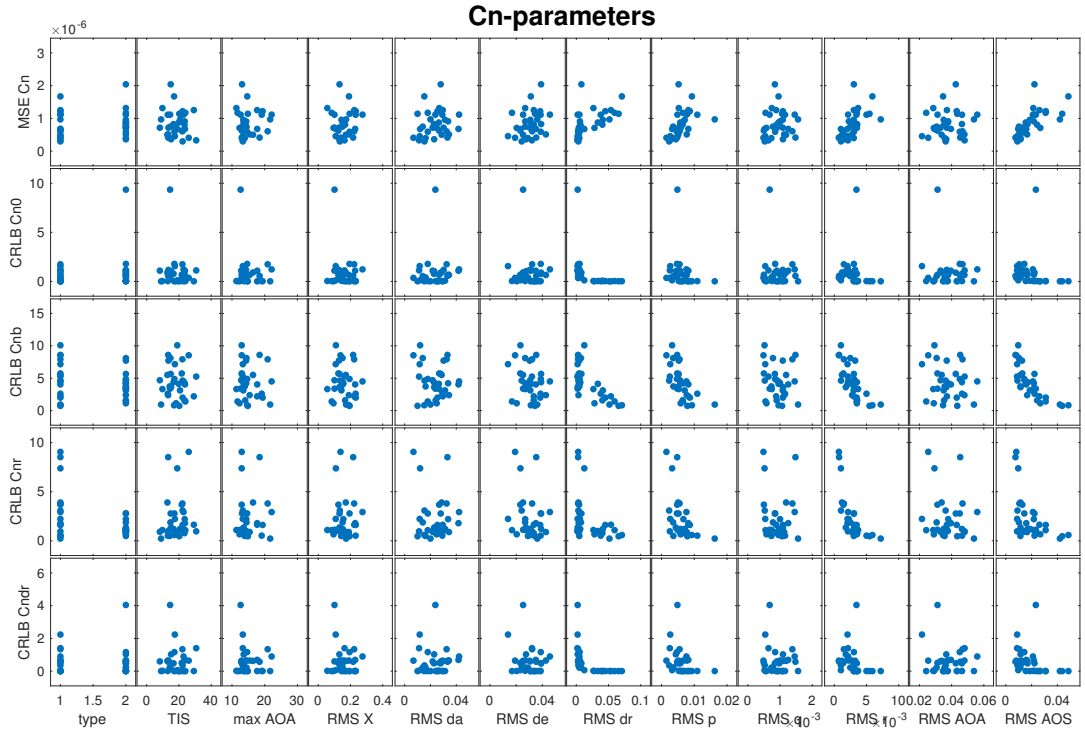

Figure F.7: Flight test maneuver analysis plots for the C_n-parameters.

G

SIMONA Implementation of Model

A critical next step in the research towards effective programs for pilot stall training is to evaluate the developed stall model in a human-in-the-loop simulation. This will take place in SIMONA, the research simulator of the research group in which this thesis was performed. This Appendix briefly describes the current state of the project on this matter, and lists several next steps to be taken.

G.1. Current State of SIMONA Implementation

The current version of the Citation II stall model has been implemented in the same way as the normal flight envelope model. This normal model is used for demonstration purposes, and can be found in the DUECA project `CitationDemo`. For the stall model, a new project was created, called `CitationStall`. Both projects can be checked out of the repository.

The aerodynamic force and moment models themselves are implemented as part of the complete Citation II aircraft models in Simulink. These Simulink files are included in the repository project files. When these models are verified to work, Simulink's Code Generation tool (on Mac: Cmd+B, on Windows: Ctrl+B) is used to export the models to a series of C files. These files are placed in the module `CitationModel` and communicate with the rest of the C++ code. For this to work, the Simulink model inputs and outputs needs to be defined according a specific format. DUECA supports exported code by Matlab 2016b, and several older versions.

Besides the aerodynamic model the Simulink model contains an engine model, a landing gear model, a mass model, an atmospheric model, and a gravity model. Figure G.1 shows what this looks like. Figure G.2 shows what is inside the aerodynamic model block. The current stall model is implemented as stand-alone (i.e., only the stall model is included, not the normal flight envelope model), is not trimmed, and has not been thoroughly tested.

G.2. Recommended Next Steps

During next steps of the research, the simulator is thought to become an important tool during model development. To facilitate this, it will be useful to have a convenient interface for quickly implementing variations of (stall) models. Generated code from Simulink models is a good way to approach this, since offline testing is made easy. However, there are several improvements that could be made that will make work easier:

- First of all, there are two bugs in the model that were clearly noticeable during a first test in SIMONA: there is an unexplained roll moment to the left, and uncontrollable pitch oscillations start near the stall. These bugs should not be in the model.
- Second, a general update of the Simulink model would be helpful. The division of functionalities in sub-blocks is clear, but the signal routing between them is not. Muxes, buses, input/output blocks, goto/from blocks, and selectors are all used interchangeably. The current model contains contributions from multiple authors, so it will be beneficial for one person to obtain a deep understanding of all its parts.
- Next to that, many parts of the model are quite old and stem from a Simulink version when Matlab Function blocks were not available yet. They are difficult to understand, and could definitely use an

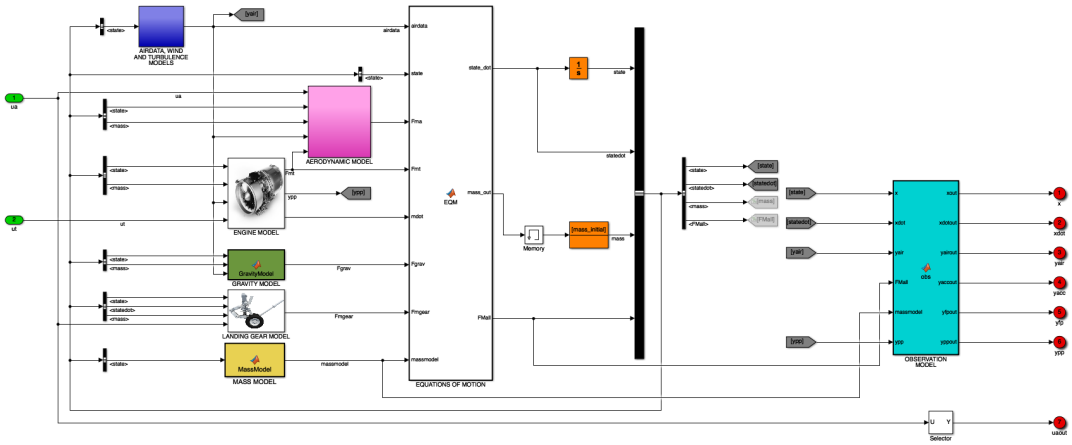

Figure G.1: Overview of the complete Citation II aircraft model as implemented in Simulink

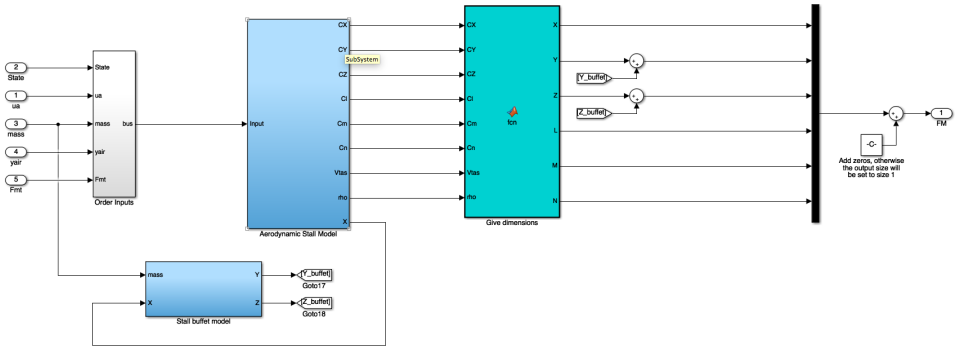

Figure G.2: Aerodynamic stall model part of the Simulink model.

update. Using as many Matlab Function blocks is highly recommended for this update, they are flexible, can be easily inspected, and result in nicely generated C code.

- The way in which the current stall model has been implemented is not ideal, and is not very flexible for making quick changes and fixes. It will pay off to think about a convenient way to interface with this.
- The `m`-files that are used to initialize the model could use an update, many functions in them are not actively used anymore.
- A trim input has not been determined for the initial conditions yet. Solving for a trim input is a nonlinear optimization problem, but is vital for testing errors
- During this thesis, it was seen that the engine model very likely contains errors, so an update is desired. If and when this is done, it is instrumental to also implement these changes to the methods used to pre-process any Citation II flight data, as this is a completely separate routine!
- The stall model should be combined with the regular flight envelope model. One thing to keep in mind during that, is that the regular flight envelope model could potentially also benefit from including a term related to C_T, to account for engine model errors.

Furthermore, considering the DUECA project, also there several next steps are recommended:

- Inside the `CitationModel` module, a clear folder structure for all the files generated by Simulink, and others that are required should be created. Currently, it is very easy to forget updating one or more of these after editing the Simulink model and generating new code.
- Finally a way to run several (stall) model simultaneously in DUECA will be very helpful during experiments. It will enable rapid switching between normal or stall models, or different variants of stall models.

H

List of Recommendations for Future Research

The developed stall modeling methodology is concluded to be suitable for extending the envelope of the obtained model. This final Appendix contains the most important recommendations for possible future research endeavours into stall modeling based on the findings from this thesis.

- One of the first upcoming steps should be to perform a human-in-the-loop experiment using the current stall model. This will be instrumental in identifying which aspects of a stall model are important for a convincing simulator experience, and will determine future research steps. For this, the Simulink implementation of the stall model will have to be debugged and thoroughly tested, as explained in Appendix G.

- If the stall modeling methodology developed in this thesis is to be applied to extending the obtained stall model, new flight tests will have to be done. Regarding these **flight tests**, several recommendations can be made:

  - In general, it was found to be beneficial to achieve a high angle of attack that is as high as possible.
  - If the degradation of control surfaces is to be modeled, it is important to excite the aircraft with the control surface of interest both during the stall, as well as right before the stall. Both the stall and this extra maneuver should be included in the same data set. For example, a 3-2-1-1 or doublet could be added at the start of the data set.
  - For the identification of dynamic aircraft responses (i.e., to body rotation rates), it is also important to excite the aircraft both outside of and during the stall. For this, the same maneuvers as described in previous bullet will be effective.
  - All control surfaces should be excited during the stall, also including the rudder.
  - The aircraft response to large rudder inputs during the stall is more unpredictable than the response due to aileron or elevator deflections. It is recommended to be careful when applying the rudder input disturbances.
  - Avoid very rapid oscillatory control surface excitations during the flight tests. During the flight tests, the aircraft response to such inputs was seen to be limited. The expected reason for this is that the aircraft dynamics act as a damper system, so high-frequency components of the control inputs do not enter into the measured dynamics. During system identification, this effect can be mistaken for a reduction in control surface effectiveness that is not really there.

- Regarding the **model structure selection** method:

  - New mathematical transformations of X should be tested as candidate regressors.
  - It was unexpected that no terms that model the changes in aileron and rudder effectiveness were found. Future research should focus on finding these effects, or proving that they do not exist.
  - It was also unexpected that no terms depending on q were identified. Also this should be a point of attention in future research.

  - A special focus should be placed on evaluating the effect of (simple) spline terms as regressors. In the model for C_L, it was found that even a simple spline was beneficial to model quality. Due to their local effects, splines are and ideal tool for modeling configuration-dependent effects of stall (e.g., tail shadowing).
  - The presence of the terms relating to C_T is unconventional, and expected to be caused by errors in the engine model. The engine model should be updated, and these terms should be removed from the model if possible.
  - Currently, a lot of manual work is involved in the model structure selection step. While this is not necessarily a bad thing, it could be interesting to investigate an increase in automation. Especially when the modeling methodology is to be used to expand the current model, this could save a lot of development time.

- Regarding **parameter estimation**:

  - During following research, identify dimensionless variants of τ_1 and τ_2, as the airspeed at which stall occurs varies quite significantly with altitude.
  - It would be interesting to see what is the effect on model quality of estimating the X-parameters using C_D or C_m instead of C_L. It is expected that this will change the estimated parameters significantly, and possibly this has a strong positive effect on the model quality for C_D or C_m. If this is the case, it could be considered to have multiple variants of X. Note that this will increase the number of parameters and complexity of the model.

- In this research, the buffet model was not treated. The first version of the buffet model was developed during previous research [57]. The new flight data should be used to either validate and/or update the buffet model.

- Finally, considering the data pre-processing, novel and more accurate state reconstruction methods can be considered, such as the unbiased adaptive maximum a posteriori (UAMAP) algorithm, or a multi-rate Kalman filter. Furthermore, the effects of low-pass filtering and resampling of data can be investigated further.